91-02066/

Environment Canada
Environnement Canada

PROCEEDINGS OF THE WORKSHOP ON APPLICATIONS OF REMOTE SENSING IN HYDROLOGY

COMPTES RENDUS DE L'ATELIER SUR LES APPLICATIONS DE LA TÉLÉDÉTECTION EN HYDROLOGIE

Saskatoon, Saskatchewan
13 and 14 February 1990 / Le 13 et 14 février 1990

Canadian Climate Centre
Centre climatologique canadien

National Hydrology Research Institute
Centre national de recherche en hydrologie

Canadian Water Resources Association
Association canadienne des ressources hydriques

Editors / Rédacteurs
G. W. Kite and A. Wankiewicz

Canadä

En 36-512/5E
NHRI Symposium No. 5

ISSN 0838 1984
ISBN 0-662-17687-1

TABLE OF CONTENTS

PREFACE.. 1

ACKNOWLEDGEMENTS... 3

EXECUTIVE SUMMARY
M. Brugman & A. Stanley.................................... 5

RÉSUMÉ POUR LA DIRECTION................................... 9

OPENING REMARKS
T.M. Dick.. 13
D.G. Schaefer.. 15

SESSION 1A: Hydrologic Models I

Session Chairman: G.W. Kite

Effective Use of Satellite-Observed Snow Cover Data in the Snowmelt-Runoff Model; A. Rango..................... 19

Contribution of GOES Data to Hydrologic Regionalization; R.M. Leith.. 33

Application of Remotely Sensed Data in a Distributed-Parameter Watershed Model; G.H. Leavesley & L.G. Stannard.. 47

Using GOES Visible Data to Extend Snow Course Data in Southern Ontario; J.R. Donald, E.D. Soulis, N. Thompson & S.B. Malla................................. 69

Determination of Characteristics for Hydrologic Modelling Using Remote Sensing; J. Whiting.......................... 79

SESSION 1B: Hydrologic Models II

Session Chairman: J. Whiting

Enhancing Rainfall-Runoff Modelling of Mixed Land Use/ Land Cover Areas with Remote Sensing; N. Kouwen, E.D. Soulis & A. Peitroniro............................... 94

Surface Hydrology in Climate Models: The Role of Remote Sensing; G. Thomas.. 109

Modelling the Kootenay Watershed with Satellite Data; G.W. Kite... 123

Progress Report on the Implementation of an Algorithm to Estimate Regional Evapotranspiration Using Satellite Data; N. Bussières, P.Y.T. Louie & W. Hogg...................... 135

Updating Hydrological Model Forecasts; H. Assaf & M.C. Quick.. 149

HYDROTEL - A Hydrological Model Designed to Make Use of Remotely Sensed and GIS Data; J-P. Fortin, J-P. Villeneuve, C. Bocquillon, R. Leconte & K.D. Harvey.................. 177

SESSION 1C: Hydrologic Models III

Session Chairman: B.E. Goodison

Using a Surface Energy Budget Model to Estimate Evapotranspiration; T.Y. Gan.............................. 189

A Qualitative Evaluation of Data Networks for Streamflow Simulation in Manitoba; A.A. Warkentin.................... 215

WORKSHOP SESSION 1: Remote Sensing in Hydrologic Modelling

Session Chairman: G.W. Kite

Working Group Questions................................... 227

Summary.. 229

SESSION 2A: RADAR Remote Sensing and Soil Microwave Radiometry

Session Chairman: A. Wankiewicz

Utilisation of SAR Data in the Monitoring of Snowpacks and Wetlands; R. Leconte & T.J. Pultz......................... 233

Interpretation of Passive and Active Microwave Imagery over Snow-covered Lakes and Rivers near Fairbanks, Alaska; R.A. Melloh & L.W. Gatto........................... 259

Use of Microwave Remotely Sensed Soil Moisture in Hydrologic Modeling; E.T. Engman.......................... 279

Retrieval of Land Surface Temperature and Soil Moisture with SSM/I Brightness Temperatures; M.J. McFarland, R.L. Miller & C.M.U. Neale................ 293

SESSION 2B: Snow Microwave Radiometry

Session Chairman: R. Perla

Determination of Snow Water Equivalent on the Canadian Prairies using Near Real-Time Passive Microwave Data; B.E. Goodison, A.E. Walker & F.W. Thirkettle 297

Average Areal Snow Water Equivalent Determination in a Mountain Basin using Passive Microwave Satellite Data; A. Rango 317

Analysis of MOS-1 Microwave Scanning Radiometer Data for Canadian Prairie Snow Cover; A.E. Walker, S.A. Gray, B.E. Goodison & R.A. O'Neill 319

Microwave Satellite Spring Runoff Correlations; A. Wankiewicz 331

Classification of Snow and Frozen Ground Surfaces with SSM/I Signatures; C.M.U. Neale, M.J. McFarland & M.M. Batchelor 345

WORKSHOP SESSION 2: Radar & Microwave Radiometry

Session Chairman: A. Wankiewicz

Working Groups & Questions 359

Summary 361

INVITED PAPER:

Opportunities for Remote Sensing within a Canadian GEWEX program; R.G. Lawford 365

POSTER PAPER:

Snowmelt Stages on Landsat Images; G.A. Fuller & R.D. Hofer 375

LIST OF PARTICIPANTS 381

PREFACE

The Workshop on the Applications of Remote Sensing in Hydrology held at the National Hydrology Research Centre, Saskatoon, Saskatchewan on February 13 and 14, 1990, was a collaborative initiative of the Canadian Climate Centre (CCC) and the National Hydrology Research Institute (NHRI) in association with the Canadian Water Resources Association (CWRA).

As hydrology develops, simple lumped parametric models are giving way to more physically-based distributed models which need vastly increased numbers of data. At the same time, the number of ground-based data collection points is decreasing due to economic constraints. These two opposite trends of need and availablity serve to emphasise the potential usefullness of remotely-sensed data for hydrologic modelling. Satellites not only provide distributed values of data but can also provide data unobtainable from other sources. The Hydrologic Models session of the workshop concentrated on applications of GOES, NOAA and Landsat data in various hydrologic watershed models and contained discussion on means of increasing the utility of satellites for hydrologic modellers. There were thirteen oral presentations in this session followed by three workshop group discussions and a plenary session on Remote Sensing in Hydrologic Modelling. Also part of this session were five computer demonstrations, two by commercial companies, and a poster paper.

Satellite surveillance is about to revolutionise hydrology. Cloud-penetrating microwaves now have the potential for continuous monitoring of water and land processes. Microwave emission and RADAR reflection has been found to be sensitive to the unique physical signatures of water or snow. The high temporal resolution of microwave remote sensing will complement information obtained by short-wave sensors. The Microwave Hydrology Session focused on promising applications. Included were recent developments in: determining snowpack for streamflow forecasting; monitoring soil moisture status; classifying land and ice condition; and monitoring surface freeze-thaw. This session emphasised the benefits of microwave remote data collection for hydrologic monitoring, modelling and forecasting at field and basin scales. There were nine presentations in this session, followed by three workshop group discussions and a plenary session on RADAR and Microwave Radiometry.

ACKNOWLEDGEMENTS

The organisers, Geoff Kite, of CCC, and Anthony Wankiewicz, of NHRI, gratefully acknowledge the assistance of the many individuals who contributed to the success of the workshop. We thank Milne Dick and Garry Schaefer for making the facilities of NHRI and CCC available for the workshop. Wally Nikolaichuk and John and Mary Gillies assisted by providing the facilities of CWRA. We are grateful to the general chairman, Alan Stanley, for the efficiency with which he ensured that the workshop operated on schedule and that all participants were provided with the necessary information.

The discussions following the presentations formed an important part of the workshop and we wanted to include the flavour of these in the proceedings. Mindy Brugman transcribed the questions and answers from tape and a selection of these have been included after the papers. The executive summary of the workshop was prepared by Alan Stanley and Mindy Brugman and was translated by Gisèle Piché and Simon Ommanney.

We also thank the session chairmen, the authors of papers and demonstrations and the chairmen and rapporteurs of the workshops for their role in ensuring a smooth proceedings. The reports from each workshop session have been summarised and are included in the relevant parts of the proceedings.

Thanks are also due to all those who assisted with the technical and social arrangements, particularly Brenda Doell for managing the registration and lists of participants, Sandra Forsberg for coordinating the large amount of office work needed, Karen Morin for coordinating activities with CWRA and Philip Gregory for creating the graphics and ensuring successful printing of the circulars and proceedings. We are pleased to acknowledge the technical support for projecting, sound recording and lighting arrangements provided by Dan Matthews, Gary Lawrence and Newell Hedstrom.

The organisers were also pleased to provide facilities for representatives of Ph.D. Associates and PCI Inc. to demonstrate their products.

EXECUTIVE SUMMARY

Melinda M. Brugman and Alan Stanley
National Hydrology Research Institute

The focus of this meeting "Applications of Remote Sensing in Hydrology" was on two main topics: hydrological modelling (Session 1) and microwave radiometry (Session 2A included radar and 2B dealing with snow). In addition, there were displays by Canadian private industry, Ph.D. Associates and PCI Inc., demonstrating the latest innovations for handling remotely sensed data using a personal computer. Each topic at the meeting was dealt with by individual scientific presentations followed by group discussions to address key questions posed by workshop organisers. Discussions at the individual workshops were reported back at plenary sessions together with a summary of the recommendations. These recommendations are included in the meeting summary given below.

HYDROLOGIC MODELLING

To take advantage of the data acquired through remote sensing, future development of hydrologic models needs to be physically based and distributed. Digital-terrain-analysis procedures coupled with modelling provide a promising method to objectively study the hydrologic characteristics of a watershed or region. This modelling is still at the stage of parameter-estimation at different spatial scales, because the field situation is too complicated to be accurately determined by physically based models using the presently available data resolution from satellites. The data obtained by remote-sensing needs to be better related to the physical parameter being measured. The physics of the interaction of electromagnetic energy with complex land surfaces is not well understood at the present time and this limits interpretation of satellite images and the direct incorporation of satellite data into hydrologic models. Recent advancements in computer technology and in the quality of image processing has led to greater data accessibility, although there is considerable room for further improvements.

For immediate improvement of hydrologic forecast models, the empirical approach is still necessary, and has clearly been shown to give good results for selected basins. Despite the fact that algorithms to extract hydrological information from satellite data are still primarily qualitative, they have been effectively used to test and improve hydrological models. One prime example is the increased ability to forecast more accurately river discharge. If data resolution and availability were significantly increased, then scientific advancements in this field would progress much more rapidly. Large-scale hydrologic models still rely heavily upon field data obtained from long-term ground-based studies. Additional information is needed on actual surface roughness at different scale lengths, and on the character of vegetation, cloud cover, soil moisture and grain-size distribution, surface emission and albedo at different measurement angles, extent of ground- and lake-ice, spatial variation of snow crystal type and size, image calibration and location methodology. Future research should be aimed at comparing direct and remotely sensed data based on physical principles, while continuing to increase the capability to make timely and accurate hydrologic forecasts.

MICROWAVE HYDROLOGY

Microwave radiation (wavelength 1 millimeter to 1 meter) is able to penetrate clouds, to indicate snow under dry or partially wet conditions and to partially penetrate vegetation cover. RADAR and airborne radiometers have similar resolution to shortwave sensors (on order of 1 centimeter to 1 kilometer). However, satellite microwave radiometers currently have very poor resolution (15 to 150 kilometers, depending upon frequency). Several papers presented enticing correlations between microwave brightness and snow water equivalent and soil moisture, but operational models remain to be developed.

Both passive and active microwave studies were presented. RADAR studies involved Synthetic Aperture Radar (SAR) in the X- and C-bands obtained by Canada and the quadpolarized (HH, VV, HV, and VH) C-, L- and P-bands of the U.S. Jet Propulsion Laboratory's SAR. Results were presented for dry snow, and it was shown that the effects of water content and grain size distribution are still not well understood.

Reported correlations between microwave brightness and surface hydrologic characteristics varied from location to location and between the different wavelengths used in a study. The scatter of data for each correlation must be reduced for operational application of the algorithms. The details of the statistical correlations were usually not extensively discussed. Due to the large averaging footprint, physical variables, such as snow areal coverage and water equivalence, derived from microwave data for basins with complex topography and vegetation require extensive "ground truth". Several participants expressed caution in tests of algorithm accuracy using several remotely measured variables that are physically interrelated.

Overall, microwave radiation is a useful indicator of snow areal extent, snow water content, snow water equivalence and soil moisture. However, the methods are not a panacea for hydrological problems. Several different independent methods such as snow courses will continue to be needed in order to verify algorithms used to map physical variables from remote sensing data.

Microwave sensing is an imperfect predictive tool, but a much better understanding of the data available and the range of its use in hydrologic modelling has been developed.

FUTURE DEVELOPMENTS

Development of hydrologic networks should take into account information that will be available from remote sensing. Where possible the networks should be arranged to provide ground truth, continuously if possible, and to obtain the benefits of other types of surveys, such as those using gamma rays. Ground-based data are necessary now even more than ever to understand results obtained from aircraft and satellites, in order to advance scientists ability to interpret remotely sensed variables in hydrology.

The needs of operational agencies include information on snow cover extent and water content, soil moisture, surface water distribution and vegetation cover. These variables can also be used to test theories about regional and global climate change and climate variability, so that we can prepare for environmental changes predicted by some studies.

Remotely sensed data should be available as soon as possible after it has been received. Several solutions were put forward to satisfy the needs of operational engineers and of scientists. Remote sensing information could be provided through some central agency which has already processed the raw data and has made the information available together with user-friendly software packages to facilitate its further use. A second solution was for information to be more efficiently and more widely disseminated by reducing the cost of the data, by increasing its availability, and by increasing funding of research that involves applications of remote sensing to hydrological problems. The high cost and difficulties of obtaining data were cited as obstacles to more rapid advance of research in this field. Combined together, both proposals offer a solution to current obstacles caused by high cost of using the data, lack of data availability and incomplete knowledge of potential data applications.

RÉSUMÉ POUR LA DIRECTION

par Melinda M. Brugman et Alan Stanley
Institut national de recherche en hydrologie

Cette réunion "Applications de la télédétection en hydrologie" a porté sur deux grands sujets: la modélisation hydrologique (séance 1) et la radiométrie des micro-ondes (séance 2A comprenait le radar et séance 2B portait sur la neige). De plus, il y avait des étalages faits par l'industrie privée canadienne, Ph. D Associates and PCI Inc., qui démontraient les innovations les plus récentes en matière de traitement des données de télédétection sur ordinateur personnel. Chaque sujet, de la réunion, a fait l'objet de présentations scientifiques séparées, suivies de discussions de groupe sur les principales questions soulevées par les organisateurs des ateliers. Des comptes rendus des discussions menées lors des différents ateliers ont été présentés lors des séances plénières en même temps qu'un résumé des recommandations. Ces recommandations sont comprises dans le résumé de la réunion, donné ci-dessous.

MODÉLISATION HYDROLOGIQUE

Afin de profiter des données recueillies par télédétection, les prochains développements de modèles hydrologiques doivent avoir une base physique et être diffusés. Les méthodes d'analyse numérique du terrain, combinées à la modélisation, constituent une méthode prometteuse pour étudier objectivement les caractéristiques hydrologiques d'un bassin versant ou d'une région. Cette modélisation en est toujours à l'étape de l'estimation des paramètres à différentes échelles spatiales parce que la situation sur le terrain est trop complexe pour être représentée avec exactitude par des modèles de processus physiques en utilisant la résolution des données actuellement accessibles par satellites. Les données recueillies par la télédétection doivent être mieux reliées au paramètre physique étant mesuré. La physique de l'interaction de l'énergie électromagnétique avec des reliefs terrestres complexes est actuellement mal comprise, ce qui restreint l'interprétation des images-satellites et l'entrée directe des données-satellites dans les modèles hydrologiques. Des progrès récents en matière de technologie informatique et de qualité du traitement des images ont mené à une plus grande accessibilité des données, quoiqu'il y soit encore possible de les améliorer.

Pour améliorer immédiatement les modèles hydrologiques prévisionnels, il est encore nécessaire de recourir à l'approche empirique qui a nettement donné de bons résultats pour certains bassins. Même si les algorithmes d'extraction de l'information hydrologique contenus dans les données-satellites sont encore essentiellement qualitatifs, ils ont été utilisés efficacement pour éprouver et améliorer les modèles hydrologiques. Citons notamment l'amélioration de la capacité de prévoir plus exactement le débit des cours d'eau. Si la résolution et la disponibilité des données étaient sensiblement accrues, les progrès scientifiques dans ce domaine se multiplieraient beaucoup plus rapidement. Les modèles hydrologiques à grande échelle reposent encore dans une certaine mesure sur des données recueillies sur le terrain dans le cadre d'études au sol à long terme. Il faut recueillir d'autre information sur la rugosité actuelle de la surface à différentes échelles et sur la nature de la végétation, la nebulosité, la teneur en humidité et la granulométrie des sols, le rayonnement émis par la surface et l'albédo selon différents angles de mesure, l'étendue des glaces terrestres et lacustres, la variation totale d'une région des types et des tailles des cristaux de neige, l'étalonnage des images et les méthodes de localisation. Les recherches futures devraient viser à comparer les données directes et les données de télédéction selon des principes de physique, tout en continuant d'accroître la capacité de faire des prévisions hydrologiques opportunes et exactes.

HYDROLOGIE ET MICRO-ONDES

Les micro-ondes (longueur d'onde de 1 millimètre à 1 mètre) peuvent pénétrer dans les nuages pour indiquer la présence de la neige dans des conditions sèches ou partiellement humides, et pénétrer partiellement la couverture de végétation. Le radar et les radiomètres aéroportés ont des résolutions voisines de celle des détecteurs d'ondes courtes (de l'ordre de 1 centimètre à 1 kilomètre). Cependant, les radiomètres à micro-ondes des satellites ont actuellement des résolutions très médiocres (de 15 à 150 kilomètres selon la fréquence). Plusieurs communications ont décrit des corrélations séduisantes entre la brillance des micro-ondes et l'équivalent en eau de la neige et la teneur en humidité du sol, mais il reste à mettre au point des modèles opérationnels.

Des études sur l'utilisation tant active que passive des micoondes ont été présentées. Les études sur le radar portaient sur le radar à ouverture synthétique (ROS) dans les bandes X et C obtenus par le Canada et sur les bandes C, L, et P quadpolarisées (HH, VV, HV et VH) du ROS de l'U.S. Jet Propulsion Laboratory. Les résultats ont été présentés pour la neige sèche, et il a été montré que les effets de la teneur en eau et de la granulométrie sont encore mal comprises.

Les corrélations signalées entre la brillance des micro-ondes et les caractéristiques hydrologiques de surface variaient selon l'endroit et la longueur d'onde utilisée dans l'étude. La dispersion des données pour chaque corrélation doit être réduite pour que les algorithmes soient applicables et opérationnels.

Les corrélations statistiques n'ont en général pas été discutées de façon approfondie. A cause de l'étendue de l'empreinte pour établir les moyennes, les variables physiques tels que la couverture superficielle de neige et l'équivalence en eau, calculées à partir de données de micro-ondes pour des bassins au relief et à la végétation complexes, nécessitent un important travail de "réalité de terrain". Plusieurs participants ont exprimé des réserves quant à l'utilisation de plusieurs variables télémesurées qui sont physiquement reliées pour vérifier la précision des algorithmes.

Globalement, les micro-ondes peuvent indiquer efficacement l'étendue de la couverture de neige, de la teneur en eau de la neige, de l'équivalence en eau de la neige et de la teneur en humidité du sol. Cependant, les méthodes ne sont pas une panacée pour les problèmes hydrologiques. Plusieurs méthodes indépendantes différentes telles que les cours sur la neige continueront à être nécessaires pour vérifier les algorithmes utilisés dans la cartographie des variables physiques à partir de données de télédétection. La détection par micro-ondes est un outil de prévision imparfait, mais elle a permis de comprendre beaucoup mieux les données disponibles et leur marge d'utilisation dans la modélisation hydrologique.

PERSPECTIVES D'AVENIR

Dans l'élaboration des réseaux hydrologiques, il faudrait tenir compte de l'information qui parviendra de la télédétection. Le cas échéant, les réseaux devraient être montés pour offrir la réalité de terrain, en continu si possible, et pour tirer profit des autres types de sondages comme ceux par rayons gamme. Les données recueillies au sol sont maintenant plus que jamais nécessaires pour comprendre les résultats obtenus par aéronef et par satellite afin d'améliorer l'interprétation des scientifiques vis-à-vis les variables hydrologiques de télédétection en hydrologie.

Les organismes d'exploitation ont besoin d'information sur l'étendue de la couverture et de la teneur en eau de la neige, la teneur en humidité du sol, la répartition des eaux de surface et la couverture de végétation. Ces variables peuvent aussi être uilisées pour vérifier des théories sur le changement et la variabilité du climat à l'échelle planétaire, de sorte que nous puissions nous préparer aux changements environnementaux prévus par certaines études.

Les données de télédétection devraient être disponibles dès leur réception. Plusieurs solutions ont été proposées pour répondre aux besoins des ingénieurs opérationnels et des scientifiques. L'information de la télédétection pourrait être fournie par l'intermédiaire d'un organisme central qui aurait déjà traité les données brutes et présenterait l'information sous forme prologiciels convivaux facilitant son utilisation complémentaire. Une autre solution consisterait à diffuser l'information de façon plus efficace à un auditoire plus large en réduisant les coûts des données, en facilitant son accessibilité et en augmentant les fonds de recherche portant sur l'application de la télédétection aux problèmes hydrologiques. Le coût élevé et les difficultés d'acquisition des données ont été cités comme des obstacles à l'avancement rapide de la recherche dans ce domaine. Ensemble, les deux propositions permettent d'éliminer les obstacles actuels que sont le coût élevé d'utilisation des données, le manque de disponibilité des données et la méconnaissance des applications potentielles des données.

OPENING REMARKS

T.M. Dick, Director, NHRC

Good morning everyone, Welcome to Sunny Saskatoon. Bonjour à tous au pays du congélateur. First of all, I would like to thank both the AES-Hydrometeorological Research Division and the Institute's Physical Hydrology Division for taking the initiative to jointly organize this workshop under the leadership of Geoff Kite of AES-HRD, Anthony Wankiewicz and Ron Perla of NHRI. They were supported by Karen Morin and Brenda Doell of NHRI and Sandra Forsberg of AES-HRD. This workshop provides an excellent example of inter-service collaboration.

I would also like to mention here that we have two people who have travelled some distance to be here. The first is Professor Thien Yew Gan from the Asian Institute of Technology, Bangkok, and once again, John Stewart from the Institute of Hydrology, Wallingford, England.

Je voudrais également adresser quelques mots à nos invités francophones. Au nom du comité d'organisation, j'aimerais vous accueillir chaleureusement au Centre et à cet atelier. Je suis assuré que cet atelier vous profitera grandement et vous donnera une bonne occasion d'avoir des discussions à la fois agréable et informatives. J'espère aussi que ces rencontres pourront encore avoir lieu dans l'avenir.

In the next decade hydrological science must develop almost routine ways to handle meso-scale and by extension macroscale models of basins or regions. Larger basins introduce problems of dealing with basin variables which may have very complex spatial relationships. Bearing in mind, that any model is an approximation of reality, the problem is to establish reliable models which contain an acceptable error and behave consistently. That is the error should be systemic rather than random. In addition there must be a consistent relationship to real physical and environmental parameters and variables. It must be evident also, that in order to correctly assess the effects on water resources if there are changes in climate averages, that the models must reflect reality in a consistent way.

At this time the rapidly developing capability to obtain spatially related data by remote sensing methods and the ability to combine data bases in one model makes possible to have models which are physically based rather than local calibrations.

It is also evident that the interpretation of remote sensing signals will need systematic evaluation and calibration. The scope and task is quite clearly formidable and will benefit greatly if various research groups can find ways to work together on various aspects of the problem. This workshop provides an opportunity to exchange information and ideas. There will be a proceedings produced to place on record the papers and discussions. I wish you all every success and an interesting time in the next two days.

OPENING REMARKS

D.G. Schaefer, Acting Chief
Hydrometeorological Research Division, CCC

Good morning ladies and gentlemen. It is my great pleasure to welcome you to today's workshop on behalf of the Canadian Climate Centre. I'd like that to be an especially warm greeting to our out-of-city, out-of-province and out-of-country guests.

For those of you not familiar with Canada's government bureaucracy I'll say that Milne Dick's NHRI and our Canadian Climate Centre are units of sister services in Environment Canada. Both services have a long standing interest in remote sensing, ours beginning with meteorological applications and, now, increasingly oriented towards applications in hydrology. The Canadian Climate Centre's research program is carried out by the Hydrometeorology and Marine Division at our Toronto headquarters and by the Hydrometeorological Research Division here in the Centre.

I'd like, now, to acknowledge the good work done by the program committee comprised of Geoff Kite, Tony Wankiewicz and Ron Perla. You will hear from each of them as the program unfolds.

On a personal note, I'm glad to have the opportunity to meet, once again, a number of colleagues from across the country as well as to make some new aquaintances from among those working in the field of remote sensing in hydrology. I'm sure we'll have a good two days. Thank you all for being here.

SESSION 1A
HYDROLOGIC MODELS I

Session Chairman: G.W. Kite, Canadian Climate Centre

EFFECTIVE USE OF SATELLITE-OBSERVED SNOW COVER DATA IN THE SNOWMELT-RUNOFF MODEL (SRM)

A. RANGO
USDA Hydrology Laboratory, Agricultural Research Service, Beltsville, Maryland 20705, U.S.A.

ABSTRACT The Snowmelt-Runoff Model (SRM) employs direct input of remotely-sensed snow cover extent data for simulation and forecasting of snowmelt runoff. An increasing number of snowmelt-runoff models are using remote sensing inputs. SRM can accept snow cover extent data from a wide variety of sources including ground, aircraft, and satellite observations. The National Weather Service provides operational snow cover maps using NOAA-AVHRR observations for about 4000 basins in North America. Because of its daily coverage, NOAA-AVHRR data are very appropriate for snowmelt-runoff applications, but its 1.1 km resolution limits its use to basins larger than about 200 km^2.

SRM has been tested extensively worldwide with excellent simulation results. The quality of hydrograph simulations only drops when basins are extremely large, the data network is sparse, data quality is poor, and users are inexperienced. The development of a forecasting methodology for SRM has been tested on the Rio Grande basin in Colorado. It is necessary to develop modified snow cover depletion curves (snow cover area versus accumulated snowmelt) for each elevation zone. The appropriate modified depletion curve for a given year is selected by using the April 1 snow water equivalent. Tests of the forecasting approach in both the realtime and post-analysis mode were successful. A simple updating approach provided improvement of the forecast and additional updating techniques are being considered. SRM is now distributed in microcomputer format, and it has proved easy to use.

INTRODUCTION

Many hydrological models have been developed to approximate the movement of water through various stages of the hydrological cycle shown in Figure 1. For use in basins where snowmelt contributes a significant amount to runoff, special snowmelt algorithms have been developed to represent the snowmelt-runoff process. There are many models that can be used to simulate the snowmelt-runoff hydrograph, and eleven different models formally participated in the World Meteorological Organization Intercomparison of Models of Snowmelt Runoff (World Meteorological Organization, 1986). Most of these models employed the degree-day approach for calculating runoff, and the remaining few models used an energy balance approach. At the time of the actual Intercomparison (1982), only one of models, the Snowmelt-Runoff Model (SRM), employed distributed input data supplied by remote sensing. Since 1982, more and more models have started to use remote sensing inputs. Examples of these recent developments are Leavesley and Stannard (1990), Kite (1989), and Fortin et al. (1990). This trend will likely continue because the remote sensing data allow the models to take advantage of the areally distributed capabilities incorporated in most of them.

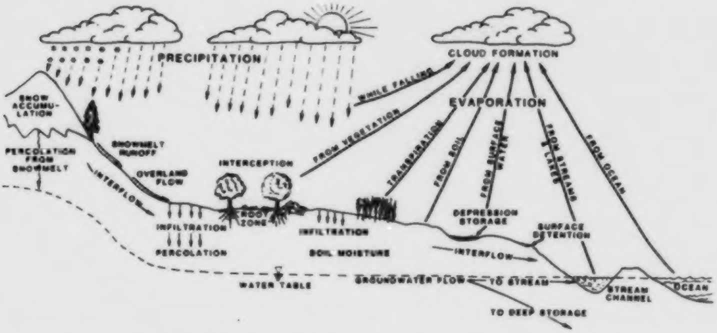
PRECIPITATION
CLOUD FORMATION
WHILE FALLING
EVAPORATION
SNOW ACCUMU-LATION
PERCOLATION FROM SNOWMELT
SNOWMELT RUNOFF
INTERFLOW
OVERLAND FLOW
INTERCEPTION
FROM VEGETATION
TRANSPIRATION
FROM SOIL
FROM SURFACE WATER
FROM STREAMS & LAKES
FROM OCEAN
ROOT ZONE
INFILTRATION
PERCOLATION
INFILTRATION
SOIL MOISTURE
DEPRESSION STORAGE
SURFACE DETENTION
INTERFLOW
WATER TABLE
GROUNDWATER FLOW
TO STREAM
STREAM CHANNEL
OCEAN
TO DEEP STORAGE

Fig. 1. Circulation of water through the hydrological cycle.

DESIGN AND INPUT REQUIREMENTS OF SRM

SRM was developed by Martinec (1975) for small mountainous basins and subsequent development facilitated the use of various types of satellite remote sensing inputs (Rango and Martinec, 1979; Martinec et al., 1983). The structure of SRM is adequately discussed in Rango and Martinec (1979) and Martinec et al. (1983). SRM requires three input variables, namely, daily values of temperature, precipitation, and snow-covered area. The temperature data, used for calculating snowmelt degree days, and the precipitation data, used for assessing incremental additions to the snowmelt hydrograph, are obtained from conventional ground measurements. The snow-covered area data are obtained from some form of remote sensing to be discussed in a later section.

The temperature data used in SRM is most commonly obtained as maximum and minimum daily values. These values are used to directly calculate the daily degree-day value which in turn is used in the snowmelt calculation. The precipitation data required are 24 hour totals. Shorter time interval data can be handled, but are not needed. It is preferred that the temperature and precipitation data be obtained at the mean elevation of each elevation zone, at the mean elevation of the entire basin, or somewhere in the drainage basin, in order of priority. Failing this, data from somewhere in the basin vicinity can be utilized.

The remote sensing input of the areal extent of snow cover is extremely critical to the operation of SRM because these data are used to areally specify where the temperature and precipitation algorithms should be applied in the basin. The more frequently these snow cover data are obtained, the better. The desired frequency of observation of snow coverage is once per week. As is the case for the location of the climate stations, the desired frequency of observation is seldom obtained. The minimum coverage that the model has been run with is two observations during the entire snowmelt runoff season (Rango, 1985).

Questions are often raised as to why SRM does not require snow water equivalent data. In its original design, SRM took into consideration that snow cover in mountain basins did not change drastically from day-to-day. Only so much snow could be melted in a day based on a finite amount of energy available, and as a result, snow cover changes were of a gradual nature. If the snow cover could be monitored frequently enough, and the degree days applied to only the area covered by snow, then snow water equivalent information was not of a critical nature. This was confirmed as SRM was tested, and it was further found that even with minimal snow observations, the generally regular depletion of the snow cover extent obviated the need for the snow water equivalent measurements. This was fortuitous because areal snow water equivalent data are seldom available. It was found that the areal snow cover extent data were more appropriate than point snow water equivalent data for use with distributed snowmelt runoff models such as SRM.

SELECTION OF REMOTE SENSING DATA

There is a wide variety of remote sensing data available as well as a variety of ways to collect it. Because snow cover extent is required by SRM, the visible portion of the electromagnetic spectrum is usually chosen. The type of visible snow cover data selected depends heavily on basin size. The areal extent of snow cover on basins less than 10 km^2 in area can be determined by visual observations and from snow course data. In such a small basin, the visual observations can be made from one or two observation points that can reveal the snow cover in the majority of the basin. A snow course network can supplement these visual observations and can even be used to delineate the snow cover when the visual observations are not possible. Low altitude aircraft observations or higher altitude orthophotos, of course, give results superior to the methods mentioned here.

Basins exceeding 10 km^2 in area are too large for visual, ground-based snow mapping, and an aircraft observing capability is the next logical step. For basins in the range of 1-100 km^2 in area, the aircraft platform is ideal. The automated calculation of discontinuous snow cover is possible, and the observation flights can be flown when needed and as weather conditions permit.

Satellite observations can, of course, be made on basins both above and below 100 km^2 in area, especially because resolutions as good as 28.5 m are routinely available using the Landsat Thematic Mapper (TM). The use of the TM data permits digital analysis on basins as small as 2.5 km^2, although the previously mentioned observational capabilities are preferred for this small a basin. Similarly, the Landsat Multispectral Scanner Subsystem (MSS) with a 57 m resolution can be used on basins as small as 10 km^2 using digital analysis (20 km^2 using photointerpretation). It has also been found that the MSS data are cost effective on basins larger than 25 km^2 (Rango et al., 1983). As a result, TM data for most snow cover related studies should be limited to a basin size range of 2.5-25 km^2 and only when visual ground or aircraft observations are not possible.

The best satellite for providing highly repetitive coverage of a basin is NOAA with imagery from the Advanced Very High Resolution Radiometer (AVHRR). In the visible channel (0.56-0.72 μm), the resolution is about 1.1 km near nadir. Although this resolution is much poorer than either of the Landsat sensors, NOAA provides coverage twice per 24 hour period (one daytime and one nighttime overpass). This is a big improvement over the Landsat coverage of once every 16 days. Because of the poorer resolution, however, the minimum basin or zonal size is about 200 km^2 with digital analysis (500 km^2 with photointerpretation). A more extensive discussion of the various snow mapping capabilities is given in Rango et al. (1985).

As development of a snow mapping capability has proceeded, the National Weather Service (NWS) has created a National Remote Sensing Hydrology Program (NRSHP) which produces operational digital maps of areal extent of snow cover. The NOAA-AVHRR sensor is used to produce these maps on approximately 4000 basins in North America in 1990. Additionally, the snow cover statistics are calculated by elevation zone for about 400 of these river basins in the western United States. The snow cover extent data from AVHRR are generated approximately once a week depending on cloud cover. The digital snow cover data are available electronically to end users in real time (Carroll, 1990).

SRM SIMULATION PERFORMANCE

Since its development, SRM has been tested on a variety of basins in the simulation mode, i.e., all necessary input data were known and the model operators were trying to duplicate, as closely as possible, the observed hydrograph. These tests were performed successfully on 24 basins and documented by Martinec and Rango (1986). These basins ranged in size from 0.77 to 4000 km^2 and in elevation from 171 to 6000 m a.s.l. Eleven countries were represented in the tests. The performance of SRM evaluated statistically was quite successful. The average R^2 value, measuring correspondence of daily flows, was 0.84, and the average difference in seasonal volumes, D_v, was 4.4%. Since 1986, the average performance criteria have remained about the same, and the total number of basins now exceeds 30 with several new countries represented. The upper end of the basin area and elevation ranges have been extended to 64,000 km^2 and 7690 m, respectively.

In evaluating performance, emphasis should be on the worst model performance in order to analyze problems, recommend solutions, and generally improve model simulations. As would be expected, SRM performance suffers when basins are extremely large, the data network is sparse, data quality is poor, and users are inexperienced. The size problem is not usually significant, except when it is coupled with inadequate data observations and quality. The data quality problems involve meteorological data observed both far from the basin and at very low elevations. The data must be extrapolated over great horizontal and vertical distances. As a result, the input of temperature and precipitation to SRM may not be very representative of the area of the basin where snowmelt occurs. The other problem is poor snow cover data which then intensifies the input data problem.

Anything that can be done to minimize these data problems will tend to improve SRM performance. The problem with inexperienced users can be solved with training or development of expert systems (Engman et al., 1989).

SRM CONVERSION TO FORECAST MODE

One of the basins we have used for testing of SRM and development of a forecasting method is the Rio Grande basin above Del Norte, Colorado (3419 km^2). This basin is valuable in that it has a hydrologic data base that is complete throughout the effective period of remote sensing satellite observations (1972-1989). During this period there are only a few yeas with inadequate Landsat snow cover observations, namely, 1980, 1981, and 1985. Additionally, the NWS/NRSHP selected the Rio Grande as one of its early target basins and has been producing elevation zone snow cover maps for the Rio Grande for several years. Figure 2 shows the three elevation zones of the Rio Grande used for snow mapping. In the ten Rio Grande simulation years (1973-1979; 1982-1984), the data base was complete. SRM used data from these years to provide successful simulations. In these years, the average R^2 was 0.86 and the average D_v was 1.7%. Both of these statistical measures are better than the average values for all basins on which SRM has been tested. Figure 3 shows the SRM simulation for 1984 on the Rio Grande basin.

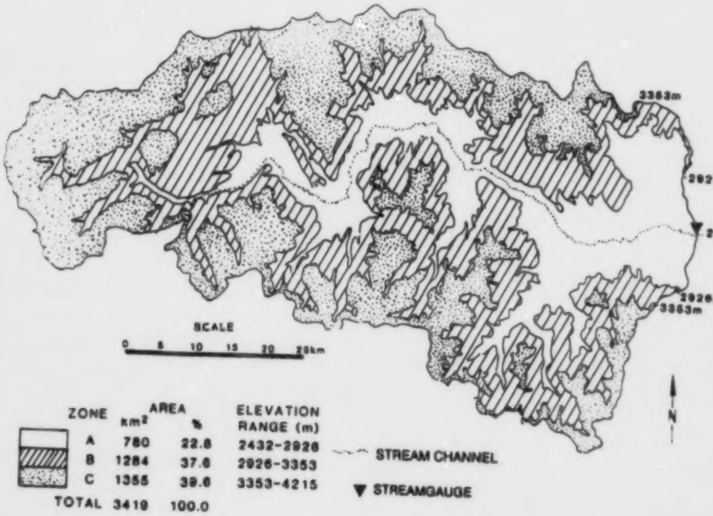
3353m
2926m
2432m
2926m
3353m
SCALE
0 5 10 15 20 25km
N
ZONE
AREA
km²
%
ELEVATION RANGE (m)
A 780 22.8 2432-2926
B 1284 37.6 2926-3353
C 1355 39.6 3353-4215
TOTAL 3419 100.0
STREAM CHANNEL
▼ STREAMGAUGE

Fig. 2. Elevation zones and areas of the Rio Grande basin near Del Norte, Colorado, U.S.A.

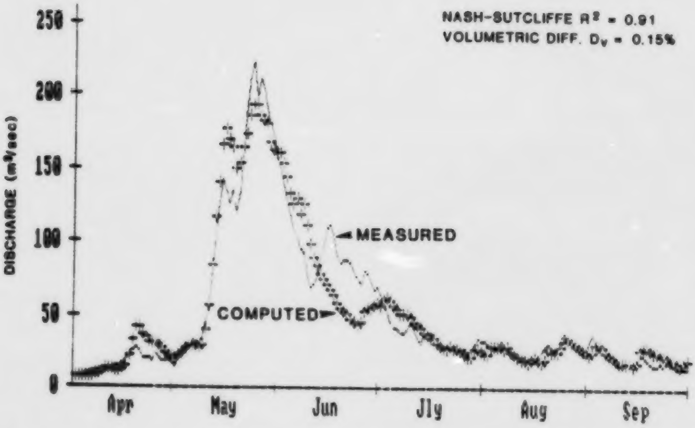

Fig. 3. Snowmelt runoff simulation for 1984 on the Rio Grande basin near Del Norte, Colorado using SRM.

The step from simulation, when all input and output data are known, to a true forecast situation, when no data past the forecast date are known, is not simple. If we were to forecast for the Rio Grande basin on April 1, we would not know the snow cover extent after April 1 and perhaps not even know it before April 1, depending on cloud cover conditions. This will be true for temperature and precipitation after April 1 as well. It was found that a series of small steps was necessary to develop a working methodology.

The first logical step was to attempt to make a forecast on April 1 with no snow cover information available. To be able to do this, we looked at each of the ten Rio Grande simulation years in reference to the zonal snow cover depletion, SRM calculated snowmelt, the observed April 1 snow water equivalent in the basin, and the SRM computed snow water equivalent. The use of modified depletion curves, which plot snow extent versus snowmelt rather than versus time (Martinec, 1985), permitted development of a family of modified snow cover depletion curves as shown in Figure 4. These modified zonal depletion curves can be labelled with the measured area under the curve to develop a family of curves for each elevation zone. In order to obtain the value to use to select a curve in a forecast situation, a regression equation for each zone is used to convert the measured snow water equivalent to an estimation of the actual snow water equivalent that would be computed by SRM. The weakness of the method involves the use of the measured snow water equivalent to estimate the SRM computed snow water equivalent value which is necessary to select the modified snow cover depletion curve in Figure 4. The better the snow water equivalent measurement network, the better the relationship, and the better the selection of a modified snow cover depletion curve for forecasting. Presently, the measured snow water equivalent is obtained from the snow course network, but it might be obtained from Snotel data or microwave remote sensing operations in the future.

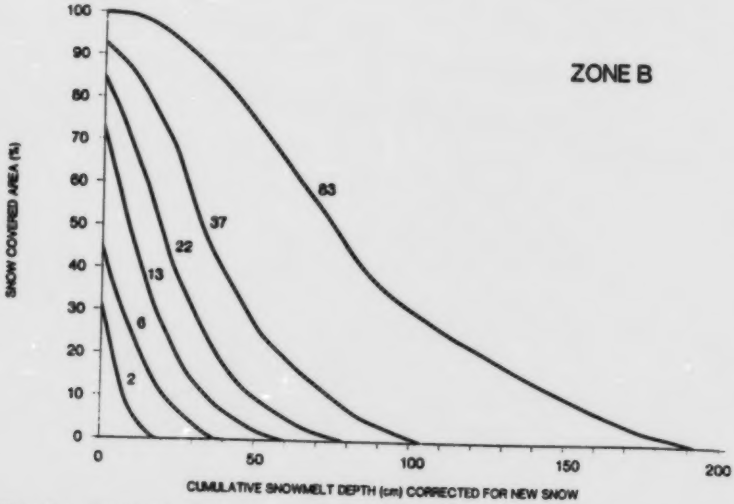

Fig. 4. Modified snow cover depletion curves for elevation zone B of the Rio Grande basin labelled with estimated snow water equivalent values (cm).

The years 1980, 1981, and 1985 were not included in the ten year simulation data base because there were not enough Landsat satellite snow cover observations to develop conventional snow cover depletion curves for input to SRM. With the existence of the family of modified snow cover depletion curves in Figure 4 and snow water equivalent observations for April 1 in 1980, 1981, and 1985, these three years could be treated as quasi-forecast situations. To simplify the forecast problem, actual temperature and precipitation data were used and the only forecast input was the snow cover.

The measured snow water equivalent data were used to get estimated SRM computed snow water equivalent values for April 1 for each year for each elevation zone. These values were used in families of curves like Figure 4 to pick a modified depletion curve for each year for each elevation zone. Figure 5 shows the modified depletion curves for elevation zone B selected for 1980, 1981, and 1985. The snow cover depletion curves thus obtained were used to extract the daily snow cover data needed by SRM. SRM was run for each quasi-forecast year and the results were similar to the results in the ten year simulation data base. Figure 6 shows the resulting quasi-forecast hydrograph for 1985.

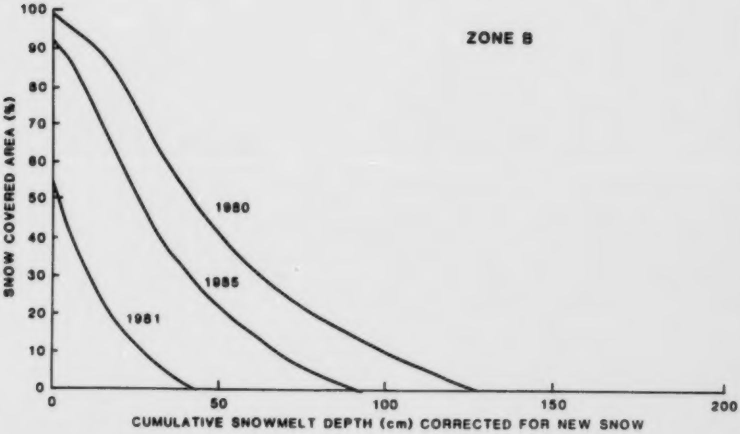

Fig. 5. Modified snow cover depletion curves for elevation zone B of the Rio Grande basin for 1980, 1981, and 1985 determined using estimated snow water equivalent values.

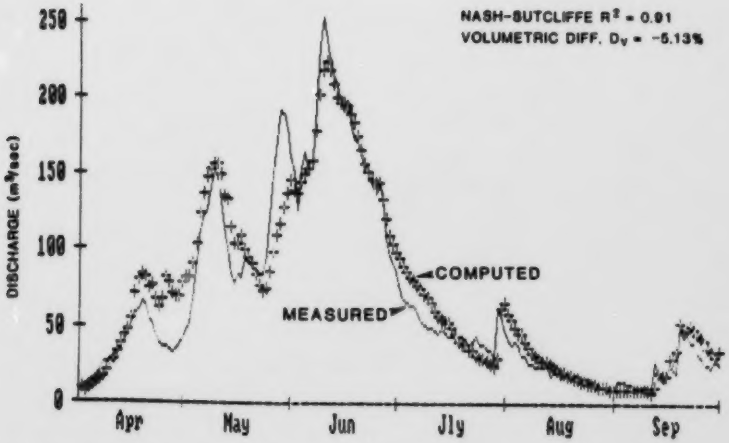

Fig. 6. Snowmelt runoff hydrograph for 1985 on the Rio Grande basin using forecast snow cover input data and SRM.

Because of the success of this controlled forecast situation with SRM, the U.S. Soil Conservation Service (SCS) urged us to carry the development further and combine forecast temperature and precipitation data with the forecast snow cover data. SCS determined in the early spring of 1987 that the Rio Grande basin had the potential for heavy runoff and possible flooding. SCS supplied their best estimate of 1987 forecast temperature and precipitation data, namely, long term average daily maximum and minimum temperatures and 110% of monthly precipitation randomly scattered through the specific month. The forecast snow cover on April 1 came from a modified depletion curve selected from Figure 4.

The resulting forecast and actual hydrographs for 1987 are shown in Figure 7. The results, as expected, are not as good as prior simulations or even the quasi forecasts, but still very useful. Because such forecasts would be done in real time with observed streamflow values available, it was decided to update the forecast hydrograph with observed streamflow every seven days, an option currently available in SRM. An improvement results as shown in Figure 8. Additional updating techniques making use of observed snow cover, temperature, and precipitation could also be used to improve the forecasting techniques. Development continues in order to perfect the forecasting methodology for SRM. More detailed discussion of the development to date can be found in Rango and van Katwijk (1990).

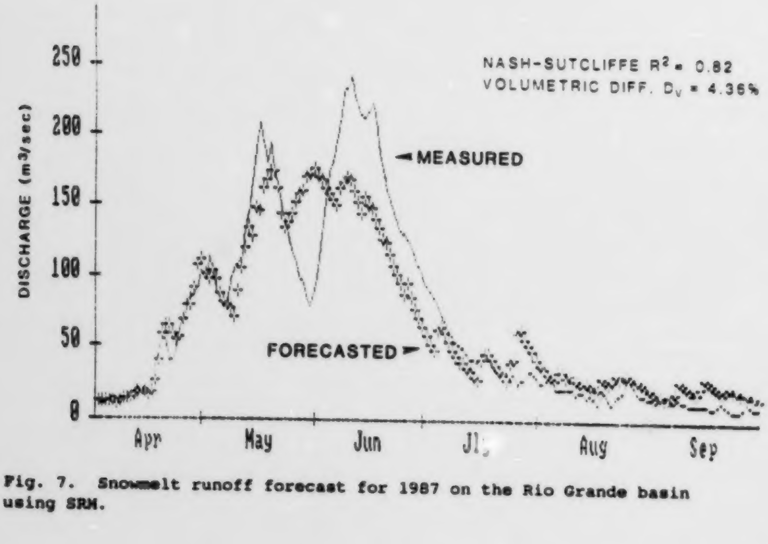

Fig. 7. Snowmelt runoff forecast for 1987 on the Rio Grande basin using SRM.

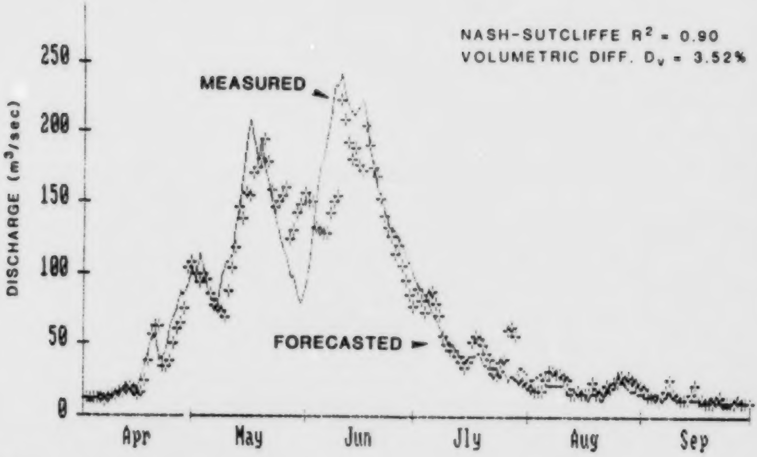

Fig. 8. Snowmelt runoff forecast for 1987 on the Rio Grande basin using SRM and actual streamflow updates every seven days.

SRM AVAILABILITY

SRM is currently distributed in a microcomputer version (Micro-SRM) to interested users. Micro-SRM (Version 2.01) was designed to operate on the IBM personal computer (PC) and all PC compatibles generating standard scan codes for keyboard function and special-use keys. The minimum system requirements for Micro-SRM include 640K of random access memory and one external (3 1/2" or 5 1/4") disk drive. Micro-SRM is compatible with most common video adapter modes (Mono, GGA, EGA, VGA, Hercules) and can display several program plot products on appropriately equipped systems. Compressed-print capability is recommended to support Version 2.01's 132-character printer output format. Printed copies of program plots can be generated on a variety of printers using a graphics driver imbedded in Micro-SRM. A configuration utility included with Micro-SRM allows the user to modify model defaults for screen display colors, compressed-print printer control codes, and video adapter modes. Micro-SRM, Version 2.01 is written in Microsoft's QuickBASIC 4.5 and includes several subroutines from Cresent Software's QuickPak Professional.

Micro-SRM is designed to be highly interactive and provides user interfaces through text, data, and menu screens. As a result, it is user friendly and it is very easy to apply. Sample diskettes, containing the executable code, supporting files, and example data files, have been provided to over 60 institutions worldwide. We have received valuable feedback from Micro-SRM users that has allowed us to debug and improve the software. A diskette of Micro-SRM, Version 2.01, can be obtained by contacting the author of this paper.

REFERENCES

Carroll, T. (1990) Operational remote sensing of snow cover in the U.S. and Canada. Proceedings of the 1990 National Conference on Hydraulic Engineering, American Society of Civil Engineers, San Diego.

Engman, E. T., Rango, A., and Martinec, J. (1989) EXSRM, an expert system for snowmelt runoff model (SRM). New Directions for Surface Water Modeling (Proceedings of the Baltimore Symposium), iahs Publication No. 181, 417-426.

Fortin, J-P., Villeneuve, J-P., Bocquillon, C., Leconte, R., and Harvey, K. D. (1990) HYDROTEL - A hydrological model designed to make use of remotely sensed and GIS data. Proceedings of the Workshop on Application of Remote Sensing in Hydrology, National Hydrology Research Institute, Saskatoon, Saskatchawan.

Kite, G. (1989) Hydrologic modeling with remotely sensed data. Proceedings of the 57th Annual Western Snow Conference, Fort Collins, Colorado, 1-8.

Leavesley, G. H. and Stannard, L. G. (1990) Application of remotely sensed data in a distributed-parameter watershed model. Proceedings of the Workshop on Application of Remote Sensing in Hydrology, National Hydrology Research Institute, Saskatoon, Saskatchewan.

Martinec, J. (1975) Snowmelt-runoff model for stream flow forecasts. Nordic Hydrology, 6(3), 145-154.

Martinec, J. (1985) Snowmelt runoff models for operational forecasts. Nordic Hydrology, 16, 129-136.

Martinec, J. and Rango, A. (1986) Parameter values for snowmelt runoff modelling. Journal of Hydrology, 84, 197-219.

Martinec, J., Rango, A., and Major, E. (1983) The snowmelt-runoff model (SRM) user's manual. NASA Reference Publication 1100, Washington, D.C., 118 pp.

Rango, A. (1985) The snowmelt-runoff model. Proceedings of the ARS Natural Resources Modeling Symposium, USDA-ARS-30, Pingree Park, CO, 321-325.

Rango, A. and Martinec, J. (1979) Application of a snowmelt-runoff model using Landsat data. Nordic Hydrology, 10, 225-238.

Rango, A. and van Katwijk, V. (1990) Development and testing of a snowmelt-runoff forecasting technique. Water Resources Bulletin, 26.

Rango, A., Feldman, A., George, T., and Ragan, R. (1983) Effective use of Landsat data in hydrologic models. Water Resources Bulletin, 19(2), 165-174.

Rango, A., Martinec, J., Foster, J., and Marks, D. (1985) Resolution in operational remote sensing of snow cover. Hydrological Applications of Remote Sensing and Remote Data Transmission (Proceedings of the Hamburg Symposium) IAHS Publication No. 145, 371-382.

World Meteorological Organization (1986) Intercomparison of models of snowmelt runoff. Operational Hydrology Report No. 23, Geneva, Switzerland.

Questions and Answers

John Stewart: With reference to the study of global climate change in which you shifted the parameters; how many parameters does the model have?

Al Rango: If you recall the slide that I showed with the variables on one side and the parameters on the other, there are about six or seven parameters that are needed to input to the model.

John Stewart: How much would these parameters be shifted for this behavior and how did you decide on how much shift?

Al Rango: We haven't finalized how much we would shift all the parameters yet. Some of them wouldn't be affected, such as the stable things like basin area. However, it turns out that if we run an analysis using historical temperature data and then look at an increase of two, three, four, five, six degrees we will see a time shift in a certain way. What happens is that the snowmelt season starts to move back into the calender, so that April 1st becomes March 15th, for example. So we are looking at these kind of analyses to see what kind of shifts in time we have to make, as well as any shifts in the magnitude of the parameter itself. We are trying to let the data that we already have guide us in that kind of a shift. It looks for this particular study, as I recall, we shifted the temperatures for three degrees by twenty days back into the calender. So April 1st was more like March 7th or 8th.

John Stewart: Okay, so the shifts in parameters were essentially guided by previous data.

Al Rango: Climatological data, is what we looked at (ie. a series of temperature data and so on).

Hamed Assaf: The curves that you developed for depth versus snow-covered area, are they from measurements or are from simulations?

Al Rango: The curves that we developed are from prior year simulations. For each year, we were able to come up with one of these modified depletion curves. And if you measure the area under the curve, that is exactly what the average water equivalent has to be in that elevation zone to have the model produce that runoff. So if we believe the model, and the statistics in these years are all very good, then we can say that is what has to be there. So these are computed water equivalent values on an areal basis and we have a relation between that and the measured snow water equivalent at snow courses. So that we can take the measured values, put them in a regression and come up with the areal value that we need to pick the proper curve for forecasting.

Hamed Assef Are these just for that basin or ...?

Al Rango: They are just for that basin and the procedure would have to be done for each basin.

Tony Wankiewicz: Yes, I was just wondering about the limitation of satellite data which is highlighted by your model, you say that the basins should be larger than 100 square kilometers, for example. What kind of limitation does tree cover play, or very rough terrain, or could you use your model for glacierized basins with this limitation of 100 square kilometer?

Al Rango: With reference to the glaciers; as long as they don't make up a vast percentage of the basin you really shouldn't have any problem applying this model. The tree cover is always a problem when you are interpreting any kind of remote sensing data. The lower the resolution of the data the more problem you have with vegetation. So, you always have to be aware of that, but, fortunately, the vegetation does not change very rapidly. Once you become experienced with a basin, the interpretation should go fairly well, unless it is an unbelievably dense tree cover with no openings whatsoever. Was there another part of the question?

Tony Wankiewicz: Well, does this this particular basin have a large amount of alpine area in it?

Al Rango: The vast majority of zone "C" (the upper zone) is alpine. The zones "A" and "B" are forest snow zones, but in the Rio Grande it's not a real dense forest so you can see the snow very easily. When you get into the northwest then you have to rely on clearcuts, and so on, to see this snow cover.

Alf Warkentin: I wasn't sure about your snow melt routines, would you suggest a three-day factor or...?

Al Rango: We are using a degree day approach with a degree day factor to melt the snowpack. This is very similar to most models used in snowmelt runoff except for a few. We will hear about one in a couple of papers; George Leavesley's model uses a different approach. Ours is just a normal degree-day approach to snowmelt runoff prediction.

CONTRIBUTION OF GOES DATA TO HYDROLOGIC REGIONALIZATION

R.M. Leith, Water Survey of Canada, Vancouver, B.C.

Introduction

This paper describes two applications of remote sensing data to hydrologic regionalization in southern British Columbia. In this context, hydrologic regionalization is a clustering exercise in which basins are classified according to geographic region. Within the classes or regions the hydrologic response can to some extent be predicted, however, there will be variation about the regional pattern. The objectives of regionalization are the identification of regions and the development of means by which estimates of hydrologic quantities may be made within regions.

The first application described in this paper concerns partitioning of a geographic area based upon clustering of a bivariate plot of basin runoff versus a basin property produced from the remote sensing data. The second application involves the estimation of precipitation and net radiation at the earth's surface and the input of these quantities to simple model to produce runoff.

These applications are part of the ongoing examination by the Water Survey of Canada, Pacific and Yukon Region, of the relationships between streamflow and other data.

The remote sensing data is Geostationary Operational Environmental Satellite (GOES) data from the Visible Infrared Spin Scan Radiometer (VESSR) subsystem. The data is in digital format which offers the benefits of objectivity and direct compatibility with computer analysis (Blanchard, 1975) as well as dynamic coverage in time and extensive spatial coverage. Previous hydrologic regionalization studies have used static quantities such as physiographic indices of elevations and shapes, or point measures such as precipitation and temperature (Leith, 1978). The use of a series of remote sensing images allows the development of dynamic predictions, but these predictions require the images to be precisely located with reference to the earth's surface (Blanchard, 1978), a procedure referred to as geographic registration or navigation. In this study a sequence of images over 48 months was used.

The study area covers 116° west to 127° west and 48° north to 51° north, ie. approximately 300 kilometres north-south and 700 km east-west. In this area of complex hydrologic response (west coast rain forests to desert) the Water Survey of Canada gauges many basins of which 65 were selected on the basis of availability and quality of data.

Data

The GOES data was purchased from the United States Department of Commerce, National Oceanic and Atmospheric Administration, Satellite Data Services Division in Off-line Data Ingest System (ODIS) format on magnetic tape. 96 images were ordered, one visible band and one infrared band at noon local time on the last day of each month from November 1978 to October 1982.

The resolution or nominal earth surface coverage was the smallest available in both visible band (0.9 km) and infrared band (8 km north-south by 4 km west-east).

The runoff for each of 65 basins over the 48 month period was taken from Water Survey of Canada data. Runoff in millimetres (mm) is the volume of water flowing from a basin divided by the drainage area of the basin. The basins chosen for this study produce essentially undisturbed flow.

Last-day-of-the-month radiation data came from Monthly Radiation Summary (Volume 19, No. 11 to Volume 23, No. 10). The quantity extracted was the total Global Solar Radiation, incoming solar radiation from the whole dome of the sky (Radiation Field 1).

Precipitation and temperature data from 85 stations in the study area as well as solar radiation, hours of sunshine, and cloud cover from four stations were extracted from Atmospheric Environment Service files.

Model

The model, based on Turc (1954), was chosen because of its simplicity and wide applicability. The model assumes that if mean values of the components of the water budget are calculated over a sufficiently long period, the variation in storage of both surface and groundwater is negligible in relation to other terms in the water balance. A further assumption is that the groundwater component of water budget is negligible compared to precipitation and evapotranspiration. With these assumptions, the following equations form the model's algorithm:

$$RO = P - AEV$$

$$AEV = \frac{P}{\mathrm{SQRT}\left(0.9 + \frac{P^2}{PE^2}\right)}$$

RO = runoff (mm)
P = precipitation (mm)
AEV = actual evapotranspiration (mm)
PE = potential evapotranspiration (mm)

The modification to Turc's model involves estimating the potential evapotranspiration from estimates of net radiation (NR) rather than temperature, as in the original model. The net radiation is assumed to be equal to the total incident solar radiation minus the reflected short-wave and emitted long-wave radiation. The potential evaporation is the depth of water which would be evaporated by the net radiation.

$$PE = 0.34\ NR$$

PE is potential evapotranspiration in millimetres.
NR is net radiation in megajoules/square metres.

Precipitation and solar radiation have been inferred from satellite data in earlier studies. Estimating precipitation from satellite data has been examined by: Scofield and Oliver (1977), Whitney and Herman (1981), Ingraham (1980), and Barrett (1981), to name a few. Although all methods used in the above-mentioned studies are similar in concept, they vary greatly in approach, purpose and degree of objectivity. Several researchers, such as Vonder Haar and Ellis (1978), Gautier et al (1980), Solomon et al (1981), Dedieu et al (1983), have studied the use of Geostationary Satellite data for inferring the solar irradiance at the surface of the earth. However, combining these estimates to obtain estimates of evapotranspiration and runoff was not attempted.

Procedure

The first step required for the GOES data extraction was navigation to establish for each image the location of picture elements (pixels) corresponding to river basins and to areas surrounding meteorologic stations.

Analog images were produced by assigning a series of print characters to a digital value; these print characters were overprinted to produce a range of grey levels with the low digital values showing dark. The analog images have pixel coordinates along the edges so that coordinates of identifiable points (landmarks) could be established. These landmarks are usually contact points between land and water.

A computer program produced the relationship between pixel coordinates and latitude and longitude. The program used the satellite attitude and orbit parameters to establish the image plane and the landmarks to refine the transformation between coordinates.

Each river basin was outlined on topographic maps and the latitude and longitude of selected points on the boundary were entered into a file. For one particularly clear image, from which many landmarks could be identified, the latitudes and longitudes of these boundary points were converted to pixel coordinates. The points on each basin boundary were joined by straight lines to form a polygon approximation of the boundary. The boundary and interior pixels were then coded to form a silhouette or a template for data extraction. The sizes and shapes of the templates were checked on several other clear day images. Once established, the templates could be located on a navigated image and digital values associated with basins be extracted.

For meteorological stations the extraction of digital data was carried out in a procedure similar to that for drainage basins. Each station was taken to be located at the center of a twenty-one by twenty-one visible band pixel area, five pixels by three pixels in the infrared band. These expanded windows were taken to allow for integration of the dynamic effects of the atmosphere, (Solomon et al, 1981); the extraction of the digital data then proceeded as for the drainage basins.

To develop a relation between ground based observations of precipitation and the GOES digital data, the values of total precipitation over 48 months recorded at the 85 precipitation stations in the study area were plotted against mean digital counts values from both visible and infrared bands.

The relationship between incoming solar radiation and GOES digital count data had to be developed using the four solar radiation stations in the study area: Mount Kohau, Nanaimo Departure Bay, Summerland CDA, and Vancouver UBC. The Mount Kohau station was discontinued during the study period.

For each visible band image, a regression equation was developed between global solar radiation field (RFI) and the mean GOES digital counts in a window around the station. Figure 1 shows an example for the 29 February 1980. For the few days for which no statistically significant regression equation could be developed, the mean value of the solar radiation recorded at the observation stations was applied throughout the study area. The radiation for each sample day was summed and multiplied by 1461/46 as 46 of the possible 1461 days had been sampled.

A check on the estimated radiation was made by comparing the total recorded solar radiation at Nanaimo Departure Bay over 48 months (17253 MJ/m^2) with the estimated total (16551 MJ/m^2).

The short wave reflected radiation was estimated through an albedo or reflection coefficient. An albedo was estimated for each basin by searching the 46 basin mean GOES digital counts in the visible band for a minimum. This minimum was assumed to be proportional to the minimum albedo for the basin and was considered to represent the reflectance as recorded under clear sky condition, ie. not affected by clouds or haze.

To convert the minimum digital counts value to an albedo, a relationship between albedo and GOES digital counts was developed using accepted values of the albedo for various scenes, (Kondratyev et al. 1981) such as water, forest and snow. From these values, the following relationship was derived:

Albedo = -0.27 + 0.0053 Digital Counts Value

The long wave radiation from each basin was estimated from the Stefan-Boltzmann equation. According to Kondratyev et al (1981) emissivities for snow, water, vegetated surfaces or bare soil are close to one. The temperature of each basin was estimated from a regression equation using elevation, latitude and longitude (Shawinigan, 1970).

The long wave radiation was assumed to take place only when the sky is clear, ie. digital counts value less than 110. This is a simplifying assumption, since losses do take place even when cloud cover exists, but a complete radiation model was beyond the scope of this study.

Results

Figure 2 shows the plot of mean basin runoff against mean basin reflectance (digital counts in the visible band). The plotted numbers indicate the numbers of observations falling in a plotting cell; the dots indicate the regression equation fitted to the complete data set. When the plotted points are associated with geographic location of the basins, the upper cluster with high runoff and little relationship with reflectance is composed of basins on the West Coast of Vancouver Island and exposed basins in the coastal mainland; the lower cluster parallel to the mean basin reflectance axis is composed of dry interior basins; the middle cluster which shows a pronounced relationship are wet interior basins in the coastal mountains and the West Kootenay area. The regions are shown in Figure 3.

For the precipitation stations in the study area, plots of mean digital counts values showed no correlation or regional association for the infrared data, however the visible band data do show a regional pattern, Figure 4. The threshold, 110, was taken so that only cloudy occurrences contributed to the mean value.

Using the regional regression equation to estimate precipitation and the estimate of the net radiation, estimates of runoff were made for all basins in the study area. Table 1 shows the distribution of relative errors for three sets of the estimates: all 65 basins, all basins with drainage areas greater than 100 km², and all basins except those in the dry interior. The largest errors are usually incurred for smaller basins and basins in the Dry Interior Region, although some basins in these categories were closely estimated by the model. The large errors are associated with small estimates of evaporation probably due to high estimates of long wave radiation.

Table 1 Distribution of Relative Errors in Estimation of Basin Runoff

Range of Errors	All Basins	Basins > 100 km²	Basins other than Dry Interior
> - 100%	6	3	0
-100% - 75%	3	2	0
- 75% - 50%	9	2	4
- 50% - 25%	5	4	2
- 25% 0%	12	7	8
0% 25%	11	8	10
25% 50%	11	7	9
50% 75%	8	6	7
75% 100%	0	0	0

Conclusions

The digital data from GOES provides a means of subdividing Southern British Columbia into hydrologic regions as indicated by the clustering on the plot of runoff versus mean digital counts.

Estimates of runoff can be produced by a simple model using inputs of precipitation and evaporation estimated from GOES data. The model appears to produce better results for basins in higher runoff regions and for basins larger than 100 km². When applied to these larger basins with higher runoff volumes, the model appears to have a bias towards underproducing probably due to underestimating precipitation.

REFERENCES

Barrett, E.C., "Satellite Rainfall Estimation by Cloud Indexing Methods for Desert Locust Survey and Control", Satellite Hydrology, Fifth Annual William T. Pecora Memorial Symposium, American Water Resources Assoc., Sioux Falls, S.D., June, 1981.

Blanchard, B.J., "Remote Sensing Techniques for Prediction of Watershed Runoff", Paper W-15, NASA Earth Resources Survey Symposium, June, 1975.

Dedieu, G., P.Y. Deschamps, and Y.H. Kerr, "Solar Irradiance at the Surface from METEOSAT Visible Data", Eighth Canadian Symposium on Remote Sensing, Montreal, P.Q., May 3-6, 1983.

Gautier, C., G. Diak, And S. Mass, "A Simple Physical Model to Estimate Incident Solar Radiation at the Surface from GOES Satellite Data", Journal Applied Meteorology, Vol. 19, 1980.

Griffith, C.G., W.L. Woodley, S. Browner, J. Teieiro, H. Maier, D.W. Martin, J. Stout and D.N. Sikdar, "Rainfall Estimation from Geosynchronous Satellite Imagery During Daylight Hours", NOAA Technical Report, ERL-356-WMPO-7, 1976.

Ingraham, D.V., "Rainfall Estimation from Satellite Images", PH.D. dissertation, University of British Columbia, Vancouver, British Columbia, 1980.

Kondratyev, K.Y., V.I. Korzov, V.V. Mukhenberg, and L.N. Dyachenko, "Shortwave Albedo and Surface Emissivity", Paper presented at World Climate Research Program Study conference, WMO/ICSO, Joint Scientific Committee, Greenbelt, Maryland, January 5-10, 1981.

Leith, R.M., "Streamflow Regionalization in British Columbia, No. 4, Regression of Low Flows on Physiographic Parameters", Report Series No. 57, Inland Waters Directorate, Pacific Region, Water Resources Branch, 1978.

Scofield, R.A., and V.J. Oliver, "A Scheme for Estimating Convective Rainfall from Satellite Imagery", NOAA Technical Memo. NESS 86, April, 1977.

Scofield, R.A., "Using Satellite Imagery to Detect and Estimate Rainfall from Flash-Flood Producing Thunderstorms", Proceedings of AMS Conference on Weather Forecasting and Analysis and Aviation Meteorology, October, 1978.

Shawinigan Engineering Company Ltd., "Hydrometric Network Planning Study for Western and Northern Canada", Report 5019-1-70, February, 1971.

Solomon, S.I., D.C. McKay, A. Beaulac, and B.J. Swain, "Solar Radiation Estimation Using GOES Satellite Data", 7th Canadian Symposium on Remote Sensing, Winnipeg, Man., Sept. 8-11, 1981.

Turc, L., "Le Bilan d'Eau des Sols. Relation entre les Précipitations, l'évaporation et l'écoulement", Ann. Agron. Vol. 5, 1954.

Vonder Haar, T.H., and J.S. Ellis. "Determination of Solar Energy Microclimate of United Sates Using Satellite Data", Proceedings of the Canadian Solar Radiation Data Workshop, sponsored by Atmospheric Environment Service and National Research Council, April 19, 1978.

Whitney, A.G., and L.K. Herman, "A Statistical Approach to Rainfall Estimation Using Satellite Data", Satellite Hydrology, Fifth Annual William T. Pecora Memorial Symposium, American Water Resources Assoc., Sioux Falls, S.D., June, 1981.

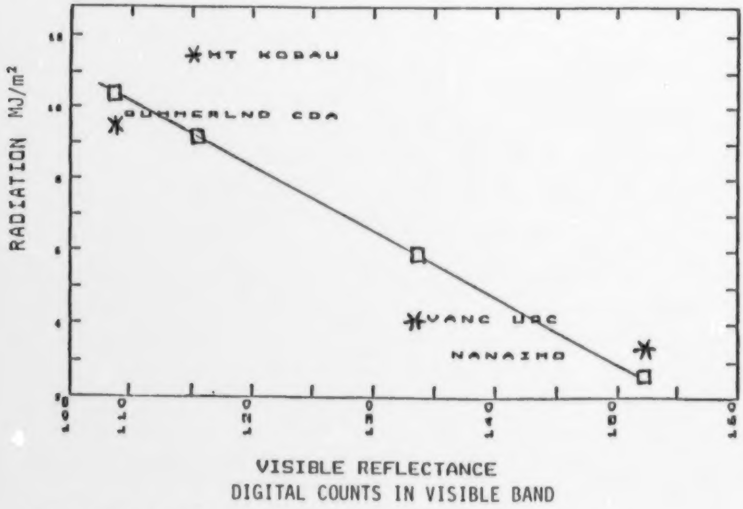

```
29 FEBRUARY 1980
STATION                  REFLECTANCE RADIATION✱  BEST-FIT □

MT KOBAU                   115.07      11.17     8.99048
NANAIMO DB                 151.84      3.12      2.42131
SUMMERLND CDA              108.28      9.15      10.2036
VANC UBC                   133.07      3.95      5.77468

Correlation coefficient is -.899875

Intercept A is  29.5484  Standard error on A is  8.30199

Slope B is     -.178656  Standard error on B is .648593E-01
```

Figure 1. Relationship of Solar Radiation and Visible Reflectance (GOES Digital Data in Visible Band) for 29 February 1980.

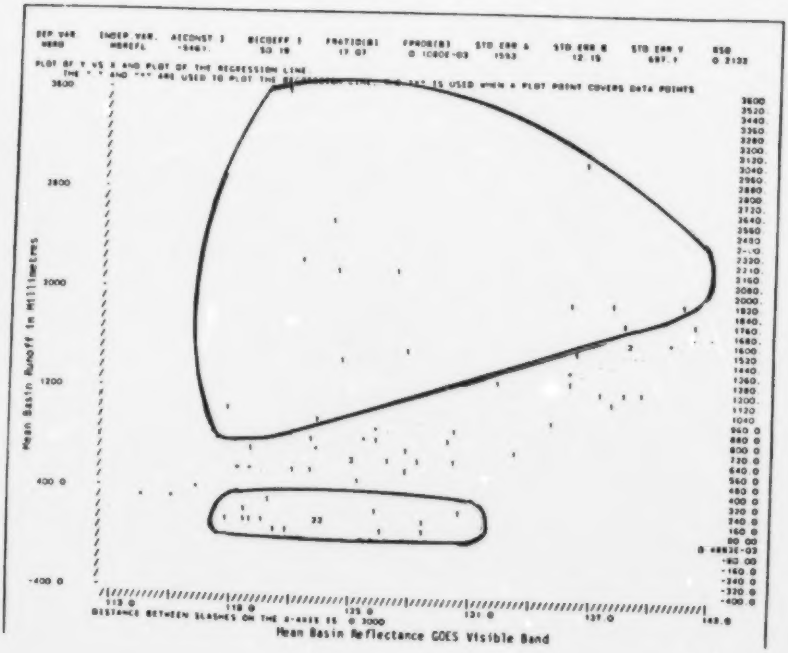

Figure 2. Mean Basin Runoff versus Mean Basin Digital Count i Visible Band.

Dry Interior basins fall on the lower horizontal band.

Wet Interior basins fall near the regression line.

Very Wet West Coast of Vancouver Island and Mainland basins fall above the regression line.

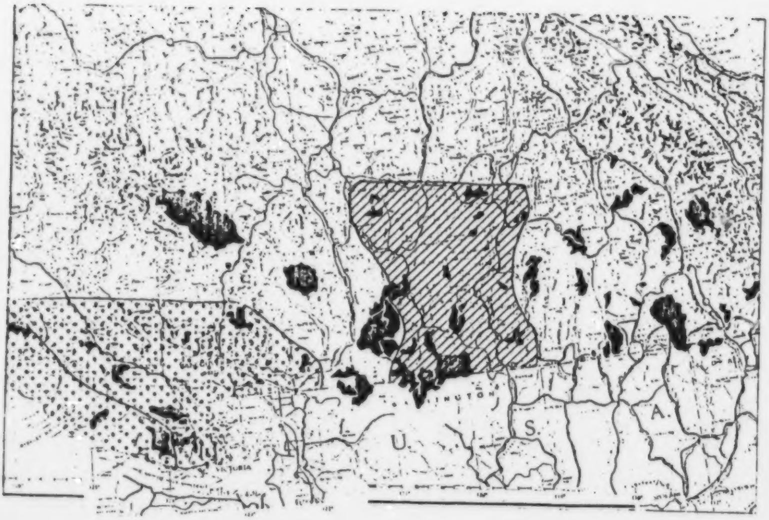

Figure 3. Delineation of Hydrologic Regions (refer to Figure 2.).

Basins are indicated in black.

▨ Dry Interior Region

░ Vancouver Island and
Lower Mainland

☐ Wet Interior Region
- remaining study region

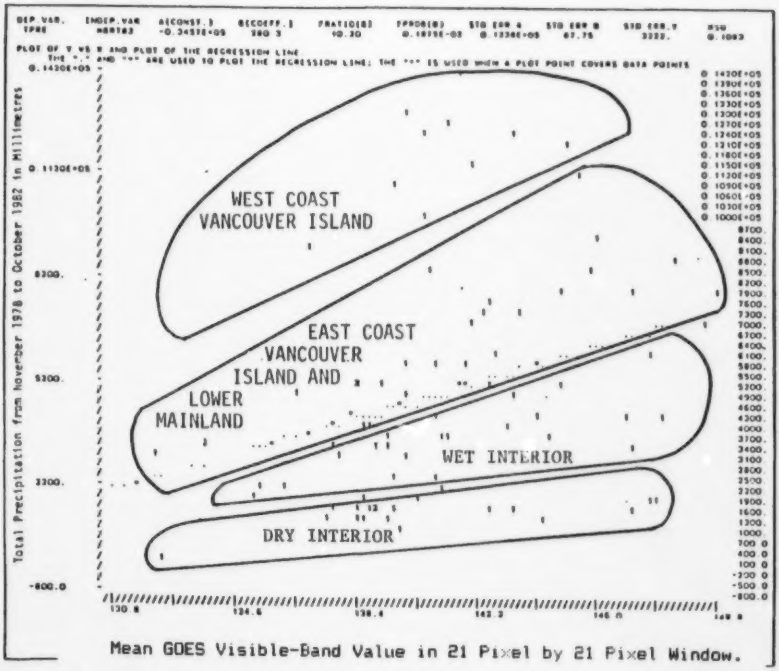

Figure 4. Total Precipitation versus GOES Visible Data.

Questions and Answers

John Stewart: I didn't quite follow the method in the sense that you were using one GOES image each month?

Rory Leith: That's right.

John Stewart: So you weren't choosing to have cloud-free images?

Rory Leith: No, definitely not, it was the last day of each month. If that were cloudy, so be it; if it were clear, so be it.

John Stewart: I don't really understand what you are measuring because the amount of cloud over a particular area won't actually be representative of average cloud over that mountain, or is that sort of implicit in the assumption?

Rory Leith: Well, I suppose it's implicit in the assumption; I go back to that sampling example I gave you for Summerland.

John Stewart: Yes, but then what do you think this represents actually? I mean you had this runoff versus GOES-VIS data and you were showing that they actually separated geographically, into sort of climatic zones, let us say.

Rory Leith: Okay; yes the feature space could be partitioned and, yes, essentially for each particular zone if it is cloudier, it is wetter.

John Stewart: Oh, then is each of those points an average of forty-eight values?

Rory Leith: Yes.

John Stewart: That is what I missed.

Al Rango: Rory, just to follow up on that point; GOES observations come streaming in at one every half hour or so. You used the last day. Did you average all of the available GOES observations over a 24 hour period or ...?

Rory Leith: No, I said "noon local time" so it is one image per day.

John Stewart: Just another cautionary note. I have just come from a conference where Catherine Gautier and her colleagues were estimating input of solar radiation to the ground and they showned that they can do it extremely well. But, only after they had recalibrated the GOES data, and what I found extremely worrying was that the conversion of digital numbers to calibrated radiance actually varied very strongly, seasonally. I think that they said it varied something like thirty percent. There was a seasonal variation in the calibration factors to go from digital numers to measured radiance.

Rory Leith: Yes, I think I agree with you. Tom Vanderhaar has found pretty much the same thing.

John Stewart: So that may introduce a systematic error. But again presumably these are averages of the forty-eight?

Rory Leith: This is sample by sample. So this is one particular sample, let's see which one is this...yes...it is labeled "the 29th Feb. 1980". So that is for that one particular image.

John Stewart: So that variation in calibration factor could affect the results?

Rory Leith: Oh yes, the calibration to calibration is different. This is just one particular example. You get a lot of different responses. Yes, very definitely. The only thing I fall back on is the "Law of Large Numbers", and the principle of insufficient reason.

Al Rango: Could you put your results graph up again and say a few words about it?

Rory Leith: Okay; for twenty-three of the basins the estimated runoff volume over that forty-eight month period was within plus or minus twenty-five percent of the observed volume

Al Rango: And those twenty-three basins were better than the other thirty-nine. Were those twenty-three in a certain geographic area?

Rory Leith: The model operated fairly well throughout the entire study area; that is the entire southern part of British Columbia. Except that it did not do so well with small basins and did not do so well with the dry interior basins at Thompson Plateau. But even within the Thompson Plateau, there were a couple of basins that were estimated to within two percent. So, the geographical factor was a mild one.

Application of Remotely Sensed Data in a Distributed-Parameter Watershed Model

by G.H. Leavesley and L.G. Stannard

ABSTRACT

The U.S. Geological Survey's Precipitation-Runoff Modeling System (PRMS) is a modular, distributed-parameter, watershed-modeling system developed for use in evaluating the effects of various combinations of climate and land use on hydrologic-system response. Major problems in applying PRMS include: (1) Determination of the optimal subdivision and characterization of a watershed to account for the effects of physical characteristics on hydrologic response; (2) estimation of parameter values for each subwatershed area delineated; (3) extrapolation of point data to areal-value estimates in complex, high-relief terrain; and (4) verification of the simulated hydrologic response of each subwatershed area. Remotely sensed data can provide spatial and temporal information needed to address these problems.

Remotely sensed measures of watershed characteristics, such as vegetation and land use, can be combined with digital-terrain-analysis results to aid in watershed-subdivision procedures and the estimation of selected model parameters for defined subwatershed areas. Remotely sensed snow-covered-area data provide a measure to verify subwatershed simulation results for selected snow-accumulation and snowmelt processes. Comparing simulated and measured streamflow jointly with simulated and measured snow-covered areas in the East Fork Carson River basin, California-Nevada, provided insight to snow-related processes and sources of model error not available from the individual analyses. The development of new techniques that combine snow-covered-area data with point measures of snowpack water equivalent will provide quantitative estimates of snowpack water equivalent in space and time for use in updating simulated variables and developing improved process algorithms.

INTRODUCTION

The U.S. Geological Survey's Precipitation-Runoff Modeling System (PRMS) (Leavesley and others, 1983) is a modular, distributed-parameter, watershed-modeling system developed for use in evaluating the effects of various combinations of climate and land use on watershed response. Watershed response to normal and extreme rainfall and snowmelt can be simulated to evaluate changes in water-balance relations, flow regimes, flood peaks and volumes, soil-water relations, sediment yields, and ground-water recharge.

As with all distributed-parameter hydrologic models, a variety of problems related to defining and simulating the spatial and temporal variation of hydrologic processes are encountered in the application of PRMS. These problems include: (1) Determination of the optimal subdivision and characterization of a watershed to account for the effects of physical characteristics on hydrologic response; (2) estimation of parameter values for each subwatershed area delineated; (3) extrapolation of point data to areal-value estimates in complex, high-relief terrain; and (4) verification of simulated hydrologic response of each subwatershed area. A major source of the spatial and temporal information needed to address these problems is remotely sensed data.

Research is currently (1990) being conducted to couple remotely sensed data with digital-terrain analysis and geographic-information-system (GIS) procedures for use in the application of PRMS. Initial work is being limited to watershed characterization and parameterization, and to the evaluation and verification of the snow-accumulation and snowmelt components. This paper describes these ongoing research efforts and preliminary results. It is intended to provide the workshop with points of discussion on current methodologies and future research needs in the application of remote sensing to distributed-parameter hydrologic modeling.

PRECIPITATION-RUNOFF MODELING SYSTEM

PRMS is the model component of a larger U.S. Geological Survey watershed-modeling and data-management system (Leavesley and others, 1987). The other components of this system are an interactive data-management and control program ANNIE (not an acronym) (Lumb and others, 1989) and a modified version of the National Weather Service's Extended Streamflow Prediction (ESP) program (Day, 1985). The ESP component produces a probabilistic prediction of streamflow variables, such as maximum flow, flow volume, and the date flow decreases to less than a selected value. Together, these components form a complete system that enables a user to: (1) Reduce, analyze, and prepare data for model application; (2) simulate and predict watershed response; and (3) statistically and graphically analyze model results.

The distributed-parameter capabilities of PRMS are enabled by partitioning a watershed into subwatershed areas using characteristics, such as slope, aspect, soil type, vegetation type, elevation, and precipitation distribution. Each area is assumed to be homogeneous in its hydrologic response and is termed a hydrologic response unit (HRU). A water balance and an energy balance are computed daily for each HRU. The sum of the responses of all HRU's, weighted on a unit-area basis, produces the daily watershed response.

The conceptualized hydrologic system used in PRMS is schematically depicted in figure 1. Model inputs are daily precipitation, maximum and minimum daily air temperature, and daily solar radiation. Precipitation in the form of rain, snow, or both is reduced by interception and becomes net precipitation delivered to the watershed surface. If daily solar-radiation data are unavailable, estimates of daily solar radiation are made using air temperature, precipitation, and computed potential-solar-radiation data. The energy inputs of air temperature and solar radiation drive the processes of evaporation, transpiration, sublimation, and snowmelt.

A watershed is conceptualized as a series of reservoirs whose outputs combine to produce the total watershed response. A soil-zone reservoir is defined for each HRU and represents that part of the soil mantle that can lose water through the processes of evaporation and transpiration. Average rooting depth of the predominant vegetation covering the HRU defines the depth of this zone. Water storage in the soil zone is increased by infiltration of rainfall and snowmelt, and decreased by evapotranspiration. The soil zone is treated as a two-layered system. Losses from the upper zone, termed the recharge zone, occur from evaporation and transpiration; losses from the lower zone occur only through transpiration.

When the soil-zone reservoir reaches field capacity, infiltrated water in excess of field capacity moves to the subsurface and ground-water reservoirs. The subsurface reservoir simulates the faster component of flow that might occur in the unsaturated zone during periods of rainfall and snowmelt. The ground-water reservoir simulates the slower component of flow from the saturated zone. The subsurface reservoir can be defined as being linear or nonlinear, whereas the ground-water reservoir is assumed to be linear. Subsurface and ground-water reservoirs can be defined for each HRU, or can be defined as larger areas receiving outflows from several HRU's.

The snow components of PRMS simulate the accumulation and depletion of a snowpack on each HRU. A snowpack is maintained and modified as a water reservoir and as a dynamic heat reservoir. A water balance is computed daily and an energy balance is computed twice each day. The energy-balance computations consider net shortwave and longwave radiation, approximations of convection and condensation terms, and the heat content of precipitation.

PRMS is a physical-process-based modeling system. To reproduce the hydrologic system as closely as possible, each component of the hydrologic cycle is expressed in the form of known physical laws or empirical relations that have some physical interpretation based on measurable watershed characteristics. These characteristics need to be measured or estimated for each HRU. Ground-based measurements of many of the watershed characteristics needed for model application are normally limited in availability and spatial coverage. Remotely sensed data provide the spatial measures needed for some HRU characteristics and the means to estimate or infer other HRU characteristics.

In addition, there is the potential to evaluate selected HRU responses using remotely sensed data collected periodically from the same watershed. For most model applications, the only measure of watershed response available for evaluating simulation results is a single-point measure of streamflow. This measure integrates the response of all upstream HRU's and leaves unanswered the question of whether individual HRU simulations are correct. Current data bases of remotely sensed data contain sufficient information on the spatial and temporal variation of snow-covered area to provide a tool with which to evaluate simulated snow accumulation and snowmelt. Additional sensors with improved resolution and frequency of measurement, however, will be needed to assess the full range of hydrologic processes simulated for each HRU.

BASIN CHARACTERIZATION AND PARAMETER ESTIMATION

The delineation of watershed HRU's and the measurement or estimation of physical characteristics and parameters of watershed HRU's is a data-intensive, iterative procedure that requires joint consideration of multiple data types at a variety of spatial and temporal scales. Historically, this procedure has been a labor-intensive, manual operation that involved a great deal of subjectivity. Resulting watershed characterizations reflected the interpretations and biases of the model user. The likelihood that any two model users would produce similar characterizations of the same watershed was small and became even smaller as watershed size and complexity increased.

A set of procedures has been developed for use with PRMS to provide a more objective watershed-characterization process with a reasonable degree of repeatability. The first procedure characterizes the topography using a set of computer programs (Jenson and Domingue, 1988) that use digital-elevation data in a gridded format. These programs are used to determine watershed boundaries, stream-drainage location and network configuration, and subwatershed boundaries based on a user-defined minimum subwatershed area. Resulting subwatershed areas are divided by their major drainage channel into two opposing hillslopes. Average slope and elevation, and the predominant aspect, defined by one of the eight cardinal points of a compass, are computed for each hillslope.

The output from the topographic-characterization programs also is digital data in a gridded format. The data can be further analyzed and displayed using a general purpose raster processing system or easily converted to vector format for polygon or line display and processing. ARC/INFO (Environmental Systems Research Institute, Inc., 1989), a vector-based geographic information system, currently is used to process, analyze, and display these data. Topographic contours with a 100-m interval generated from the gridded elevation data for the Lower Willow Creek watershed, a 186-km^2 watershed in western Montana, are shown in figure 2.

An ARC/INFO data layer, or coverage, is created from the topographic characterization and the computed values of slope, aspect, and elevation are added to the coverage as attributes for each hillslope. The discrete values for these attributes are categorized into ranges to simplify the watershed-characterization process. Other available spatial data can be converted to ARC/INFO coverages, georegistered to the topographic characterization, and used as overlays to assist in HRU delineation. Data overlays can be generated from available digital data bases or from remotely sensed data. Land-use and vegetation characteristics are items that can be determined for each HRU from image and digital satellite data. The polar-orbiting Landsat satellites and sun-synchronous Spot satellite are two such data sources.

An example of the overlay procedure is shown in figure 3. Hillslope boundaries computed for the Lower Willow Creek watershed are overlain by categorized coverages for vegetation, slope, aspect, and elevation. Hillslopes defined in the topographic characterization are further subdivided or aggregated to form HRU's, based on the additional information provided in the data overlays.

Data overlays not only assist in HRU delineation, but also contain information needed to estimate selected parameters for each HRU. Vegetation type and density are used to define HRU parameters for computing interception volume, evapotranspiration rate, and snowmelt rate. In regions, such as agricultural areas, where land use may change seasonally, knowledge of the dynamics of HRU vegetation characteristics can be used to temporally and spatially vary HRU characteristics and parameters.

Overlays developed from remotely sensed data also can be coupled with ground-based data to estimate selected HRU parameters. Available water holding capacity (SMAX) of the soil-zone reservoir is one example. SMAX is defined as a function of soil physical properties and the average rooting depth of the dominant vegetation on the HRU. Ground-based measures of soil physical properties can be coupled with measures of vegetation type defined from remotely sensed data and knowledge of the rooting characteristics of these vegetation types to estimate SMAX for each HRU. Where little or no soil data are available, the occurrence and type of vegetation can be combined with topographic data, such as slope and aspect, to infer soil physical properties and estimate SMAX.

HRU parameter estimation using the overlay procedure is currently done manually. Work, however, has been started on an automated procedure to estimate parameters from the data overlays. A software system called MODELBUILDER (G. Fisher, U.S. Geological Survey, written commun., 1989) that has been developed to extract watershed-model parameters from ARC/INFO coverages is being modified for use with PRMS. Currently, the software uses INFO programs to compute predefined parameters and variables from spatial data. Further enhancements to the software will include output in a format that PRMS can use directly. Expert-system technology also is being explored for incorporation in the parameter-estimation procedure.

Future research work will include the evaluation of additional remotely sensed measures of watershed characteristics to improve HRU delineation and parameterization. These measures will be combined with an evaluation of alternative methodologies for automated aggregation of watershed characteristics that more fully use the computational power available. The effects of these different aggregation procedures on model output also will be investigated.

SNOW-COVERED AREA

In the computation of daily water and twice daily energy balances for each HRU, a number of state variables are available for each HRU to permit assessment of the spatial and temporal variation of simulated hydrologic storages and fluxes in a watershed. Remotely sensed data collected repeatedly over the same area provide the opportunity to evaluate some of these storages and fluxes. Snow-covered area is the HRU state variable for which remotely sensed data currently are the most readily available. Coupled with an analysis of simulated and measured streamflow, the snow-covered-area comparisons provide integrated measures for evaluating simulated HRU snow accumulation and snowmelt.

Simulated HRU snow-covered area is a measure of the interactions of a number of complex snow-accumulation and snowmelt processes. Point measures of snowfall are extrapolated to each HRU by multiplying the point values by an adjustment factor that is user defined for each HRU. The adjustment factor is assumed to incorporate the effects of elevation, orography, and gage-catch efficiency on snow distribution. Adjustment factors can vary seasonally, but the seasonal values are assumed to be constant from year to year. Snowmelt is computed using an energy-budget approach, and is a function of measured air temperature and solar radiation adjusted for HRU slope, aspect, vegetation, and elevation. The percentage of an HRU covered by snow is computed using the areal-depletion-curve approach described by Anderson (1973). Simulated snow-covered area for a watershed is computed as the sum of the snow-covered area on each HRU.

Measured snow-covered-area data were obtained from the National Weather Service's National Remote Sensing Hydrology Center (Carroll and Allen, 1988). Through 1988, snow cover was mapped using the Geostationary Operational Environmental Satellite (GOES) visible data. In 1989, the program switched to using Advanced Very High Resolution Radiometry (AVHRR) visible and infrared data from the National Oceanic and Atmospheric Administration (NOAA) polar-orbiting satellites. Snow-cover data were reported for most of the major snow regions of the western United States for 1985-88, and coverage was expanded to include the Great Lakes and New England regions of the United States in 1989. For watersheds in the western United States, snow cover is normally reported as the percentage of an area covered in each of 2 to 5 predefined elevation bands. Although elevation-band snow-cover data are useful for some modeling approaches, they have limited value for PRMS.

The computation of HRU snow-covered area requires the use of the original raster-based pixel coverage from which the elevation-band snow-cover data were computed. Measured HRU and total watershed snow-covered area are determined by registering the raster-based pixel maps over a watershed characterization using the ARC/INFO system. Pixel resolution for these coverages is 1 km; thus, they are most appropriate for application to larger watersheds. The raster-based coverages are archived by region and are available on request from the National Remote Sensing Hydrology Center (Carroll and Allen, 1988).

The East Fork Carson River watershed, a 950-km^2 watershed in east-central California and west-central Nevada, was selected for this snow-covered area comparison. Raster-based maps of snow cover were available for multiple dates during the 1986 and 1988 snowmelt seasons. In 1986, the snowpack was greater than average, whereas in 1988, the snowpack was much less than average. The watershed was characterized into 23 HRU's and the PRMS was calibrated using data for water years 1981-83. Measured and simulated streamflow in the East Fork Carson River for water years 1986 and 1988 are shown in figures 4A and 4B. The difference in measured snowpack water equivalent for the 2 years is evident in the difference in magnitudes of the measured streamflow hydrographs. Measured and simulated snow-covered areas, expressed as a percentage of the total watershed area, are shown in figures 5A and 5B for the 1986 and 1988 snowmelt seasons.

The opportunity to jointly analyze measured and simulated streamflow and snow-covered area provides an added dimension not normally available in the assessment of the source of model errors. Assuming the input data for 1986 and 1988 are error free, errors in simulated streamflow during the snowmelt season can generally be attributed to errors in precipitation-form estimations, energy-balance computations, and snow-covered area computations. The availability of measured snow-covered-area data aids in removing some of the uncertainty in error source, and in identifying model components that need improvement.

Review of figure 4A shows that with the exception of late February, early March, and late June, measured and simulated streamflow volume and timing agree reasonably well for the 1986 snowmelt season. Measured and simulated snow-covered area for late February also agree reasonably well (fig. 5A) indicating that the overprediction of simulated streamflow in late February resulted from errors in precipitation-form estimations or energy-balance computations or both. Daily maximum air temperatures were 10 to 15 °C greater than average for this period, and precipitation occurred on 5 of the last 6 days of the month. Thus, the probable cause of error is an overprediction of snowmelt rates and the over-apportionment of daily precipitation into rain rather than snow. The overprediction of snowmelt during this period is reflected in the underprediction of snow-covered area in early March (fig. 5A).

The underprediction of streamflow in early March is caused by the apportionment of a 5.6 cm storm to predominantly snow, whereas the measured hydrograph indicates that the storm had a large component of rain. These errors result from the limited ability to apportion rain and snow using daily maximum and minimum air temperatures. However, this overprediction of snow probably compensated for the earlier overprediction of snowmelt, resulting in the smaller underprediction of snow-covered area shown in early May (fig. 5A).

The underprediction of simulated streamflow and the close agreement of measured and simulated snow-covered area in late June suggest that the snowmelt-process algorithms are underpredicting snowmelt rates for this period or that the predicted melt is not being distributed properly or both. Errors in the energy-balance computations could result from the errors in the computation of the shortwave-energy term; there are no shortwave-radiation data available for this watershed. In addition, advected energy from surrounding rock and soil masses that would be prevalent in the patchy snow cover at this time of the year are not included in the energy-balance equations. Snowmelt during patchy snow conditions also is assumed to be redistributed to part of the snow-free soil which would decrease the amount of snowmelt available for streamflow. The inclusion of remotely sensed data in the analysis of simulation results indicates that this underprediction of streamflow results from errors in model assumptions; however, the underprediction was originally attributed solely to inadequate snow cover when the analysis was limited to the use of information in the measured and simulated hydrographs.

In 1988, simulated streamflow is overpredicted during the first one-half of the snowmelt season, but matches measured streamflow during the last part of the season. Simulated snow-covered area is larger than measured at the start of the 1988 snowmelt season and remains larger for almost the entire season (fig. 5B). Although it is difficult to discount possible errors in energy-balance computations, the overprediction of snow-covered area is probably the major cause of the overprediction of simulated streamflow in 1988. The same underprediction of snowmelt rates or improper distribution of patchy snowmelt evidenced late in the melt season of 1986 probably was made for 1988 as well. This is compensated for, however, by the overprediction of snow-covered area, resulting in a reasonable streamflow simulation during this period.

Although a comparison of total watershed snow cover provides valuable information to model users and developers, an additional value of the remotely sensed data is the ability to view the spatial distribution of snow cover.

Measured and simulated spatial distribution of snow cover for two dates during the 1986 and 1988 snowmelt seasons are shown in figures 6 and 7. Some of the discrepancy in measured and simulated snow-covered areas in figures 6 and 7 results from a lack of information on the spatial distribution of simulated snow cover on an individual HRU. All HRU's with snow cover are displayed as having 100-percent snow cover even though the percentage of the area covered might be less than 100 percent. It should be noted, however, that the snow-covered-area data presented in figure 5 were calculated using the percentage snow-cover values computed for each HRU.

Dissimilarity in measured and simulated snow-covered areas in figures 6 and 7 is most pronounced on the larger HRU's, which are all located at the lower elevations of the watershed. The overprediction of snow-covered area in the February 25, 1986, comparison (fig. 6) is largely due to the display of all HRU's with snow cover as being 100-percent snow covered; comparison of measured and simulated snow-covered area for the total watershed on this date in figure 5 shows that these values are almost equal. The overprediction of snow-covered area in the southeastern part of the watershed on the other comparisons in figures 6 and 7 also might reflect some degree of this distortion of predicted HRU snow-covered area. HRU's at the higher elevations are smaller and this distortion is less pronounced. This distortion, however, does not preclude a valuable assessment of the spatial distribution of snow-covered area. A procedure to more accurately display simulated snow cover on the HRU's is being developed.

For 1986, the spatial distribution of measured and simulated snow cover agree closely in late February and again in late April (fig. 6). The only major discrepancy is the absence of simulated snow cover in the northeastern part of the watershed in late April. The reasonable agreement between measured and simulated values for streamflow volume and timing, and for spatial distribution of snow-covered area, in 1986 indicates that the HRU precipitation-adjustment factors and snowmelt parameters are reasonably well defined.

For 1988, there is an overprediction of simulated snow-covered area in early March and late April. The overprediction is somewhat greater in the southern part of the watershed in early March. By late April, the overprediction appears more equally divided across the watershed, with a large area of overprediction in the northwest corner of the watershed. Evaluation of these data indicates that the magnitudes of the HRU precipitation-adjustment factors are too large for years of less than average snowpack, and that their spatial distribution is different from that in 1986.

The comparison of point precipitation at different elevations in a watershed has shown that precipitation-adjustment factors may vary by storm, month, and season. For a 1,366-m change in elevation in the Wasatch Mountains of Utah, Peck (1972) reported that the seasonal range of precipitation-adjustment factors ranged from 2.05 to 4.31 for 1916-62. To improve the simulation capabilities of PRMS, this spatial and temporal variability in precipitation distribution needs to be incorporated. One solution is to increase the number and location of point measurements. This, however, has a number of practical and financial limitations that make it unfeasible. A better solution is to combine the available point data with the information obtained from remotely sensed data.

The methodology for using remotely sensed data is dependent on the model application. If the model is to be used for short-term, real-time streamflow prediction, then remotely sensed data could be used to update and correct simulated snow cover. The assumption that precipitation-adjustment factors are constant can be compensated by the periodic-update procedure. If the model is being used in a long-term-prediction application or to simulate the effects of changes in watershed or climate characteristics, however, then update procedures are not an option, and the model needs to adequately account for the spatial and temporal variation in precipitation distribution. In this case, remotely sensed data will provide a tool for the development and verification of additional model components to simulate the interactions of air-mass moisture, storm direction, orography, and other variables to compute precipitation-adjustment factors on a storm basis.

The strength of currently available, remotely sensed, snow-covered-area data is that they can be used to identify temporal and spatial differences in the distribution of selected model parameters, such as precipitation-adjustment factors. The limitation of these data, however, is that they do not provide a quantitative measure of the snowpack water equivalent associated with the areas covered. Consequently, the absolute values of the measured precipitation-adjustment factors for the HRU's cannot be determined. This in turn precludes the direct determination of a measure of the absolute error in the model precipitation-adjustment factors for the HRU's.

To overcome this limitation, methodologies are being investigated to couple point measures of precipitation and snowpack water equivalent with remotely sensed measures of areal snow cover to provide an estimate of the spatial distribution of snowpack water equivalent. Peck and others (1983) described a method to integrate point measurements with remote-sensing techniques, such as aerial gamma-radiation surveys and satellite measurements, to estimate mean areal values of snowpack water equivalent. Carroll and Yates (1989) described a method to couple these same point and remotely sensed data plus topographic information to estimate snowpack water equivalent on a pixel-by-pixel basis.

The integration of point and spatial measures is a complex problem that increases in complexity as the snowmelt season progresses. Snowmelt rates for HRU's are related to their topographic and vegetative characteristics, and differences in cumulative snowmelt among HRU's become more pronounced over the season. Consequently, the relations between point measures and HRU values of snowpack water equivalent will change daily. Procedures to extrapolate point measures of snowpack water equivalent need to incorporate these effects. Successful development of a methodology to integrate these measures will provide a tool for improving our understanding of the distributed nature of snow-accumulation and snowmelt processes, and for the development of improved distributed-parameter hydrologic simulation models like PRMS.

SUMMARY

Remotely sensed data provide a range of qualitative and quantitative information about the spatial and temporal variation in physical and hydrologic characteristics of watersheds. While being of value to all hydrologic models, this information is especially valuable to distributed-parameter models, which, by definition, attempt to account for and simulate the effects of this spatial and temporal variability on the hydrologic response of a watershed. A set of computerized procedures has been developed to objectively couple distributed-parameter characterizations of watersheds with individual or multiple overlays of remotely sensed data. Initial research indicates that remotely sensed measures of vegetation and land-use characteristics can be used effectively in objective watershed characterization and parameter-estimation procedures.

Remotely sensed snow-covered-area data provide a measure of the spatial and temporal information needed to evaluate distributed-parameter snow-accumulation and snowmelt-process algorithms of models like PRMS. The ability to jointly analyze measured and simulated streamflow and snow-covered area decreases the uncertainty in defining sources of model error that occurs when analysis is limited to the hydrograph alone. Underprediction of late-season snowmelt by PRMS, which was attributed to inadequate snow cover based on a hydrograph analysis, was determined to be more closely related to errors in model assumptions when snow-covered-area data were included in the analysis. As a result of this joint analysis, selected PRMS components whose improvement would substantially improve model results were identified. These include energy-balance computations and snowmelt distribution during periods of patchy snow cover, the precipitation-adjustment factor, and the determination of precipitation form. While providing the insight to identify these problems, remotely sensed snow-covered-area data also have the potential to provide needed information to solve them.

The value of currently available remotely sensed data is derived from the information they contain on spatial distribution of watershed features and the identification of feature types. The absence of quantitative measures other than areal coverage in most remotely sensed data currently available for operational use necessitates the coupling of these data with ground-based measures to estimate the spatial distribution of the magnitude of these features. Further research is needed to develop objective procedures to couple these data so that maximum use can be made of remotely sensed data in all phases of distributed-parameter model application and assessment. As advances are made in sensors, scale and frequency of coverage, and availability of operational products for remotely sensed data, these coupled estimation procedures will be replaced with direct measures of the physical and hydrologic characteristics of watersheds.

REFERENCES

Anderson, E.A., 1973, National Weather Service river forecast system--Snow accumulation and ablation model: Silver Spring, Md., U.S. Department of Commerce, National Oceanic and Atmospheric Administration Technical Memorandum NWS Hydro-17, 226P.

Carroll, T.R., and Allen, M.W., 1988, Airborne and satellite snow cover measurements--A user's guide, version 3.0: Minneapolis, Minn., National Weather Service, Office of Hydrology, 54 p.

Carroll, T.R., and Yates, G.R., 1989, Satellite, airborne, and ground-based snow cover data used to estimate basin-wide mean areal snow water equivalent on a pixel-by-pixel basis: American Geophysical Union, EOS Transactions v. 70, no. 43, p. 1108.

Day, G.N., 1985, Extended streamflow forecasting using NWSRFS: American Society of Civil Engineers, Journal of Water Resources Planning and Management, v. 111, no. 2, p. 157-170.

Environmental Systems Research Institute, 1989, ARC/INFO user's guide--Revision 5: Redlands, Calif.

Jenson, S.K., and Domingue, J.O., 1988, Software tools to extract topographic structure from digital elevation data for geographic information system analysis: Photogrammetric Engineering and Remote Sensing, v. 54, no. 11, p. 1593-1600.

Leavesley, G.H., Lichty, R.W., Troutman, B.M., and Saindon, L.G., 1983, Precipitation-runoff modeling system--User's manual: U.S. Geological Survey Water-Resources Investigations Report 83-4238, 207 p.

Leavesley, G.H., Lumb, A.M., and Saindon, L.G., 1987, A microcomputer-based watershed-modeling and data-management system: Western Snow Conference, Vancouver, British Columbia, 1987, Proceedings, v. 55, p. 108-117.

Lumb, A.M., Kittle, J.L., Jr., and Flynn, K.M., 1989, Users manual for ANNIE, a computer program for interactive hydrologic analyses and data management: U.S. Geological Survey Water-Resources Investigations Report 89-4080, 251 p.

Peck, E.L., 1972, Relation of orographic precipitation patterns to meteorological parameters, *in* Distribution of precipitation in mountainous areas, Vol. II: Geneva, World Meteorological Organization, Publication 326, p. 234-241.

Peck, E.L., Johnson, E.R., Keefer, T.N., and Rango, A., 1983, Combining measurement of hydrological variables of various sampling geometries and measurement accuracies, *in* Hydrological Applications of Remote Sensing and Remote Data Transmission: International Association of Hydrological Sciences Publication 145, p. 591-599.

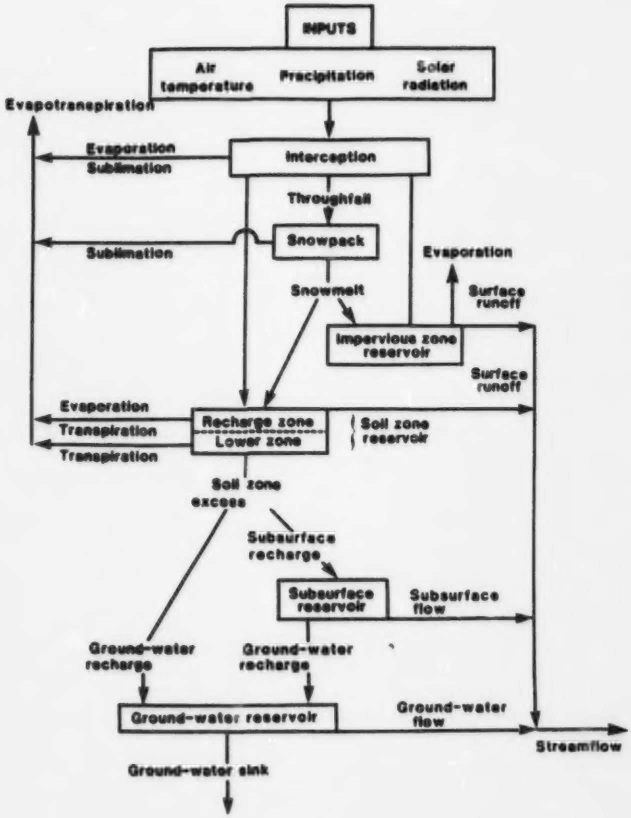
INPUTS
Air temperature
Precipitation
Solar radiation
Evapotranspiration
Evaporation
Sublimation
Interception
Throughfall
Snowpack
Sublimation
Evaporation
Snowmelt
Surface runoff
Impervious zone reservoir
Surface runoff
Evaporation
Transpiration
Transpiration
Recharge zone
Lower zone
Soil zone reservoir
Soil zone excess
Subsurface recharge
Subsurface reservoir
Subsurface flow
Ground-water recharge
Ground-water recharge
Ground-water reservoir
Ground-water flow
Streamflow
Ground-water sink

Figure 1.--Schematic diagram of precipitation-runoff modeling system (modified from Leavesley and others, 1983)

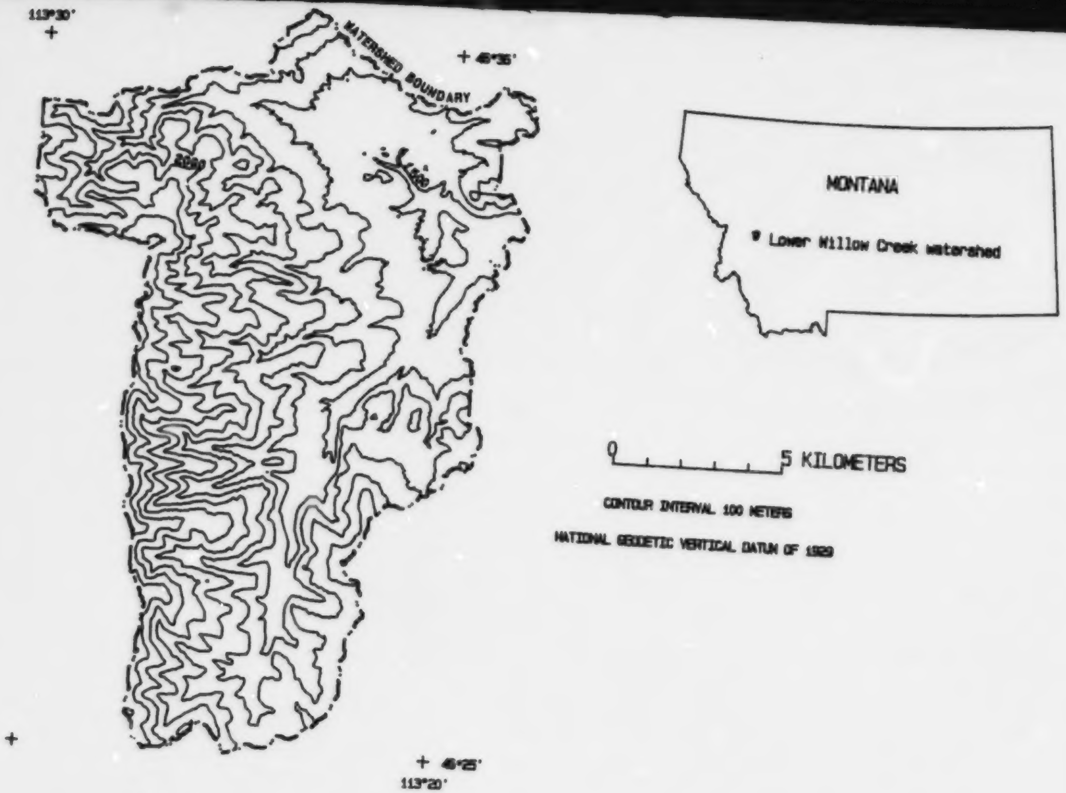
113°30'
46°35'
WATERSHED BOUNDARY
2600
1600
46°25'
113°20'
MONTANA
Lower Willow Creek watershed
0
5 KILOMETERS
CONTOUR INTERVAL 100 METERS
NATIONAL GEODETIC VERTICAL DATUM OF 1929

Figure 2.--Topographic contours generated from gridded elevation data for the Lower Willow Creek watershed, western Montana.

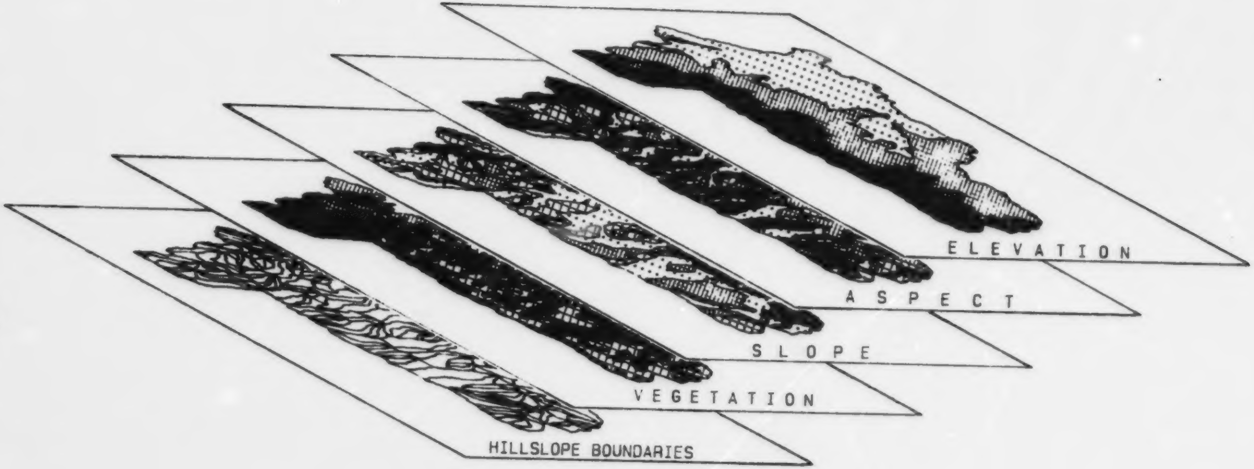
ELEVATION
ASPECT
SLOPE
VEGETATION
HILLSLOPE BOUNDARIES

Figure 3.--Overlay of vegetation, slope, aspect, and elevation coverages on computed hillslope boundaries, Lower Willow Creek watershed, western Montana.

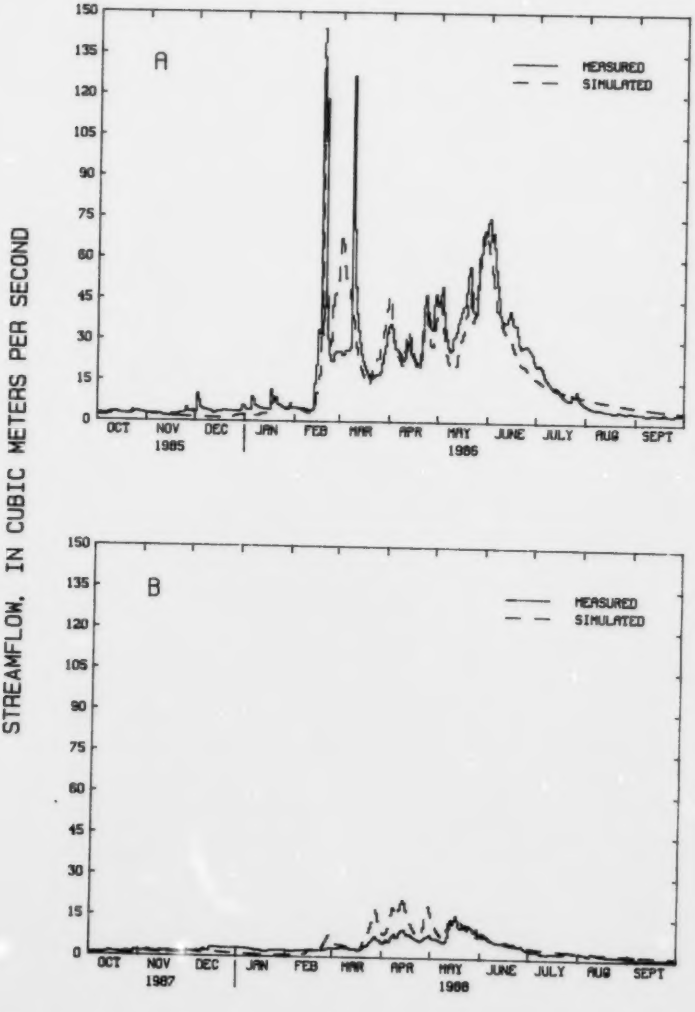

Figure 4.--Measured and simulated streamflow in the East Fork Carson River, Calif.-Nev.: A, water year 1986; and B, water year 1988.

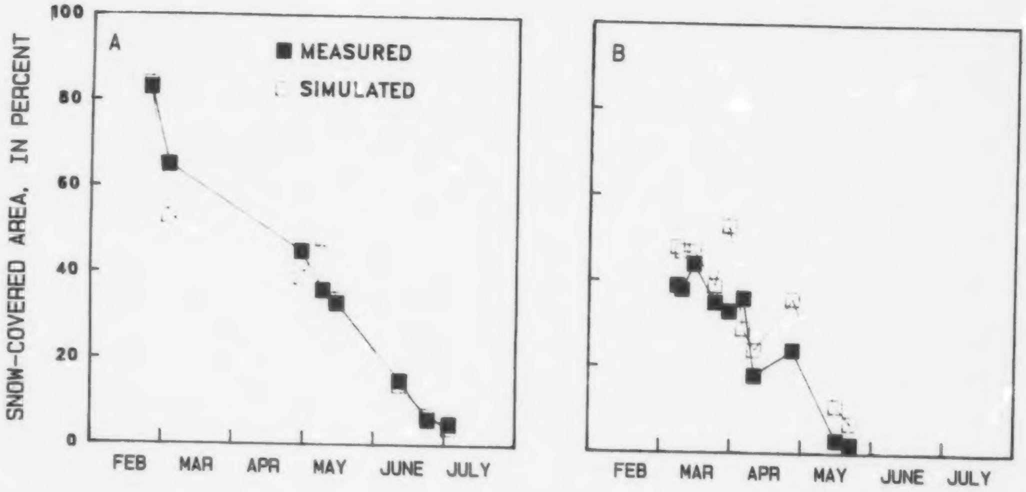

Figure 5.--Measured and simulated snow-covered area in the East Fork Carson River watershed, Calif.-Nev., expressed as a percentage of the total watershed area: A, water year 1986; and B, water year 1988.

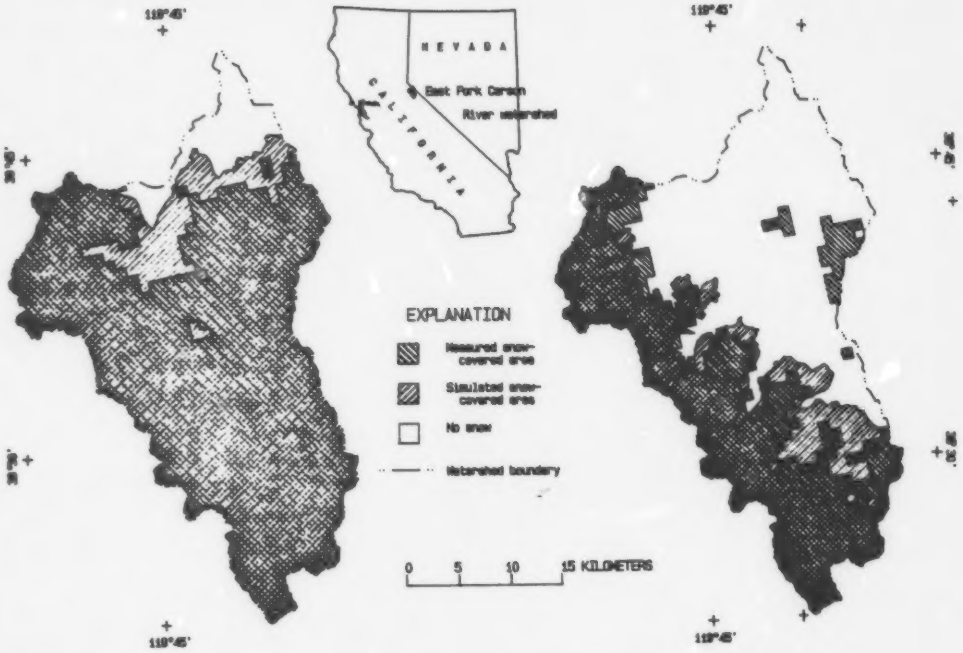
119°45'
38°45'
38°30'
NEVADA
CALIFORNIA
East Fork Carson River watershed
EXPLANATION
▧ Measured snow-covered area
▨ Simulated snow-covered area
☐ No snow
Watershed boundary
0 5 10 15 KILOMETERS

February 25, 1986

April 30, 1986

Figure 6.--Measured and simulated snow-covered area in the East Fork Carson River watershed, Calif.-Nev., February 25, and April 30, 1986.

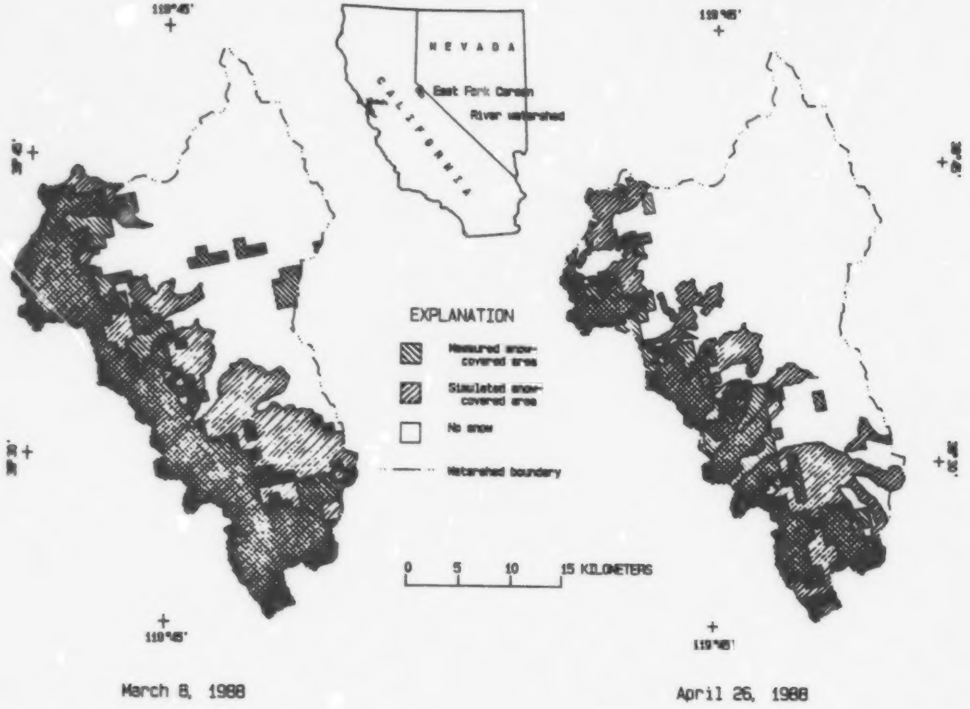

119°45'
38°45'
38°30'
NEVADA
CALIFORNIA
East Fork Carson River watershed
EXPLANATION
Measured snow-covered area
Simulated snow-covered area
No snow
Watershed boundary
0
5
10
15 KILOMETERS

March 8, 1988

April 26, 1988

Figure 7.--Measured and simulated snow-covered area in the East Fork Carson River watershed, Calif.-Nev., March 8, and April 26, 1988.

Questions and Answers

Jean-Pierre Fortin: I agree with what you are doing, because we are working largely the same way. I would like to ask what is your criterion to distinguish the hydrological response curves. I mean, do you have small units or large ones?

George Leavesley: Right now that's something we are looking at. We are looking at how to aggregate up from small units to large units and what that entails as far as what sort of smoothing you might have to do in some of your parameterizations, and how that affects your parameter estimates. The rule of thumb that we have been using for the last couple of years is that we assume anything smaller than four or five percent of the total basin area, you are not going to see in the total basin response. Unless it is a parking lot, or you pave it, or you dump a chemical on it, or you are really looking at the water quality aspects; then, you may want to be looking at something that is smaller. The one thing that I didn't mention is that with the way the hydrologic response units are distributed, I don't know if you noticed, but there are replicates. Working in a daily mode we are not routing from every hydrologic response unit. So that this area...is the same are this area...is the same as this area, for example. Because there is no routing, we can aggregate those areas together even though they are not contiguous. So we can account for the slope, aspect and vegetation because there is a lot of similarity, but it is not one large unit.

Jean-Pierre Fortin: I agree with the lower limit. But how do you get the higher limit?

George Leavesley: That is sort of driven by the objectives of the problem and the data constraints. We've done some analysis looking at if you just had one unit, or if you made five units, or if you made more. The limit becomes smaller and smaller over the single hydrologic response unit. So there is a law of diminishing return coming in here, and we find that five percent is a reasonable one.

Al Rango: When the snow cover from satellites doesn't agree with the simulated cover in the model, you had a good impression what to do when the hydrographs did not agree. But now, what happens when the model is doing fine when you compare the simulated to the measured hydrographs, but the area of snowcover from satellite doesn't agree with what the model is simulating? What's the problem then?

George Leavesley: Well, we haven't gotten to the point to really get anything in to verify the satellite data, so at this point we are kind of going on faith. This basin is particularly open and it has got vegetation cover densities that are in the order of thirty to forty percent, so we don't feel that there is a problem with heavy vegetation cover. But, that is something we haven't faced, and as we move into more and more basins we will have to consider this problem further. This is really the first basin we've looked at for applying this, and one of the reasons that we picked this basin is because we were more comfortable assuming that the satellite data was valid.

Al Rango: Then, there are more analyses to come?

George Leavesley: Yes.

Mindy Brugman: I have a question about the discrepancy between your predicted runoff curve versus that observed for the summer. The predicted was higher and you said that this was possibly due to errors in the routing method used?

George Leavesley: The predicted was lower. Yes, if you look at the 1988 curve, here it is, you notice that we did real well; at the end of the season here it matches right on. But that's the year we were way above, so the model was simulating about ten to fifteen percent more snow than was actually there. So that overestimate was enough to compensate and produce a reasonable recession. Thus, in this year if we hadn't done the analysis we would have said "we have the right amount of snow but in 1986 we were short, so we need to add more snow". When in fact, the way we are handling patchy snow is that in some cases it does not have a direct route to a channel to flow off. It is assumed to be seeping down through the soil and available for evapotranspiration over a larger area than may be appropriate. So we are going to go back and take a look at some of that.

Thian Yew Gan: What are your main parameters, how do they vary and do they vary between each area?

George Leavesley: Yes, the parameters vary. The parameters we are looking at principally for the snow melt algorithms are the available waterholding capacity of the soil (which is defined by the rooting depth and the available moisture in inches per foot of soil), the vegetative canopy density (which defines both the long wave component in the canopy as well as the transmission coefficient for the attenuation of short-wave radiation to the surface), and then built in is, of course, the slope and aspect of that area (we take the measured short wave on a horizontal surface and readjust it to that slope and aspect). So those are the primary factors affecting the energy budget of the melt on each unit, and they do vary.

Thian Yew Gan: This means you have to have a lot of data points, because one or two will be discarded?

George Leavesley: Yes, right. Or it means you have to have points from representative vegetative covers, and so what I'll often do is get some aerial photography and look at what are vegetative covers and what are some representative values. But I can go out and take some measurements in those representative areas and I can then extrapolate out to those on the basin and use that as a means.

Al Rango: In reference to the output from the basin in terms of simulated versus observed flows, with all of these hydrological response units, it seems that you have quite a big job in terms of getting the conveyance correct. It could be a fairly large source of error, perhaps. What sort of routing are you using?

George Leavesley: In the daily mode, on a basin of this size, none. What melts that day is routed through the subsurface reservoir (which is a rapid flow reservoir, treated as nonlinear), and then through the groundwater reservoir (treated as linear), and so that's the routing mechanism. If the daily melt exceeds a model threshold value, I've got surface runoff, or if I get rain on snow I can get surface runoff. Otherwise, it is assumed that all the melt infiltrates and is routed through those two reservoirs. So that takes up some of the conveyance.

Milne Dick: The difference between the recorded output and your predictions; how much of that is caused by, say, errors in concepts or problems with the model vis-a-vis differences between inout data and reality. Is there an trade-off there?

George Leavesley: The most common problems were the ones that I showed for 1986 where, because we only had daily data (it was max. and min. temperatures), you often miss rain or snow; calling it rain when it is really snow or calling snow when it is really rain. That's a very typical error. Also, when we don't have the solar radiation data, with the current algorithms used in the model, problems have occurred. For example, that first blip that I showed you with the simulated rise that didn't actually occur; that is related to the solar radiation algorithm. I think that those are the two biggest data problems. If we are going to use an energy budget approach, these errors are probably eighty to ninety percent of the errors that we have. If we have the snow on the watershed in the right distribution, we seem to be able to do reasonably well provided we have a good handle on the energy budget. So if you are going to apportion the error, from the experience of applying this model to a dozen basins, I would say that it is sixty percent or seventy percent data and thirty or twenty percent concepts. Not necessarily concepts, but simplifying assumptions that you have to make, because we don't have measures of the spatial distribution of a lot of these things.

Using GOES Visible Data to Extend Snow Course Data in Southern Ontario

J.R. Donald, E.D. Soulis, N. Thomson
Department of Civil Engineering, University of Waterloo,
Waterloo, Ontario, N2L 3G1

S.B. Malla
Water & Energy Commission Secretariat, Kathmandu, Nepal.

Abstract

The spatial variation of snow cover depth is an important input to distributed hydrologic models. Recent experience suggests that these data can be averaged over regions with areas of up to 4% of basin size. For large basins with significant snowmelt events, ground resolutions of 10 km or more are sufficient. Meteorological satellites have been used to map the areal extent of snow at this resolution but they are not normally used to determine snow cover depth. This paper examines the potential of GOES imagery to map snow cover depth in southern Ontario. GOES visible data for December 29, 1987 is compared with snow course data for December 31, 1987 and January 4, 1988. The image brightness is found to be uniform where snow depths exceed 20 cm but correlates well with shallower snow depths. Since snow packs in southern Ontario are often in this range, GOES or other meteorological satellite imagery may be useful supplements to snow course measurements.

INTRODUCTION

The spatial variation of snow cover properties, such as depth, density and water equivalent, is an important requirement for distributed hydrologic models. To provide distributed information characterizing the snow cover of a watershed, snow survey measurements must be extended to regions where no snow survey data is available. Snow surveys provide detailed information on snow pack properties but their site specific nature and infrequent occurrence limit their potential for use in operational models. Remotely-sensed satellite images can provide information that can "fill-in-the-gaps" in temporal and spatial snow survey resolution.

Satellite imagery has been quite useful in estimating the snow covered area for input to snowmelt runoff (eg., Rango and Martinec, 1979) but the use of satellite imagery in the estimation of snow depth and snow pack water equivalent for input into hydrologic models has been limited. In many instances the snow pack water equivalent has been derived from hydrologic models once a snowmelt event is complete (eg., Rango and Martinec, 1981; Søgaard and Thomsen, 1988).

Snow has a very high albedo in the visible range of the electromagnetic spectrum, therefore it is intuitive to expect the albedo of a specific area to increase as the percentage of snow covered area within the area increased. Studies have been carried out to examine the relationship between albedo and depth. This phenomenon is displayed in a study by Kung et.al. (1964), in which albedo measurements taken from a low-flying aircraft were compared to snow survey information. The data from the 1964 study (reproduced in Figure 1) show a definite relationship between albedo and surface snow depth in the farmland and farmland & forest classifications. Relationships such as these would be useful in hydrologic modelling, especially in watersheds with shallow and rapidly changing snow packs, if they could be evaluated on a real-time basis.

The purpose of this paper is to evaluate the potential of meteorological satellites, such as GOES, to extend the snow course data, by developing relationships such as that presented in Figure 1 for use in distributed hydrologic models. Meteorological satellites are attractive for this application as they can provide daily information (provided cloud-free conditions exist) as well as adequate spatial resolution for distributed modelling of large watersheds.

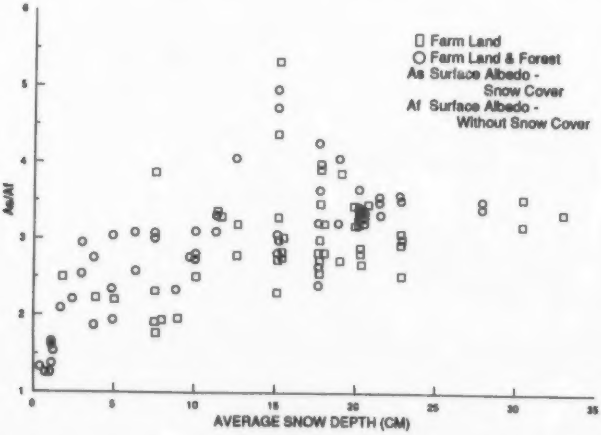

Figure 1 Surface albedo related to depth of ground snow cover (after Kung et.al., 1964)

SATELLITE DATA

Satellites in the GOES series follow a geosynchronous orbit, sampling in two operational bands: visible (0.55μm to 0.75μm) and thermal infrared (9.7μm to 12.8μm). A digitally-archived GOES image of southern Ontario at 18:01 GMT, December 29, 1987, was obtained from the Canadian Atmospheric Environment Service for use in this study. The visible band of this image, shown in Figure 2, has a ground resolution of approximately 1 kilometre by 1 kilometre at the latitude of the study region.

The image extends over latitudes 42°30″ N to 44°30″ N and longitudes 79°W to 81°W. The image was geometrically corrected using a second-order polynomial transformation with nearest neighbour interpolation to UTM coordinates at 8 known ground control points. The image is clear, except for a small cloud-covered area in the south-east corner.

Radiometric correction is not necessary for the analysis performed in this study as only the presence of a general trend is being examined. If the absolute reflectance values from different images were to be used then radiometric correction would be required.

SNOW DATA

Snow survey information was taken from Snow Cover Data (Dept. of Transport, Atmospheric Environment Service, 1988) for southern Ontario on December 31, 1987 and January 4, 1988. There are 72 standard snow courses in the region (shown on Figure 2) operated by various agencies. The snow courses report average depth and average snow water equivalent on a bi-weekly basis throughout the winter season.

Daily climate data (Canadian Atmospheric Environment Service, 1987 and 1988) indicate that a snowfall event crossed the southern region of the study area on December 28, 1987, one day before the image was taken. No significant snowfall occurred in the north and central portion of the image, but snow existed in many of these snow courses in the survey of December 15, 1987. The southern snow courses were bare in the December 15, 1987 survey.

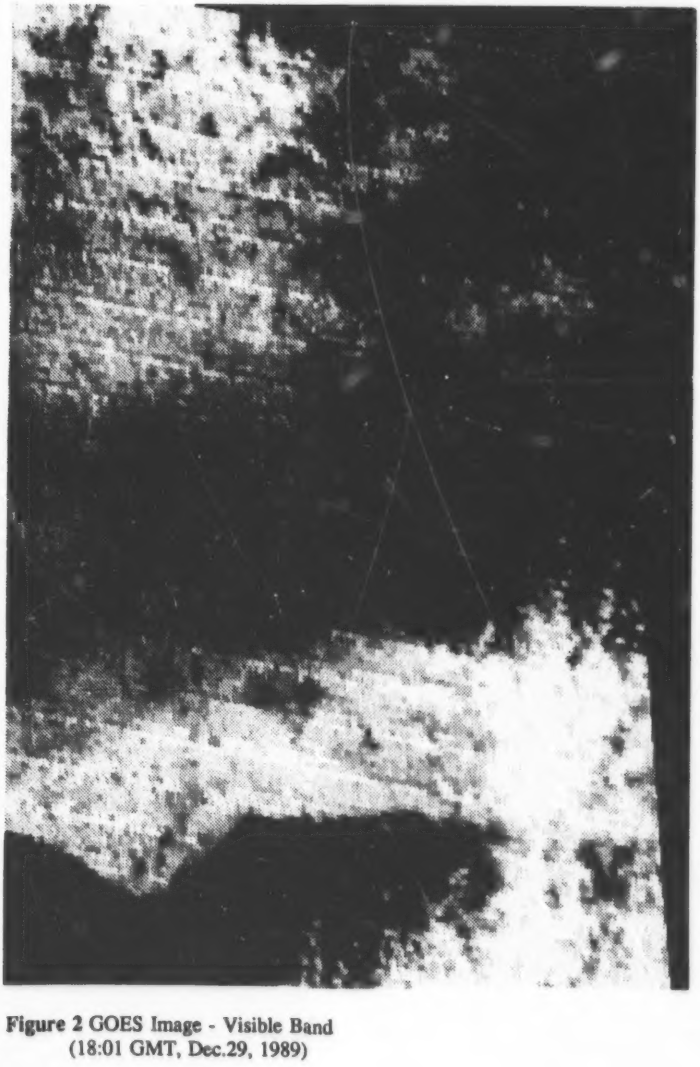

Figure 2 GOES Image - Visible Band
(18:01 GMT, Dec.29, 1989)

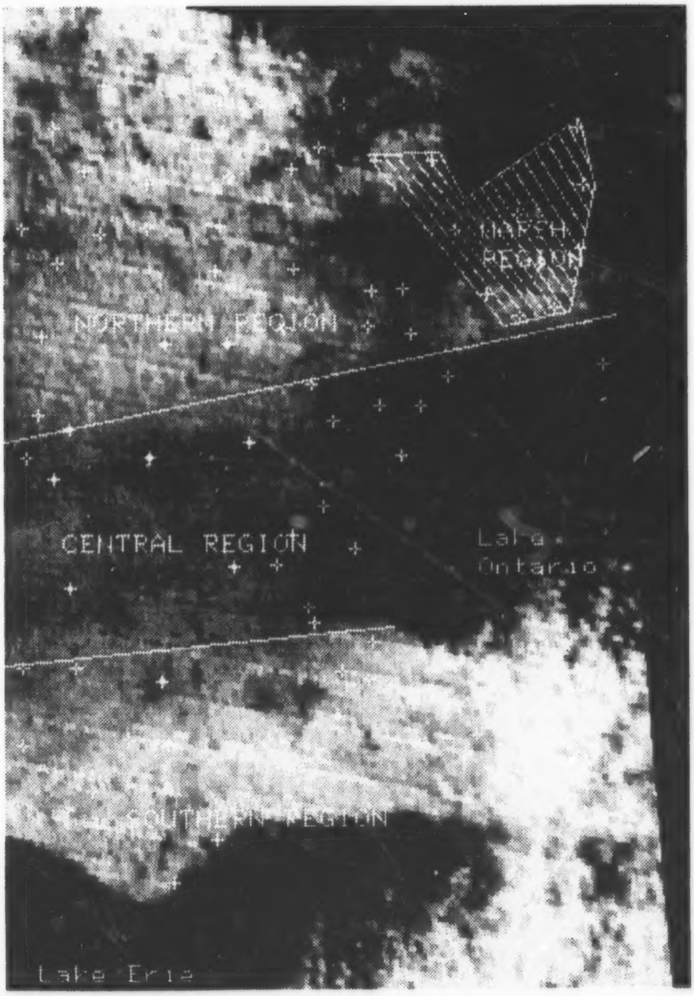
NORTHERN REGION
MARSH REGION
CENTRAL REGION
Lake Ontario
SOUTHERN REGION
Lake Erie

Figure 3 Study Region and Snow Course Locations (+)

SNOW DEPTH-REFLECTANCE RELATIONSHIP

The relationship between satellite raw reflectance digital number (DN) and the snow depth in the standard snow courses was created by plotting the reflectance value of the pixel containing each snow course against the average snow course depth. In the resulting plot (Figure 4) no relationship is immediately apparent. However, if the climatic conditions are taken into account, the relationship in Figure 5 emerges. To create Figure 5, the stations in the southern region were eliminated from the data set. It is likely that the high temperatures that occurred on December 30 and 31 were sufficient to melt most, if not all, of the snow in the region before the snow courses were sampled on December 31 or January 4.

The stations in the central and northern regions were all included in the plot with the exception of the courses in the Holland Marsh region (hatched area on Figure 3). This region displayed very high reflectance values despite low snow course depths. The Holland Marsh is a wide expanse of low-lying farm land and it is likely that this cover could have been dominated by a highly reflective thin frozen ice layer.

In Figure 5 the reflectance values increase with average snow pack depth, levelling out at approximately 20 cm. This relationship is expected to be terrain-dependent, that is, the general surface characteristics will influence the depth at which the levelling out will occur. The rougher the surface, the deeper the pack must be to completely cover the surface. Once the surface is completely covered,

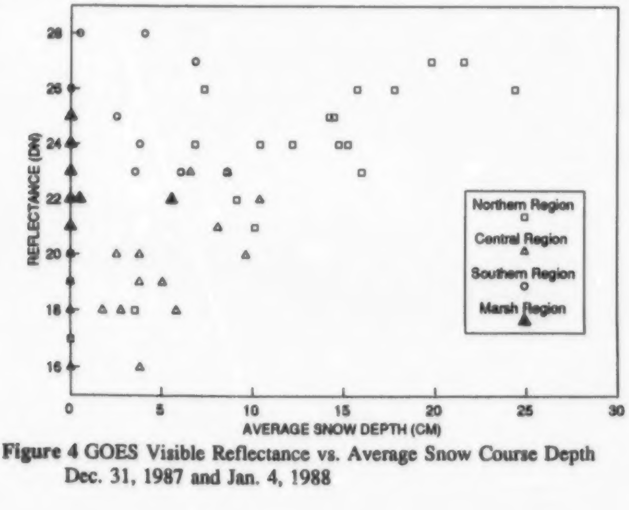

Figure 4 GOES Visible Reflectance vs. Average Snow Course Depth
Dec. 31, 1987 and Jan. 4, 1988

there is no increase in reflectance with increased depth of the snow pack. The degree of scatter in the relationship is likely to be a function of the variability in the surface type from pixel to pixel. The reflectance from a pixel is the integrated reflectance over a 1 kilometre by 1 kilometre square, thus, if all pixels have approximately the same mix of surface cover types then the scatter in the relationship will be less than if the mix varies.

The shape of the relationship shown in Figure 5 is similar to the results obtained by Kung et.al. (1964) for the farm and farm/forest regions. It is encouraging that the snow depth-reflectance relationship appears to hold at the resolution of the meteorological satellites. Most of the scatter in the snow depth - reflectance relationship occurs at zero snow depth. This is most likely caused by snow courses that are not representative of the region, but is a concern that should be examined in future studies.

Plotting the GOES reflectance vs. average snow pack water equivalent (SWE) in Figure 6 results in a relationship very similar to the reflectance-depth relationship. The reflectance increases with SWE starting at a digital number of approximately 16 at zero SWE, rising with increased SWE and levelling out at about 4 cm. This is somewhat surprising as snow water equivalent can be highly variable from

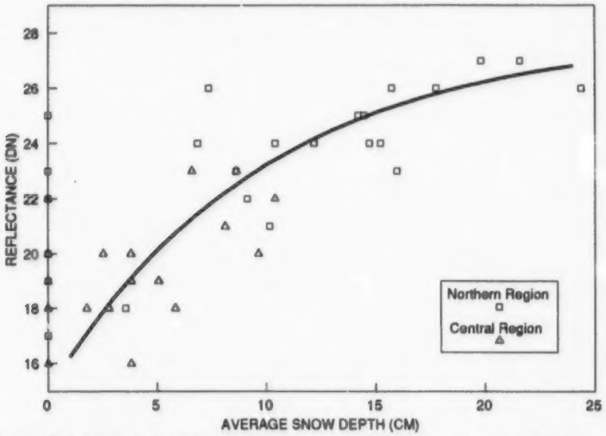

Figure 5 GOES Visible Reflectance vs. Average Snow Course Depth Northern and Central Regions, Dec. 29, 1987 & Jan. 4, 1988

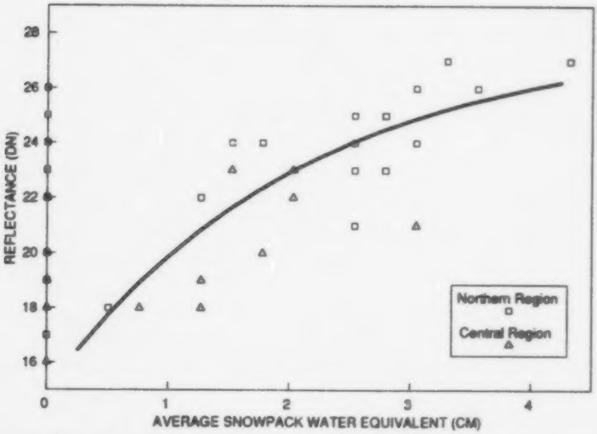

Figure 6 GOES Visible Reflectance vs. Average SWE
Northern and Central Regions, Dec.29, 1987 & Jan. 4, 1988

region to region and is not necessarily related to depth. However, the GOES visible pixels represent an average value over an area of approximately one square kilometre and the variability in snow density that would be apparent at a local scale could easily be averaged out when considering the larger scale relationship.

CONCLUSIONS

Operational hydrologic modelling of snowmelt events requires real-time input of the snow cover parameters. Snow survey information is inadequate, both spatially and temporally, in providing snow cover information for distributed snowmelt runoff models.

The results of this study indicate that a relationship exists between reflectance values measured from meteorological satellites and the snow cover properties of snow depth and snow water equivalent in southern Ontario, perhaps to an average snow pack depth of 20 cm or a snow pack water equivalent of 4 cm. Snow packs with depths and snow water equivalents of this order are very important in southern Ontario, where packs are shallow and ephemeral in nature.

If relationships such as those presented in this study can be standardized, their potential application as input to distributed snowmelt runoff models should improve operational snowmelt hydrology by providing daily information regarding the snow pack on a basin scale. The relationships are likely to be governed by terrain features and as such would have to be developed on a regional basis.

A potential operational difficulty in the operational application of the reflectance-snow depth relationship in southern Ontario is the necessity of cloud-free coverage. Significant snowmelt events are often accompanied by rain or cloud coverage for periods of days, inhibiting the utility of the meteorological satellite coverage. However, even one or two images in the course of a melt, especially if the timing of the standard snow course surveys is poor, could aid in the initialization or updating of a snowmelt model.

The methodology would be well-suited to climates such as the Prairies or perhaps even the sub-arctic, that experience a greater number of cloud-free days during the melt season, yet have shallow enough packs to make the information useful. The methodology would not be suitable for mountainous terrain, due to the rapid changes in elevation and the presence of very deep snow packs.

The next phase in the research is to attempt to standardize the relationship between reflectance and snow depth/snow pack water equivalent using additional images, taken coincident with snow course sampling dates. Once the relationship is established, the effect on real-time snowmelt runoff forecasting can be evaluated by using the information as input in a distributed hydrologic model.

REFERENCES

Dept. of Transport, Meteorological Branch (1987,1988) Snow Cover Data - Eastern Canada.

Kung,E.C., Bryson,R.A. and Lenschow, D.H. (1964) Study of a continental surface albedo on the basis of flight measurements and structure of the Earth's surface cover over North America, *Monthly Weather Review*, Vol. 92, No. 12, 543-563.

Martinec, J. and Rango,A. (1981) Areal distribution of snow water equivalent evaluated by snow cover monitoring, *Water Resources Research, Vol. 17, No.5, 1480-1488.*

Rango,A. and Martinec,J. (1979) Application of a snowmelt-runoff model using Landsat data, *Nordic Hydrology*, 10, 225-238.

Søgaard, H. and Thomsen, T. (1988) *Application of Satellite Data to Monitoring Snow Cover and Runoff in Greenland, Nordic Hydrology*, 19, 225-236.

Questions and Answers

Tony Wankiewicz: Just on the problem of non-representative snow courses. I've noticed, in the prairies, when you drive along and the snow blows in the ditches, that it is often black for some distance back from the road. You get the wrong impression looking out over the fields, because there is more snow further away from the road. I wonder if people go by and say that there is no reason for doing a snowcourse.

John Donald: Yes, well that could very well happen, especially in that marsh region where every single snow course in one specific area had zero depth and some "-99" which indicates that they did not take a snow sample for some reason. I don't know why it is. The numbers are there, and I didn't ditch the numbers without knowing really what they were. I left those in there.

Robert Miller: On your scale of reflectances where do clouds fit in?

John Donald: Clouds were about thirty-four to thirty-three range.

Mindy Brugman: Do you have any information on the snow-grain size variation north to south in your study area? I just have a hard time believing the line you drew. I didn't know if grain size varied, dust content varied, or whether there was a difference due to small snow dunes that affected the relectance of the snow.

John Donald: North to south? Well, I think that all of those things do change and in this area it would be definately be warmer in the south than the north, and the snow pack characteristics would be different. Because it is an integrated value and because the albedo of the snow is so high, you can agree that it might change from fifty percent to seventy-five percent, or something like that. I think that is what accounts for a lot of the scatter. Because it is an average value, and because we've got these curves behaving this way, we have it characterised fairly well. So far as the physics of the snow pack and how it is affecting the result, I really haven't considered that in detail.

Determination of Characteristics for Hydrological Modelling Using Remote Sensing

Jeff Whiting
Saskatchewan Research Council
Saskatoon, Canada S7N 2X8
Tel 306-933-5423

Abstract: The Saskatchewan Research Council with other agencies has investigated the use of remote sensing to provide hydrological information. Ten Projects have been conducted to assess various watershed characteristics. The following characteristics were analyzed: land cover classes for snow melt runoff modelling, snow line mapping, snow water equivalent estimation, flooded land mapping, effect of fault blocking on drainage pattern, antecedent water area, and snow catchment mapping. The adequacy of this data has been analyzed.

1. Physical Characteristics Of Hydrological Events And Their Relevance To Forecasting Models

1.1 Introduction and Definitions

A forecast is a statement of expected future occurrences; of what is predicted. A prediction is based upon the present knowledge of the states and the effects of physiographic, meteorologic, and hydrologic conditions.

A flood is a condition that occurs when water overflows the confines of a stream, or accumulates by drainage over low-lying areas. In contrast, a drought is a period of abnormally dry weather sufficiently prolonged for the lack of water to cause a serious hydrologic imbalance in affected areas. Drought severity depends upon the degree of moisture deficiency, the duration, and (to a lesser extent) the size of the affected area (Huschke 1959).

1.2 Time and Space Aspects of Extreme Events

1.2.1 Meteorological Phenomena: The meteorological 'trigger' for hydrological events varies in size, lifetime, and predictability. A severe thunderstorm may cause local heavy flooding in one part of town but it is not easily predicted, quantitatively, for more than an hour or two. On the other hand, the forecast of critically low flows on major rivers is often the result of prolonged drought where the significant meteorological trigger is the net effect of low precipitation and high temperatures, accumulated over weeks or months.

The relative importance of significant meteorological parameters relative to hydrological problems are given in Table 1. For timing of maximum monthly flow in major prairie streams, the most important parameter is the condition of the winter snow pack. The difficulty in forecasting various meteorological events can be appreciated by comparing the maximum lead times associated with each hydrological event. Lead times range from

Table 1 Streamflow Forecasting Problems and Meteorological Triggers.

Hydrological Problem	Meteorological Trigger	Size of Trigger km^2	Maximum Forecast Lead Time	
			Quantity	Quality
1. Flash floods				
a) heavy rain on saturated soil	thunderstorm	10	2 hours	12 hours
b) moderate rain on frozen ground	synoptic or meso-scale rain storm	100 - 1000	24 hours	48 hours
c) ice jam	sudden thaw and light to moderate rain	10,000	3 days	5 days
2. "Hybrid" floods	moderate to high snowmelt and rainfall over 1-2 days	10,000	24 hours	2 days
3. Annual Maximum Discharge for Water Supply Regulation	heavy winter snowfall and onset of spring thaw	continental	2 weeks	1 month
4. Annual Minimum Discharge for Water Supply Regulation	drought (prolonged heat and dryness)	continental	1 month	2-3 months

Source: Hogg et al. 1985.

under two hours for quantitative forecasts of heavy rain to two to three months quantitative indications of large scale droughts (Hogg et al 1985).

Weather satellites measure phenomena similar to those of interest to water resources (Figures 1 and 2). Repetitive views yield global cloud maps and permit the tracking of storms and the associated precipitation. The resolution of sensors on-board these satellites and their frequencies of orbit (observation) must be matched to the meteorological and hydrological event.

Phenomena with a time scale of minutes to hours (e.g., tornadoes) are difficult to monitor as they require observations of short interval. For instance, such monitoring requires many such orbiting satellites, or a stationary, geo-synchronous satellite. The GOES Satellite provides 30 minute repeat cycles over large areas (60° latitude and 75° longitude), but its resolution at Canadian latitudes is only 8 km. The NOAA satellite is a polar orbiter however only one satellite in orbit is guaranteed (although there are normally 2 in orbit). With one in orbit, 12 hour coverage (i.e. one day and one night pass) is possible. The land observation satellites, SPOT and LANDSAT, have 10 m to 60 m resolution and 14 to 16 day cycles. The French satellite, SPOT, can be pointed 5 track off nadir (within a day cycle) with 48 hour notice. The monitoring and modelling must therefore be tuned to the time scale of the phenomena.

Due to the frequency of orbit and the resolution, only meso- and macro-scale events can be tracked from space in the foreseeable future (Figure 1). The GOES satellite is suitable only for the middle meso-scale and above. The NOAA series is good for the upper meso-scale and above. LANDSAT and SPOT are fine for the upper macro-scale but these fail the time test.

1.2.2 Hydrological Phenomena: The same sort of message regarding space and time scales can be obtained from Figure 2 for hydrological phenomena. Similar monitoring problems arise from these characteristics. For example, the GOES satellite can providing information for the flash flood, and snowfall aspects for the water manager needs. The NOAA satellite data starts at the end of the snow period and includes regional floods. The LANDSAT and SPOT satellite are suitable for monitoring river plumes, lake circulation, land use change, drought and climate change end of the spectrum of events.

The primary source of water is rain and snow falling on the head water of river systems. Because these headwaters are frequently located in inaccessible regions, predictions of river flow rely on largely scattered point sources of data and on reporting by cooperative observers. We must determine the total runoff potential in the form of snow on the ground and precipitation, as well as the rate at which the water is running off. This information is needed to determine the water available for flooding and water supply. Remote sensing inherently provides areal integrated data. Synoptic scenes repetitively covered in machine format offer needed data, as well as a means for improving predictive models.

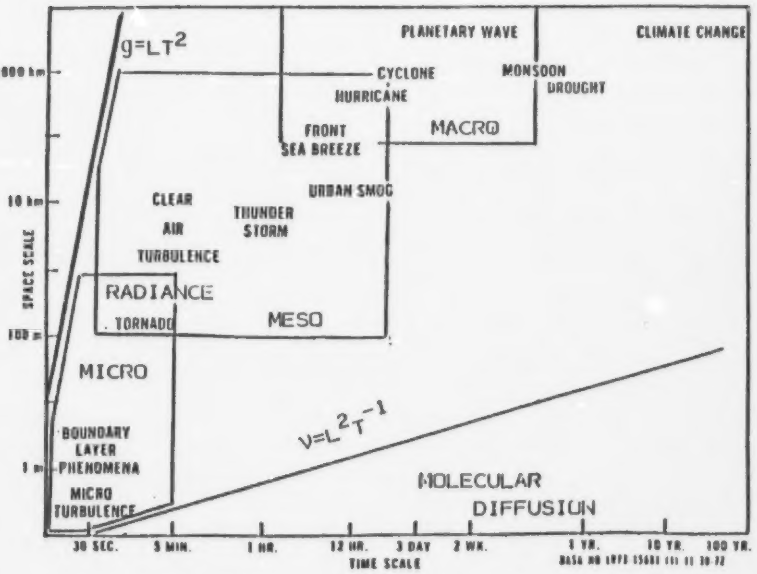

Figure 1 Time and Space Scales of Meteorological Phenomena

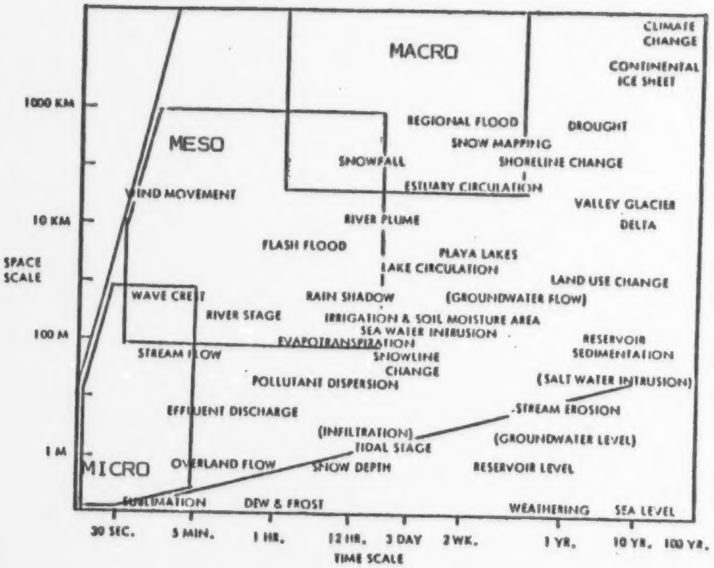

Figure 2. Time and Space Scales of Water Resources Phenomena

Taken from Remote Sensing and Management by Thomson, Lane & Csallany, AWRA, 1974.

1.2 Hydrological System Examples

The causes of flooding are varied. In British Columbia, the lifting of moist warm air from the Pacific over the coastal mountains gives the coastal areas the highest annual precipitation in Canada. With sudden melting of snow in these narrow 'V' shaped valleys, with high gradient and large impervious expanses produces very large increases in flow in rivers. The rain shadow or low precipitation areas of the Prairies are next. Nonetheless, floods can occur because eastward flowing rivers have their headwaters in the same interior Rockies. In the immature drainage basins of the Prairie streams overtopping occurs as rain on snow event are frequent. In the northwest Arctic, the spring thaw starts in the south while the northern part is still frozen. The result is ice jams and flooding.

Few studies have determined the benefit/cost of using remote sensing in forecasting. In the few that have been reported, remote sensing data has a large advantage over conventional data except over very small basins (Rango 1985). A projected benefit/cost for snow-cover data is 75:1 (Rango 1980). If the HEC-1 hydrological model uses LANDSAT data, the benefit/cost was found to be 4:1 on basins larger than 25 km^2 (Rango et al 1983). HEC-1 effectively produces peak flow calculations and SSARR (SRM) model produces highly accurate snow-melt-runoff simulations around the world. (Rango 1985).

Comparison of hydrological forecasting errors for test basins in the U.S.A. resulted in a 15% accuracy for conventional techniques and 10% accuracy for remote sensing using LANDSAT (Rango 1985). During drought trials both conventional and remote sensing data had gross percentage errors but small errors in volume (Rango 1985).

All variables related to basin characteristics, for instance terrain elevation, slope, and aspect, soils, drainage information and land-use are handled by this module. Normally an off-line procedure first prepares the data bank containing all pertinent physiological information on the basin for later use in the system. A 5 x 5 km grids is recommended initially, but the size can be changed later. Land-use and soil data can be obtained and up-dated using remote sensing. An interactive procedure is suggested to restructure the original data bank according to hydrological contributing areas.

1.4 Water Resource Manager's Requirements

It is useful to look at the complexities involved in watershed modelling. Especially, the types of information required by the hydrologists. Based upon the overall goal of the modelling exercise (i.e. the water resource issue) differing types of watershed response must be analyzed (e.g., peak flows vs. runoff volume). This realization indicates the need for a multiplicity of watershed modelling capability. Table 2 shows the issues and related information requirements (Shafer and Skaggs 1983). In addition, hydrologists need to know the depression storage and active areas of a watershed; pre-storm channel conditions; and water use in the basin; identification of

Table . 2. WATERSHED MODEL CHARACTERISTICS

Model Name	Rain	Snow	Intercept	PET	Actual ET	Infil.	Soil Moisture (Zones)	Interflow	Baseflow	Overland	Channel	Deep Perc.
ANSWERS	+		+	-		O	O (1)		-	+	+	-
BSAM	-	O		O		-		-	O			-
BURP2	O	O	O	+	O	O	O (2)					+
CREAMS	O	O		+		+				O	O	+
HEC-1	O	O		-		-				O	+	
HSPF	O	+	O	-	O	O	O (2)	O	O	O	O	O
PSRM	O		O	-		O				O	O	-
PSU-IV	-										O	
Sacramento	O			O		O	O (2)	O	O	O		O
SCSTR20	O			O		O					O	
SSARR	+	+		-		-	O (1)		O	O	O	O
STORM	O	O		-		-	-					
SWMM	O			O		O				O	O	
TVA	-		O	-		-			-	-	-	
USDAHL-74	O	O	O	-	O	+	O (1)		O	O	O	-

* + = more than adequately represented

- = rough approximation

O = acceptable representation

blank indicates process not included

Source: Env. Can. 1986

all known and potential flood areas on-line (from historic, topographic and climate data assessment).

2. Methodology

The characteristics studied were land use (% / km^2), snow line location, snow water equivalent, flooded area, drainage pattern, water area, and drainage area.

2.1 Land Cover

The purpose of this study was to identify and classify land cover types which maybe related to spring runoff in the Souris drainage basin in Saskatchewan, North Dakota and Manitoba. The specific objectives were to classify three LANDSAT images; geometrically corrected to the Universal Transverse Mercator (UTM) projection; to produce a basin outline as graphics overlay; and to produce hard copy maps.

Small areas of known land cover were classified and isolated using an interactive training procedure. Four MSS bands were used. The maximum likelihood signature was created (mean and covariance). A maximum likelihood classification was performed on each image and matched. A post classification filter was run to smooth the classification and remove erratic bits of information. These programs plus the map registration and boundary generation programs are resident on a commercial remote sensing package [DIPIX (ARIES), Ottawa](Polson and Whiting 1988 and Whiting and Polson 1988).

2.2 Snow Line

The NOAA satellite data was collected by the Atmospheric Environment Service, Toronto. This data was collected for the Prairie sector. Because the receiving station is more than 2,000 km away, some images were distorted. Geometric correction was required on all images. The data were corrected to a Lambert Conformal Conic map projection. Manual interpretation was made using a fast parallelepiped classifier (a resident commercial program [DIPIX (ARIES)]) on two channels - 2 and 4. The snow areas were identified by classifying snow covered lakes, snow covered cropland and snow covered forest areas. Cloud areas were also identified. The snow line was considered to be the line between the snow covered areas and the unclassified areas.

2.3 Snow Water Equivalent

A multi-agency snow survey experiment in 1982 provided ground snow depth and water equivalent data and airborne gamma data for calibration. These provided the basis for an algorithm between the passive microwave digital data on board the DMSP satellite using the Special Sensor Microwave/Imager (SMM/I)(Goodison 1989).

2.4 Flooded Land

Three years of LANDSAT MSS data was used to define areas of flooding. Two consecutive years of flooding occurred. The third year was used as a base year. Supervised and unsupervised classifications were used. A combination of both classifications was made.

2.5 Fault Blocking

Two LANDSAT MSS images were used over an active sand dune area. The sandstone bedrock area has been subjected to uplift forces creating fault blocks. The DIPIX ARIES program has a rigorous statistical directional filter. This program creates linear feature images for each cardinal direction (45°). A Fourier transform was used to re-combine the linear feature files into a single colour image (Whiting and Wheaton 1987). These programs enhanced each edge of the blocks. The rivers were then superimposed on the block structures to show coincidence.

2.6 Antecedent Water

LANDSAT MSS imagery was used over an area 71 km x 85 km. Band combinations were enhanced and tested to aid in classification. Unsupervised, supervised and parallelepiped classifications were performed for evaluation (Kallenback and Banga 1987).

2.7 Snow Catchment

Aerial photography were used to create a DEM. First and second derivatives were created to determine active and passive areas of the watershed. Channel volume, global and local catchment, and disposal area were resolved (Whiting and Kiss 1987).

3. Physiological Input To Models

The seven characteristics, obtained by remote sensing, are described in Table 3. This table shows the project title, remote sensing source, processing to get the characteristic, agency for which the work was fulfilled, and the model into which the data was expressed. Not all of the data went into a model.

An assessment of accuracy, value and problems was also made in Table 4. The most accurate were snow catchment, snow water equivalent, and land cover. The best value for money spent and to the public is snow water equivalent. The main problems are timing of the imagery (in terms relevance, frequency,and cloud cover), expense, and confusion with the background (ice, wet snow, forest or land cover, and wet ground).

4. Conclusion

The land cover mapping would be better if LANDSAT TM data were used. Greater detail of the waterway and channel is provided by TM data. But this detail is at the expense of area covered and of course processing and storage time.

The snow line determination is not very easy. The hardest part is geometric correction of snow covered images. Snow covers the features used to correct the image. Subjectivity also creates a problem. The training area spectral signatures are not always consistent between images.

TABLE 3 PHYSIOLOGICAL INPUT TO MODELS

PROJECT	REMOTE SENSING PRODUCT	PROCESSING	CHARACTERISTICS	AGENCY	MODEL
1.land cover(3)	MSS (April)	classification mosaic	land use & area	AES	Hydrotel SLURP
2.snowline	NOAA(daily)	density slicing of band ratios	snowline & land cover	AES	index
3.SWE	DMSP	algorithm	direct input to model	AES/PhD	HEC-2
4.flooded land	MSS (April-June)	unsupervised classification	area flooded	Sask. Agri.	payment
5.fault blocking	MSS (fall)	directional filtering	drainage pattern	SRC	--
6.antecedent water	TM series	classification	area of water	Sask. Water Corp.	
7.snow catchment(2)	digital aerial imagery	DEM, 1st & 2nd derivative	area drainage & depression storage	SRC	SSARR

notes:

MSS - LANDSAT Multi-Spectral Scanner
NOAA- National Oceanographic Atmospheric Administration
DMSP- Defence Meterological Satellite Platform
SWE - Snow Water Equivalence
TM - LANDSAT Thematic Mapper
DEM - Digital Elevation Model

TABLE 4 ACCURACY, VALUE AND PROBLEMS OF PHYSIOLOGICAL DATA

PROJECT	ACCURACY(%)	VALUE	PROBLEMS
1.land cover	82	good	timing of image
2.snowline	--	poor	cloud, difficult to register
3.SWE		excellent	ice, wet snow, forest, variable tracking of orbit
4.flooded land	60	poor	wet ground, clear water
5.fault blocking	70	good	node counting (dendritic)
6.antecedent water	40	poor	size, frequency of cloud free imagery
7.snow catchment	96	good	expense

For the snow water equivalent, the geo-location was also a problem. The snow cover maps are a real-time tool for the regional hydrologist. Initial comparisons to ground data and to the snow line data (described above) show good agreement. The spatial resolution of SSM/I is sufficient to provide useful SWE estimates in regions without ground data. Wet snow and ice cause errors (Goodison 1989).

Flooded land could not be adequately determined due to lack of ground data. There was also problems differentiating wet ground, thin water covering summerfallow and/or stubble. The ground data was found to be suspect because of the remote sensing study. This error was verified by spot checks later.

The dendritic drainage distribution depends upon directional analysis and shows bedrock control. But more work is needed to plot continuity and inter-connectivity.

The antecedent water could not be readily transformed into useable data. Areas were classified and tabulated into areas of deep water, shallow water, marsh and transition (marsh to wet field). The extent of artificially drained land could not be determined (Kallenback and Banga 1988). Higher resolution and spectral ability are needed. The unsupervised classification enhanced the vegetation differences and not the waterways or water differences. The supervised was better but not very good for the smaller depressions. The parallelepiped classifier was the best.

The active part of watersheds was delineated from depression-storage areas. The DEM gave channel volume, global and local catchment, and dispersal area. The DEM was also used to refine the snow course network. A significant (38%) of the snowmelt runoff was already in the channel. With the advent of SPOT stereo pairs, DEM's can be readily created for most watersheds.

In the long-term, new models are probably required and should consider: methods for up-dating general hydrologic land cover; algorithms to determine for snow-melt-runoff relationships from snow-covered areas [better snow-melt model]; surface soil moisture from microwave data for water budget accounting and linkage to the soil profile; vegetation indices or biomass estimates; soil infiltration rates as a function of snow cover (% of basin); information on soil frost as runoff efficiency increases from 10 to 90% with increasing frost; surface temperature for evapotranspiration and interceptions calculation; and high resolution data for channel networks and overland flow considerations.

REFERENCES

Environment Canada. 1986. Review of operational remote sensing techniques and streamflow forecasting techniques - Phase I. Contract report by A.J. Robinson & Assoc. Ottawa. Ont.

Goodison, B. 1989. Determination of Aerial SWE on the Canadian Prairies using Passive Microwave Satellite Data. IGARSS'89 and 12th Can. Sym. on Remote Sensing, Vancouver. pp 1243-1246.

Hogg, W, W. Pugsley, G. Schaefer, N. Yacowar. 1985. Meteorological inputs to streamflow forecasting. Streamflow Forecasting - Proceedings of the Technology Transfer Workshop, Downsview

______. 1983. Technical Workshop Series No. 5, Inland Waters Directorate, Ottawa pp 428-447.

Hogg, W. 1986. Production of gridded data sets through integration and objective analysis of multiple source climate data, Atmospheric Environment Service, Downsview, Ont.

______, K.J. Johnstone, A.J. Hanssen, A. Niitsoo, V.L. Polavarapu. 1986 The values of satellite rainfall estimation techniques for drought monitoring Can. Hydrology Symp. (CHS-86) Regina, National Research Council (ACH) Ottawa pp 75-87.

Huschke, R.E. (es.).1959. Glossary of Meteorology (Edition 3) Am. Met. Soc. Boston, Mass.

Kallenback, B., and Banga, A. 1987. The Determination of Depression Storage and Artificially Drained Areas in the Assiniboine Basin Using Satellite Imagery. SRC Publication No. e-905-29-B-87. Technical No. 202.

Kite, G.W. 1978. Development of a hydrological model for a Canadian watershed. Can. J. of Civil Eng. 5(1) 126-134.

Kite, G.W. 1974. Hydrologic Forecasting in the Water Resource Branch, Inland Waters Directorate, Environment Canada, Ottawa.

______. G.W. 1989. Using NOAA Data for Hydrological Modelling. IGARSS '89, 12th Can. Remote Sensing Sym, Vancouver. pp 558-62.

Polson, J and Whiting, J. 1988. Agricultural and Forest Land Cover Mapping of Saskatchewan. SRC Publication No. E-905-5-E-88.

Rango, A. 1980. Operational applications of satellite snow cover observations. Water Resources Bull. 16(6) 1066-2073.

______, A. Fieldman, T. George, and R. Regan. 1983. Effective use of LANDSAT data in hydrological models. Water Resources Bull. 19(2) 165-174.

______. 1985. Assessment of remote sensing input to hydrological models. Water Resources Bull. 21(3) 423-431.

Shafer, J. M., and R.L. Skaggs. 1983. Identification and characterization of watershed models for evaluation of impacts of climate change on hydrology. U.S.A. Dept. of Energy. USI DE 179 I21.

Thomson, K., Lane, R., and Csallany, S. 1973. Remote Sensing and Water Resources Management. Am. Water Resources Assoc.

Urbana, Ill.
World Met. Organization. 1974. International Glossary of Hydrology,WMO publication # 385. Geneva, Switzerland.
Whiting, J. 1985. Preliminary Analysis of Flooded Cropland, Contact Sask. Crop Insurance. E- 905- 1-C-85.
______, J. and Wheaton, E. 1987. A Design Of A Western Canadian Real-time System for Integrated Forecasting of Basin Specific Flood and Low Flows. SRC Publication No. E905-5-E-87. Technical Report No. 195.
______, and Kiss, J. 1987. Integration of Digital Terrain Models into Ground Based Snow and Runoff Measurement. Large Scale Effects of Seasonal Snow Cover (Proceedings of Vancouver Symposium, August 1987) IAHS Publication 166. pp 375-387.
______, and Wheaton, E. 1987. Is the Largest North American Sub-arctic Sand Dune Disappearing? The Influence of Climate Change and Climate Variability on the Hydrologic Regime and Water Resources (Proceedings of the Vancouver Symposium, August 1987). IAHS Publication No. 168. pp 339-353.
______, Epp, H., and Heyland, D. 1988. Saskatchewan Technology Enhancement Program - Summary Report. SRC Publication No. E-905-4-B-88 Technical Report No. 213. Saskatoon.
______, and Polson, J. 1988. Land Cover Clasification of Satellite imagery for Kootenay and Souris River Basins. SRC Publication No. E905-17-E-88.

Questions and Answers

Jean-Pierre Fortin: I didn't see any mention of surface temperature; I think it's useful in evapotranspiration representation. Do you have any data on that?

Jeff Whiting: Most of our work is in, let's call it, "hind-casting" and not "now-casting". I think that if you are going to get into temperature and snow-water equivalent modelling then you have to start planning into your model the capability or possibility of satellite down-linking. I have some difficulty with what is meant by surface temperature measured from a satellite.

John Stewart: Was the data corrected for varying atmospheric effects?

Jeff Whiting: Yes, it was.

Robert Miller: Can you go on a little bit more about what you were saying earlier on defining surface temperature from satellites?

Jeff Whiting: How do you calibrate satellite-measured-surface-temperature to actual-surface-temperature? Do you call it 1 metre or ½ metre screen temperature? Do you call it grass temperature? Do you call it soil temperature at 1 cm or is it some reflection of the air above it? How do you correct for the atmosphere? So, what is that number that you get out?

John Stewart: Can I just make a comment on that question, Jeff? As part of the FIFE project, we were making surface temperature measurements with ground-based instruments, and relating it to satellite and aircraft data; there is still a lot more to do. One of the other problems that comes up, if you are trying to estimate surfaces fluxes, is the problem of knowing what the satellite is exactly measuring. For example, we were getting a sparse grass situation in an area that was fairly heavily grazed. The important factor was what combination of soil and vegetation cover is actually contributing to the satellite or aircraft measured temperature. As a result, one of the queries that we ended up with is what is meant by "surface temperature"? We found that their is a difference between what some people call the "aerodynamic surface temperature" (defined as the temperature which if used with a transfer coefficient derived from micrometeorological data gives you the correct sensible heat-flux into the atmosphere) and the "radiative surface temperature" (as attained by an infra-red thermometer). It is also suggested by our study results that these temperatures are in turn different to what is called the "kinetic temperature". So, there are certainly unresolved problems in measuring a radiative surface, even when you're not having to go through a large piece of atmosphere to do it. We know that when there is a large piece of atmosphere, as well, there are additional problems. If indeed that atmosphere has a lot of water vapor in it, then you've also got large atmospheric corrections corrections to put into your computation to get to a "true" radiative surface temperature. Then, as I say, one has this problem of what is meant by "radiative surface temperature".

SESSION 1B
HYDROLOGIC MODELS II

Session Chairman: J. Whiting, Saskatchewan Research Council

Enhancing Rainfall-Runoff Modelling of Mixed Land Use / Land Cover Areas with Remote Sensing

by

N. Kouwen, E.D. Soulis and A. Pietroniro.
Department of Civil Engineering
University of Waterloo
Waterloo, Ontario, Canada, N2L 3G1

ABSTRACT

WATFLOOD, a micro-computer based watershed management system, and SIMPLE, its complementary distributed hydrologic model are described. Both are co-ordinate based and specifically designed to incorporate remotely sensed data. Calibration and validation results are presented for rainfall-runoff events on Ontario watersheds.

INTRODUCTION

The rainfall-runoff process is a non-linear process and is strongly affected by the vegetative cover and soil characteristics of a watershed. There has been a trend towards distributed, process-based modelling of the rainfall-runoff process to eliminate the need to lump the various contributing factors. To some extent, the need to lump hydrologic parameters for mixed land uses and land covers has prevented progress in the development of hydrologic models larger than the field scale because the parameter values have reflected the mix of the land surface characteristics rather than physically meaningful parameters such as permeability or resistance coefficients.

Some new models have appeared (Abbot et al., 1986; Kouwen, 1987) and older well known models such as the SSARR model (Rockwood et al., 1988) are being revised to reflect the physical processes affecting runoff. Regardless of the modelling approach, remotely sensed imagery provides some of the detailed watershed data required to improve hydrologic modelling by allowing the use of sub-watersheds or "elements" that can be considered as hydrologically homogeneous.

The paper describes how remotely sensed data is used in a micro-computer based flood forecasting system. The data management system and the hydrologic model are called WATFLOOD and SIMPLE respectively. WATFLOOD provides the menu-driven interface for entering and checking rainfall, streamflow and reservoir release data. SIMPLE is a distributed rainfall-runoff model.

WATFLOOD DATA MANAGEMENT SYSTEM

It is generally accepted that hydrologic models can still be improved. This is obvious from the regular appearance of new models in the literature. Presumably, each one was created as a solution to a particular problem or a claimed improvement of existing models. In this regard, SIMPLE is no exception. It was originally developed as a model for flash flood forecasting in a real-time situation. It is equally obvious that hydrologic models must become much more "user friendly". Fortunately, the introduction of powerful micro-computer systems has made both goals attainable.

First, micro-computers have greatly reduced the cost of developing programs. It is estimated that the main-frame computing cost of developing SIMPLE would have been at least 0.5 million dollars in computer time alone. Instead, most of the original computational work was done on equipment costing roughly $20,000. Secondly, inexpensive software development tools are available for micro-computers. The result is that menu driven data management systems are relatively easily developed. The Micro Interactive Design of Urban Stormwater Systems (MIDUSS) and WATFLOOD are examples.

The WATFLOOD system is used through a main menu (Figure 1) and a utilities menu (Figure 2). The main menu takes the user through each of the steps required to produce a flood forecast. The items in the main menu are self-explanatory. If weather radar is available for a particular watershed, the radar rainfall data can be downloaded in the CAPPI (Constant Altitude PreciPitation Index) format. The CONVERT CAPPI entry on the menu initiates software to convert rainfall index values to rainfall rates and extracts the data for the watershed being modelled. If radar data is not available, or if the radar data needs to be adjusted to raingauge data, raingauge rainfall data can be entered in a spreadsheet format as shown in Figure 3.

The utilities menu allows the user to execute SIMPLE in several modes, namely a model calibration mode, a forecast mode in which the initial soil moisture is updated before a forecast is made, and a single run mode in which all parameter values are pre-specified. In addition, the utilities menu allows the simulation of a historic event that has been previously entered as a data set or it can initiate a new set of files so new data can be entered through the spreadsheet-like data entry screens as shown in Figure 3. This figure shows the screen layout for entering raingauge data. Similar screens appear when the user selects the streamflow and reservoir input menu items.

Not seen by the user are several basin files. These files contain the locations of rainfall and streamflow gauges as well as reservoirs located in the watershed. The largest file is the basin file. This file contains all the watershed information, including the land cover classifications for each element of the watershed. It also contains information about the drainage pattern, stream slopes, and basin coordinates. Another file contains the values of all model parameters such as roughness and permeability. These files are created only once for each watershed and are formatted files created with any standard editor. The WATFLOOD system becomes user friendly once these files exist. A users manual provides all the information needed to create these files (Kouwen, 1986).

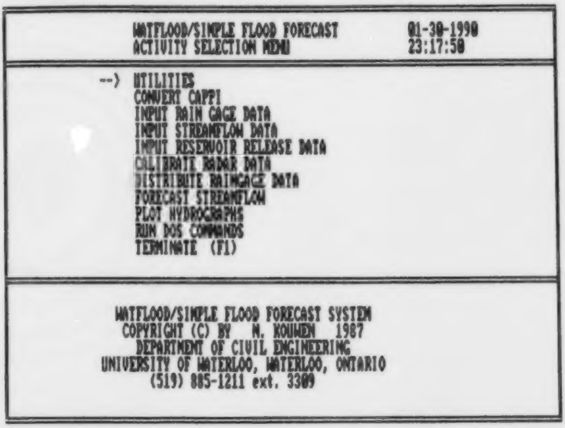

```
        WATFLOOD/SIMPLE FLOOD FORECAST          01-30-1990
        ACTIVITY SELECTION MENU                 23:17:50

    --) UTILITIES
        CONVERT CAPPI
        INPUT RAIN GAGE DATA
        INPUT STREAMFLOW DATA
        INPUT RESERVOIR RELEASE DATA
        CALIBRATE RADAR DATA
        DISTRIBUTE RAINGAGE DATA
        FORECAST STREAMFLOW
        PLOT HYDROGRAPHS
        RUN DOS COMMANDS
        TERMINATE  (F1)

      WATFLOOD/SIMPLE FLOOD FORECAST SYSTEM
       COPYRIGHT (C) BY   N. KOUWEN   1987
        DEPARTMENT OF CIVIL ENGINEERING
    UNIVERSITY OF WATERLOO, WATERLOO, ONTARIO
           (519) 885-1211 ext. 3309
```

Figure 1 - Main menu for the WATFLOOD data management system

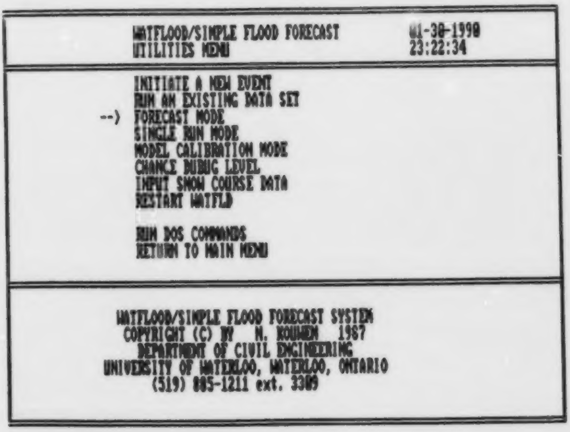

```
        WATFLOOD/SIMPLE FLOOD FORECAST          01-30-1990
        UTILITIES MENU                          23:22:34

        INITIATE A NEW EVENT
        RUN AN EXISTING DATA SET
    --) FORECAST MODE
        SINGLE RUN MODE
        MODEL CALIBRATION MODE
        CHANGE DUBUG LEVEL
        INPUT SNOW COURSE DATA
        RESTART WATFLD

        RUN DOS COMMANDS
        RETURN TO MAIN MENU

      WATFLOOD/SIMPLE FLOOD FORECAST SYSTEM
       COPYRIGHT (C) BY   N. KOUWEN   1987
        DEPARTMENT OF CIVIL ENGINEERING
    UNIVERSITY OF WATERLOO, WATERLOO, ONTARIO
           (519) 885-1211 ext. 3309
```

Figure 2 - Utilities menu for the WATFLOOD data management system

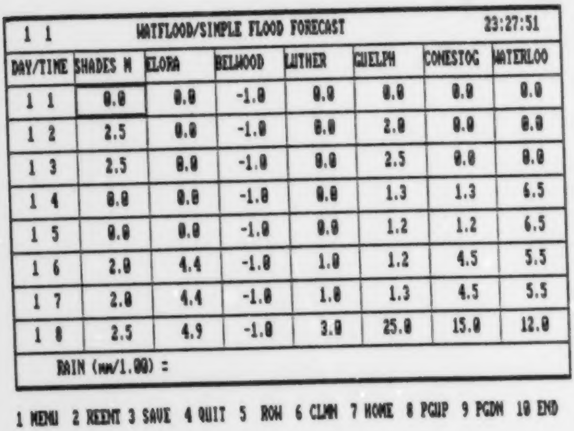

1 1 WATFLOOD/SIMPLE FLOOD FORECAST 23:27:51

DAY/TIME	SHADES M	ELORA	BELWOOD	LUTHER	GUELPH	CONESTOG	WATERLOO
1 1	0.0	0.0	-1.0	0.0	0.0	0.0	0.0
1 2	2.5	0.0	-1.0	0.0	2.0	0.0	0.0
1 3	2.5	0.0	-1.0	0.0	2.5	0.0	0.0
1 4	0.0	0.0	-1.0	0.0	1.3	1.3	6.5
1 5	0.0	0.0	-1.0	0.0	1.2	1.2	6.5
1 6	2.0	4.4	-1.0	1.0	1.2	4.5	5.5
1 7	2.0	4.4	-1.0	1.0	1.3	4.5	5.5
1 8	2.5	4.9	-1.0	3.0	25.0	15.0	12.0

RAIN (mm/1.00) =

1 MENU 2 REENT 3 SAVE 4 QUIT 5 ROW 6 CLMN 7 HOME 8 PGUP 9 PGDN 10 END

Figure 3 - Raingauge data input template

HYDROLOGIC MODEL

SIMPLE is a conventional hydrologic model using textbook hydrologic abstractions such as the Philip (1954) infiltration equation and storage routing. However, SIMPLE is unconventional in that the runoff in each sub-basin element is calculated as separate contributions for each of six different land cover classes as inferred from LANDSAT Multi-Spectral Scanner (MSS) imagery. The runoff from these separately contributing areas is then combined and routed jointly in the river system.

Furthermore, SIMPLE utilizes a coordinate based or square grid approach to delineate sub-catchments. Huggins and Monke (1966) appear to be early promoters of this type of model. When work on SIMPLE was started in 1972, it was becoming apparent that remotely sensed data such as LANDSAT imagery and radar constant altitude precipitation index maps would be available to the hydrologist in the future. The most direct method to incorporate such data is a coordinate based model (Kouwen, 1973).

In SIMPLE, it is assumed that the hydrologic response is uniquely related to the land cover classes as inferred form LANDSAT MSS imagery. This approach has been applied to the Grand, Saugeen, Humber, and Eastern Metropolitan Toronto watersheds by calibrating the model to the Grand River watershed above Cambridge, Ontario and then performing validation on the other basins. The predicted hydrographs closely resemble the measured hydrographs in shape, time to peak, and total runoff. Some typical results are shown in a later section.

As with other rainfall-runoff models, SIMPLE is to some extent a reflection of its creators perception of nature. A perusal of any modern hydrology textbook reveals many approaches to represent each component of the hydrologic cycle. However, the main criteria for selecting each of the model's components were that they should affect the short term contribution to river flow, be computationally efficient, be of approximately the same level of sophistication, and represent the physical processes as closely as the first two criteria allow. Based on these selection criteria, the following processes were included in SIMPLE:

interception - exponential relationship with accumulated precipitation (Linsley et al., 1949)
infiltration - the hydraulic conductivity formula (Green and Ampt, 1911; Philip, 1954)
depression storage - maximum amounts (ASCE, 1969)
interflow - linear storage-discharge function
base flow - recession curve
overland flow - storage routing with Manning's formula
channel flow - storage routing with Manning's formula

The processes that are modelled occur primarily at the surface, and are thus most likely to benefit from an improved land cover description (Tao and Kouwen, 1989). The exclusion of other factors such as snowmelt and evaporation has no significant effects on the results in this paper since the model was tested only for rainfall-induced flood forecasting in moderate climates. Research is in progress to incorporate longer term phenomena in order to extend SIMPLE's range of applicability.

In SIMPLE, the Philip formula (Philip, 1954) is used to calculate the infiltration rate. The formula is identical to the Green and Ampt (1911) formula with the exception that surface ponding is added to the capillary potential to calculate the hydraulic gradient. As well, Philip provided a straightforward method to calculate the capillary potential as a function of soil permeability.

The entire routing sequence is based on storage (simple) routing, which is one of the reasons for naming the model SIMPLE. A number of other routing schemes have been compared for Southern Ontario rivers but all provide similar results (Kouwen, 1983; Kouwen and Ding 1986; unpublished student papers). The storage routing method has the advantages of computational efficiency and insensitivity to grid size (Kouwen and Garland, 1989; Tao and Kouwen, 1989a)

Resolution Requirements -A tendency in hydrologic modelling is to use elemental areas that are small enough to be considered homogeneous from a hydrologic point of view. Bathurst (1986) suggests that a watershed may have to be divided into at least 100 sub-watersheds for the purpose of modelling the rainfall-runoff process. In the extreme, the smallest resolution that could be considered for areas such as Southern Ontario is the 79 m pixel of the imagery being used to classify the land cover. This is because digital LANDSAT composite colour imagery shows variation in most individual pixels, indicating at least some difference in vegetation or underlying soil characteristics between each neighbouring pixel.

Depending on the purpose of the model, and therefore the number of physical processes modelled, vast amounts of computational effort might be needed. If the purpose of the model is flood forecasting, the turn around time for data input, data correction and the production of the forecast needs to be very short and the computer on which the work is carried out must be able to continue irrespective of power outages and communications breakdowns. The micro-computers available today ideally suit this purpose as long as the spatial resolution of the model is not so excessive that execution time becomes too long.

Previous research with SIMPLE has dealt with the resolution requirements for modelling flood flows on the Grand River watershed and several of its sub-watersheds, with drainage areas ranging from 125 to 3520 kilometers square. It was concluded that from five to 25 elements adequately represent the drainage area and pattern of the basins as long as spatial variations in the rainfall were adequately preserved. This requirement leads to an element size of no more than approximately 10 km by 10 km when modelling flash floods (Kouwen and Garland, 1989).

Based on the above criteria, the grid sizes used in this paper were 10 km by 10 km for the Grand and Saugeen watersheds, which have drainage areas of 3520 and 4056 square km respectively. For the Humber and the Eastern Metropolitan Toronto basins, a 4 km by 4 km grid size was used for areas ranging from 350 to 900 square km. Such a grid size results in a mix of different land cover classes in each element and therefore sub-basin or element based parameters would reflect the relative amounts of each class in a sub-watershed. For this reason each computational element is subdivided into six contributing areas: one for each hydrologically significant land cover class and proportioned according the the number of pixels designated to each class by a maximum likelihood classifier. The model parameters were then calibrated for each of four identifiable land cover classes namely, barren land, lightly vegetated land (cropland), forest, and wetland. Water covered areas were also extracted but no parameters needed to be estimated for this class.

Urban areas were grouped with barren areas. Subsequently, the impervious area was estimated through the use of commonly accepted textbook values.

METHODOLOGY AND RESULTS

Calibration - Three events were linked in one run to calibrate the model parameters on the Grand River watershed. Since all the land cover classes are represented in each computational element and each sub-watershed (based on Canada Water Survey streamgauge locations), the calibration can only be successful if the relative amounts of each class varies among sub-watersheds. Tables 1 and 2 show the percentages of each land cover class for each of five sub-watersheds of the Grand. Ideally, the ratio of the classes would vary more. A more consistent set of parameters would likely be found. However, even variations shown in these tables appear adequate for the purpose of calibrating the model parameters.

TABLE 1 - Percent of Land Cover Classes on the Grand River Watershed

Basin Number	Barren %	Forest %	Cropland %	Wetland %	Water %
1	12	14	48	26	0
2	10	4	70	16	0
3	6	11	61	20	0
4	11	14	47	28	0
5	6	18	62	13	0

TABLE 2 - Percent of Land Cover Classes on the Saugeen River Watershed

Basin Number	Barren %	Forest %	Cropland %	Wetland %	Water %
1	15	19	52	12	2
2	18	14	50	15	3
3	11	21	56	10	2
4	8	25	45	20	2
5	14	14	62	6	4

Figure 4 shows the results of the calibration. The measured peak flows are plotted along the horizontal axis and the computed peak flows along the vertical axis. If the computed flow is equal to the measured flow, the point falls on the diagonal line. The crosses compare the peak flows for three events at eight Canada Water Survey streamflow gauges. There is a substantial amount of scatter, which is due to measurement errors as well as modelling errors. However, the peak flows used for the calibration are relatively small and experience with the model indicates it performs better for events having more rainfall, which is to be expected given the model's emphasis on flood forecasting.

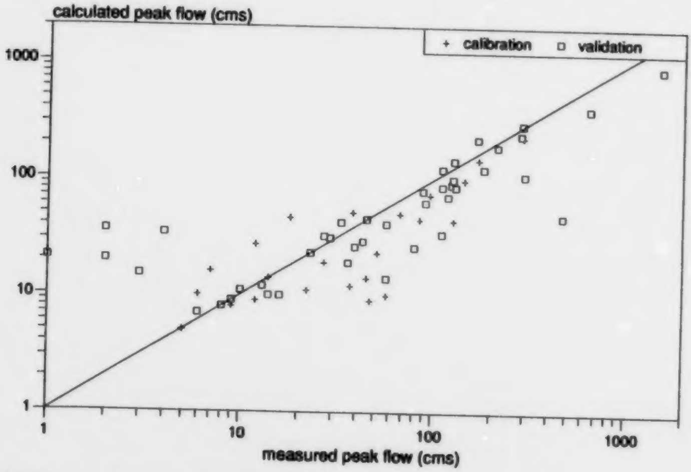

Figure 4 - **Measured versus calculated peak flows for the Grand River Calibration and validation in time**

Validation - Next the model was used to simulate eight different events over the Grand River basin, seven on the Saugeen and Humber River basins, and five on the watersheds just east of Metropolitan Toronto. Figure 4 also shows the result of the validation in time for the Grand River. In this figure the boxes compare the calculated to the measured flows. These results are encouraging because the scatter for the validation points appears to be slightly less than for the calibration runs for many of the basins.

The points at the left side of the figure are for the Eramosa watershed, which is located near the Niagara escarpment on limestone and has karst drainage system. This results in systematic over estimation of the flow. Fortunately, the flows are very small and do not contribute significantly to downstream flood flows. One other point on the right side of the graph is greatly in error. This point is for a September 1986 event when the raingauges appear to have missed much of the rainfall.

Figures 5, 6, and 7 show the results of the validation runs for the Saugeen, Humber, and Eastern Metropolitan Toronto Rivers respectively. The results for the Saugeen indicate that the model parameters calibrated to the Grand River data can be applied to the Saugeen River basin. The results for the Rouge River to Oshawa Creek watershed are not as good as for the Saugeen and the Humber River simulation produced unsatisfactory results.

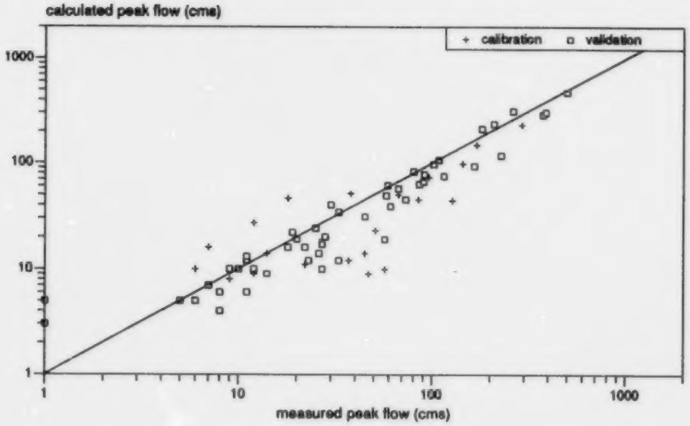

Figure 5 - Measured versus calculated peak flows for the Saugeen River Calibration and validation in space

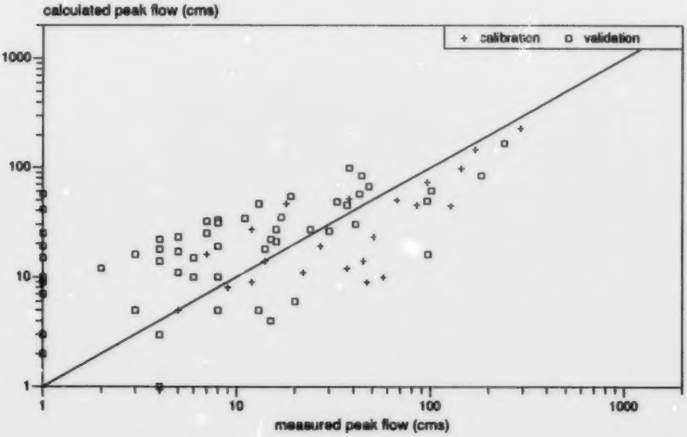

Figure 6 - Measured versus calculated peak flows for the Humber River Calibration and validation in space

Parameter sensitivity - As a check on the validity of the calibration of the model, parameter values for various land cover classes were interchanged to determine the sensitivity of the model to those parameters. For instance, the permeability and interflow parameters were interchanged for forested and cropped lands. These parameters have very different values for each land cover class and have the proper relative values. Figures 8 and 9 show the effect of this exchange. Figure 8 is based on the calibrated parameters and Figure 9 is based on the wrong parameters for a September 1986 event on the Grand River watershed. The degradation of the computed hydrograph is clear. This lends some validity to the calibration process.

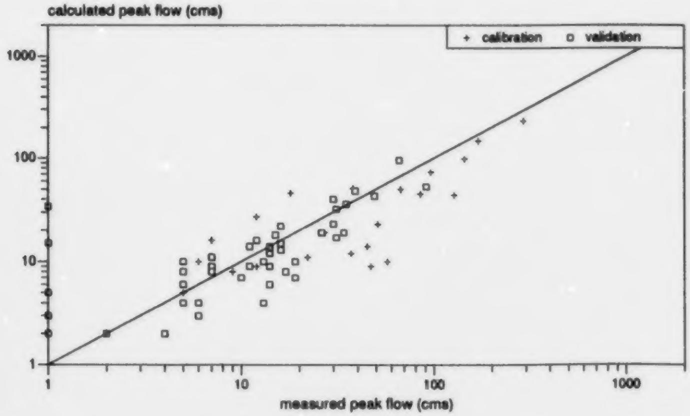

Figure 7 - Measured versus calculated flows - East Metro Toronto basins
Calibration and validation in space

DISCUSSION

The universality of the parameters for particular land cover classes has not been conclusively established by the results shown above because the figures show that the validation in space is most successful for the watershed that is most like the Grand River in terms of the land cover mix. The Eastern Metropolitan Toronto watersheds are somewhat like the Grand River and the Humber River is the most unlike the Grand River because it is heavily urbanized in its lower parts. The problems with the Humber River may have resulted from the method used to classify the LANDSAT image or the very poor distribution of the raingauges in the basin. The urbanized area was combined as one class rather than treating the pervious and the impervious areas as two distinct classes during the classification of the image. At the time of writing the images are being reclassified in an effort to delineate impervious areas from LANDSAT MSS data and radar imagery is being included to improve the rainfall input to the model.

However, while the universality of the parameters in a particular physiographic region will not be proven until the validation results are equally as good as those for the Saugeen River for a watershed having a substantially different mix of vegetative cover, the method of calibrating parameters on a land cover class basis appears promising and research is continuing to gain more confidence in the method.

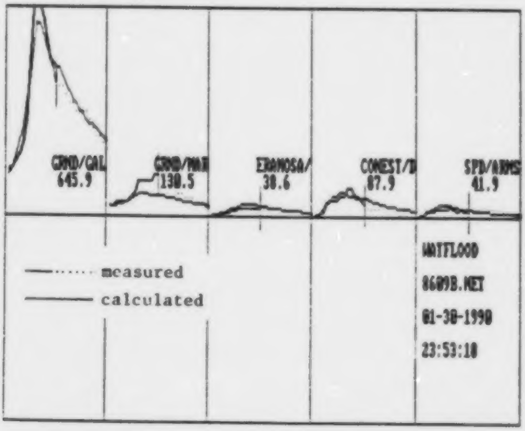

Figure 8 - Parameter sensitivity analysis: correct parameters

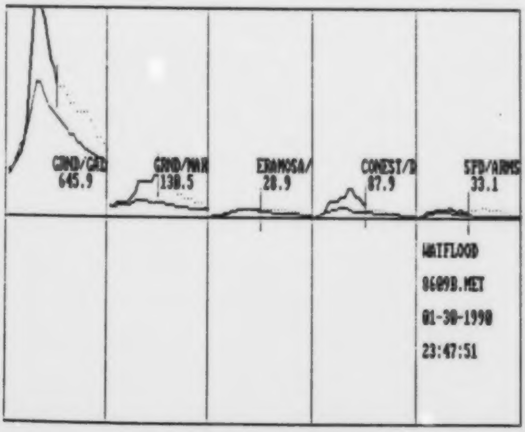

Figure 9 - Parameter sensitivity analysis: incorrect parameters

REFERENCES

Abbot, M.B., Bathurst, J.C., Cunge, J.A., O'Connell, P.E., and Rasmussen, J., 1986, "An Introduction to the European Hydrological System - Systeme Hydrologique Europeen, 'SHE', 1: History and Phylosophy of a Physically-based, Distrubuted Modelling System", Journal of Hydrology, Vol. 87, pp. 45-59.

ASCE (1969) "Design and Construction of Sanitary and Storm Sewers", Manuals and Reports on Engineering Practice-No 37 (WFCF Manual of Practice No. 9), Am. Society of Civil Engineers, New York, NY.

Bathurst, J.C., 1986, "Sensitivity Analysis of the Systeme Hydrologique Europeen for an Upland Catchment", Journal of Hydrology, Vol. 87, pp. 103-123.

Brandes, E.A. 1975: "Optimizing rainfall estimates with the aid of radar", J. of Applied Meteorology, vol.14, no.10, pp.1339-1345.

Browning K.A. and C.G. Collier, 1989, "Nowcasting of Precipitation Systems", Rev. of Geophysics, Vol. 27, No. 3, August, pp. 345-370

Green, W.H., and Ampt, G.A., 1911, "Studies in Soil Physics, 1, The Flow of Air and Water through Soils", Journal of Agricultural Science, Vol. 4, pp. 1-24.

Huggins, L.F. and E.J. Monke, 1966, "The Mathematical Simulation of the Hydrology of Small Watersheds", Purdue University, Water Resources Research Center, Technical Report No. 1, August.

Linsley, R.K., Kohler, M.A., and Paulhus, J.L.H., 1949: Applied Hydrology, McGraw-Hill, 689pp.

Kouwen, N. and G. Garland, 1989, "Resolution Considerations in Using Radar Rainfall Data for Flood Forecasting", Canadian Journal of Civil Engineering. June, pp. 279-289.

----------, 1988: "WATFLOOD: a micro-computer based flood forecasting system based on real-time weather radar", Canadian Water Resources Journal, vol.13, no.1, pp.62-77.

---------- and J. Ding, 1986, "Dynamic Wave Flood Routing Sensitivity Study", Proceedings, CSCE Annual Conference, Toronto, May, Vol. 3, 25 pages.

----------, 1986, "SIMPLE - A Watershed Model for Flood Forecasting", Users Manual, Department of Civil Engineering, University of Waterloo, Waterloo, Ontario. March, 92 pages.

----------, 1983, "VSC Flood Routing for Ontario Rivers on Apple II", Proceedings, Engineering Foundation Conference; Emerging Computer Techniques in Stormwater and Flood Management, Nov.

----------, "Watershed Modelling Using a Square Grid Technique", Proceedings, First Canadian Hydraulics Conference, Edmonton, Alta., May 1973, pp. 418-434.

Philip, J.R. 1954: "An infiltration equation with physical significance", Soil Science, vol.77, January-June.

Rockwood, D.M., D.D. Speers, E. Davis, 1988, "Operational Forecasting in Complex River Basins with SSARR-Micro Versus Mainframe Computer", Proceedings, 3rd Water Resources Operations Management Workshop, Water Resources Planning and Management Division, ASCE, Colorado State University, Fort Collins, Colorado, June 27-30, pp. 302-312.

Smith, A.A., 1986, "MIDUSS User's Mannual", Version 3.2 for the IBM-PC, etc., Alan A Smith Inc., Dundas, Ontario, Canada.

Tao T., and N. Kouwen, 1989, "Remote Sensing and Fully Distributed Modeling for FloodForecasting", Journal of Water Resources Planning and Management, ASCE, Vol. 115, No. 6, November, pp. 809-823.

Tao T and N. Kouwen, 1989a, "Spatial Resolution in Hydrologic Modelling", Proceedings of the Internatgional Conference for Centennial of Manning's Formula and the Kuichling's Rational Formula, University od Virginia, 22-26 May, pp. 166-175.

Questions and Answers

Michael Quick: Where is the base for sediment production from?

Nick Kouwen: It is a two part model that is being developed by the Department of Agriculture in Fort Collins and it is a detachment from a transport model. It is somewhat different and is more like the model of Dave Hartley who published on this topic a few years ago.

Michael Quick: It is calibrated on their data, is it?

Nick Kouwen: No, it is not really calibrated at all. I am just using some values that we guessed at relative to what they have used for crops. It is not a calibrated model; we are just getting to the point where we have sediments coming off.

Michael Quick: It is not calibrated by you, but it's been pre-calibrated by them with their data set?

Nick Kouwen: It is agricultural though, with the emphasis on the forest-logging type of situation, so we just included it. In the Tri-Creek area we do have sediment data over a period of about 15 years as logging progressed. But it has not been very helpful, just yet, because it seems that most of the sediment is coming from roads, rather than from the areas that are logged. So, we can make this model do almost anything, but we do not know the origin of the sediment.

Jeff Whiting: Do you have any feel for why the Landsat data is giving you some increase in accuracy?

Nick Kouwen: Why it is? Well, it's simply because if you don't use the Landsat data then the parameters for a basin really reflect a mix of vegetation. So, if you have 50% of vegetation and 50% of pasture, or 50% forest and 50% pasture, you get a parameter for that watershed for, say, permeability or roughness. When you change those ratios, then your roughness changes, not because it changes in the forest or on the pasture, but because the overall ratio changes. People are used to using weighted coefficients for roughness or runoff coefficients and so on, but you do not have to do any weighting with this method at all. You simply find the coefficient for a particular vegetative cover. That is why we could move the model to the Saugeen basin with exactly the same parameters; granted it's a similar geographic area, so that is why these same parameters probably work. Now, we are just trying this model out around Thunder Bay, and I expect the parameters to be quite different.

SURFACE HYDROLOGY IN CLIMATE MODELS: THE ROLE OF REMOTE SENSING

G. Thomas, Dept. of Geography, University of British
Columbia, 1984 West Mall, Vancouver, B.C. V6T 1W5.

1. Introduction

The emergence of a coherent greenhouse theory of climate change has prompted a number of important developments in the atmospheric sciences. The physical foundations for the theory have been firmly laid by developments in radiative transfer and absorption-line measurements. Translating the radiative effects of altered atmospheric chemistry into adjustments in the climatological regime of the earth has been made possible by developments in numerical modeling techniques. Thus, general circulation climate model (GCM) studies suggest that current trends in atmospheric carbon dioxide and other radiatively active trace gase concentrations will result in historically significant increases in global temperature and changes in global and regional precipitation patterns (e.g. Hansen et al., 1988; Rind, 1988). Providing a consistent picture of the impacts of such changes presents one of the most difficult and as yet unresolved challenges of the next few decades. Considerable emphasis is currently being placed on the role of climate models as a means of providing realistic projections of climate change. One of the most important consequences of future climate change may be an alteration of the surface hydrologic balance, including changes in streamflow and soil moisture and ground water recharge. Since water is a basic resource of human activities, any variations in the distribution and availability of surface water will undoubtedly result in some socio-economic adjustments.

This paper reviews the current status of the parameterization of land-surface processes in climate models. The role of remote sensing as an aid to their design and as a means of increasing understanding of the role of surface processes is emphasised.

2. The Use of Climate Models in Hydrological Impact Studies

Recent years have witnessed an increased use of the results of climate model sensitivity studies as a means of providing climate forcing for hydrologic models. In addition, the hydrologic quantities calculated in climate models are being directly interpreted as representing the potential sensitivity of surface processes to climate change. However, considerable caution should be exercised in both these cases. As described in the following section, climate models differ fundamentally in their representation of surface moisture transfer processes. In particular the model hydrologic processes and parameters may bear little relation to their hydrologic definitions. While it is apparent that GCMs provide a considerable lack of consistency in terms of the nature of regional climate change, the results are also sensitive to the complexity of representation of surface processes.

2.1 Parameterization of terrestrial processes

Although the rationale for incorporating a physically realistic representation of surface processes in GCMs is clear, the reality of the modelling is not. Consequently there exist a variety of modelling approaches in current use (Table 1). All of these parameterization schemes are to some degree physically based and therefore represent an improvement upon the 'bucket' style schemes used previously (e.g. Shukla and Mintz, 1982). Much recent work has focussed on improved representations of terrestrial hydrology and explicit modelling of vegetative canopy processes. In particular canopy interception of radiation and moisture and the role of plant physiology in controlling transpiration through stomatal resistance may be incorporated directly. The results of recent numerical experiments (e.g. Hunt, 1985; Dickinson and Henderson-Sellers, 1988) suggest that the Budyko 'bucket' formulation (e.g. Manabe, 1969) is generally inadequate for the representation of terrestrial surface and sub-surface moisture flows. Thus, single layer sub-surface thermal and hydrological representations are being replaced by multilayer models. This allows horizontal moisture transfer to be incorporated. An additional requirement is the need to take account of subgrid-scale variability of both precipitation and surface properties. Currently, only two of the available parameterization schemes explicitly incorporate some measure of spatial variablity of processes and parameters within the model grid-element. Overall, the past decade has seen the development of land-surface parameterization schemes that are underlain by a firmer physical basis. Recent model integrations suggest that the incorporation of these improved parameterization schemes produces a more realistic partitioning of energy at the land surface (e.g. Sato et al., 1989). However, coincident with such improvements in the ability to model land-surface processes are a number of unresolved problems. In particular, assessments of the validity of the more sophisticated parameterization schemes are limited by poor parameterization of surface forcing terms such as solar radiation and precipitation. Following on from this is the urgent need for both 'parametric' data for initialization of the models and 'observed' surface variables to allow validation of the model performance. Such data is required at an appropriate resolution.

2.2 GCM representation of global and continental-scale hydrology

The observed average annual precipitation and runoff for the terrestrial surface of the earth are shown in Figure 1 together with the values for three versions of the National Centre for Atmospheric Research (NCAR) Community Climate Model (CCM). The model is spectral in nature although physical processes are still calculated on a Gaussian grid (consequently the model spatial resolution is described rather than the spectral wavenumber truncation). T42 is a version of the model with a horizontal spatial resolution of 2.8 latitude and 2.8 longitude and with a 'bucket' style surface hydrological representation. R15 is a coarser resolution (horizontal spatial resolution of 4.5 latitude and 7.5 longitude) version also with a bucket style surface hydrology. R15B also has a horizontal resolution of 4.5 latitude and 7.5 longitude, but incorporates a 'complex' model of the surface hydrological processes. Clearly the modeled values are excessive compared to the observed. The models produce approximately 35% in excess of the observed precipitation and 31% in excess of the observed runoff. T42 is the 'wettest' model with R15B and R15 being somewhat drier. The ratio of runoff to precipitation (i.e. the runoff ratio) for the mean values of the observations is 0.36 compared to 0.38, 0.33 and 0.35 for T42, R15B and R15 respectively. Thus the models produce the same proportion of runoff compared to precipitation as do the observations.

The observed and modeled average annual precipitation and runoff for the (inhabited) continents are shown in Figures 2 and 3 respectively. In terms of the observed precipitation there is little variation in the mean values for the continents of North America, Europe, Asia and Africa (although the spread in the observed estimates is noticeably larger for the first three of these continents). South America and Australia are the 'wettest' and 'driest' of the continents respectively. The modeled continental average precipitation exhibits a number of features. For North and South America and Africa there is a tendency for each version of the CCM to produce too much precipitation. This is particularly the case for T42 for South America which produces more than 2500 mm compared to the observed value of approximately 1500 mm. T42 also produces the largest average values for Africa and Australia. There is much better agreement in terms of the modeled precipitation for Europe and Asia, while all three model versions uniformly overestimate the average annual precipitation for North America.

The observed runoff for the continents basically reflects the variation in precipitation. South America produces the largest runoff value of approximately

650 mm. There is little variation in the magnitude of runoff for North America, Europe and Asia. Africa produces approximately half the runoff of these three continents, while Australia produces less than half of the African value. The latter reflects the proportion of desert found in these two continents. The variation in observed estimates for individual continents is greatest for North and South America. The modeled continental average runoff exhibits somewhat greater variation than is the case for precipitation. In particular the runoff values for South America vary from 566 mm for R15 to 1139 for T42 compared to the observed figure of approximately 680 mm. Both Africa and Europe exhibit a wider variation in simulated runoff values, while for Asia and Australia there is a much better agreement between the observed and modeled figures. The models uniformly overestimate the total runoff for North America. The observed runoff ratios for North and South America, Europe and Asia are all within the range 0..39–0.43. For Africa the ratio is 0.21 and for Australia 0.09.

It is clear that at the largest spatial scales a number of difficulties remain in the representation of surface hydrology. Although the above results are inconclusive regarding the major problem of determining the required complexity of surface processes necessary for incorporation in climate models, they do imply that an adequate test of the hydrologic representation requires a much higher resolution. These results should be kept in mind in interpreting specific model studies of the hydrologic response to climate change, as described in the following section.

2.3 GCM sensitivity studies

There have been a number of recent climate modelling studies designed to investigate the (modelled) climate sensitivity to perturbations in surface properties and processes (Table 2). A number of modelling studies have focussed on the role of surface albedo changes in modifying climate. Recently, Laval and Picon (1986) used the LMD GCM to investigate the sensitivity to a prescribed change in the surface albedo of the Sahel region. In response to the specification of an 'anomalous' albedo of 0.35, they reported reduced precipitation and evaporation rates. In addition, the zonal circulation over the Sahel was perturbed. Cunnington and Rowntree (1986) also report results of a study designed to test the sensitivity of the Sahelian climate to surface proceses. In particular, they report that the use of more realistic albedos tends to transfer rainfall from regions of higher albedo (e.g. deserts) to regions of lower albedo (e.g. forests). Shukla and Mintz (1982) and Delworth and Manabe (1988) provide some interesting insights into the role of evapotranspiration in determining climate sensitivity. The former study involves a global prescription of 'wet' and 'dry' land surfaces. The latter study discusses the influence of potential evaporation on the variabilities of simulated soil wetness and climate. Sud and Smith (1985) and Heasman (1987) have used GCMs to investigate the effect of changing surface roughness length. In the former study, the roughness length of the globe's deserts was reduced from 45 cm to 0.2 mm. This resulted in a decrease in precipitation in the perturbation experiments, which was attributed to reduced horizontal water vapour convergence into the region and to cooling of the boundary layer. Heasman (1987) tested the sensitivity of the UKMO GCM to an increase in the surface roughness for all land points. Increasing surface roughness resulted in an improved (shallower) simulation near the Aleutians and the Western United States. The climate response to soil moisture anomalies has been the focus of a number of numerical modelling studies. For example, Rind (1982) used a coarse-resolution GCM to examine the effect of continent wide reductions in soil moisture. The model predicted an increase in surface temperature and a decrease in precipitation. Oglesby and Erickson (1989) examined the climate response to an imposed soil moisture anomaly over North America. A reduction in summertime soil moisture resulted in an increase in surface temperature, lower surface pressure, increased ridging aloft and a northward shift of the jet stream. Precipitation was also reduced due to reduction in evaporation and enhanced subsidence aloft. A number of additional studies have investigated the climate response to aggregated changes in surface parameters presumed to occur as a result of vegetation removal. Henderson-Sellers and Gornitz (1984) considered the impact of removing the Amazon tropical forest in the GISS GCM. Changes in albedo, roughness and soil moisture holding capacity resulted in reduced regional precipitation, evaporation and cloud. The study by Cunnington and Rowntree (1988) investigates the sensitivity of a GCM to changes in atmospheric watercontent, soil moisture content, radiation scheme and albedo. The results reveal the importance for a good Saharan simulation of the initial atmospheric and surface moisture specifications. In addition, an extension of Charney's hypothesis to include moisture is proposed in which any increase in diabatic heating, whether due to reduced albedo or increased moisture availability, must be compensated by increased cold advection. Lean and Warrilow (1989) investigated the sensitivity of the Amazon region to deforestation. Changes in roughness and albedo resulted in reductions in precipitation and evaporation.

In conclusion, it is apparent that model sensitivity studies demonstrate that the specification of surface parameters has important consequences for atmospheric fields. In particular, changes in surface hydrology appear at least as important as changes in albedo. Although such results are sensitive to the parameterizations inherent in the models there exists considerable evidence to substantiate the important role of terrestrial processes in climate change studies.

3. Remote sensing possibilitites

The previous sections demonstrate a clear requirement to provide data on a variety of surface parameters and processes. Table 3 summarises the current status of satellite observation. There exists a clear requirement to obtain well discriminated and interpretable data. The role of remote sensing is central to this goal. However, the procedures and algorithms for extracting important state variables from satellite data are not well developed. However, a number of international research programs have been initiated to examine this issue (e.g. ISLSCP, IGBP). Currently, the parameters required in the specification of surface processes in climate models are specified from site-specific studies as a function of 'typical' grid-box specifications of land-cover and soil type. A number of such global archives are currently available (see Henderson-Sellers et al., 1985 for a review of such archives).

Comparative studies (and in particular the prospect of satellite up-dating) of the information content of the available data archives are still being undertaken . For example, a preliminary investigation of the use of the NOAA Global Vegetation Index for the derivation of land cover characteristics by Thomas and Henderson-Sellers (1987) reveals that substantial difficulties remain before consistent information suitable for climate model studies can be abstracted from remote data sources. Figure 4 shows the NOAA GVI land-surface characterisation for a region in North America. Although a broad similarity between the GVI classes and other data archives was demonstrated, there were some notable differences. Clearly, there is an urgent need to obtain validated global data archives for use in climate related studies.

4. Summary and conclusions

The current status of the parameterization of land-surface hydrology in GCMs has been summarized. Clearly, a variety of approaches are currently being investigated. The importance of deriving a physically realistic approach is demonstrated with respect to the GCM representation of the continental annual and monthly water balance. In addition, climate model sensitivity studies reveal the influence of land-surface parameterization for the interpretation of climate change experiments. Substantial difficulties remain in terms of adequately representing many hydrological processes at the GCM scale. The role of remote sensing is central to this goal. However, it is important to be aware of the nature of the information required for global climate studeis. Many GCMs prescribe surface parameters on the basis of the predominant grid area land-cover. Thus, a number of archives of such data have been constructed. Intercomparisons of the available archives with satellite data are urgently required. In addition the possibilitites of providing data on surface parameters required by climate models directly from remote sensing requires further research.

Table 1 Current parameterization schemes designed for inclusion in climate models

Reference	GCM	Subgrid-scale variability	Explicit vegetative canopy
Abramopoulos et al. (1988)	GISS		X
Dickinson et al. (1986)	NCAR		X
Entekhabi and Eagleson (1989)	?	X	X
Sellers et al. (1986)	GFDL		X
Warrilow et al. (1986)	UKMO	X	

Table 2 Model sensitivity studies to land surface modification

Surface Perturbation Category				
albedo	roughness	Evaporation	Soil Moisture	Combined
Sud and Fennesy (1982)	Sud and Smith (1985)	Shukla and Mintz (1982)	Rind (1982)	Henderson-Sellers and Gornitz (1984)
Laval and Picon (1986)	Heasman (1987)	Delworth and Manabe (1988)	Rowntree and Bolton (1983)	Cunnington and Rowntree (1986)
			Yeh et al. (1984)	Dickinson and Henderson-Sellers (1988)
			Oglesby and Erickson (1989)	Lean and Warrilow (1989)

Table 3 Sustained long term measurements of global variables important for the study of land-surface characteristics and climate

Variable	Importance	Analysis Product Quality
Surface radiating temperature	Substantial	No information
Incident solar flux	Substantial	Useful, poor discrimination
Snow cover	Substantial	Useful, poor discrimination
Snow water equivalent	Substantial	No information
River runoff	Substantial	Well discriminated, absolute accuracy doubtful
Surface parameters (for albedo, roughness, infrared and microwave emittance)	Substantial	Useful, poor discrimination
Index of land-use changes	High	No information
Index of vegetation cover	Essential	Qualitative index, interpretation doubful
Index of surface wetness	Substantial	No information
Soil moisture	Essential	No information
Biome extent, productivity, and nutrient cycling	Essential	No information

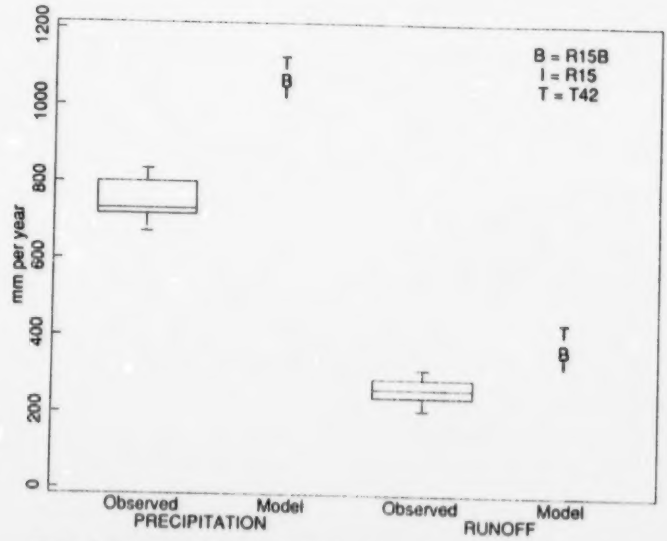

Figure 1 The observed average annual precipitation and runoff for the terrestrial surface of the earth together with values for three versions of the NCAR CCM.

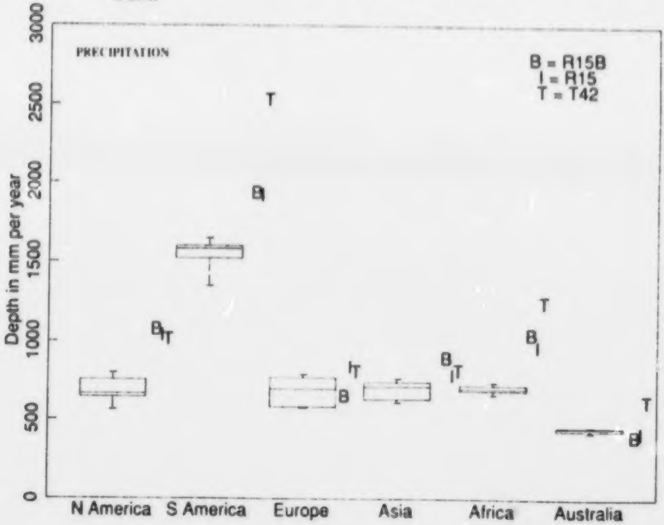

Figure 2 The observed and modeled average annual precipitation for the continents.

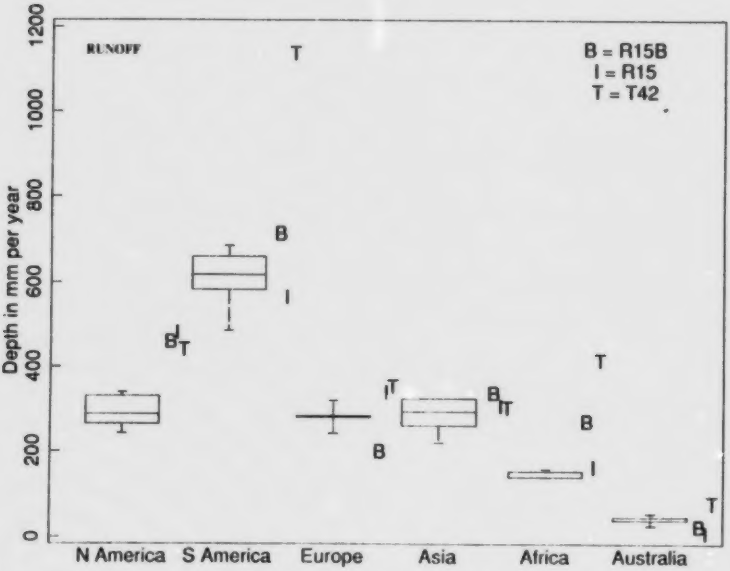

Figure 3 The observed and modeled average annual runoff for the continents.

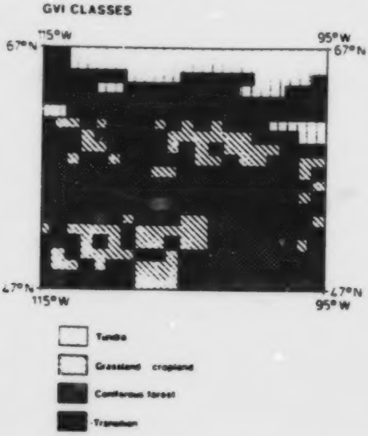
GVI CLASSES
115°W
95°W
67°N
67°N
47°N
47°N
115°W
95°W
Tundra
Grassland cropland
Coniferous forest
Transition

Figure 4 The GVI land-surface characterisation of a region of North America.

References

Abramapoulos, Rosenzweig, C. and Choudhury, B., 1988, Improved ground hydrology calculations for global climate models (GCMs): Soil water movement and evapotranspiration, *J. Climate*, **9**, 921–941

Cunnington, W. M. and Rowntree, P. R., 1986, Simulations of the Saharan atmosphere-dependence on moisture and albedo, *Q. J. Roy. Met. Soc.*, **112**, 971–999

Delworth, T. and Manabe, S., 1988, The influence of potential evapotranspiration on the variabilities of simulated soil wetness and climate, *Journal of Climate*, **5**, 445–470

Dickinson, R. E. and Henderson-Sellers, A., 1988, Modeling tropical deforestation: A study of GCM land-surface parameterizations, *Q. J. Roy. Met. Soc.*, **114**, 439–462

Dickinson, R. E., Kennedy, P. J., Henderson-Sellers, A. and Wilson, M. F., 1986, *Biosphere-Atmosphere Transfer Scheme (BATS) for the NCAR Community Climate Model*, NCAR Tech. Note, NCAR/TN-275+STR

Entekhabi, D. and Eagleson, P. S., 1989, Land surface hydrology parameterization for atmospheric general circulation models including subgrid scale varaiability, *Journal of Climate*, **8**, 816–831

Hansen, J., Russell, G., Rind, D., Lacis, A., Lebedeff, S., Ruedy, R. and Travis, L., 1983, Efficient three-dimensional global models for climate studies: Models I and II, *Mon. Wea. Rev.*, **111**, 9341–9364

Heasman, C., 1987, Sensitivity of the Met. O. 20 11–layer model to increased land-surface roughness length, DCTN 49, UKMO, Bracknell, 18pp

Hansen, J., Fung, I., Lacis, A., Rind, D., Lebedeff, S., Ruedy, R. and Russell, G., 1988, Global climate changes as forecast by Goddard Institute for Space Studies three-dimensional model, *J. Geophys. Res.*, **93**, 9341–9364

Henderson-Sellers, A. and Gornitz, V., 1984, Possible impacts of land cover transformations, with particular emphasis on tropical deforestation, *Climatic Change*, **6**, 231–258

Hunt, B. G., Amodel study of some aspects of soil hydrology relevant to climate modeling, *Q. J. Roy. Met. Soc.*, **111**, 1071–1085

Kellogg, W. W. and Zhao, Z.-C., 1988, Sensitivity of soil moisture to doubling of carbon dioxide in climate model experiments. Part I: North America, *J. Climate*, **1**, 348–366

Laval, K. and Picon, L., 1986, Effect of a change of the surface albedo of the Sahel on climate, *J. Atmos. Sci.*, **43**, 2418–2429

Lean, J. and Warrilow, D. A., 1989, Simulation of the regional climatic impact of Amazon deforestation, *Nature*, **342**, 411–412

Manabe, S., 1969, Climate and ocean circulationl: The atmospheric circulation and hydrology of the earth's surface, *Mon. Wea. Rev.*, **97**, 739–774

Manabe, S. and Wetherald, W. T., 1986, Reduction in summer soil wetness induced by an increase in atmospheric carbon dioxide, *Science*, **232**, , 626–628

Meehl, G. A. and Washington, W. M., 1988, A comparison of soil moisture sensitivity in two global climate models, *J. Atmos. Sci.*, **45**, 1476–1492

Milly, P. C. D. and Eagleson, P. J., 1988, Effects of spatial variability on annual average water balance, *Wat. Res. Res.*, **23**, 2135–2143

Mitchell, J. F. B. and Lupton, G., 1984, A 4 x CO_2 experiment with prescribed changes in sea temperatures, *Prog. Biomet.*, **3**, 353–374

Mitchell, J. F. B. and Warrilow, D. A., 1987, Summer dryness in northern mid-latitudes due to increased CO_2, *Nature*, **330**, 238–240

Oglesby, R. J. and Erickson, D. J., 1989, Soil moisture and the persistence of North American drought, *J. Climate*, **2**, 1362–1380

Rind, D., 1982, The influence of ground moisture conditions in North America on summer climate as modeled in the GISS GCM, *Mon. Wea. Rev.*, **110**, 1487–1494

Rind, D., 1988, The doubled CO_2 climate and the sensitivity of the modeled hydrologic cycle, *J. Geophys. Res.*, **93**, 5385–5412

Rowntree, P. R. and Bolton, J. R., 1983, Simulation of the atmospheric response to soil moisture anomalies over Europe, *Q. J. Roy. Met. Soc.*, **109**, 501–526

Sato, N., Sellers, P. J., Randall, D. A., Schneider, E. K., Shukla, J., Kinter, J. L., Hou, Y-T. and Albertazzi, E., 1989, Effects of implementing the Simple Biosphere Model in a general circulation model, *J Atmos. Sci.*, **46**, 2757–2782

Sellers, P. J., Mintz, Y., Sud, Y. C., and Dalcher, A., 1986, A simple biosphere (SiB) model for use within general circulation climate models, *J. Atmos. Sci.*, **43**, 505–531

Shukla, J. and Mintz, Y., 1982, Influence of land-surface evapotranspiration on the Earth's climate, *Science*, **215**, 1498–1501

Sud, Y. C. and Smith, W. E., 1985, The influence of deserts on the July circulation, *B. Layer Met.*, **33**, 15–49

Thomas, G. and Henderson-Sellers, A., 1987, Evaluation of satellite derived land cover characteristics for global climate modeling, *Climatic Change*, **11**, 313–347

Warrilow, D. A., Sangster, A. B. and Slingo, A., 1986, Modeling of land-surface processes and their influence on European climate, *Dynamical Climatology Technical Note*, **38**, 92pp

Yeh, T.-C., Wetherald, R. T. and Manabe, S., 1984, The effect of soil moisture on the short-term climate and hydrology change-a numerical experiment, *Mon. Wea. Rev.*, **112**, 474–490

Questions and Answers

Geoff Kite: One of the reasons we need detailed hydrologic models is because people are interpreting the results of the general circulation models for specific basins on the basis of inadequate hydrologic models. Do you agree?

Graham Thomas: Yes, the interpretation of climate model results is fraught with difficulties. In the hydrological sense this is particularly true because the parameters that come out of the models do not have hydrologic definitions. For example "field capacity" isn't even "depth of moisture" over a grid cell, it's not an integrated variable over a given drainage basin; it takes no account of the physical complexity of an individual drainage basin.

George Leavesley: From a hydrologic standpoint, you're looking at aggregating up from basin-scale information to your global-scale or to meso-scale. As a hydrologist trying to apply the GCM information, we're looking at the output problem, disaggregating that information down. Do you have any suggestions or insight on what should be done?

Graham Thomas: Well, the current attempts to do that are in terms of using embedded meso-scale models as means of generating finer resolution precipitation and other hydrological inputs. So here on this diagram we are looking at a coarse resolution GCM representation of the mean July precipitation for Australia. I have not cleaned up in any sense the following data set which is a meso-scale model, so we have sixty-kilometer resolution here, but we have on the order of three by three degree resolution there, and we have some observed data. There are a considerable number of difficulties that must be overcome in order to tie together a meso-scale model and a climate model, to embed it, because you provide very smoothed information to a sixty-kilometer grid resolution meso-scale model from a GCM. Also, we use the same physical parameterization, the same determination of runoff and evapo-transpiration, as we move down the scale. My concern is to test the validity of that approach, and whether or not it is required. I am very interested in the model that you were describing. I am trying to get to it the other way in a sense, down to the very fine scale needed to test these parameterizations.

Modelling the Kootenay Watershed with Satellite Data

G.W. Kite
Hydromet. Research Division, Canadian Climate Centre
Atmospheric Environment Service
Saskatoon, Saskatchewan.

Abstract

The SLURP (Simple LUmped Reservoir Parametric) hydrologic model is a simple lumped parametric model with a history of applications in Canada and abroad. It has recently been extensively upgraded to incorporate snow-course data and satellite data and to operate on personal computers as part of a larger study of the utility of satellite data for hydrologic modelling.

Hydrologic modelling is developing rapidly and satellites offer the only practical way of obtaining the vast amounts of distributed data needed.

This paper describes the SLURP model and its application to a mountain basin in western Canada. Results of using the model with various types of satellite data are compared to the results obtained using ground data only and preliminary conclusions are drawn on the utility of these satellite data for hydrologic modelling.

A brief description is also given of the larger study of which this is a component. The objectives of the larger study are to investigate the usefullness of different types of satellite data in hydrologic modelling for different physiographic zones, to develop a more physically-based distributed model using remotely-sensed data, and to develop a land-phase component for global circulation models.

Introduction

A hydrologic model is a representation of the processes which convert precipitation into streamflow. Simpler models generally approximate the processes with parametric relationships but more complex models incorporate more of the watershed physics and split the watershed into smaller components. As a result, these models need much more data. There is also a tendency for data collection agencies to economise by cutting back on the number of data collection stations.

One possible solution to the data availability problem is to use satellites for hydrologic modelling. An on-going study is looking at the utility of satellite data for modelling in different physiographic and climatic zones of Canada. The longer term objectives of the study are to develop a model with physics-based components developed specifically for satellite data and, eventually, to expand the scale of the model so that it could be used as a land-phase component of a global circulation model.

Complex distributed hydrologic models are difficult and time-consuming to calibrate and to run and it was therefore decided to use a easier model in a first approach to this study. The simple SLURP model is used to investigate the response of the basin and to remove obvious errors in input data as a preliminary to use of more complex models.

The choice of satellites with hydrologically useful data includes SPOT, Landsat, NOAA and GOES. Considering the resolution, frequency of image availability and the cost of images (see Table 1), it was decided to use daily NOAA imagery for snow and cloud cover analyses and to use one Landsat image per watershed for land-use classification. One NOAA image (5 channels) per watershed per week is obtained on magnetic tape from AES, Edmonton, and data for the intermediate days are video-digitised from NOAA visible and near-IR photographs.

A database to combine the ground-based point data (climatic and hydrometric) with physiographic data, land-use data and the distributed cloud and snow data from satellite was written in Fortran for a microcomputer. The model accesses data directly from this databank.

Watersheds in two different climatic and physiographic zones were selected for the study; the Kootenay watershed in south-eastern British Columbia and the Souris watershed in south-eastern Saskatchewan, south-western Manitoba and northern North Dakota. This paper describes the application of the model to the Kootenay watershed shown in Figure 1.

The Model

i) Introduction

SLURP was originally written for a mainframe computer (Kite,1978) but the latest version is for use on a microcomputer using a menu system, full-screen data entry and on-screen graphics. It has 13 parameters (see Table 2) and is very easy to operate.

The watershed is represented by three tanks, one for snowpack, one for a combined surface storage and top soil layer storage and the third for groundwater. The three tanks have specified initial contents and maximum allowable depths. On a particular day, the sequence of steps within the model might be as follows:

- Precipitation is converted to an estimated areal average. Optionally, precipitation data may be modified to reflect the percentage of the watershed covered by cloud as observed from satellite.

- If the daily mean temperature is above a critical temperature, then the precipitation is assumed to be rainfall and enters the surface storage tank. If the supplemented surface storage exceeds a specified maximum depth, the excess runs off. The surface storage is depleted to both runoff and groundwater. At the same time, the snowpack (if it exists) is depleted by snowmelt to the surface tank and to the groundwater tank. A proportion of the snowmelt will run off directly and the remainder will infiltrate to groundwater

- If, on the other hand, the daily mean temperature is below the critical level, then the precipitation is assumed to be snow and is added to any snowpack. In this case, there would be no snowmelt but the surface storage would again contribute both to runoff and to groundwater. If snow-course data are available, then the calculated snow water equivalent may be adjusted to agree with the measured data.

- Melt from snow-covered areas may, optionally, be modified by the areal extent of snowcover estimated by supervised multispectral classification of NOAA images.

- Evapotranspiration is satisfied, if possible, first from the snowpack and then from the surface storage.

- Runoffs from snowmelt, surface storage and groundwater may be lagged and may be combined with streamflows from an upstream basin.

ii) Data

Data types used in the model are listed in Table 2. The first four data types are all essential, the remainder are optional. Streamflow data are needed only for calibration runs; the long-term mean flows are used only to calculate one of the calibration criteria and the last three data types will be used only if specified.

Daily mean temperature and daily precipitation are derived within the database by averaging data from any set of up to five climate stations; missing data are accounted for in the averaging process. Monthly dewpoint and air temperatures and hours of bright sunshine are used to estimate monthly values of areal evaporation using Morton (1983). Daily evapotranspiration is then interpolated from monthly evaporation using daily hours of bright sunshine and wind-run.

The daily snow and cloud cover are calculated from the database files containing the percentages of snow and cloud for each grid square of the watershed. Snow water equivalent data are the averages, for a given day, of the figures reported from as many snow courses as possible.

iii) The Program

At the main menu the user enters the watershed name and the program will retrieve the appropriate command file and display the latest set of run-control options. There are options to control the data input -

> start and end dates for simulation,
> optimisation type, if any,
> units of the data (metric/Imperial),
> whether satellite cloud cover or snow cover data are to be used,
> whether snowcourse data are to be used,
> the name of the file containing upstream flows, if any,

and options to control the program output -

> plots of hydrographs,
> WMO statistics,
> time increment for printed output (daily, monthly, annually or no printout),
> the name of a file to contain simulated streamflows.

The user accepts or modifies the default options and moves to a screen of operational parameters. When the options and parameters are all correct, the updated values are written back to the command file.

For each year of simulation, the observed and computed hydrographs will be displayed on screen (see, for example, Figure 2). The daily rainfall is plotted along the top of the graph. Figure 2 shows the difference between the two hydrographs in a wave pattern if the computed runoff is greater and in a brick pattern if the observed runoff is greater.

The final screen of a model run includes three measures of efficiency which may be used to measure the effectiveness of a calibration. The Nash/Sutcliffe (1970) efficiency is defined as:

$$F^2 = \frac{F^2{}_m - F^2{}_d}{F^2{}_m} \qquad (1)$$

where

$$F^2{}_m = \frac{1}{n} \sum_{i=1}^{n} (q_i - \bar{q})^2 \qquad (2)$$

and

$$F^2{}_d = \frac{1}{n} \sum_{i=1}^{n} (q_i - c_i)^2 \qquad (3)$$

q_i is the observed flow and c_i is the calculated flow on day i. This criterion compares the simulation to a 'forecast' consisting

of the average flow, $\bar{q}$.

The efficiency measure proposed by Garrick et al (1978) replaces $F^2{}_m$ in equation 2 by:

$$F^2{}_m = \frac{1}{n} \sum_{i=1}^{n} (q_i - \bar{q}_i)^2 \qquad (4)$$

where $\bar{q}_i$ is the long term mean flow on day i. This criterion compares the model simulation on a particular day to a 'forecast' consisting of the long term mean flow for that particular day.

If one had no other information, one might forecast the flow on day i to be the same as the flow on the previous day, i-1, taking advantage of the persistence component of river flows. The third criterion is based on this forecast and replaces $F^2{}_m$ in equation 2 with:

$$F^2{}_m = \frac{1}{n-1} \sum_{i=2}^{n} (q_i - q_{i-1})^2 \qquad (5)$$

Method

i) Calibration

The model was calibrated for the Kootenay watershed (Figure 1) using daily data for January to December 1988. Daily evapotranspirations were estimated using data from Cranbrook airport. Daily mean temperatures and daily total precipitations were averaged from four climate stations. Daily streamflows at Skookumchuck were used for calibration. Snow water equivalent data were averaged from four snowcourses.

The model was first run without satellite data; the results indicated that the model had the correct volume of runoff and that the maximum daily error was just over twice the mean observed daily flow and just less than one half of the maximum observed flow. The total evapotranspiration actually extracted by the model was about 70% of the theoretically calculated evapotranspiration.

The model was then run again with satellite-observed cloud cover. All the parameter values remained the same although the initial snow water equivalent was changed to accommodate the modifying effect of the cloud data. The average cloud cover on the 184 days with precipitation was 60% while the monthly average cloud cover in 1988 varied from 43% in October to 78% in March. Finally, the model was run for a third time using both satellite snowcover and cloudcover. Again, all parameters remained as in the first run but the initial snow water equivalent was changed. The results are shown in the upper half of Table 3alues.

ii) Verification

The model was verified using daily data for January 1 to July 31, 1989. The calibrated parameter values were maintained and the model was run three times; once with no satellite data, then with satellite cloud cover and, finally, with both satellite snowcover and cloudcover. The resulting statistics are given in the lower part of Table 3. The best of the three runs uses satellite snow cover data, next is the run with no satellite data and, last, is the run using both satellite snow and cloud cover data. The standard error of the verification runs averaged about 50% greater than for the calibration runs.

Conclusions

A simple model has been used to demonstrate that satellite data, such as extent of snow cover, can improve the performance of a hydrologic model. Using cloud cover as an indicator of precipitation didn't work, indicating that a better method of deriving precipitation from satellite data should be used.

In deriving the evapotranspiration for the verification period, only preliminary climatic data were available. These contain many periods of missing data. This probably influenced the model simulation and it is expected that better results will be obtained when quality-controlled data are available.

The next step in the study will be to include more verification runs for longer periods of data and in different watersheds. The study will also investigate using different types of satellite data such as passive microwave temperatures as measures of snow water equivalent, soil surface temperature and soil moisture. The way in which the watershed is represented in the model will also be changed to increase the physics and decrease the dependence on parameters.

There is a limit to the development of such a simple model, however. Basically, a lumped model cannot provide an accurate response from a mountainous watershed because the concept of average precipitation and temperature is not valid for such a watershed. Therefore, once the simple model has served it's purpose, further stages of the study will use a more sophisticated distributed model.

References

Garrick, M., Cunnane, C. & J.E. Nash, 1978. A Criterion for Efficiency of Rainfall-Runoff Models. Journal of Hydrology, 36, 375-381.

Kite, G.W., 1978. Development of a Hydrologic Model for a Canadian Watershed. Can,. J. Civil Engineering, Vol. 5.

Kite, G.W., 1989. Hydrologic Modelling with Remotely Sensed Data. Proc. 57th Annual Western Snow Conference. Ft. Collins, Co., April 18-20, pp 1-8.

Morton, F.I., 1983. Operational Estimates of Areal Evapotranspiration and their Significance to the Science and Practice of Hydrology. Journal of Hydrology, 66, pp.77-100.

Nash, J.E. & J.V. Sutcliffe, 1970. River Flow Forecasting through Conceptual Models; Part I - A Discussion of Principles. Journal of Hydrology, 10(3), pp.282-290.

Table 1
Practical Choice of Satellite

	Resolution	Frequency	Cost, C$/Image
Landsat 5 - TM	30 m.	8/16 days	3840
Landsat 5 - MSS	80 m.	8/16 days	795
SPOT - MSLA	20 m.	2 per day	1855
SPOT - Pan.	10 m.	2 per day	2205
NOAA	1 km.	2 per day	55
GOES	1 km./ 8 km.	1/2 hour	100

Table 2
Data and Parameters used by the SLURP Model

Data type	Units
temperature	C°
precipitation	mm.
areal evap.	mm.
streamflow	m^3/s
long-term mean flows	m^3/s
cloud cover	percentage
snow cover	percentage
snow water equivalent	mm.

Parameter	Typical Value
Initial value of snowpack (mm)	180
Initial value of surface storage (mm)	4.2
Initial value of groundwater (mm)	13.9
Proportion of snowmelt to runoff	0.04
Proportion of surface storage to runoff	0.19
Proportion of groundwater to runoff	0.05
Proportion of surface storage to groundwater	0.70
Maximum depth of surface storage (mm)	270.0
Precipitation multiplication factor	1.17
Rain/snow division temperature (C)	9.5
Snowmelt rate (mm/degree/day)	5.5
Lag time for surface runoff (days)	0
Lag time for groundwater (days)	1

Table 3
Model Calibration and Verification, Kootenay Watershed

Statistic	No Sat. Data	With Sat. Snowcover Data	With Sat. Snowcover & Cloud Data
a) Calibration, Jan 1 - Dec 31, 1988.			
Nash/Sutcliffe criterion	0.85	0.87	0.86
Garrick et al. criterion	0.46	0.5	10.47
Previous-day criterion	-2.94	-2.57	-2.86
b) Verification, Jan 1 - Jul 31, 1989.			
Nash/Sutcliffe criterion	0.83	0.85	0.79
Garrick et al. criterion	0.40	0.46	0.25
Previous-day criterion	-6.68	-5.96	-8.66

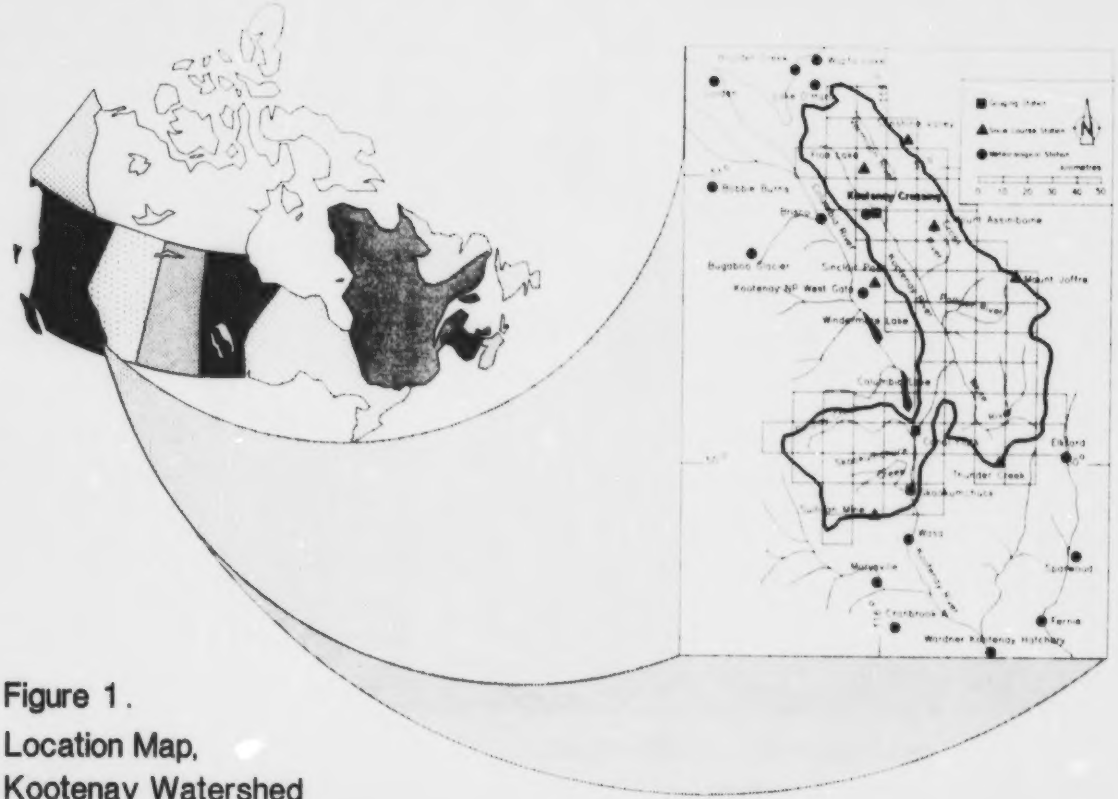
Wapta Lake
Lake O'Hara
Robbie Burns
Brisco
Bugaboo Glacier
Kootenay Crossing
Floe Lake
Mount Assiniboine
Sinclair Pass
Kootenay NP West Gate
Windermere Lake
Mount Joffre
Columbia Lake
Kootenay River
Columbia River
Elkford
Thunder Creek
Skookumchuck
Sullivan Mine
Wasa
Marysville
Cranbrook A
Sparwood
Fernie
Wardner Kootenay Hatchery
Gauging Station
Snow Course Station
Meteorological Station
kilometres
0
10
20
30
40
50
N

Figure 1.
Location Map,
Kootenay Watershed

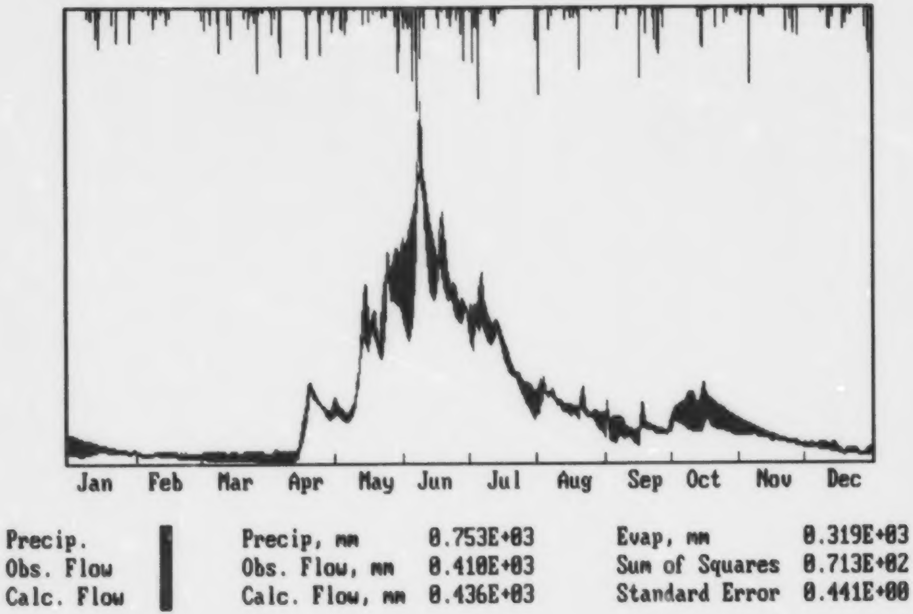

Figure 2.
Simulated and Recorded Hydrographs,
Kootenay River at Skookumchuck, 1988.

Questions and Answers

Michael Quick: Perhaps you could say a word about why your putting satellite cloud cover in the model made things worse?

Geoff Kite: Yes. The reason is because we were using a such a simplistic process. We were taking NOAA images, once per day, measuring the cloud cover over the basin and taking that as an index of precipitation and, basically, it isn't a good index. For satellite snow cover, on the other hand, the daily images are a very good index. This diagram shows you, for example, the percent snow-cover over the Kootenay basin from daily NOAA images versus cumulative positive temperature during spring melt. Looking at that in a different way, this diagram shows the percent snow-cover from NOAA images versus Julian day during the snowmelt period in the spring, and that's not a bad measure. But when you come to look at the daily cloud cover and relate that to the precipitation, this diagram shows that there is no relationship there at all. Basically, the approach that we used was just too simple-minded and we have to try something more sophisticated than that.

Thian Yew Gan: Do you have any ideas on what other methods you
should apply?

Geoff Kite: Not from NOAA data, they are just too infrequent to use for cloud cover. If we were to go to GOES data, then yes, there are established methods but the data manipulation problems of using GOES data on a grid square basis for long periods of time is difficult. It is something we have to think about.

Gary Schaefer: You called the images usable for snow mapping if they had less 100% cloud cover. What if they had 90% cloud cover?

Geoff Kite: We have an algorithm which, if a grid square is cloud-covered, looks at the image from the previous day. If we had a good image the previous day, then we accepted the previous day's percent snow cover.

PROGRESS REPORT ON THE IMPLEMENTATION OF AN ALGORITHM TO ESTIMATE REGIONAL EVAPOTRANSPIRATION USING SATELLITE DATA

N. Bussières, P.Y.T. Louie and W. Hogg
Canadian Climate Centre
Atmospheric Environment Service
Downsview, Ontario, M3H 5T4

ABSTRACT

Project CLIGRID was developed to accept both remotely sensed and conventional data and to transform them into mapped outputs of climatic variables. The authors describe the implementation, within this project environment, of a simple scheme to estimate evapotranspiration from satellite radiance measurements, in cloud free situations. Although the primary objective was to estimate the evapotranspiration field, the methodology required the derivation of several intermediate fields which included albedo, surface temperature and net radiation. These intermediate fields have great value in various applications. The schemes uses visible and infrared channels from GOES, plus air temperature and upper air soundings of temperature and moisture. Data requirements and processing are discussed in detail. Validation and error assessment of intermediate data fields are made.

RÉSUMÉ

Les objectifs du projet CLIGRID étaient l'ingestion de données conventionnelles et de télédétection ainsi que leur transformation en des matrices de variables climatologiques. Les auteurs décrivent l'implantation d'une méthode simple d'estimation de l'évapotranspiration, en utilisant les ressources fournies par CLIGRID. Cette méthode fait appel à de mesures des radiances observées par satellites en absence de nuages. Bien que l'objectif principal est d'estimer la matrice d'évapotranspiration, la méthodologie nécessite que soient dérivés plusieurs champs intermédiaires, incluant l'albédo, la température de surface et le rayonnement net. Ces champs intermédiaires ont une valeur intrinsèque dans de nombreuses applications. La méthode présentée utilise les canaux visible et infrarouge de GOES, ainsi que la température de l'air et les sondages de température et d'humidité. On discute en détail des besoins en données. On effectue la validation et le constat des erreurs qui apparaissent dans les champs intermédiaires.

INTRODUCTION

Evapotranspiration (ET) is an important process in many climatological applications. In agriculture, hydrology and climate modeling, it is a key component of the water and energy budgets. Direct ET measurements are difficult to make and at best provide only point values. Presently, regional values of ET must be estimated by models using standard meteorological network data as input. Remotely sensed data from meteorological satellites have the potential for improving regional estimates of ET. Recognizing this potential, many researchers have worked on developing ET models that accept remotely sensed measurements as input variables.

Bussières and Louie (1987) conducted a study to determine the feasibility of producing operational ET estimates on the regional scale. The study classified satellite data techniques into two groups: a) iterative energy-balance model inversion (Taconet et al 1986) and b) residual energy budget (Jackson et al 1977).

Method (a) uses an energy balance model to estimate the surface temperature. Iterations are made until the estimated temperature compares, within pre-determined limits, to a temperature value estimated from remotely sensed data. At this point, the model is inverted, giving the fluxes. This method may provide an excellent representation of reality but its use is currently limited to case studies in the vicinity of amply instrumented land stations.

Method (b) is simpler and is considered more suitable for operational use as well as for spatial estimates; the latent heat flux is computed as a residual of the energy budget equation formulated to use remotely sensed data. In the following, this method is applied to daily estimates of ET, under non-cloudy conditions. Chapter two describes the method and its implementation in a multi-data set environment. Chapter three describes validation of the generated fields and points out some unresolved problems.

2. IMPLEMENTATION OF THE RESIDUAL ENERGY BUDGET METHOD

The rate of ET is controlled by temperature, humidity, net radiation and wind. It depends also on the availability of water at or below the surface, the nature of the surface and the physiological state of the vegetation.

2.1 Description of the method

Termed "residual energy budget" by Rambal et al (1985), the method was introduced by Jackson et al (1977). Their concept was to use remotely sensed temperature in the evaluation of the expression:

$$LE^{24} = R_n{}^{24} - B\,(T_s - T_a)^i \qquad (1)$$

$$B = (R_n{}^{24} / R_n{}^i)\ \rho\,\overline{c_p} / \overline{r^i_{ah}} \qquad (2)$$

where:

LE^{24} = 24 hour total ET

R_n^{24} = 24 hour net radiation

$(T_s - T_a)^i$ = instantaneous canopy to air temperature difference near midday

R_n^i = instantaneous net radiation around midday

r^i_{ah} = turbulent diffusion resistance to heat transport (a function of wind velocity, atmospheric stability and surface roughness)

ρ = air density

c_p = specific heat of air

Equation 1 represents the energy budget, for a duration of 24 hours, and with the ground heat component neglected. Peculiar, however, is the heat flux term. It uses temperature measurements made at a point in time to produce a heat flux valid for the duration of a day. Time scale conversion is thus handled as shown in Equation 2. Selection of midday for the time of measurement corresponds often to the time of maximum heat flux.

Seguin and Itier (1983) estimated errors of the method below 10 and 20 percent for monthly sums of their ET outputs. The reader is directed to their work for an excellent discussion on the physical aspects of the method. As in Jackson et al (1977), the same authors suggested some values for the "B" coefficient. Rambal et al (1985) also illustrated how to model the values of "B" for 4 types of vegetation from data on 4 different days.

Because of limitations in the modeled estimates of the B term, due for example to neglecting the effect of wind and soil moisture, large errors in individual estimates of ET can be expected in a number of cases. Improvement of the data base and better calibration efforts would certainly help to overcome this classical problem.

The "B" coefficient involves the aerodynamic and surface resistances which are well known (Serafini 1987) sources of uncertainty. Nieuwenhuis et al (1986) discussed the limitations of the "B" term. It must be tuned according to the climate and the surface with clear days being essential for applying the method. The same authors suggested the following alternative form:

$$LE^{24} = LE_p^{24} - B' (T_c - T_c^*) \qquad (3)$$

where:

B' = calibration constant

T_c^* = temperature of the crop that is potentially transpiring under optimal soil moisture condition

T_c = temperature of the crop under the restriction of soil moisture condition

LE_p^{24} = 24 hour potential ET flux (see for example Monteith 1973)

T_c^* and T_c are estimated from thermal IR data. Areas known to be adequately supplied with water (possibly low elevation areas) would be selected for the estimation of T_c . Equation 3 states the reduction in ET based on the difference in crop temperatures. The authors of this technique presented heat images showing the variability of temperature with vegetation in connection with computed maps of the deficit in ET. They concluded that this type of analysis over cultivated land is valid only with remote sensing from aircraft, which has the necessary resolution. Remote sensing by satellite provides adequate time coverage but its spatial resolution is inadequate for the size of cultivated plots. Because of the necessity of determining the difference between T_c^* and T_c, this seems indeed to be a limitation for using the method of Nieuwenhuis et al (1985) with satellite data.

Reiniger and Seguin (1986) provided an intercomparison of the iterative energy balance model inversion (TERGRA, TELL-US, TELOP and SEAL models) and the residual energy budget methods. They concluded that all methods must be used in parallel with ground truth since they are more suited for delineating relative changes in ET patterns than absolute values.

The same authors approved the use of Equation 1 as an alternative solution to complex modeling. They also concluded that the use of the consecutive night/day temperature difference (suggested by Price, 1980) would not improve ET estimates. Price (1980) used the difference between maximum and minimum temperature as an approximation for the derivative of the temperature relative to time, to compute the transfer of energy through the ground. This term of the energy balance is neglected in the derivation of Equation 1.

2.2 Implementation

Our example for an implementation strategy uses the equations and values given in Rambal et al (1985):

$$LE^{24} = R_n^{24} - B\,(T_s - T_a)^{3/2} \qquad \text{for } T_s > T_a \qquad (4)$$

This is the unstable case, and B, expressed in mm /°C - day, is given as: 0.32 for shrubland, 0.43 for open woodland, 0.68 for mid-dense woodland. For dense woodland, the value of B is 2.4, which, according to Rambal et al, is probably an overestimate. More values can be found in the literature.

Stable conditions ($Ts < Ta$) are likely to occur only under advective conditions at midday. In their study of the stable case, Seguin and Itier (1983) suggested the use of Jackson et al (1977) equation, with B values smaller than in the unstable case:

$$LE^{24} = R_n^{24} - B\,(T_s - T_a) \qquad \text{for } T_s < T_a \qquad (5)$$

Uncertainty in Equations 4 and 5 depends on the uncertainty in the temperature difference, the B coefficient and the net radiation estimate. In a case study, Cooper et al (1984) determined uncertainty values of $(T_s - T_a)$, to be about ± 3.8 °C. In our evaluation, if B is 0.32 (for shrubland), the corresponding uncertainty due to temperature in the $B(Ts - Ta)$ term is ± 1.2 mm/day. In energy terms, with the latent heat of evaporation of water being (2.45×10^6) Joule/Kg, the corresponding uncertainty is:

$$U = \pm\, 1.2 \times 10^{-3}\ \frac{m}{day} \quad \times\ 2.45 \times 10^{6}\ \frac{Joule}{Kg} \quad \times\ 1000\ \frac{Kg}{m^3}$$

$$U = \pm\, 2.9\ MJ / day\ m^2$$

This is rather significant compared to the incoming solar daily radiation range of 17.5 to 28.5 MJ m^{-2} reported for the cases studied by Rambal et al. Absolute values of ET can be obtained but the merit of the results will lie more in delineating the areal variation in ET.

For test implementation of the technique, an environment that accepted both remotely sensed and objectively analyzed conventional data was required. The CLI-GRID system (Hogg et al 1986) was used. CLI-GRID allows the production of various independent gridded fields that could be combined to give an ET map. CLI-GRID mesh size is about 4 km.

In order for the reader to better judge the level of effort required, it is convenient to consider the implementation of methodologies for building each field and data set as separate modules. Contrary to the iterative model inversion method, the residual energy budget method does not suppose an implicitly balanced equation set. Since more input variables are used than in modeling, more errors are possible. This imposes a need for verification of intermediate steps (point comparisons and allowance for possible ranges). The existence of intermediate data sets is on the other hand particularly useful. Albedo, surface temperature and net radiation data fields have great value in various applications. The following implementation scenario is tailored to facilitate the examination of intermediate data.

Figure 1 illustrates the relationship between the data sets required. Squares represent co-located gridded arrays (256 x 128 elements in CLI-GRID). Disk volume symbols represent ungridded data sets. Processes applied to data sets are indicated in plain language between the various surfaces. Building of arrays and testing proceeds from top of the diagram towards the bottom right. Arrows indicate the directions of the data flow. Satellite data are used extensively. Details of particular data sets are given below.

DATA SETS B.3 A/B: 1800 UCT satellite Infrared and visible digital counts.

The infrared data should come from NOAA Polar orbiter satellites, for which most of the work was done for atmospheric corrections and for the evapotranspiration method. To be consistent, the visible data should come from the same satellite, but there is no problem using GOES data to create the cloud mask data field.

DATA SET B.4 Cloud mask

GOES data has a resolution of about 2 km (VIS) and 8 km (IR) GOES. According to Tsonis (1983), clear daytime conditions occur when the GOES VIS count, normalized for the solar zenith angle, is below 23. Under these conditions, the VIS sensors respond mostly to solar radiation reflected by the surface. Under cloudy areas, ET is not available with this method and all processing requiring satellite data is skipped for grid locations classified as cloudy.

DATA SET B.6: Albedo map

It is deduced from GOES VIS maps and is strictly valid from the satellite point. Clear sky albedo is proportional to the observed radiance from a pixel. Benchimol and Hay (1986) quote the following expression:

$$A = \frac{(K_{\uparrow} - K_o \alpha_i)}{S \ [1 - a(u_2)] \ (1 - \alpha_i)} \qquad (6)$$

with:

$$S = Ko \ (1 - \alpha_i) \ (1 - a(u_1)) \qquad (7)$$

where:

$K_{\uparrow}$ = radiance monitored by the satellite

K_o = extraterrestrial irradiance a function of the latitude, solar declination angle and time of day

S = solar radiation incident at the surface
$a(u_1)$, = water vapor absorption coefficients for solar
$a(u_2)$ zenith and satellite viewing angles, respectively
α, α_1' = Rayleigh scattering coefficients for direct and diffuse radiations
u_1, u_2 = precipitable water content along the path

Detailed guidelines for correctly evaluating these expressions are given in their paper and in Chapter 3 of Benchimol (1985). The value of $K_\uparrow$ must be properly determined and corrected from the satellite radiance calibration to relate to the digital count given by its sensor. An albedo map provides a convenient intermediate step for data verification.

DATA SET B.8: Instantaneous net radiation fields (Rni).

These are estimated from satellite data sources. Approximately:

$$R_n^{i} = (1 - A)\, S + R_{\downarrow} - e_{sfc}\, \sigma T_s^{4} \qquad (8)$$

where:

e_{sfc} = IR emissivity of the surface
σ = Stefan-Boltzmann constant

Tabulated values of emissivity of various surfaces are available in the literature. The albedo (Equation 6) might be replaced directly in (8). The $R_{\downarrow}$ term can be evaluated approximately with Brunt's empirical formula:

$$R_{\downarrow} = e_{air}\, \sigma T^{4}_{air} \; (.61 + .05\, (v)^{1/2}) \qquad (9)$$

where:

v = vapor pressure (mm Hg).
e_{air} = IR emissivity of air

DATA SET B.10: A gridded surface inventory and look-up data.

A gridded surface inventory was provided in digital format by Robinson and Associates (1988). Codes and identifications of surface are given in Table 2. Corresponding to each class, a value of surface emissivity and of B coefficient were assigned.

TABLE 1 : Surface classification for gridded inventory.

code	predominant surface	B coefficient	emissivity
1	Open	.32	.90
2	Forest	.68	.90
3	Water	1.0	.94
4	Urban	.5	.90
5	Open / forest	.5	.90
6	Open / water	.66	.92
7	Water / forest	.84	.92
8	Water / urban	.41	.90
9	Urban / forest	.75	.92
10	no predominance	.51	.90

This type of classification can be generated from various data sources, including satellite data (Justice et al 1985). It is used in the computation of coefficient B. Many authors now use the normalised difference vegetation index for this purpose.

DATA SET B.11: Daily net radiation fields (Rn24)

Net radiation is a key product of this method. To obtain an estimate of this field, a relationship was computed from July-August (1985) data for Elora and Toronto reference stations. With regression coefficients of r=.72 for Elora and r=.77 for Toronto, the following relation between the daily net radiation and the 1800 UCT instantaneous (Rn^i) net radiation was obtained:

$$R_n^{24}\ (\text{Joules/m}^2) \quad = \quad 3\ 10^3 \ + \ 6\ R_n^{\ i}\ (\text{Joules/m}^2) \qquad (10)$$

3. VALIDATION AND ERROR ESTIMATES

The following describes tests of an implementation scenario using the residual energy budget technique based on Jackson et al (1977). The test results are also described in more detail in an unpublished paper by Bussières and Louie (1989), which contains colour pictures of the test fields.

The implementation scenario required that each of the input fields be properly integrated. Getting the NOAA satellite data was difficult and GOES data was used. Changes were made to the scenario to accommodate deficiencies in the data base. Verification of the computed fields were made with real data extracted from climate archives.

The following section describes validation of fields generated for July 24, 1985. The Canadian Meteorological Centre weather chart for 1800 UCT on that day showed a low pressure area at the western tip of Lake Superior, with a quasistationnary front extending towards James Bay. The 1800 UCT winds were from the south sector, in the range 15 to 25 km/hour Clouds were present near the frontal region but clear conditions were reported over various locations of the CLI-GRID area.

3.1 Data sets

IR to surface temperature conversion table

The LOWTRAN method requires knowledge of satellite sensor response. GOES satellite was used due to the difficulty in obtaining properly navigated 1800 UCT NOAA data. As GOES sensor characteristics could not be obtained, METEOSAT characteristics were used in first approximation. A rural aerosol level and visibility of 20 km were assumed. A correction to the IR brightness temperature was thus computed for the angle of the satellite as function of earth location. Additive correction to an IR temperature of 20°C at 45°N was about +5.2°C at 1800 UCT on July 24, 1985.

1800 UCT satellite visible and infrared digital counts.

A large portion of the satellite images was cloud free with VIS < 23 and contrast between water bodies and land was well marked.

Cloud mask

The cloud mask was computed by taking as cloudy all pixels with VIS > 22. Surface observations of cloud opacities at aviation weather sites (Sudbury, North Bay, etc.) were available from the AES digital archives. The opacities in a scale from one to 10 were compared with the cloud mask. Station opacities above 4 tenths were found over areas classified by satellite as cloudy. Cloud opacity of 2 at Wiarton (N44°45', W81°06') was consistent with IR detectable warm cloudiness over southern Lake Huron and Georgian Bay. Based on VIS signal alone, pixels over this region were classified as non-cloudy. These should have been classified as cloudy since cloud contamination over the same pixels resulted in low estimates of lake surface temperatures. Future cloud classification for this evapotranspiration algorithm will be based on a combination of VIS and IR thresholds.

Objective analysis of the precipitable water content (u).

The use of the single Maniwaki sounding (N46°23, W75°58), linearly interpolated between 1200 UCT and 2400 UCT provided a unique precipitable water content value at 1800 UCT for the whole grid. This value, 19 mm, might be an overestimate for clear areas since the cloud/no cloud separation was right over Maniwaki.

Albedo map

Albedo was derived from GOES VIS for 1800 UCT on 24 July 1985. Except over snow or ice, typical albedo values should range from 0.05 to 0.30. All mapped values were below 0.16, with some below 0.05, indicating a possible underestimation. The ratio RF3 (reflected solar radiation) over RF1 (global solar radiation on a horizontal surface) for Toronto Research Station at 1800 UCT was 0.22.

Midday Surface temperatures estimated from satellite IR

Surface temperatures were derived from satellite for 1800 UCT. Over land, there was no routine measurement available to compare the values directly. Hottest spots were estimated in the range from 27°C to 40°C. Near the edges of the estimated cloud area , there were pixels classified with temperature values below 0°C . This is due to clouds, undetected using the single VIS threshold classification.

Over water, there are routine NOAA estimates available for lake water temperature (see Irbe et al, 1982). Maps of July 23, 0800 UCT NOAA estimated water temperatures for lake Erie indicate values from 20°C near the Northern edges of the lake to 22°C over most of the lake and above 23°C in the Southwestern sector and near the Southern edges. The ET scheme is not intended to be used over water, but since it automatically evaluates the surface temperatures at every cloud free location, these are available for comparison. The GOES surface temperature estimates gave values above 25°C near the Northern edges of lake Erie, a large central area of temperatures between 16 and 20 °C , and values between 21-22°C over the Southwestern portion of the lake. Too high values of the Northern portion of the data are explained by a navigation error of the infrared GOES data that resulted in a shift of the data to the South. Once the data was shifted to correct this error, a comparison of numerical values indicated that the lake surface temperature using GOES data were underestimated by about two degrees.

Lake Ontario GOES pattern also required a shift to the North. Temperatures ranged then from 10 to 14°C in the Northwest, to 15°C in the centre to 16-20°C near the Southern edge of the lake. NOAA lake water temperature estimates for July 23 at 0800 UCT were obtained separately. They ranged from temperatures < 14°C in a narrow band over the Northern sector of the lake to about 16°C over the middle to 18°C and above over the Southern sector. Comparison of numerical data indicates that the lake Ontario surface temperatures from GOES data were underestimated by two or three degrees.

Objective analysis of midday air temperatures (T_a) from reporting stations.

Hourly temperatures over the CLI-GRID area are available from a limited set of 15 Canadian stations. On the other hand, the climatological network provides maximum and minimum data at about 860 climatological stations. The idea is to model the diurnal temperature cycle between the maximum and the minimum temperatures and to extract an hourly temperature estimate. A simple theoretical scheme was used for this purpose. The estimates were objectively analyzed by the Gandin statistical technique (Gandin 1963) over the CLI-GRID area. Comparison of the values at the location of the 15 hourly stations provided correction parameters which were also objectively analyzed. Most analysed values of this analysis ranged from 18°C to 31°C.

Daily net radiation fields (Rn^{24})

Daily net radiation field was estimated using the 1800 UCT satellite-derived net radiation in equation 10. Highest estimated net radiation (23 to 25 Megajoules/day-m^2 .occured over lakes. Intermediate values (21-22 Megajoules/day-m^2) occurred over forests. Lower radiation values (19-20 Megajoules/day-m^2) occurred over agricultural areas. Verification data was extracted from the archives for Elora Research Station (43.39N, 80.25W). The ground truth daily value was 14.0 MJ/m^2. The satellite estimate at this location was 20 Mj/m^2. This satellite overestimate might be explained partly due to the presence of clouds during the day in that region.

At the Toronto Meteorological Research Station (43.40N, 79.24W), the ground truth was 15.3 Mj/day-m^2, but the cloud mask prevented an estimate using satellite data. The daily net radiation estimates vary from 19 to 25 Mj/day-m^2. Values over the CLI-GRID area rarely exceed 15 Mj/day-m2, which indicates that equation 10 lead towards an overestimate of the net radiation field.

B term

The B (Heat transfer) term was derived in mm/day units as described before. A large portion of the non-cloudy data was assigned a value of zero, corresponding to areas of smaller difference between air and surface temperatures. This occurs mostly over forests and lakes. Vertical heat flux occurs over agricultural areas, specially where surface temperature exceeds 25°C.

Daily evapotranspiration

Maximum values of evapotranspiration appear over water bodies with estimated evaporation of 10 mm/day. Evaporation over water bodies might suffer from errors due to non-negligible heat storage, in addition to the already mentioned error sources. An intermediate value of 9 mm/day occurs over forest areas. The lowest evapotranspiration values (1 to 8 mm/day) appear over agricultural land.

Table 2 below shows the relative contribution of the net radiation and heat transfer terms to ET at selected locations for the case of July 24, 1985. We already noted in section 2.1 that the heat transfer term would be of smaller magnitude than the net radiation term. The linear correlation coefficient between net radiation and ET from the estimates given in Table 2 is r = 0.75.

TABLE 2 : Relative Contribution of Net Radiation and Heat Flux Terms to ET estimates.

Grid coordinates	Net Radiation mm/day	Heat Transfer mm/day	ET mm/day
64, 32	10	0	10
64, 96	10	0	10
80, 45	10	0	10
80, 110	9	1	8
128, 32	9	0	9
128, 64	9	0	9
128, 96	8	2	6
140, 45	9	0	9
140, 80	8	1	7
140, 110	8	1	7
192, 64	9	0	9
192, 96	8	4	4
220, 80	8	0	8
220, 110	8	2	7
240, 110	8	0	8
245, 115	9	3	6

3.2 Discussion

The intermediate and final results showed the feasibility of generating multiple location estimates of evapotranspiration, based on satellite data. The comparison of patterns with the ground truth values indicated where improvements can be made. The significant overestimation of net radiation is the most important factor to correct. The second most important improvement would be the introduction of NOAA surface temperature estimates. The implementation approach makes it easy to add gradual refinements to the algorithms and to better the estimates.

Further development should incorporate classical treatement of the influence of winds on the B term. Effects and variability of land surface could be subject of a very detailed investigation. Finally, the model is not conceptually difficult and its application has been limited mainly due to the effort required in obtaining input data. This last problem will gradually disappear as better data assimilation systems become available. Currently, implementations using NOAA data occur very rapidly and simultaneously in many countries, with U.S., France, The Netherlands and Findland ahead of the race. The normalised difference vegetation index is already used in certain schemes.

REFERENCES

Benchimol, N., 1985: The Mesoscale Variability of Insolation Over the Lower Fraser Valley Resolved by Geostationary Satellite Data. *Canadian Climate Centre, CCC report* No. 85-8.

Benchimol, N. and J. E. Hay, 1986: An Assessment of the Ability of a Geostationary Satellite-Based Model to Characterize the Mesoscale Variability of Solar Irradiance Over the Lower Fraser Valley. *ATMOSPHERE-OCEAN*, **24**, 128-144.

Bussières, N. and P.Y.T. Louie, 1987: Estimating Regional Evapotranspiration from Satellite Data: A Feasibility Study. *Canadian Climate Centre, CCC report No. 87-12.*

Bussières, N. and P.Y.T. Louie, 1989: Implementation of an Algorithm to Estimate Regional Evapotranspiration Using Satellite Data. Unpublished report. Available on request by contacting the authors at the Hydrometoreology Division, Canadian Climate Centre (416) 739-4343.

Cooper, D.I., Russo, J.M. and E.M. Perry, 1984: Measurements Uncertainties with Satellite-Derived Surface Temperatures. Pennsylvania State University.

Gandin, L.S. 1963: Objective Analysis of Meteorological Fields. English version published through the *Israel Program for Scientific Translation (IPST)*, Jerusalem, 1965.

Hogg, W. 1986: Production of Gridded Datasets Through Integration and Objective Analysis of Multiple Source Climate Data. CLI-GRID Pilot Project Description. Unpublished *internal document*, Atmospheric Environment Service, Environment Canada.

Irbe, G.J., Cross, R.K. and A. Saulesleja, 1982: An Operational Program for Monitoring Surface Temperatures of Lakes and Coastal-Zone Waters in Canada from Polar-Orbiting Satellite Infrared Data. *NAFO Sci. Coun. Studies*, **4**, 31-39.

Jackson, R.D., Reginato, R.J., and S.B. Idso, 1977: Wheat Canopy Temperature: A Practical Tool for Evaluating Water Requirements. *Water Resour. Res.* **13**, 651-656.

Justice, C.O., Townshend, J.R.G., Holben, B.N., and C.J. Tucker, 1985: Analysis of the phenology of global vegetation using meteorological satellite data. *Int. J. Remote Sensing*, **6**, 1271-1318.

Monteith, J.L., 1973: *Principles of Environmental Physics* (London: Edward Arnold).

Nieuwenhuis, G.J.A., Smidt, E.H., and H.A.M. Thunnissen, 1985: Estimation of Regional Evapotranspiration of Arable Crops from Thermal Infrared Images. *Int. J. Remote Sensing*, **6**, 1319-1334.

Price, J.C., 1980: The Potential of Remotely Sensed Thermal Infrared Data to Infer Surface Soil Moisture and Evaporation. *Water Resour. Res.*, **16**, 787-795.

Price, J.C., 1983: Estimating Surface Temperatures from Satellite Thermal Infrared Data - A Simple Formulation for the Atmospheric Effect. *Remote Sens. Environ.* **13**, 353-361.

Rambal, S., Lacaze, B., Mazurek, H. and G. Debussche, 1985: Comparisons of Hydrologically simulated and Remotely Sensed Actual Evapotranspiration from some Mediterranean Vegetation Formations. *Int. J. Remote Sensing*, **6**, 1475-1481.

Reiniger, P. and B. Seguin, 1986: Surface Temperature as an Indicator of Evpotranspiration and Soil Moisture. *Remote Sensing Reviews*, 1, 277-310.

Seguin, B., and B. Itier, 1983. Using Midday Surface Temperature to Estimate Daily Evaporation from Satellite Thermal IR data. *Int. J. Remote Sensing*, 4, 371-383.

Serafini, V.V., 1987: Estimation of the evapotranspiration using surface and satellite data. *Int. J. Remote Sensing*, 8, 1547-1562.

Taconet, O., Bernard, R., and D., Vidal-Madjar, 1986: Evapotranspiration over an Agricultural Region Using a Surface Flux/Temperature Model Based on NOAA-AVHRR Data. *J. Clim. Appl. Meteorol.*, 25, 284-307.

Tsonis, A.A., 1983: Examination of the Spectral and Spatial Characteristics of the Visible and Infrared GOES Images and applications. Environment Canada, Atmospheric Environment Service, Atmospheric Research Directorate, *Internal Report* No. **ARPB 116 P 39**.

Questions and Answers

Jean-Pierre Fortin: The air temperature you refer to is the 1.5 metre temperature. What are you doing to correct air temperature over trees?

Normand Bussières: Right now, there is no correction made but the method is not as sensitive over forested areas as over agricultural areas.

Jean-Pierre Fortin: All experiments have been made over wilderness areas with areas of mixed land use. So what are you doing with mixed land use?

Normand Bussières: The algorithm uses the predominant classification so that, for example, if an area has 60% forest and 40% lake, then the method would use forest.

John Stewart: Did "B" value depend on roughness of vegetation?

Normand Bussières: It was a constant value.

John Stewart: Did you find a difference in albedo between forest and prairie? It looked from your estimates that if albedo decreased from 0.25 over the prairie to 0.10 over the forest, then the net radiation should have gone up by 15% in the forested area.

Normand Bussières: Yes, there is a consistent difference in albedo.

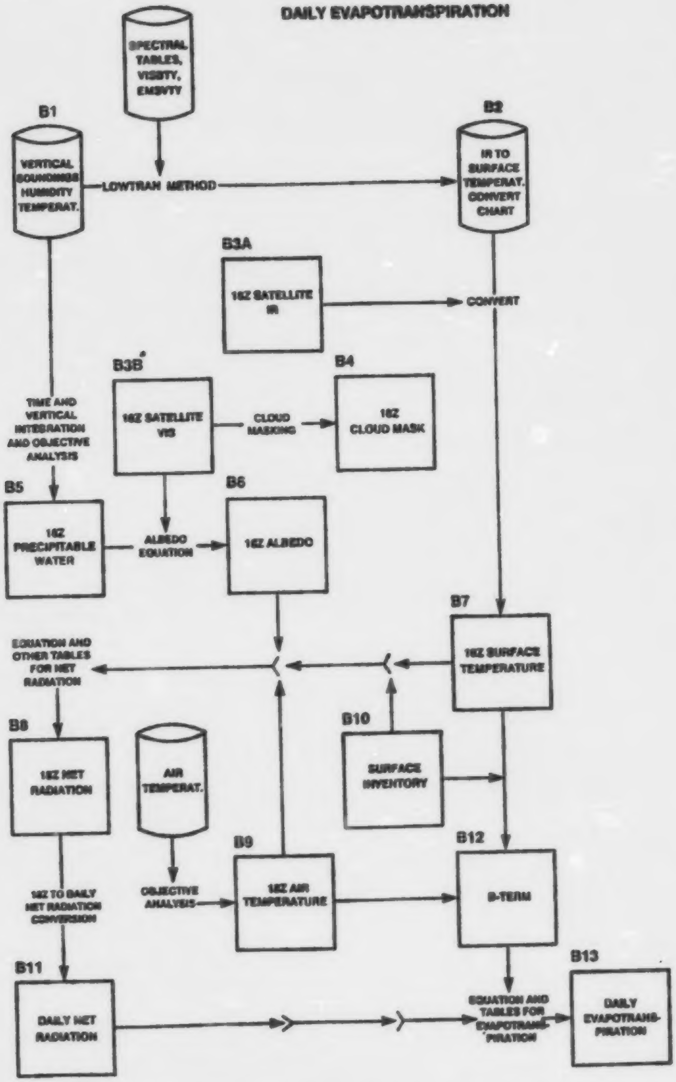
DAILY EVAPOTRANSPIRATION
SPECTRAL TABLES, VISBTY, EMSVTY
B1
VERTICAL SOUNDINGS HUMIDITY TEMPERAT.
LOWTRAN METHOD
B2
IR TO SURFACE TEMPERAT. CONVERT CHART
B3A
18Z SATELLITE IR
CONVERT
B3B*
18Z SATELLITE VIS
CLOUD MASKING
B4
18Z CLOUD MASK
TIME AND VERTICAL INTEGRATION AND OBJECTIVE ANALYSIS
B5
18Z PRECIPITABLE WATER
ALBEDO EQUATION
B6
18Z ALBEDO
B7
18Z SURFACE TEMPERATURE
EQUATION AND OTHER TABLES FOR NET RADIATION
B8
18Z NET RADIATION
AIR TEMPERAT.
B10
SURFACE INVENTORY
B9
18Z AIR TEMPERATURE
OBJECTIVE ANALYSIS
B12
B-TERM
18Z TO DAILY NET RADIATION CONVERSION
B11
DAILY NET RADIATION
B13
EQUATION AND TABLES FOR EVAPOTRANSPIRATION
DAILY EVAPOTRANSPIRATION

Figure 1. Data Flow Diagram for implementation of ET algorithm

UPDATING HYDROLOGICAL MODEL FORECASTS

Hamed Assaf and Michael C. Quick[*]

February 23, 1990

Abstract

A flow updating model is presented in which the flow is estimated using outputs from a physically-based watershed model(UBC watershed model) and a feedback of the most recent flow measurement. These outputs(the flow components) are modified by certain parameters that are updated whenever a flow measurement is available. The updating process is based on a state-space model where Kalman filter technique is used to update the parameters from their past values and the most recent flow measurement. The extent of updating is controlled by the relative uncertainties in the flow measurements and the parameters. The updating model has been applied on the Illecilewaet basin and the flow forecasts have shown great improvement over the ones obtained by using the UBC watershed model only.

The flow updating model is formulated based on an assumption that the errors in the watershed model output are of a certain linear structure. The validity of such assumption could be tested by comparing some statistical measures of performance.

1 Introduction

Operation and management of watershed systems require accurate and reliable flow forecasts on short period basis. These short term forecasts are also very essential for effective flood control measures.

In the late sixties the philosophy behind flow forecasting was to develop physically-based models that simulates the behavior of the watershed system based on "presumably" error-free input(precipitation, temperatures, etc..). The flow measurements were not used as feedback except in the calibration mode where historical flow records were used for selecting values of the model parameters that produces flow forecasts that best fit these records. To incorporate flow

---

[*] Respectively, Graduate Student and Professor, Dept. of Civil Engineering, University of British Columbia, Vancouver, B.C., Canada, V6J 1Z9

measurements in the forecasting process early concepts of the filtering theory were applied to design simple linear models that simulate the input-output behavior of the watershed system. Treating the watershed system as a black box is a mathematical convenience that ignores the watershed system physical behavior and relies heavily on an oversimplified short-term input-output relationship. These assumptions made these models unreliable and inaccurate especially for medium and long forecast leads.

New developments in the filtering theory and its successful application in other fields of engineering led to more application of its concepts in hydrology. In particular the hydrologist is able to describe some of the hydrological processes in difference equations that can then be formulated in a state-space format. This format is a very convenient form for applying filtering theory to update certain parameters in the model using the runoff data as feedback. Many models have been developed using this approach and they range widely in their complexity and application.

In the current work, outputs from an off-line deterministic model (UBC watershed model) are coupled with the most recent flow measurement in a state-space format to update flow forecasts for a given forecast lead. The updating process is achieved using a Kalman filtering scheme. The flow updating model has been based on the output of UBC model to avoid dealing with the nonlinear structure of UBC model. Measurement noise variance and model uncertainty are the main factors that control the updating process. The flow updating model is quite flexible and produces accurate and reliable flow forecasts even for long forecast leads.

The present work is not meant to be the ultimate updating model to be used in operation. It only serves as an illustration of flow updating techniques. More work is being done to develop flow updating methods based on snowpack or snow-covered area, which are expected to show the greatest longterm improvement in forecast.

2 General Description Of The UBC Watershed Model

UBC watershed model is designed based on a mathematical representation of the physical processes that control the watershed system. Therefore, the UBC model belongs to the family of deterministic models. The model is designed primarily for watershed systems that are mainly driven by snowmelt. The model requires daily inputs of maximum and minimum temperatures and precipitation. The model calculates on daily basis the time distribution of streamflow leaving the catchment as a result of snowmelt and rainfall.

A general schematic description of the model is shown in Fig. 1[1]. As can be seen from Fig. 1, the precipitation is distributed into snow or rain according to the maximum and minimum temperatures. Then, the slow components of rain and snow melt are combined to give the groundwater flow component Q_{GW}. The fast component of snowmelt is distributed using a fast unit hydrograph to yield the snowmelt flow component Q_{SN}. And the fast component of rain is distributed using another fast unit hydrograph to produce the rain flow component Q_{RN}. The flow at the basin outlet is then estimated as the sum of these three components :-

---

[1] Other irrelevant details have been left out.

(1) $Q_{CAL} = Q_{SN} + Q_{RN} + Q_{GW}$

3 The Scheme Of The Flow Updating Model

3.1 Modifying the UBC Watershed Model

The flow updating model is developed based on modifying Eq. 1 by estimating the flow as a weighted sum of the three flow components Q_{SN}, Q_{RN} and Q_{GW}, i.e.:

(2) $Q_{EST}(t) = A_{SN}(t) * Q_{SN}(t) + A_{RN}(t) * Q_{RN}(t) + A_{GW}(t) * Q_{GW}(t)$

where Q_{EST} is the estimated flow; and A_{SN}, A_{RN} and A_{GW} are the weighting factors for the flow components Q_{SN}, Q_{RN} and Q_{GW}, respectively. These weighting factors are assumed to be stochastic and normally distributed[1] variables. It is the objective of the updating model to estimate the means and the variances of these weighting factors. The means serve as the best estimates of these factors; while the variances determine the confidence limits of these estimates. The updating process is achieved by applying kalman filter scheme using the most recent flow measurement.

The model scheme is based on the assumption that the forecast residual (or error) from UBC watershed model is linearly related to the corresponding flow components. The validity of this assumption is very important for the updating model to be effective, especially for long forecast leads. This assumption has been proved to be valid for the data record of the Illecilewaet basin. A simple statistical test could be applied to test the validity of such assumption, as will be shown in a later section.

3.2 The State-Space Format of the Updating Model

The weighting factors A_{SN}, A_{RN} and A_{GW} are assumed, as mentioned in the previous section, to be stochastic variables. So they could be expressed as follows :

$$A_{SN}(t) = A_{SN}(t-1) + W_{SN}(t-1)$$

---

[1] i.e. they can be fully described by their first two moments the mean and the variance.

$$\text{(3)}\quad \begin{aligned} A_{RN}(t) &= A_{RN}(t-1) &+W_{RN}(t-1) \\ A_{GW}(t) &= A_{GW}(t-1) &+W_{GW}(t-1) \end{aligned}$$

Where:

W_{SN}, W_{RN} and W_G are random errors (or white noise processes) of zero means and variances VAR_{SN}, VAR_{RN} and VAR_{GW}, respectively. This can be expressed as follows: -

$$\begin{aligned} W_{SN} &\sim N(0, VAR_{SN}) \\ W_{RN} &\sim N(0, VAR_{RN}) \\ W_{GW} &\sim N(0, VAR_{GW}) \end{aligned}$$

The series $\{A_{SN}\}, \{A_{RN}\}$ and $\{A_{GW}\}$ are therefore random walk processes.[2] The behavior of the weighting factor in time can be expressed as in Fig. 2. The solid lines in Fig. 2 represent the best estimates of the weighting factors (i.e. their means) ; while the points represent their possible values that lie within boundaries determined by the corresponding variances. The larger the variances the wider these boundaries and the more scattered the possible values are. Therefore, the variances is a measure of the accuracy of the estimates: large values mean poor accuracy, and vice versa.

In the Baysian approach the probability density function (*pdf*) of a certain variable can be updated (or refined) whenever a new relevant information is available. Since a Gaussian (normally distributed) *pdf* is fully described by its mean and variance, it can be updated by updating its mean and variance. The recursive solution of this problem has been formulated by Kalman (1960) and Kalman and Bucy (1961). This solution has since then been referred to as Kalman filter.

Assuming that the weighting factors are normally distributed processes of means (M_{SN}, M_{RN} and M_{GW}, respectively) and variances (P_{SN}, P_{RN} and P_{GW}, Kalman filter can be applied on the following state-space model to update the flow estimates whenever a new flow measurement is available.

$$\left.\begin{aligned} A_{SN}(t) &= A_{SN}(t-1) &+W_{SN}(t-1) \\ A_{RN}(t) &= A_{RN}(t-1) &+W_{RN}(t-1) \\ A_{GW}(t) &= A_{GW}(t-1) &+W_{GW}(t-1) \end{aligned}\right\}\text{State Equation}$$

$$\text{(4)}\quad \left.\begin{aligned} Q_{OBS}(t) = {} & A_{SN}(t) * Q_{SN}(t) + A_{RN}(t) * Q_{RN}(t) + \\ & A_{GW}(t) * Q_{GW}(t) + V(t) \end{aligned}\right\}\begin{array}{c}\text{Measurement}\\ \text{Equation}\end{array}$$

Where: $V(t)$ is the measurement noise and is a random process (white noise) of zero mean and variance R. R is an index of the measurement quality. Good measurement yields small variance; while bad one results in a large variance. As will be explained later, the updating process is controlled by the relative values of the measurement and state variances. Therefore, it is crucial to select the ratio of measurement variance to state variances that produces the best performance of the model. However, the absolute values of the variances are important for calculating the confidence limits of the flow forecasts.

---

[2] Random walk process is expressed as:- $X(t) = X(t-1) + V(t-1)$

3.3 Model Algorithm

A) At time $T = 0$, the weighting factors are estimated to be equal to unity, i.e. :

$$\begin{aligned} \hat{A}_{SN}(0) &= 1.0 \ ; \\ \hat{A}_{RN}(0) &= 1.0 \ ; \quad \text{and} \\ \hat{A}_{GW}(0) &= 1.0 \end{aligned}$$

These values are selected assuming no previous knowledge of the weighting factors. The initial values of the weighting factors variances are assumed to be equal to fixed percentages of the corresponding weighting factors. Selecting this percentage to be equal to 10% :

$$\begin{aligned} \hat{P}_{SN}(0) &= (0.1 * \hat{A}_{SN}(0))^2 \ ; \\ \hat{P}_{RN}(0) &= (0.1 * \hat{A}_{RN}(0))^2 \ ; \quad \text{and} \\ \hat{P}_{GW}(0) &= (0.1 * \hat{A}_{GW}(0))^2 \end{aligned}$$

B) (Prediction step) The values of the weighting factors and their corresponding variances for the next forecast lead period (FL days) could be predicted from Eq. 4 as follows :

$$\begin{aligned} \hat{A}_{SN}(0+FL)_- &= \hat{A}_{SN}(0) \\ \hat{A}_{RN}(0+FL)_- &= \hat{A}_{RN}(0) \\ \hat{A}_{GW}(0+FL)_- &= \hat{A}_{GW}(0) \end{aligned} \tag{5}$$

$$\begin{aligned} \hat{P}_{SN}(0+FL)_- &= \hat{P}_{SN}(0) + VAR_{SN}(0) \\ \hat{P}_{RN}(0+FL)_- &= \hat{P}_{RN}(0) + VAR_{RN}(0) \\ \hat{P}_{GW}(0+FL)_- &= \hat{P}_{GW}(0) + VAR_{GW}(0) \end{aligned} \tag{6}$$

Where the hat sign $\hat{()}$ indicates that these values are only estimates ; and the negative sign ($_-$) indicates that these estimates are calculated before a new measurement is available

C) The flow for time ($t = 0 + FL$) is estimated as follows :

$$\begin{aligned} Q_{EST}(0+FL) = &\ \hat{A}_{SN}(0+FL) * Q_{SN}(0+FL) + \\ &\ \hat{A}_{RN}(0+FL) * Q_{RN}(0+FL) + \\ &\ \hat{A}_{GW}(0+FL) * Q_{GW}(0+FL) \end{aligned} \tag{7}$$

D) Once a new measurement is available the prediction error (residual) could be calculated as follows;-

(8) $ERR(0+FL) = Q_{OBS}(0+FL) - Q_{EST}(0+FL)$

E) The Kalman gain $\mathbf{K}(0+FL)$ to be used in the next updating step is calculated as follows :
let

$$\hat{\mathbf{P}}(t) = \begin{bmatrix} P_{SN}(t) & COV(A_{SN}(t), A_{RN}(t)) & COV(A_{SN}(t), A_{GW}(t)) \\ COV(A_{RN}(t), A_{SN}(t)) & P_{RN}(t) & COV(A_{RN}(t), A_{GW}(t)) \\ COV(A_{GW}(t), A_{SN}(t)) & COV(A_{GW}(t), A_{RN}(t)) & P_{GW}(t) \end{bmatrix}$$

where for example: $COV(A_{SN}(t), A_{RN}(t))$ is the covariance of the weighting factors A_{SN} and A_{RN} at time t.
Let,

$$\mathbf{H}(t) = [\ Q_{SN}(t) \quad Q_{RN}(t) \quad Q_{GW}(t)\ ]$$

Then,

$$\begin{aligned} \mathbf{K}(0+FL) &= \hat{\mathbf{P}}(0+FL)_- * \mathbf{H}(0+FL)^T * \\ &\quad \left[\mathbf{H}(0+FL) * \hat{\mathbf{P}}(0+FL)_- * \mathbf{H}(0+FL)^T + \mathbf{R}(0+FL)\right]^{-1} \end{aligned} \quad (9)$$

F) (Updating step) The prediction error and the kalman filter gain $\mathbf{K}(0+FL)$ are used in the following equation to give new estimates of the weighting factors and their corresponding variances:
Let,

$$\hat{\mathbf{A}}(t) = \begin{bmatrix} \hat{A}_{SN}(t) \\ \hat{A}_{RN}(t) \\ \hat{A}_{GW}(t) \end{bmatrix}$$

(10) $\hat{\mathbf{A}}(0+FL)_+ = \hat{\mathbf{A}}(0+FL)_- + \mathbf{K}(0+FL) * ERR(0+FL)$

(11) $\hat{\mathbf{P}}(0+FL)_+ = [\mathbf{I} - \mathbf{K}(0+FL) * \mathbf{H}(0+FL)] * \hat{\mathbf{P}}(0+FL)_-$

Where,
$\mathbf{I}$ is the identity matrix, and the positive sign $(_+)$ indicates that the estimates are calculated after obtaining a new flow measurement.

G) The values of the weighting factors and their corresponding variances for the next forecast period are predicted as in step (**B**). Using general terms, at time t_k the weighting factors can be predicted for the time $(t_{k+1} = t_k + FL)$ as follows :

(12) $\hat{\mathbf{A}}(t_{k+1})_- = \hat{\mathbf{A}}(t_k)_+$

(13) $\hat{\mathbf{P}}(t_{k+1})_- = \hat{\mathbf{P}}(t_k)_+ + \mathbf{VAR}(t_k)$

Where :

$$\mathbf{VAR}(t) = \begin{bmatrix} VAR_{SN}(t) & 0 & 0 \\ 0 & VAR_{RN}(t) & 0 \\ 0 & 0 & VAR_{GW}(t) \end{bmatrix}$$

In general terms, steps **C** to **F** can be expressed as follow :-

- Estimating the flow for the next forecast period :

(14) $Q_{EST}(t_{k+1}) = \mathbf{H}(t_{k+1}) * \hat{\mathbf{A}}(t_{k+1})_-$

- Calculating the prediction residual :

(15) $ERR(t_{k+1}) = Q_{OBS}(t_{k+1}) - Q_{EST}(t_{k+1})$

- Calculating Kalman gain $\mathbf{K}(t_{k+1})$

$$\mathbf{K}(t_{k+1}) = \hat{\mathbf{P}}(t_{k+1})_- * \mathbf{H}(t_{k+1})^T * \left[\mathbf{H}(t_{k+1}) * \hat{\mathbf{P}}(t_{k+1})_- * \mathbf{H}(t_{k+1})^T + \mathbf{R}(t_{k+1})\right]^{-1} \quad (16)$$

- Updating the estimates of the weighting factors :

(17) $\hat{\mathbf{A}}(t_{k+1})_+ = \hat{\mathbf{A}}(t_{k+1})_- + \mathbf{K}(t_{k+1}) * ERR(t_{k+1})$

(18) $\hat{\mathbf{P}}(t_{k+1})_+ = [\mathbf{I} - \mathbf{K}(t_{k+1}) * \mathbf{H}(t_{k+1})] * \hat{\mathbf{P}}(t_{k+1})_-$

So, Eqs. 12 to 18 represent the general algorithm of the flow updating model.

4 The Role Of The Measurement And State Variances in the Updating process

Examining Eq. 17, it can be seen that the extent by which the weighting factors $\hat{\mathbf{A}}(t)$ are updated depends on Kalman gain $\mathbf{K}(t)$. Smaller $\mathbf{K}$ results in minimal updating and vice versa.

From Eq. 16, it can be seen that $\mathbf{K}(t)$ is a function of the relative values of the covariance matrix ($\hat{\mathbf{P}}$) and the measurement variance $\mathbf{R}$. Since $\hat{\mathbf{P}}$ is a function of the state variances **VAR** and **R** (Eqs. 13 and 18) $\mathbf{K}(t)$ is ,therefore, a function of the relative values of **VAR** and **R** which increases with increasing **VAR** and decreasing **R**. Thus, the updating process is controlled by the relative variances (or accuracies) of the measurements and the output of UBC watershed model. For example, if there are good quality measurements but inaccurate output from the UBC watershed model, then a large value of $\mathbf{K}$ will result, and this will produce a significant updating[3] of the weighting factor estimates (Eq. 17) leading to a major updating of the flow forecast (Eq. 14). Alternatively, for bad measurements (high $\mathbf{R}$) combined with good output of UBC watershed model a small value of $\mathbf{K}$ will result, and this will produce insignificant updating. Therefore, it is of great importance to select a ratio of state to measurement variance that will produce a good flow forecast update. The absolute values of the variances are needed for calculating the covariance matrix $\hat{\mathbf{P}}$ (Eqs. 13 and 18) to define the confidence limits of the estimates.

In the present work the variances are assumed to be proportional to a an unknown positive quantity σ^2. The maximum likelihood estimate of σ^2 could be expressed[4]as follows :

$$(19)\quad \sigma^2 = \frac{\sum_{i=1}^{m} \frac{\mathbf{ERR}^2(t)}{\mathbf{VAR}_{ERR}(t)}}{N}$$

Where :

$$N = \sum_{i=1}^{m} FL \text{ is the record length in days;}$$

m is the number of flow observations available for updating; and
$\mathbf{VAR}_{ERR}$ is the variance of the prediction error (ERR) calculated as follows :

$$(20)\quad \mathbf{VAR}_{ERR}(t) = \mathbf{R} + \mathbf{H}(t) * \hat{\mathbf{P}}_{-}(t) * \mathbf{H}^T(t)$$

Then, the absolute values of the variances could be estimated from σ^2.

5 Model Performance Criterion

For evaluating the general performance of the model on a given period the criterion NTD has been used. NTD is defined as follows:

$$(21)\quad NTD = \frac{S_{OBS} - S}{S_{OBS}}$$

Where:

$$S = \sum_{i=1}^{N}(Q_{OBS}(i) - Q_{EST}(i))^2 \quad ;$$

$$S_{OBS} = \sum_{i=1}^{N}(Q_{OBS}(i) - \overline{Q}_{OBS})^2 \qquad ; \text{and}$$

---

[3] Providingthat the residual (ERR) is not very small

[4] Harvey (1981), page14, equation 2.21

$\overline{Q}_{OBS}$ is the observed mean flow for the given record.

So, NTD measure the performance of the flow updating model against the mean of the observed flows using the criterion of the sum of squares of errors.A positive value of NTD indicates that the updating model is doing better than just estimating the flow by its mean. A negative value indicates otherwise. An NTD value of unity means that the updating model perfectly forecasted the flow.

6 Sensitivity Analysis Of The Variances

Since the ratio of the state to measurement variances is the only factor that controls the updating process, it would be sufficient to apply sensitivity analysis of the model performance versus either the measurement or the state variances and fix the other variance(s).

In the present work, the model performance has been tested in relation with the measurement variance and fixing the values of the state variances at 0.01, calculated as the square of 10% of the initial values of the weighting factors (which are equal to unity) as shown below:

$$\begin{aligned} VAR_{SN} &= (0.1 * A_{SN}(0))^2 &= (0.1 * 1.0)^2 &= 0.01 \\ VAR_{RN} &= (0.1 * A_{RN}(0))^2 &= (0.1 * 1.0)^2 &= 0.01 \\ VAR_{GW} &= (0.1 * A_{GW}(0))^2 &= (0.1 * 1.0)^2 &= 0.01 \end{aligned}$$

The performance of the model has been tested for measurement variances between 0 and 20,000 CMS^2. The test has been applied for several forecast leads (1, 5, 10, 15, 20, 25 and 30 days.) The results are shown in Figs. 3 and 4. Fig. 3 shows the sensitivity analysis of the updating model on the Illecilewaet basin for the period April 15 to July 15, 1970. This period has been selected since it represents the period of the summer season in which snowmelt is the dominant source of flow. This results in the highest and most rapidly changing flows that are very important yet difficult to forecast. It is important to point out that forecasting the flow for the Illecilewaet basin using the UBC watershed model has not been fully developed. Therefore, better performance of the UBC model can be achieved using a more accurate calibration.

It can be noticed from Fig. 3 that in general the NTD is relatively insensitive to the measurement variance and attains its highest levels for measurement variance values between 200 CMS^2 and 500 CMS^2. However, very high values of measurement variance drastically affects the performance of the model especially for long forecast leads as can be seen from Fig. 4 (with an extended scale of measurement variance up to 20,000 CMS^2.) The performance of the model for forecast lead of 30 days decays to levels very close to that of the performance of the UBC Watershed model without updating as the variance becomes very high ; while the performance of the updating model for forecast lead of 1 day is still at high values of NTD even for high values of measurement variance

(Fig. 4.) This behavior could be explained by the fact that high measurement variance causes a minimal updating of the estimates of the states. However, in the case of small forecast lead this effect is reduced by the presence of relatively large number of measurements (eg. 92 measurements in the case of a one day forecast lead) available for updating; while in the case of a long forecast lead, much less number of observations (4 measurements in the case of the 30 day forecast.) are available for updating.

Fig. 3 shows that, in general, very small measurement variance causes a reduction in the model performance and might lead to very poor results (as the case of forecast lead of 20 days.) This is due to the fact that very small measurement variance makes the updating model very sensitive to the measurements causing the model to perform badly if some of the measurements contain large errors.

Another approach of selecting measurement variance is to set it equal to the square of a certain percentage of the observed flow. This is probably a reasonable assumption because the variance will probably increase with the flow. The state variances could similarly be set equal to the squares of given percentages of their corresponding weighting factors.

Fig. 5 shows the NTD .vs. measurement variance estimated as the square of given percentages (from 0% to 100%) of the observed flow. The state variances have been set equal to the square of 10% of their corresponding weighting factors. Starting with 0% measurement variance, the NTD increases with measurement variance up to a certain peak. From there it declines with a rate related to the forecast lead. The shorter the forecast lead the slower the rate of decline and vice versa. This behavior is similar to the result observed for fixed measurement variance. However, the peak is generally flatter in the latter. In other words, the updating model is more sensitive to the measurement variance as $(\% \text{ flow})^2$ than to fixed variance. This is expected, since the scale of square of 0% to 100% of observed flow is roughly equivalent to 0 to 10000 CMS^2 for an average observed flow of 100 CMS which is a little less than the actual average. The model attains its highest levels of performance for measurement variances between 10% to 20%. Which is a conveniently wide range to choose the from.

The approach of recursively estimating one or both of the measurement and the state variances from flow observations is called adaptive Kalman filtering. Most of the methods using this approach utilize the condition that the prediction errors (residuals) from the application of Kalman filter have to be uncorrelated with each other (i.e belong to white noise process.) However, imperfect conditions of any application case result in residuals that tend to be correlated. Variances could then be recursively updated on the basis of minimizing the correlation between residuals.

Some of the methods reviewed require strict conditions that do not apply for the current work. Others are complex and require estimation of many parameters (see Mehra (1970) and Todini (1978) .) However, an algorithm that updates the state variance has been developed based on the work of Kitanidis and Bras (1978b). No significant differences have been noticed between the adaptive and the non-adaptive models. This is not unexpected, since the adaptive algorithm is designed for slow time-varying variances. And since the model performance is relatively insensitive to the variances no significant improvement is expected from small changes in the variances.

For the present work, adaptive filtering does not give any significant improvement and is also complex, time consuming and generally requires the knowledge of additional parameters. Consequently, fixed or percentage-wise variances are sufficient for obtaining good and reliable flow forecasts. Fixed values of 200 CMS^2 for the measurement variance and 0.01 for the state variances have been selected for the application case to be presented in the next section.

7 Application

The flow updating model is applied to the output of UBC Watershed Model and to the flow observations of the Illecilewaet basin for the period April 15 to July 15, 1970. The diagonal elements of the initial covariance matrix $\hat{\mathbf{P}}(0)$ are set equal to the corresponding state variances (i.e. 0.01.) The initial values of the weighting factors are set at values equal to unity.

The Hydrographs of the observed flow, the flow calculated by the UBC watershed model , the updated flows for forecast leads of 1 day, 10 days, 20 days and 30 days and their corresponding residuals are shown in Figs. 6a,b,c &d, respectively. Fig. 6a shows that the daily updated hydrograph fits the observed flow hydrograph more closely than the UBC calculated hydrograph. The model performance measured by the NTD is improved by 20%, from 0.741 to 0.945 as can be seen from Table 1. Although much less number of measurements are available for updating for a forecast lead of 10 days the flow updating is still doing very well as can be seen from Fig. 6b. This is reflected in the high NTD value of 0.926. Fig. 6c shows that the high performance of the flow updating model is not very much affected for a forecast lead of 20 days where less number of measurements are available for updating. The NTD is still high at value of 0.92. for a forecast lead of 30 days, a very small number of measurements are available for updating, especially in the high flow region. This causes minimal updating until a later stage(after June 16) where improvement in the forecasting is noticed (Fig. 6d .) This causes an increase in the NTD value from 0.741 to 0.813.

8 Testing Model Performance Using Other Least Square Criteria

Several features of model performance can be tested using different least square criteria. Their definitions and the results of their applications on the model forecast are listed below :-

1. The coefficient of determination "R" defined as follows :

$$(22) \quad R = \frac{S_{OBS} - S_{REG}}{S_{OBS}}$$

Where,
S_{OBS} is as define before in section (5); and

$$S_{REG} = \sum_{i=1}^{N} (Q_{OBS}(i) - Q_{REG}(i))^2$$

where $Q_{REG}(i)$ is the flow calculated from linear regression of the observed flow against the flow calculated by the model. Therefore, R measures the performance of the model after removing errors that are linearly related to the flow calculated by the model. This leads to the conclusion that the difference between the values of the NTD and R is equal to the normalized[5] sum of squares of errors that are linearly correlated with the calculated flow (shortly referred to as linear errors.) For example, the flow forecast of UBC watershed model produces an NTD equal to 0.741 and R equal to 0.940. This means that the normalized sum of squares of linear errors is equal to $(0.940 - 0.741 = 0.199)$ as compared to $(1 - 0.741 = 0.259)$ for total normalized sum of squares of errors. This makes up about 77% of the total errors. The idea of comparing the NTD value with R for the purpose of assessing linear errors has been mentioned by Kitanidis (1980b). A more general and precise method is developed based on similar approach. This method, which will be presented in the next section, is used for testing the validity of the Kalman filter flow updating model.

2. The coefficient of persistence C_P, defined as follows :-

$$(23) \quad C_P = \frac{S_P - S}{S_P}$$

Where,
S is as define before in section (5); and

$$S_P = \sum_{i=1}^{N} (Q_{OBS}(i) - Q_{OBS}(i - FL))^2$$

---

[5] Normalized to S_{OBS}

Table 1: Results From Testing Model Performances Using Different Criteria

Model	NTD	Coefficient of Determination	Coefficient of Persistence	Coefficient of Extrapolation	Accumulated Volume Error,CMS^3
Q_{UBC}	0.741	0.940	-2.259, FL=1 0.623, FL=10 0.761, FL=20 0.815, FL=30	-1.833, FL=1 0.973, FL=10 0.990, FL=20 0.995, FL=30	1671.8
Q_{UP1}	0.945	0.946	0.305	0.395	37.7
Q_{UP10}	0.926	0.932	0.892	0.992	-389.3
Q_{UP20}	0.920	0.924	0.926	0.997	-369.3
Q_{UP30}	0.813	0.878	0.865	0.997	470.4

So, C_P is a measure of the performance of the model compared to the performance of a naive model that estimates the flow by the most recent flow measurement. A C_P value over zero means that the tested model performs better than the naive model. A value less than zero indicates the opposite.

From Table 1, C_P for the UBC model is equal to -2.259 for a forecast lead of one day; while it goes above zero value for longer forecast leads. This means that the naive model does better than the UBC model for short forecast leads. As the forecast lead becomes longer the opposite is observed. This is not unexpected, since daily consecutive flows are strongly correlated. This correlation is much weaker for sparsely measured flows, making the naive model impractical for long forecast leads. On the other hand, the C_P values for the flow updating model are well above zero for all forecast leads. This indicates that the flow updating model is a better choice than the persistence model even for the shortest forecast lead(one day).

3. The coefficient of extrapolation C_E, defined as follows;-

$$(24) \quad C_E = \frac{S_E - S}{S_E}$$

Where,
S is as define before in section (5); and

$$S_E = \sum_{i=1}^{N}(Q_{OBS}(i) - Q_E(i))^2$$

Where, $Q_E(i)$ is the flow calculated from the extrapolation of the most two recent observed flows. A positive C_E value indicates that the tested model performs better than the extrapolation model. A negative value indicates the opposite. The results for the extrapolation model are similar to those of the persistence model, high performance for short forecast lead and inferior one for long forecast leads. This is expected since the extrapolation model is also based on the characteristic of the flow hydrograph that consecutive flows are highly correlated.

9 Detection of Linear Errors in the Output of a Flow Forecasting Model

The flow updating model presented in this paper is based on the assumption that the errors in the UBC Waterched model are linearly related to its prefinal output, namely: the flow components Q_{SN}, Q_{RN} and Q_{GW}. This assumption could be satisfactorily tested by comparing the values of the NTD of the UBC Watershed model output and the coefficient of determination R from linear regression of the observed flow (Q_{OBS}) on the calculated flow components Q_{SN}, Q_{RN} and Q_{GW}. The difference between these values is equal to the normalized sum of squares of errors that have been removed by the linear regression. This difference is therefore a measure of the errors that are linearly related to the flow components, including the bias term[6]. So, the term PLE (Percentage of Linear errors) defined as below:

$$PLE = \frac{R - NTD}{1 - NTD} * 100$$

is a measure of the percentage of errors that can be corrected by applying linear regression.

Since Kalman filter approach is based on minimizing the sum of squares of errors, PLE could be used to test the possibility of improving flow forecasts using Kalman filter approach. In the present work PLE is calculated from the NTD of the UBC Watershed model and R from linear regression of Q_{OBS} on Q_{SN}, Q_{RN} and Q_{GW}. NTD is equal to 0.741, while R is equal to 0.941, so

---

[6] The bias term has not been accounted for in the flow updating model. The inclusion of the bias term is currently under study.

$$PLE = \frac{0.941 - 0.741}{1 - 0.741} * 100 = 77\%$$

This means that 77% of the errors are linearly related Q_{SN}, Q_{RN} and Q_{GW} and there is a great potential of improving flow forecast using the flow updating model. This is shown in the improvement of NTD from 0.741 to 0.945 (for forecast lead of one day.) That results in removing

$$\frac{0.945 - 0.741}{1 - 0.741} = 78.6\%$$

of the errors.

The PLE could be used in the process of selecting the state-space structure of the flow updating model, avoiding the time consuming and expensive process of implementing each model. This could be done by calculating the PLE values of each model and then selecting the model with the highest PLE value.

10 Conclusion

The flow updating model has been formulated on the assumption that the errors in the flow forecast of the UBC Watershed model are highly linearly related to its prefinal outputs: the flow components Q_{SN}, Q_{RN} and Q_{GW}. This assumption has been verified by the improvement in the flow forecast even for long forecast leads. The flow updating model incorporates flow measurement, whenever they are available, to update the flow forecast. Flow measurement are assumed to contain random errors of fixed or flow-related variances. The updating procedure is a function of the ratio of state to measurement variances. Fixing the values of the state variance, it is found that the model performance is not very sensitive to the measurement variance. This makes it possible to select the measurement variance as a fixed value or as a square of a given percentage of the flow without a sacrifice in model performance. The insensitivity of the model performance to the variances and the lack of large number of observations, especially for long forecast leads, make the use of adaptive Kalman filtering impractical.

Feedback from flow measurements is not a replacement for a well-structured model, especially for practical forecast leads. This could be seen from the performance of the persistence and extrapolation models. Although they outperform the UBC Watershed model for one day forecast lead due to the high correlation between flow measurements, they badly trailed behind the UBC model for longer forecast leads. On the other hand, the flow updating model outperforms trivial models and the UBC model on all forecast leads. This shows the ability of the flow updating model to successfully incorporate both the flow measurement and the UBC model output to give a better flow forecast. The ability of the flow updating model to perform well for long forecast leads (10 and 20 days) is due to the fact that it is partially based on the output of the well-structured UBC model and also that the errors in the flow forecast of UBC model are highly linear.

The proportion and form of linear errors in the output of a flow forecasting model can be determined by the quantity *PLE*. *PLE* could also be used in the process of selecting the structure of the flow updating model. The results of the current work shows the potential of updating flow forecasts using the feedback of flow measurements for practical forecast leads. Other forms of flow updating models are under investigation.

REFERENCES

Kalman, R.E. (1960), "A New Approach to Linear Filtering and Prediction Problems," *Transactions of the ASME, Journal of Basic Engineering, series D*, vol. 82, pp. 34-45.

Kalman, R.E. and R.S. Bucy (1961), "New Results In Linear Filtering and Prediction Theory, " *Transactions of the ASME, Journal of Basic Engineering, series D*, vol. 83, pp. 95-108.

Kitanidis, P. K., and R. L. Bras (1978b), "Error Identification In Conceptual Hydrologic Models, In *Application of Kalman Filter to Hydrology, Hydraulics and Water Resources*, edited by C. L. Chiu, University of Pittsburgh, Pittsburg, Pa., pp. 325-354.

Kitanidis, P. K. (1980b), "Real-Time Forecasting with a Conceptual Hydrologic Model :- 2 Applications and Results ", *Water Resources Research, Vol. 16, No.6*, pp. 1034-1044.

Mehra, R. K. (1970), On the Identification of Variances and Adaptive Kalman Filtering," *IEEE Transactions of Automatic Control*, vol. AC-15, pp. 175-184.

Todini, E.(1978), "Mutually Interactive State - Parameter (MISP) Estimation", In *Application of Kalman Filter to Hydrology, Hydraulics and Water Resources*, edited by C. L. Chiu, University of Pittsburgh, Pittsburg, Pa., pp. 325-353.

BIBLIOGRAPHY

Gelb, A (1986), "Applied Optimal Estimation," M.I.T. Press.

Harvey, A.C. (1981), "Time Series Models," John Wiley & Sons, New York.

IMSL, "User's Manual," Problem Solving Software Systems, IMSL, 1987.

Kitanidis, P. K. (1980a), "Real-Time Forecasting with a Conceptual Hydrologic Model :- 1 Analysis of Uncertainty", *Water Resources Research, Vol. 16, No.6*, pp. 1025-1033.

Ljung, L. (1983), "System Identification, Theory for the User," Prentice - Hall, Information and System Sciences Series.

Ljung, L. and T. Söderström (1987), " Theory and Practice of Recursive Identifications, The M.I.T. Press.

Mehra, R. K. (1972), "Approaches to Adaptive Filtering," *IEEE Transactions on Automatic Control*, pp. 693-698.

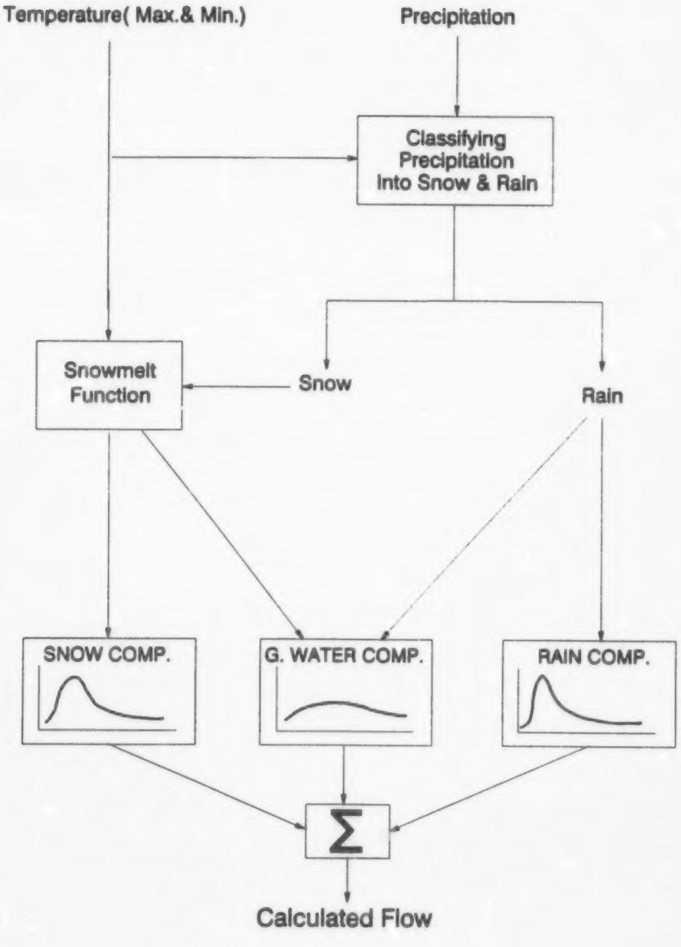
Temperature(Max.& Min.)
Precipitation
Classifying Precipitation Into Snow & Rain
Snowmelt Function
Snow
Rain
SNOW COMP.
G. WATER COMP.
RAIN COMP.
Σ
Calculated Flow

Fig. 1 The General Flow Chart of UBC Watershed Model.

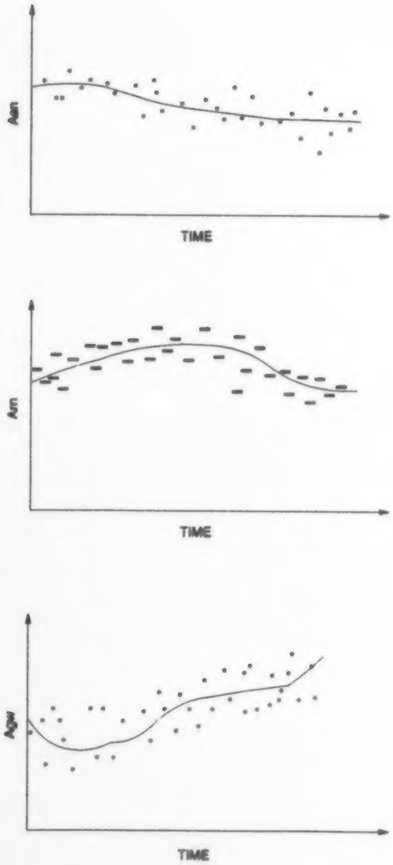

Fig. 2 The Means and Possible Values of the Weighting Factors.

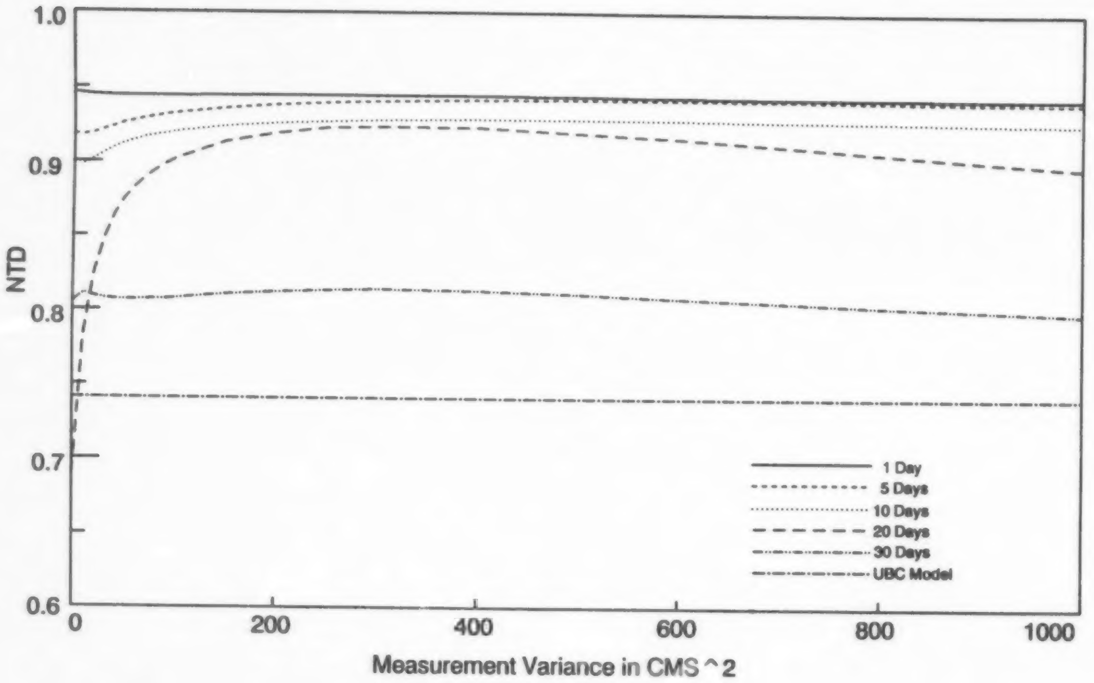

Fig.3 NTD versus Measurement Variance For Different Forecast Leads

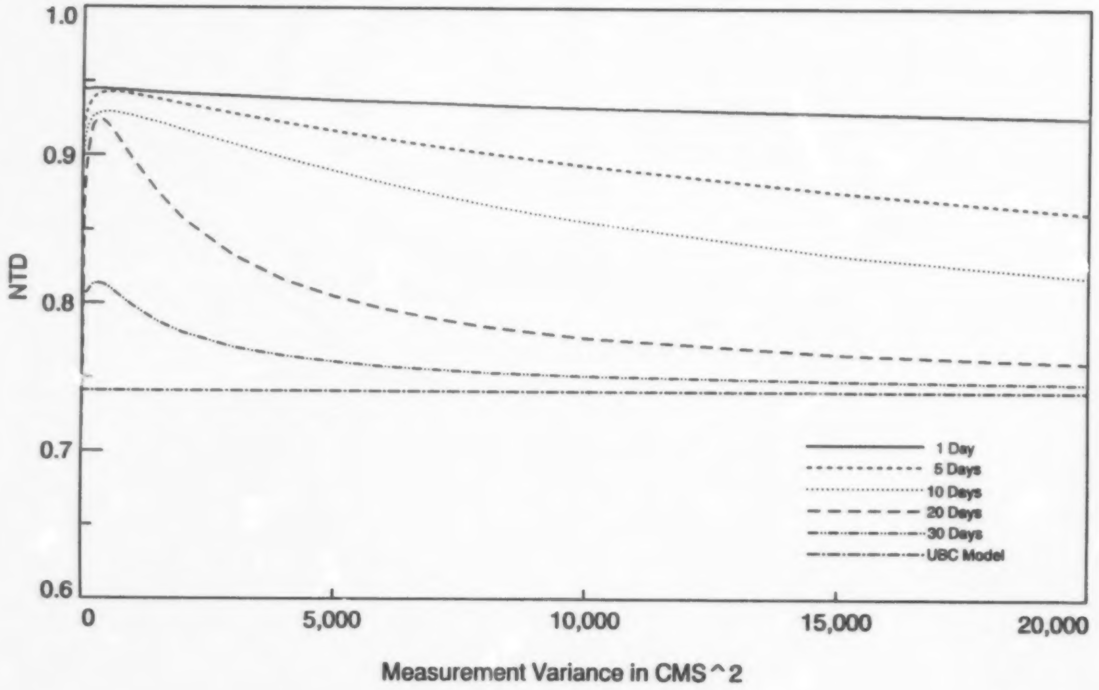

Fig.4 NTD versus Measurement Variance For Different Forecast Leads

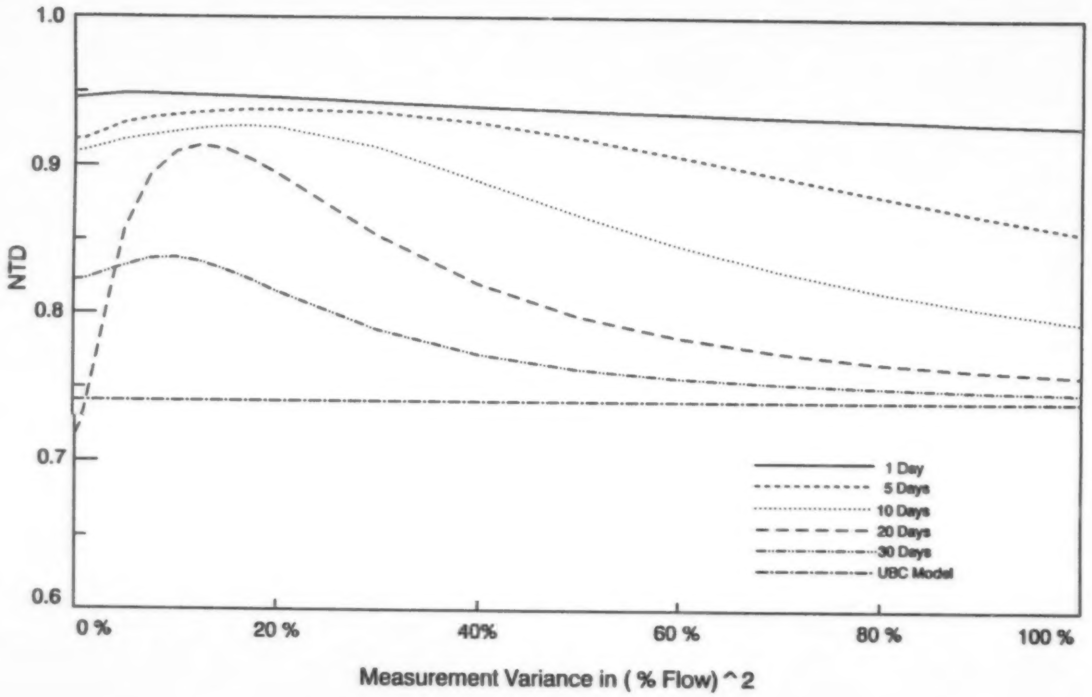

Fig.5 NTD versus Measurement Variance For Different Forecast Leads

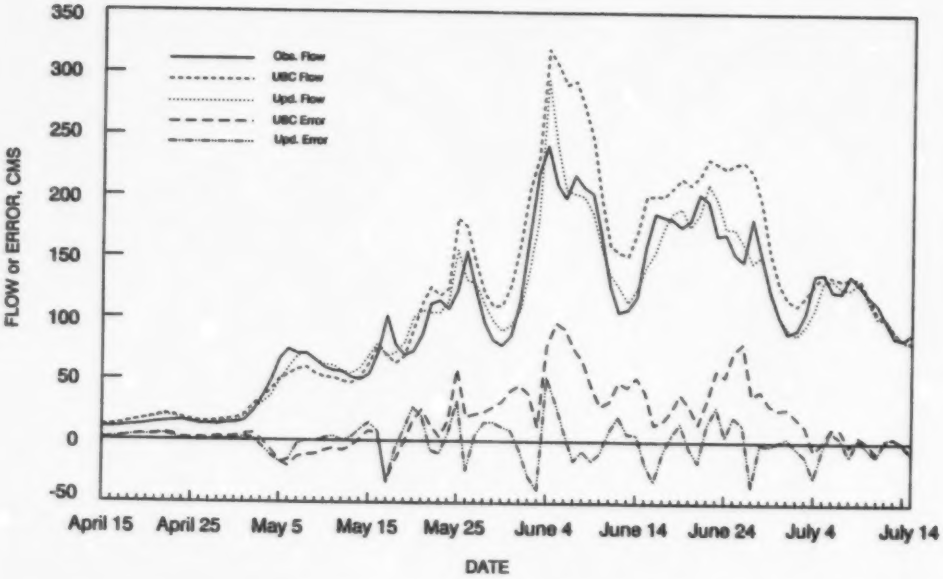

Fig. 6a The Hydrographs of the Observed, UBC and Updated Flows and Their Errors For Forecast Lead of One Day, (April 15 - July 15), 1970.

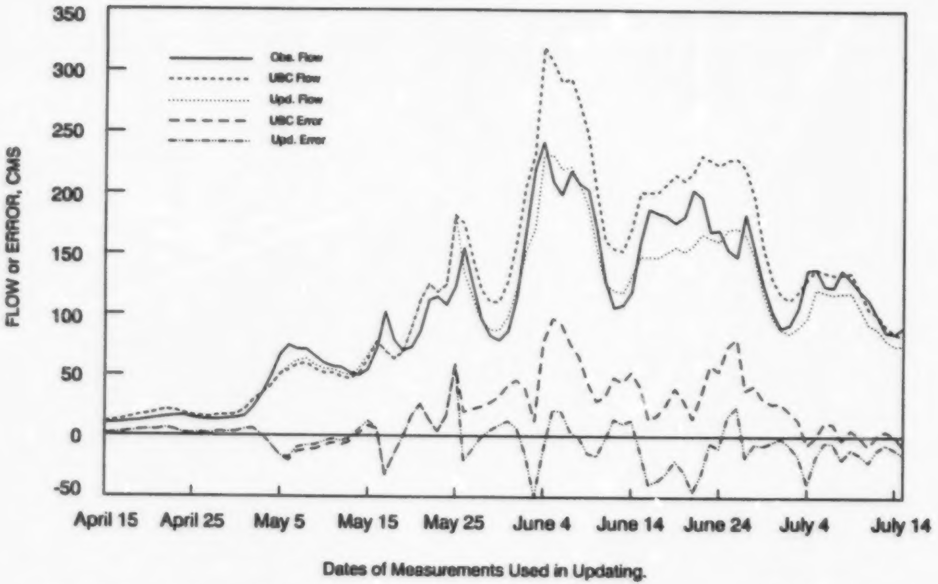

Fig. 6b The Hydrographs of the Observed, UBC and Updated Flows and Their Errors For Forecast Lead of 10 Days, (April 15 - July 15), 1970.

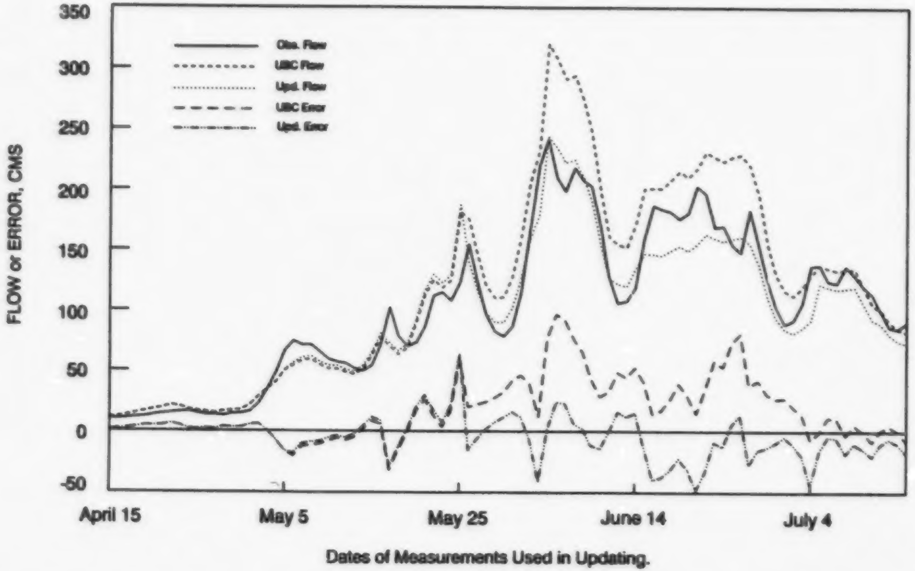

Fig. 6c The Hydrographs of the Observed, UBC and Updated Flows and Their Errors For Forecast Lead of 20 Days, (April 15 - July 15), 1970.

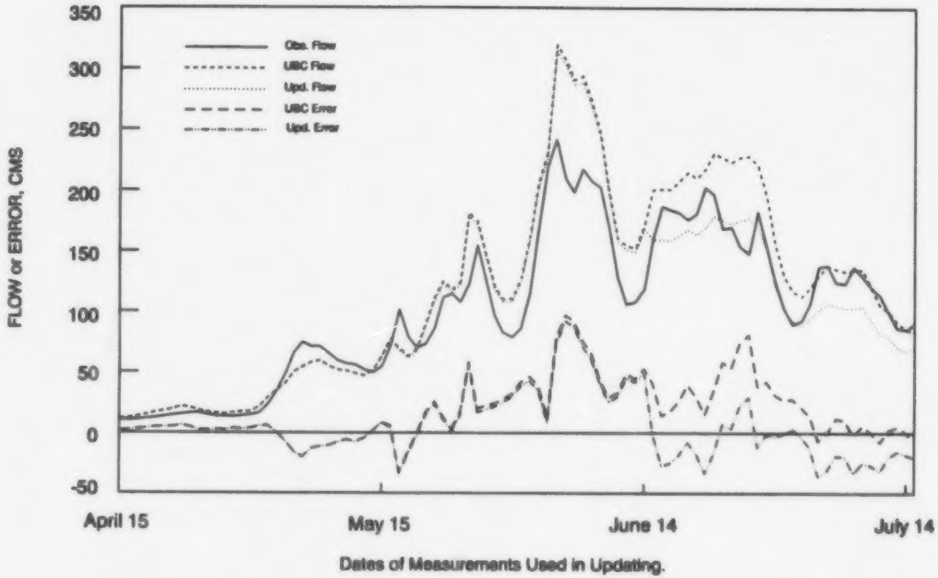

Fig. 6d The Hydrographs of the Observed, UBC and Updated Flows and Their Errors For Forecast Lead of 30 Days, (April 15 - July 15), 1970.

Questions and Answers

Alf Warkentin: I want to clarify if, in your updating procedure, you are really redistributing in time the same volume? Because, you had your snowmelt flow and snowmelt paths arranged with slightly different constants in front of those terms and you are optimizing those constants. Is that correct?

Hamed Assaf: That's correct.

Alf Warkentin: Are you redistributing the same volume in your optimization scheme? You start with the same volume and assume that you always forecast it that way. Is this correct?

Hamed Assaf: Well, the volume would be distributed into at least three flow components. So what I do, actually, is that I update those values. It would not necessarily be the same volume used in different model runs. It could be that, if the coefficients are lower than one, then generally you would use the same volume. As you suggest, it would be better to update the snowmelt function starting from the upstream side, and that is the approach I am actually dealing with right now. But in this paper we are dealing with the downstream side, when we deal with the flow.

HYDROTEL, a hydrological model designed to make use of remotely sensed and GIS data.

by

Jean-Pierre Fortin[1]
Jean-Pierre Villeneuve[1]
Claude Bocquillon[2]
Robert Leconte[3]
K. David Harvey[4]

1. INRS-Eau, bureau 105, Carrefour Molson, 2800, rue Einstein, Québec (QC) G1X 4N8, CANADA
2. Laboratoire hydrologie et modélisation. U.S.T.L. Place Eugène Bataillon, 34060 Montpellier CEDEX, FRANCE
3. Canadian Center for Remote Sensing, 1547, Marivale Road, Ottawa, Ontario, K1A 0Y7
4. Water Resources Branch, Environnement Canada, Ottawa, Ontario, K1A 0H3

ABSTRACT

A new hydrological model with spatially distributed variables, is currently being developed at INRS-Eau and LHM, in cooperation with Environment Canada and the Canadian Center for Remote Sensing, both agencies funding the project and participating in the development. This model has a modular structure and is able to make good use of remotely sensed data and digital terrain models. It is made out of three complementary software programs designed for use on microcomputers, each of them presented with a user's friendly interactive interface. Specific tasks devoted to hydrological simulation are grouped in the HYDROTEL program, whereas tasks related to image processing are integrated in the IMATEL program and those allowing the structuration of data for a given basin can be found in the PHYSITEL program. The links between those complementary programs are explained together with a description of the mean characteristics of each program and of the way remotely sensed data are processed for use in HYDROTEL. The model is applied to the Clifton watershed, in Southern Quebec.

RÉSUMÉ

Un nouveau modèle hydrologique discrétisé, conçu selon une approche modulaire, et capable de bénéficier des données acquises par télédétection et de modèles numériques de terrain est en cours de développement à l'INRS-Eau et au LHM, avec la coopération d'Environnement Canada et du Centre canadien de télédétection, les deux organismes finançant le projet et participant au développement. Ce modèle est constitué de trois logiciels exécutés sur micro-ordinateurs et comportant des interfaces interactives facilitant leur utilisation par l'usager. Les tâches spécifiques de modélisation hydrologique sont concentrées dans le logiciel HYDROTEL, alors que les tâches de traitement d'images sont réunies dans le logiciel IMATEL et celles permettant de structurer les données pour un bassin donné se retrouvent dans PHYSITEL. Les liens entre ces logiciels ainsi que leurs principales caractéristiques sont expliqués. On insiste sur la façon dont les données acquises par télédétection sont utilisées. Le modèle est appliqué au bassin de la rivière Clifton, dans le sud du Québec.

INTRODUCTION

Development of hydrological modelling and remote sensing has been done mostly independently until the beginning of the 80's. Thus, it was not a surprise that Peck et al. (1981) at the end of a study sponsored by NASA, concluded that: "The most obvious conclusion of the study is that most hydrologic models in their present configuration do not have a significant potential for using remotely sensed observations (...). Hydrologic modeling can be improved through the development of a new generation of models or subroutines for existing models which recognize the characteristics of the new remote sensing capabilities".

A few years later, Rango (1985) was writing: "Currently, much research remains to be done to allow effective input of the remote sensing data to the models. From the results coming out of the remote sensing and modeling experiments so far, it appears that any effort in modifying or designing hydrologic models to be compatible with remote sensing data is easily justified on the basis of potential improved simulation accuracies (...). Model modification or development should accomodate microwave and thermal infrared data that will be more widely available in the future". New models and new approaches had to be developed. Work has effectively been done to that effect by various authors (Fortin et al., 1985; Schultz, 1989; ...).

On the other hand, even if they were offering a large number of tasks, general purpose image analysis systems and geographic information systems did not necessarily offer tasks that would be useful, if not essential, for specific hydrological purposes. More over, most of those systems were run on large or mini-computers.

Recognizing the fact that microcomputers were becoming more and more powerful and that there would be a need for microcomputer based software, a joint program was undertaken by INRS-Eau and LHM for the development of a hydrological model able to make good use of remotely sensed data and digital terrain models. This program is now being pursued in cooperation with Environment Canada and the Canadian Center for Remote Sensing, both agencies funding the project and participating in the development.

GENERAL CHARACTERISTICS

The list of tasks intended for the original model has effectively lead to three complementary software programs (fig. 1) designed for use on microcomputers, each of them presented with a user's friendly, interactive interface. Specific tasks devoted to hydrological simulation are grouped in the HYDROTEL program, whereas tasks related to image processing are integrated in the IMATEL program and those allowing the structuration of data for a given basin can be found in the PHYSITEL program. It is also possible to use another image analysis system to process remotely sensed imagery or another GIS system, provided that those systems do have the necessary tasks and can provide output data compatible with HYDROTEL. To that effect, an effort has already been made to use formats as compatible as possible with other programs. For instance PHYSITEL can exchange data with SPANS (a GIS system from TYDAC), whereas IMATEL can read image files from EASY PACE (an image analysis system from PCI).

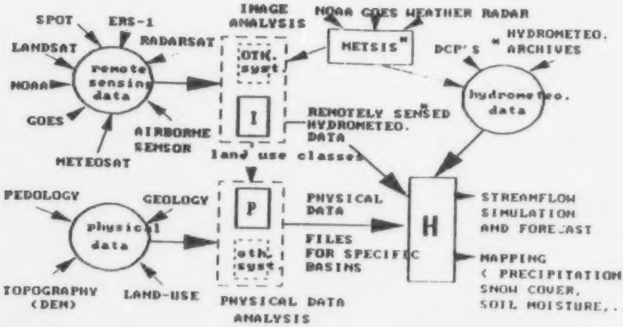
SPOT
ERS-1
LANDSAT
RADARSAT
NOAA
GOES
METEOSAT
AIRBORNE SENSOR
remote sensing data
IMAGE ANALYSIS
OTH. syst
I
NOAA GOES WEATHER RADAR
METSIS*
DCP'S
* HYDROMETEO. ARCHIVES
hydrometeo. data
REMOTELY SENSED* HYDROMETEO. DATA
land use classes
PEDOLOGY
GEOLOGY
physical data
TOPOGRAPHY (DEM)
LAND-USE
P
oth. syst
PHYSICAL DATA ANALYSIS
PHYSICAL DATA
FILES FOR SPECIFIC BASINS
H
STREAMFLOW SIMULATION AND FORECAST
MAPPING (PRECIPITATION, SNOW COVER, SOIL MOISTURE,...)

Figure 1 Integrated analysis of physical remotely sensed and meteorological data for streamflow simulation and forecasting by PHYSITEL, IMATEL and HYDROTEL.

Also, a modular structure has been adopted for all three programs in order to facilitate future integration of new modules, either by the authors or by users.

HYDROLOGICAL SIMULATION WITH HYDROTEL

The HYDROTEL simulation model can make good use of remotely sensed data when available, but does not need R.S. data necessarily. This approach is mandatory for real time operation, when a forecast has to be issued even if R.S. data are not available.

Since meteorological and hydrological processes are distributed, a distributed structure has been adopted for the simulation of those processes, making use of spatial informations available from remote sensing and G.I.S. (fig. 2).

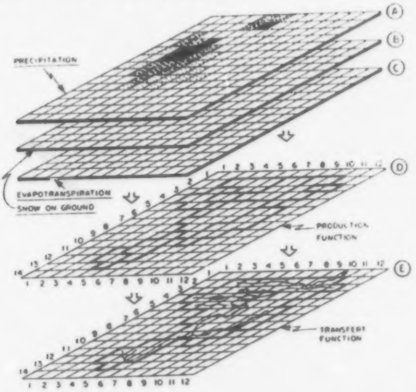

Figure 2 Spatial structure of the model

The spatial variability of basin characteristics (including topography, pedology and land-use) is taking care of by the definition of "homogeneous" hydrological units derived from spatial integration, in PHYSITEL, of the original raster data. The vertical water budget is first estimated for each of those "homogeneous" hydrological units (HHU), from interpolated station values. The outflow from these HHU is then routed as surface and sub-surface flow to the nearest river reach, where it is routed downstream as river flow.

A modular structure has also been adopted for the simulation of each component of the water budget, namely precipitation, snowmelt, evapotranspiration and soil moisture. Each component module is further divided into options allowing the user to select the one option he considers best, among those offered (table 1). As an example, various equations allowing estimation of evapotranspiration can be selected (fig. 3), permitting to take the available data into account. More over, this modular approach allows a user to add its own sub-models to those already offered. Thus, a particular user has the opportunity to develop his own model for a specific component of the water cycle, say the vertical water budget for a soil submitted to permafrost, without having to write a complete simulation program including simulation of the other components of the water cycle, as well as utility fonctions (input, output, display). The information to do this is given in the user's manual and the menus for the selection of the appropriate sub-model already contain the option "user's defined sub-model".

TABLE 1

SIMULATION OPTIONS AVAILABLE IN HYDROTEL 2.0

1. Interpolation of solid and liquid precipitation	1.1	Thiessen polygons
	1.2	Weighted mean of nearest three stations
	1.3	Arithmetic mean of nearest three stations
2. Snowcover variation and melt	2.1	Modified degree-day method
3. Potential evapotranspiration	3.1	Thorthwaite
	3.2	Linacre
	3.3	Penman
	3.4	Priestley-Taylor
4. Vertical water budget	4.1	CEQUEAU (modified)
	4.2	BV3C
5. Surface runoff	5.1	Kinematic wave
6. Channel routing	6.1	Kinematic wave
	6.2	Diffusion wave

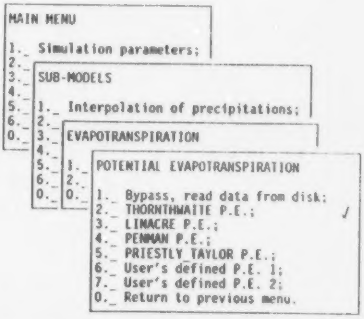
MAIN MENU
1._ Simulation parameters;
2._
3._
4._
5._
6._
0._
SUB-MODELS
1._ Interpolation of precipitations;
2._
3._
4._
5._
6._
0._
EVAPOTRANSPIRATION
1._
2._
0._
POTENTIAL EVAPOTRANSPIRATION
1._ Bypass, read data from disk;
2._ THORNTHWAITE P.E.; √
3._ LINACRE P.E.;
4._ PENMAN P.E.;
5._ PRIESTLY_TAYLOR P.E.;
6._ User's defined P.E. 1;
7._ User's defined P.E. 2;
0._ Return to previous menu.

Figure 3 Sub-menu #3.3.1 in Hydrotel: available options for estimation of potential evapotranspiration

In order to make a better use of the potential of remotely sensed as well as DTM data, a new sub-model for the simulation of the vertical distribution of soil moisture together with outflow from the HHU has been developed. As requested by Peck (1981), its variables and fluxes have been defined so as to represent as much as possible physical processes taking place during water redistribution in the soil column. They are by no means an exact representation of the much more complex reality of water movements and storage in the soil. Nevertheless, they should represent what happens on the average. In particular, the soil profile is divided into three layers (fig. 4). Each HHU may be characterized by a particular mean soil type, leading to θ_s, θ_{cc} and θ_{pf}, the water contents at saturation, at field capacity and at the permanent wilting point, k_s, the hydraulic conductivity at saturation, ψ_s, the matrix potential at "saturation", and λ, the pore size distribution (Rawls and Brakensiek, 1989). Also, the first layer is limited to 10-20 cm, at most, in order to be compatible with measurements of soil moisture by remote sensing.

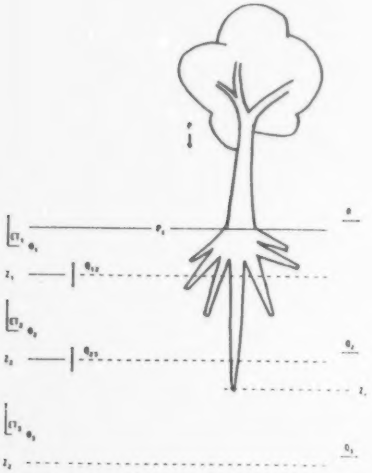

Figure 4 Vertical water budget in BV3C

With HYDROTEL, it is also possible to test a particular component without having to simulate all other components at the same time. This is made possible by saving intermediate results from the various components of the model and reading those from disk on subsequent runs (fig. 3). This may shorten appreciably the time of each test simulation.

IMAGE ANALYSIS WITH IMATEL

As mentionned above, processing of remotely sensed imagery for hydrological purposes is done by IMATEL. Following the approach favored with HYDROTEL, PHYSITEL and IMATEL, R.S. data can be related directly or indirectly to model variables (fig. 5). Measurement of the length of a river reach is an example of direct use of R.S. information, as shown in path 1. The river length obtained from a SPOT or TM image becomes a direct input for river routing by either kinematic of diffusive wave equations. On the other hand, land-use classes derived from R.S. imagery can be characterized by quantitative attributes which are then input to the model. This is an example of an indirect relation between image data and model variables, as shown in path 2. For development purposes, on the Clifton watershed, located in Soutern Quebec, near Sherbrooke, the following classes are considered: coniferous forest, deciduous forest, clear-cuts, large and deep rivers and lakes, small streams, highways, gravel (and assimilated type) pits, bare fields, waste, lands, marshes, pastures, crops. Only classes that behave differently from an hydrological point-of-view will be kept for operational application of the model. As an example of the transformation of R.S. information into useful modelling information, let us take the class "deciduous forest". It can be characterized by tree height (from which roughness values are derived), root depth and albedo, which are variables used to compute actual evapotranspiration.

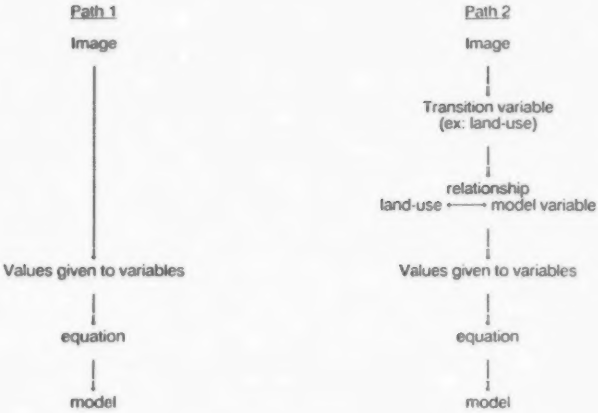

Figure 5 Transformation of remotely sensed data into usable data for hydrological simulation

STRUCTURING WATERSHED DATA BASES WITH PHYSITEL

The preparation of the physiographic and land-use data bases for use in HYDROTEL is done in PHYSITEL.

The PHYSITEL program allows definition of regional as well as watershed data bases in which data can be stored. Regional data bases, as expected, correspond to large geographical areas (Southern Quebec, Northern Saskatchewan, ...) which may contain many watersheds. A specific cartographic projection is chosen for a particular data base and the various types of data which are input into the RDB keep their original accuracy but their spatial coordinates are changed to that of the RDB. Then, from input data already stored in regional data bases, a watershed data base for a particular watershed can be created by (1) spatial integration of the original data (land-use, DTM, soil type, ...) to the selected cell size, (2) processing of DTM data (original or spatially integrated values) to obtain the drainage structure of a watershed (including slope, aspect and altitude of each cell), and (3) spatial integration of cells into homogeneous hydrological units.

Processing of DTM data to obtain surface drainage, as well as data on river reaches can be done using also informations coming from R.S. imagery to complement DTM data.

TESTING OF THE MODEL

While it is being developed at INRS-Eau and LHM, prototype versions of the model are being or will be tested at both Environment Canada and CCRS, on various basins througout Canada.

The Eaton basin, as mentionned above, has been chosen as our basin, for various reasons. Among those, the basin had been selected for intensive studies during the International Hydrological Decade (1965-1975) so that a lot of meteorological, hydrological, geological and pedological data were available.

The spatial distribution of land-use classes throughout the basin was obtained from analysis of TM and SPOT data. As for the characteristics of river reaches, they were measured temporarily on aerial photographies and maps, but will be obtained directly from TM and SPOT images integrated with DTM data, as soon as all the tasks to do so are implemented in IMATEL and PHYSITEL. Soil types come from a survey by Environment Quebec. Cartographic informations obtained from that survey will be used to define HHU's. One of the objectives of this sub-project is to find out if and how RS and DTM data can be used later on to obtain those HHU's. DTM data also are temporary. They were extracted manually from 1:50000 maps, as mean evaluated altitudes of 1 X 1 km squares on UTM maps.

Figure 7 shows results obtained with the model. The upper graph contains meteorological informations, whereas that in the middle shows, as an example, the outflow from the vertical profile of the square located at the outlet of the basin. The simulated and measured hydrographs are drawn in the lower graph. It should be mentionned here that these results were obtained without modification of the initial parameters. In other words, they do not come from a series of tests to optimize the parameter values. More specifically precipitations were interpolated using Thiessen polygons, the vertical water budget was simulated by CEQUEAU and the diffusive wave equation was use for channel routing.

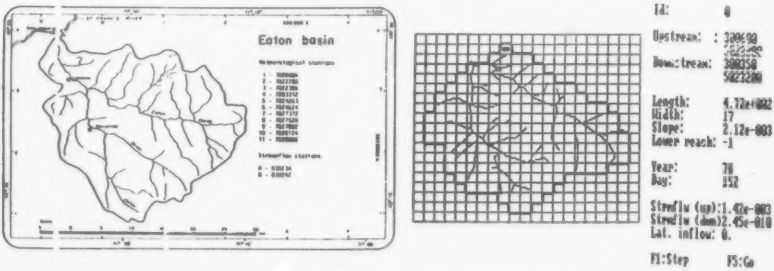

```
Id:              0

Upstream:      : 309?90
                 [illegible]
Downstream:      308358
                 5023200

Length:          4.72e+002
Width:           17
Slope:           2.12e-003
Lower reach:     -1

Year:            78
Day:             152

Strmflw (up):1.42e-003
Strmflw (dwn)2.45e-010
Lat. inflow: 0.

F1:Step          F5:Go
```

Figure 6 The Eaton basin in Southern Quebec a) Meteorological and stream flow stations b) Tabular informations on variables related to reaches for the Clifton sub-basin

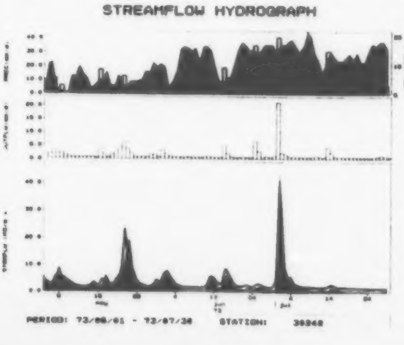

Figure 7 Streamflow hydrograph for the Clifton sub-basin

CONCLUSION

An integrated software package is now being developed. The results obtained to date are promising, but more remains to do.

An objective sub-program to optimize model parameters as well as an updating sub-program for forecasting purposes will be added. Spatial distribution of precipitation from integration of weather radar data with station data will be taken care of by a fourth complementary program.

ACKNOWLEDGMENTS

The project is being funded by DSS contract no: KE 144-8-4443.

The authors want to mention the participation of Agriculture Canada and Environment Quebec for field measurements.

Special thanks to our computer analysis, Claude Blanchette, Martin Montminy and Jérôme Benoît who have done a tremendous job in a relatively short time.

Finally, IMATEL is being programmed by Octographe Inc., with algorithms developed both at Octographe and INRS-Eau.

BIBLIOGRAPHIE

FORTIN, J.P., J.P. VILLENEUVE, A. GUILBOT et B. SÉGUIN (9186). Development of a modular hydrological forecasting model based of remotely sensed data, for interactive utilization on a microcomputer. International Workshop on Hydrologic Applications of Space Technology. Cocoa Beach, Florida, August 18-25, p. 307-319.

PECK, E.L., T.N. KEEPER and E.R. JOHNSON (1981). Strategies for using remotely sensed data in hydrologic models. NASA-CR-666729, 77 p.

RANGO, A. (1985). Assessment of remote sensing input to hydrologic models. Water Resources Bulletin, 21(3): 423-432.

RAWLS, W.J. and D.L. BRAKENSIEK (1989). Estimation of soil water retention and hydraulic properties, in: Unsaturated flow in hydrologic modeling. Theory and Practive, p. 275-300. H.J. Morel-Seytoux (ed.). Kluwer Academic Pub.

SCHULTZ, G.A. (1989). Remote sensing of watershed characteristics and rainfall input, in: Unsaturated flow in hydrologic modeling. Theory and Practice, p. 301-323. H.J. Morel-Seytoux (ed.) Kluwer Academic Pub.

Questions and Aswers

Ric Soulis: What is your time scale on the bottom of your last graph? Is it daily?

Jean-Pierre Fortin: Yes, daily. But the model was planned to have variable time steps, so it actually could work at one, four, six, ten, twelve or 24 hours.

Thian Yew Gan: What sort of resolution of remote sensing data do you use in your model?

Jean-Pierre Fortin: Those that we have in the past example are one kilometer in size, but the model is actually being tested on two other basins. At these basins resolutions of two and twelve kilometers are being used.

SESSION 1C
HYDROLOGIC MODELS III

Session Chairman: B.E. Goodison, Canadian Climate Centre

USING A SURFACE ENERGY BUDGET MODEL TO ESTIMATE EVAPOTRANSPIRATION

Thian Yew Gan
Division of Water Resources Engineering
Asian Institute of Technology
Bangkok, Thailand

ABSTRACT

At present, estimation of regional actual evapotranspiration ET is often based on the potential rate derived from empirical or Penman type equations, or the open water pan measurements adjusted to soil evaporation and plant transpiration. In deterministic hydrologic models, factors that limit the actual ET are the soil moisture status usually represented by the amount of "fictitous" water present in the conceptual storages and the hierachy of moisture extraction priority from the storages. The mass balance and heat balance equations for an evaporating surface are seldom used because surface temperature, the variable common to both equations, is rarely available from routine measurements. But now surface and canopy temperature data on a regional scale can be processed from thermal infrared images collected from satellites such as NOAA-AVHRR or others. Also, energy budget models using such remotely sensed surface temperatures and some soil-water/heat transfer models using surface soil moisture data inferred from airborne radar measurements with/or surface temperature data have been demonstrated experimentally to model actual ET for bare soils and agricultural areas adequately. The merits and disadvantages of some representative past works on these two types of models using airborne and satellite data are reviewed. A model to estimate the actual basin ET by an energy balance approach for an earth-atmosphere system is presented. In this model, the evaporative flux, ET equals to the net radiation R_n (sum of absorbed solar shortwave and net absorbed longwave fluxes) minus the gain in soil energy fluxes G and sensible heat H to the atmosphere. If no direct measurement of solar radiation is available, it can be estimated from expressions that include the solar radiation formula, Brunt (1932) or Brusaert (1975) or Satterlund (1979)'s formula for atmospheric emissivity, and the blackbody irradiance formula. The sensible heat H is based on a turbulance transport function and G a heat transfer in soil or empirical formulae. A simple study based field collected surface temperature data (not remotely sensed) and other meteorological data shows that this surface energy model can predict adequate point daily ET values if accurate meteorological measurements are available.

INTRODUCTION

Evapotranspiration is a major component of the hydrologic cycle; however, it is also one of the most difficult processes to model accurately. In arid climate regions and particularly during hot seasons, ET generally exceeds effective rainfall. Under such circumstances, low soil moisture will stifle crop growth unless there are proper irrigation schemes to make up the deficit in water supply. Thus for regions where agriculture is important, reliable estimation of ET as part of a regional water budget analysis for irrigation and water supply control becomes essential. However, large scale ET estimation is nontrivial because the complex process of water transforming to water vapor in a natural environment is not fully understood, and sufficient field measurements needed, especially in large hydrologically nonuniform areas, for a reliable analysis are too costly to obtain. The second factor is more crucial than the first because in a large scale context only an approximate but fairly representative estimation is needed and the present state of art in modeling evapotranspiration is sufficient to achieve this objective. But now it is possible to overcome the data shortage problem since areal measurements collected from space can complement or even replace the limited point measurements collected from ground. Given that more and more high precision satellite images are acquired at times of day (early morning or early afternoon) optimum for study involving the energy balance of the earth's surface, and the technique for taking active and passive microwave radar measurements is refined enough to accurately infer soil dielectric properties highly related to surface soil moisture, the time has come for using remotely sensed data with either energy budget or soil-water/heat transfer models to estimate regional evapotranspiration.

EVAPOTRANSPIRATION EQUATIONS

In majority of present deterministic hydrologic models, actual ET is adjusted either from the potential rate derived from empirical or physically based, i.e., Penman type equations, or from direct measurements such as the open water evaporation pan and lysimeters. Methods used for estimating potential evapotranspiration E_p is primarily based on a few more popular approaches such as Thornthwaite method, Blaney-Criddle formula, Penman equation (1948) and its simplified version, the Priestley-Taylor equation (1972). Penman's model is a combination of the energy and aerodynamic equations solved simultaneously.

$$E_p = \frac{R_n \Delta + \gamma E_a}{\Delta + \gamma} \tag{1}$$

Penman equation (1) requires a knowledge of the net radiation R_n (Wm^{-2}), the gradient of the saturated vapor pressure curve at air temperature Δ (mb/^oC), the psychrometric constant γ (0.66 mb/^oC), and the contribution of mass-transfer to evaporation E_a (m/day) such that

$$E_a = f(u)(e_s - e_a) \tag{2}$$

where u is the windspeed (m/day) usually measured at a height of 2 meters above the ground, e_s the saturation vapor pressure, and e_a the atmospheric vapor pressure at air temperature T_a.

It is by far one of the most versatile equations to estimate potential ET for small basins. In case that some of these climatological data are unavailable, a simpler equation requiring less data must be used. Priestley and Taylor (1972) found that for ET over large areas, energy balance is the primary factor governing ET and the second term E_a of Equation (1) is approximately 25 to 30 percent of the first, so that (1) can be simplified as

$$E_p = m \frac{\Delta R_n}{\Delta + \gamma} \tag{3}$$

where m = 1.25 to 1.3.

In case that even less data are available, it might be necessary to just use empirical formulae based upon single climate variables. For example, a less accurate method, like that of Thornthwaite which only uses air temperature as an index of the energy available for ET, might be used if air temperature is the only data one has.

Evaporation from the bare soil surface and from plants (called transpiration) which are influenced by radiation, wind effects, vapor pressure deficit, land surface roughness, and canopy stomatal resistance (for plants), will occur at the potential rate if water is plentiful. In real life situations, the actual ET rate is usually limited by the amount of water available to meet the evaporative demand of the atmosphere.

In a water balance study, spatial measurements of soil moisture states below the land surface is required to estimate actual ET but they are too costly and impossible to collect on a regional scale. Thus in lumped-parameter hydrologic modeling, where no spatial variability is considered, the soil moisture status is usually represented by the "fictitous or conceptual" water available in the model's conceptual storages derived from calibrations. For complex soil moisture acounting models such as the Sacramento Model (Burnash et al, 1973) of the National Weather Service of USA, factors considered to estimate ET include the hierachy of moisture extraction priority and the water available on each conceptual storage. The algorithms for computing ET extraction rates are simple approximations based on linear ratio of the states of several storages versus their respective maximum water storages such as

$$E_u = E_p \frac{UZTWC}{UZTWM} \tag{4}$$

where E_u is the ET from the upper tension zone, UZTWC the upper zone tension water content, and UZTWM the upper zone tension water maximum.

In simpler models, a similar, single-equation approach is also applied, i.e., Haan (1972) and Holton et al. (1975). This simple approach of using the ratio of water balances represented by Equation (4) will only yield approximate ET volumes.

Saxton et al. (1974a & b) introduced a soil-plant-air system to estimate ET and soil moisture of small basins by a more comprehensive water balance approach. Their model calculates interception evaporation, soil water evaporation, and plant transpiration separately and combines them to provide daily ET estimates. Calculations are based on the characteristics of soil moisture and soil hydraulic properties, crop canopy, and root distributions which are difficult to obtain. Though the model applied to two research watersheds produces good estimates of ET and accurate soil moisture profiles, given its data requirements, it is difficult to apply on large catchments.

A more complex version of Penman Equation is the Penman-Monteith equation (Monteith, 1973),

$$E = \frac{\Delta R_n + \rho C\ (e_s - e_a)/r_a}{\Delta + \gamma(1 + r_c/r_a)} \qquad (5)$$

where ρ is the density of air (kg m^{-3}), r_a the aerodynamic resistance to water vapor transport, and r_c the canopy resistance to water vapor flow.

In general the more complex the model, the more realistic it is physically. Among several ET equations available in the Systeme Hydrologique European (SHE) model (Abbot et al., 1986), a highly sophisticated, physically-based, distributed hydrologic system built in Europe, Equation(5) is the most complex for ET estimation. With the parameter r_c included, Equation(5) computes the actual ET directly. This is desirable because it does not have to go through the type of water budget manipulations mentioned earlier before it can compute actual ET. Instead, the reduction in ET rates due to water shortage is accounted for implicitly by the stomatal resistance term r_c since water shortage is directly related to the surface resistance to water flow from the canopy to the atmosphere. Unfortunately, r_c needs to be measured by botanical methods and are difficult to extrapolate to other crops. Even in SHE, r_c is assumed to be a constant or an arbitrary function of soil moisture tension and vegetation type. Therefore, Equation (5) is only applicable in a research context.

APPLICATIONS OF REMOTE SENSING

Without adequate field data, the predicament of hydrologists to estimate basin ET is obvious. ET estimated from the moisture accounting approach of even the more comprehensive hydrologic models such as the Sacramento Model is accurate only on a long term basis even though the model accounts for all the major components of the hydrologic cycle (Gan, 1988). Even if detailed hydrologic data is available, the vast complexities of the subsurface hydrologic processes will still prevent an effective linkage between ET and soil moisture on a regional scale, no matter how complicated and vigorous the model is.

As mentioned before, using crop stomatal resistance as an index to estimate regional ET is also impractical because it requires intensive field measurements. But with the aid of remote sensing(RS) data, it is now possible to adopt a new modeling philosophy to overcome these problems. The potential of RS is yet to be fully explored; however, many preliminary research works have already demonstrated that such measurements, which provide specific information from particular spectral bands, are valuable to model specific components of the hydrologic processes. Engman(1986), Oliver (1985)and others envisaged an ever-increasing role to be played by RS in hydrologic modeling. RS cannot provide direct information of ET but pertinent variables that affect the evaporative flux from the land surface such as albedo, surface temperature, spectral vegetative indices, and soil moisture of the surface layer are obtainable from such measurements. It is noted here that surface temperature, the variable common to both the mass balance and energy balance equations for an evaporating surface (bare soil or land with vegetation) is not used in evaporation equations, even in Penman Equation, because it is seldom available from routine measurements. But since 1978, the launching of Heat Capacity Mapping Mission, HCMM, and Tiros-N, the first two satellites to acquire high-resolution thermal infrared data at times of day optimal for measuring daily maximum and minimum surface temperatures, the situation has changed.

In addition to providing extra parameters, on a regional basis, RS data is generally more informative than measurements collected from the ground because it contains spatially integrated information of the entire scenes of satellite images, while ground data only provide point information (Engman, 1986). RS's ability to integrate variability in the horizontal plane gives the potential to replace point data with areal data in hydrologic modeling. To assimilate the spatial information of RS data, distributed models should be used and basins should be modeled with grid systems at resolutions compatible with that of the data. With remotely sensed surface temperature and meteorological data available, ET can be calculated from an energy budget model built for a land-atmosphere system. Several attempts using this approach have already been made and they will be discussed in greater details later. In general, surface temperature from bare soils and canopy temperature from vegetation are estimated from the thermal infrared red IR bands (10.5 - 12.5 μm) of satellites and sometimes from the microwave spectrum of airborne radar images. According to Schultz(1988), there is yet a microwave sensor carried by satellites which fulfill the requirements of hydrology and that is why microwave data used are airborne measurements.

Another approach to model ET with RS data is to use a combined water and heat flow model. The electromagnetic properties of soil, highly related to its moisture content, are measurable remotely by microwaves MW(1 cm to 50 cm). The brightness temperature of passive MW and backscattering coefficients of active MW have been shown to have direct relationships with the top soil moisture collected from bare soils and agricultural plots (Schmugge et al, 1979).

For several reasons, this combination approach is more difficult to apply. The soil moisture information derived from MW images is at most limited to the top 10 cm of the surface soil layer. Remotely sensed soil moisture measurements are primarily limited to bare grounds or lands covered with sparse vegetations. Moreover, some pertinent data to model the subsurface water movement by numerical schemes such as soil properties and root distributions cannot be obtained by means of remote sensing. However, using the parameterization schemes of Girard(1974) and Deardorff(1977) to model soil fluxes of the land component, researchers such as Ottle et al.,(1989) and Soares et al. (1988) have some apparent success. So far, the method is validated more substantially with agricultural plots or bared grounds and so more testing is required for applications to basins with dense vegetation such as forests.

SOIL-WATER/HEAT TRANSFER MODELS

The earlier models usually treat the soil-water/heat transfer processes in a local continuum and then extend them to a regional scale by some kinds of scaling concept. These processes are represented by physically based models which are usually solved numerically. However, in order to assimilate data containing spatial information on a regional scale, the later trend has been towards models of more modest computational requirements.

Bernard et al. (1981) presented a method to predict bare soil evaporation from simulated microwave radar data. The average soil moisture over the first 5 cm of the soil layer is inferred from the backscattering coefficient (MW radar data) via a simple relationship

$$\sigma_o(\mathrm{dB}) = \frac{14.5\theta_o}{FC} - 15.817 \qquad \sigma_o \leq 8\ \mathrm{dB} \tag{6}$$

where $\sigma_0(\mathrm{dB})$ is the radar backscattering parameter, σ_0 is the average soil moisture over the first 5 cm soil layer, and FC is the soil field capacity. Then using the soil moisture data as the upper boundary condition, Richard's 1-D equation for soil water movement in the unsaturated zone is solved numerically to estimate evaporation and other boundary fluxes.

Other than its computation burden, a major problem to their method is the validity of extending the local transfer model to the regional scale by scaling the field heterogeneities with a similar media concept. Moreover, the spatial variability of soils modeled by this concept is incompatible with the surface averaging made by radar observations.

In a later paper of 1986, Bernard et al. conceded that even if the soil hydraulic properties for solving Richard's equation are known, the soil water simulation is still "local" and thus is not compatible with RS data which provides regional surface properties.

The same numerical approach to estimate evaporation from bare soil was tested again, but this time with real microwave data for a field in France (Prevot et al., 1984). Both the backscattering coefficient - surface soil moisture relationship and the hydraulic characteristics of soil were established via calibrations. The field data of water content profiles needed for the calibrations were measured with neutron probes at daily intervals. Despite the intensive field data collection effort, the final calibrated model still underpredicted evaporation substantially when rainfall was considered in the simulations. It is obvious that the difficulty lies in simulating sudden large changes of fluxes because when no rain was considered, the prediction was much better. The lack of radar data between the rain events also contributed to the underestimation of evaporation.

A even more complicated numerical model that accounts for the mositure and energy balances at the upper soil (~2 m) and lower atmospheric boundary layer was developed by Camillo et al.(1983). This model considers the feedback mechanisms between the heat and moisture fluxes in the soil component by coupling them according to Philip and de Vries (1957) equations

$$\frac{\partial\theta}{\partial t} = -D\frac{\partial\theta}{\partial z} - D_T\frac{\partial T}{\partial z} - K \tag{7}$$

$$\frac{\partial T}{\partial t} = -\lambda\frac{\partial T}{\partial Z} - L\,D_{\theta,\ vap}\frac{\partial\theta}{\partial Z} \tag{8}$$

where θ is the soil moisture content, z the soil depth (increasing downward), k the hydraulic conductivity, t the time, and D_∂, D_T, and $D_{\theta,vap}$ are the moisture, temperature and water vapor diffusion coefficients respectively. The surface fluxes for solving these two equations numerically are derived from standard meteorological data. Remotely sensed surface temperature and soil moisture data are used for calibration. The model was tested with data taken from a bare field in Ruthe, West Germany. Good agreements were found between measured and simulated temperature. However, the model is more for studying the sensitivity of the heat process to various parameters such as the soil heat capacity, thermal conductivity and aerodynamic roughness than for estimating regional evaporation because solving these equations over long periond of time is expensive and nontrivial, and using few RS data on equations with many soil related parameters is unfounded.

With all the unknowns in the soil and lack of adequate soil moisture and temperature data, using a system involving feedback mechanisms in heat and water balance is superfluous. In view of all the drawbacks and with the present state of art, it is obvious that using a numericl scheme on the soil water movement to estimate regional evaporation is not practical.

Bernard et al. (1986) replaced the numerical models of Richards equation with a simple water budget model for a soil surface layer first proposed by Deardorff (1977). With some modifications, they showed that this two-layer model (see Figure 1), with the first layer 10 cm deep to accommodate the surface soil water information from the radar data, can derive the hydraulic properties (pseudo-diffusivity) of different fields in a region. The water movements between the two layers are calculated by a force restore method given as

$$\frac{\partial W_1}{\partial t} = - \frac{E}{d_1} + C_s(W_2 - W_1) \qquad (9)$$

$$\frac{\partial W_2}{\partial t} = - \frac{E}{d_2} \qquad (10)$$

Where W_1 and W_2 are the soil moisture of the first and the second layers respectively, E is evaporation, C_S is a pseudo-diffusivity of unit T^{-1}, and d_1 and d_2 are the respective depths of the two layers.

Soares et al. (1988) extended this concept to include the soil heat flow so that the two-layer soil system (see Figure 2) is now represented by two sets of equations, with one concerning the water flow and the other, the heat flow. The two are indirectly coupled by the interdependency of soil water and soil thermal properties. Then by linking the soil and the atmosphere through heat and mass (evaporation) transfers described by the energy budget at the interface, and with remotely sensed surface temperature (thermal infrared) and surface water content (active microwave), they could derive regional soil water content and evaporation of a bare site. The estimated evaporation was found to agree closely with ground-based measurements. The good agreements between the measured (by a Doppler SODAR equipment) and simulated sensible heat fluxes also show that realistic energy fluxes can be estimated. Conceptually, this system is similar to that of Camillo et al. (1983) but it is much simpler, and probably more effective as a model to estimate regional evaporation. However, the requirement for two types of remotely sensed data is a drawback, and especially the soil moisture data measured by airborne radars is very expensive.

Ottle et al. (1989) also used the 2-layer surface parameterization model of Bernard et al (1986) to simulate the water and energy budgets at the soil surface. But they didn't model the heat flow of surface soil. Instead, the real evaporation was estimated by merely applying a simple adjustment factor to the potential evaporation which is part of the input data. However, they explored the possibility of updating the model state variables regularly with new data derived from thermal infrared satellite images. This is an effective way of controling the output error which, if unchecked, will generally increase with time. To do this, the Stress-Degree-Day (SDD) index of Jackson et al. (1977), a plant water stress index given by the canopy-air temperature difference measured post-noon, is used to correlate with the simulated soil water budget.

From their study based on one of the sites of the HAPEX-MOBILITY experiment located in south western France, using the surface temperature derived from the channel 4 (10.5 - 11.3 μm) of NOAA9-AVHRR images, they found that the SDD computed with satellite and climatic (air temperature) data is not sufficient to follow the simulated water budget because atmospheric forcing like wind and vapor pressure deficit will also influence the canopy-air temperature difference. They suggested using the Crop Water Stress Index (CWSI) of Jackson et al. (1981) for future research. Apparently, the remotely sensed surface temperature alone is more useful to estimate regional evaporation than to update the state variables of water budget model. But their idea of using new remotely sensed data to update model state variables is very useful for future hydrologic modeling.

We have reviewed some representative research works on exploring the possibility of estimating regional evaporation, and in some instances also soil water fluxes, with soil-water/heat transfer models using remotely sensed surface temperature data and sometimes, together with surface soil moisture data.

ENERGY BUDGET METHODS

If regional evapotranspiration is the only variable required, it is probably sufficient to just use the energy budget equation instead of the soil water transfer model, though it may not give the best results. In such a case, surface temperature will be the only remotely sensed data needed. This does not imply that meteorological factors can be ignored because other than radiative fluxes, key factors that influence the remotely sensed surface temperature also include wind, aerodynamic surface roughness, rainfall, and evaporative rate of the land surface. The key factors sensitive to surface temperature should be incorporated into the energy balance models in order to account for their influence on the satellite data. But on the other hand, the models should be parsimonious in the use of parameters to avoid unnecessary complexity which may leads to unwieldy computations in the model analysis. Moreover, more parameters are likely to require more ground data.

The concepts and theoretical analysis of using thermal infrared imagery to infer evaporation and surface soil moisture have been studied substantially for the past decade on bare fields or agricultural areas (Huntley, 1978; Prevot, 1980; Carlson, 1985; Taconet et al. 1986; Ottle et al., 1989). Many investigators (Prevot, 1980; Soares, 1980; Hatfield et al. 1983; Seguin and Itier, 1983) calculated evapotranspiration from energy balance models with surface temperature processed from thermal IR data. The results are generally encouraging but more research is needed to further develop the technique before it can be operational. An energy balance model, which comprises of a meteorological data to compute regional evapotranspiration, is presented below:

A simplified form of the energy budget method for practical applications at the land-atmosphere interface is

$$R_n = L.E + G + H \qquad (11)$$

where E is the evaporative flux from soil and transpirative flux from vegetation, R_n the net radiation, G the soil heat flux, H the sensible heat (energy to heat the air), and L the latent heat of vaporization of water (about 2.45×10^6 J kg^{-1}). R_n, G, and H are in units of J $m^{-2}s^{-1}$ or Wm^{-2} while E is of unit kg $m^{-2}s^{-1}$.

R_n is the net of incoming and outgoing radiative fluxes expressed as

$$R_n = R_s(1-\alpha_s) + R_{\ell n} \qquad (12)$$

where R_s is the incoming short-wave (solar) radiation, $R_{\ell n}$ the net absorbed longwave (infrared) radiation, and α_s the short-wave albedo of the surface. Approximate mean albedo values of α_s for various natural surfaces are available from various literature such as Brusaert (1984) and Dunne and Leopold (1978)(see Table A.2). Other than surface temperature, albedo can also be derived from satellite data but the process is more difficult. Direct measurements of R_s are available from most national weather services and some agricultural organizations.

In case that direct measurements are not available, R_s is estimated from Eq. (13) where δ is the solar declination, ϕ the latitude of the point observed, h the hour angle or the angle through which the earth must turn to bring the meridian of P directly under the sun, S the solar constant (2 cal cm^{-2} min^{-1}), V the atmospheric transmittence, Z the zenith angle (see Figure 3), and R_{se} the solar radiation per day received on a horizontal plane in the absence of the atmosphere.

$$R_s = R_{se} V \qquad (13)$$

where R_{se} is given by Eq. (14).

$$R_{se} = \frac{1440}{\pi} S \left(\frac{\bar{x}}{x}\right)^2 (Q\sin\phi\sin\delta + \cos\phi\cos\delta\sin Q) \qquad (14)$$

where $\frac{\bar{x}}{x}$, ratio of the instantaneous and mean distances of the earth from the sun, ranges from 1.0344 on January 3 to 0.9674 on July 5; R_{se} are given in tables such as that given in Dunne & Leopold(1978,p.107). On cloudy days R_{se}, based on an integration of the diurnal trend of solar radiation, could be over estimated.

$$\mathrm{Cos}\ Q = -\tan\phi\tan\delta \qquad (15)$$

V can be estimated from an empirical equation proposed by Prescott (1940) (Eq. 16) and is given in Brusaert (1984, p. 132).

$$V = a + b\frac{n}{N} \tag{16}$$

where a, b are constants depended on the location, the season and the state of the atmosphere, n the actual number of hours of bright sunshine, and N the number of daylight hours. N is expressed by Jackson et al. (1983) as

$$N = 0.945\ \{\beta + \alpha \sin^2 |\pi(D + 10)/365|\} \tag{17}$$

where β and α are latitude dependent constants, and D is the day of the year. β is the length of the daylight period for the shortest day of the year and α is the amount that must be added to β to obtain the daylight period for the longest day of the year.

β and α expressed as functions of latitude ϕ are

$$\beta = 12.0 - 5.69 \times 10^{-2}\phi - 2.02 \times 10^{-4}\phi^2 + 8.25 \times 10^{-6}\phi^3 - 3.15 \times 10^{-7}\phi^4 \tag{18}$$

$$\alpha = 0.123\phi - 3.10 \times 10^{-4}\phi^2 + 8.00 \times 10^{-7}\phi^3 + 4.99 \times 10^{-7}\phi^4 \tag{19}$$

where ϕ the latitude of the observed point is expressed in degrees. Suppose C is the mean fractional cloud cover, then

$$f\,C + \frac{n}{N} = 1 \tag{20}$$

since $\frac{n}{N}$ represents the fraction of the day during which the sun is not obstructed by clouds. f is a constant ranges from 1 to about 1.5. Such simple equations are merely approximate subsititute of direct measurements of R_s which should always be used if available. The cloud cover measured by satellite is instantaneous and it is not likely to represent the mean daily cloud cover.

$R_{\ell n}$, the average daily, net absorbed longwave radiation (Price,1980) is

$$R_{\ell n} = \epsilon_{\ell e}\sigma\{\epsilon_{\ell a}T_a^4\ (1+\eta C^q) \quad - \quad (T_s^4 + 0.75\ T_s^2\ (T_{max}-T_{min})^2)\} \tag{21}$$

where T_{max}, T_{min}, and T_s are the remotely sensed surface temperatures, T_a the air temperature, $\epsilon_{\ell a}$ the atmospheric emissivity under clear skies, $\epsilon_{\ell e}$ the surface emissivity, η (cloud dependant) and q are constants, and σ (= 5.6697 x 10^{-8} $Wm^{-2}K^{-4}$) the Stefan-Boltzmann constant. Examples of values of η and q are found in Brusaert (1984) and Budyko (1974).

The values of $\epsilon_{\ell e}$ based on literature are 0.95-0.97 for bare soil, 0.96-0.98 for vegetation, and 0.99 for fresh snow.

For $\epsilon_{\ell a}$, most of the expressions derived are empirical, such as Brunt's formula(1932)(Eq. 23) and Satterlund (1979)(Eq.24); but Brusaert (1984) derived a physically based expression in 1975, given as

$$\varepsilon_{\ell a} = 1.24 \left(\frac{e_a}{T_a}\right)^{1/7} \tag{22}$$

where e_a is the vapor pressure of air in mb and T_a in ^{o}K.
Brunt's formula (1932) is popular but

$$\varepsilon_{\ell a} = \nu + \psi e_a^{1/2} \tag{23}$$

the geographical constants υ and ψ given by various researchers (see Brutsaert, 1984) vary quite Substantially which is a setback. Brusaert found that Eqs.(22) and (23) gave comparable results and recommended Eq.(22) because it includes the effect of atmospheric humidity.

Satterlund's formula (Eq. 24) which uses the same variables as Brutsaert's, is found to be better for situations below freezing.

$$\varepsilon_{\ell a} = 1.08 \left[1 - \exp\left(- e_a^{T_a/2016}\right)\right] \tag{24}$$

The sensible heat flux H is governed by a turbulent heat transport process related to the vertical temperature gradient $(T_s - T_a)$, the Von Karman's constant $K(=0.38)$, the Specific heat of air at Constant pressure C_p, the density of air ρ , the wind speed $u(ms^{-1})$, the surface roughness Z_o, the height at which the air temperature is measured, $Z_a(m)$, and d the zeroplane displacement(m),

$$H = \frac{\rho C_p (T_s - T_a)}{r_a} \tag{25}$$

where the aerodynamic resistance r_a is a function of the stability of the atmosphere just above the surface and its expression depends on the stability condition. Seguin and Itier(1983)'s results on $(E-R_n)$ versus $(T_s - T_a)$ seemed to indicate that midday values of $(T_s - T_a)$, though only a one time value of the day, may be representative of the entire day (at least for clear days). when $T_s \approx T_a$ (neutral stability),

$$r_a = \frac{\left\{\ell n \left[\frac{Z_a - d}{Z_o}\right]\right\}^2}{K^2 u} \tag{26}$$

However, for using remotely sensed surface temperatures in evaporatranspiration calculations, this condition (Eq.26) is of little interest.

Suggested operational values for the surface roughness parameter Z_o for various surfaces are given in Table A.1. Monteith (1973) established a simple relation for Z_o

$$Z_o = 0.13\, h_c \tag{27}$$

where h_c is the vegetation height.

There are complicated expressions to estimate r_a under stable ($T_s < T_a$) and unstable conditions ($T_s > T_a$) such as those derived by Businger and Dyer (given in Soer, 1980) but may require iterative solution techniques. A simpler approach suggested by Hatfield et al (1983) is to approximately account for stability by including the Richardson number such that

$$r_{ac} = r_a \left[1-n(z_a-d)g\ (T_a-T_s)/T_o u^2 \right] \qquad (28)$$

where r_{ac} is the aerodynamic resistance corrected for stability, g is the gravitational constant, T_o is the average temperature usually assumed to be T_a, and n is a constant which Monteith(1973) suggested a value of 5. H is therefore computed from Eq.(25) with r_a replaced by r_{ac} which was shown by Hatfield et al. to be a significant parameter in determing H.

The flow of heat flux G through the soil mantle is mainly dependant on the vertical soil temperature profile $\frac{\partial T}{\partial z}$ and the soil thermal conductivity $\lambda(\theta)$ which depends on the soil moisture content θ,

$$G = -\lambda(\theta) \frac{\partial T}{\partial z} \qquad (29)$$

Unfortunately this theoretical concept has little practical implication since $\frac{\partial T}{\partial z}$ is rarely available. For a land covered with vegetation, the soil heat flux G is an order or more of magnitude smaller than other terms in Eg.(11). An analytical heat transfer solution for the simple case of an infinitely thin, homogeneous soil layer subjected to an harmonic temperature variation at the surface is

$$G = \Delta T_s (\omega C_s \lambda)^{\frac{1}{2}} \sin(\omega t + \frac{\pi}{4}) \qquad (30)$$

where ΔT_s is half the difference between the maximum and minimum surface temperature, W ($= \frac{2\pi}{P}$) the frequency of oscillation, P the period of oscillation (24 hours for daily computation), and C_s the soil heat capacity. From Sellers (1965, p.132), C_s is 0.585, 0.417, and 0.246 for sand, clay, and peat. $(C_s \lambda)^{1/2}$ is referred to as the thermal inertia while $(WC_s \lambda)^{1/2}$ the diurnal heat capacity(Price,1980). Price also derived a linearized equation of the diurnal heat capacity (denoted us D in his paper of 1980) expressed in terms of T_{max} and T_{min} for air and for the surface, L.E., and other radiative terms. Naturally to obtain ΔT_s, there should be at least two satellite measurements per day, probably one taken at midday(1330 hr.) and another at might(0230 hr.) so that $\Delta T_s = T_s(1330) - T_s(0230)$. If C_s, and λ are difficult to estimate, the diurnal heat capacity term $(\omega C_s \lambda)^{1/2}$ of Eq.(30) can be approximately computed from Price's equatiion (given as Eq.11 in his paper) which, however, requires a foreknowledge of change of L.E. with respect to T_s. A check for the value of G derived from Eq.(30) is by using simple assumptions like

$$G = a_h H \qquad (31)$$

or

$$G = a_r R_n \qquad (32)$$

where G is assumed to be equal to a certain fraction of H (a_h) or R_n(a_r). Suggested values for the empirical constants a_h and a_r are found in literature such as Kasahara and Washington(1971) and Fuchs and Hadas(1972). For bare soils, good values for a_h and a_r are about 0.3 to 0.4. They are negligible for land with vegetation covers. By solving the relevant equations for R_n, H, and G, i.e., Eqs. 12 to 32, evapotranspiration E can be obtained from Eq.(11), i.e.,

$$L.E = R_n - G - H \qquad (33)$$

when there is plenty of water, most of the solar energy from R_n goes into LE and so H is small compared to LE. When water is limited, more of R_n is used to heat the air, and H is large compared to LE, introducing uncertanties into estimating LE.

This model is a combination of various physically based and empirical algorithms, some of which have been demonstrated to calculate evapotranspiration that agree closely with the measured values. No iterative technique is required to solve any of the equations.

Tables 1 and 2 provide the lists of data required and the empirical parameters involved to calculate evapotranspiration using the energy balance method proposed. Initial estimates for majority of the fifteen parameters are available from values given in the literature, some of which are given in the Appendix. Not all parameters will be needed, unless Eqs.(23),(31) or(32) are chosen in the analysis. Since the model is quasi physical, the empirical parameters may need calibration which is only possible if field data on evapotranspiration is available. The calibrated model should be validated with independent set of data.

To facilitate the assimilation of remotely sensed data, this model should be applied in a square(or other shapes) grid information system with an appropriate resolution. A geographic information system GIS is recommended for data handling since the data involved might be enormous. Ideally, there should be 2 satellite measurements for the surface temperature per day to estimate ΔT_s, mean daily T_s, and the mean (T_s-T_a) approximately.

ENERGY BUDGET MODEL TEST

Evapotranspiration rates were estimated using the surface energy model given by Equations (11) to (33) for data collected from an agrometeorological station located in the agricultural plots of the Asian Institute of Technology, Bangkok. All the ground based data are available but unfortunately the remotely sensed surface temperature data are not because for the past several months during the preparation of this paper no appropiate NOAA-AVHRR data for Thailand was available. The author even went to Malaysia but still could not obtain any data and the NOAA data ordered from USA at the end of last year is yet to arrive. Under such circumstances, in order to test the model, point data of soil surface temperature collected from the ground covered with grass of height 10 - 15 cm are used as the surface temperature T_s, instead of the satellite-IR temperature that represents a spatially integrated value over a square kilometer. Maximum and minimum temperatures which are supposed to be remotely sensed are also taken from ground measurements. In this case, the model is tested in a restricted sense and interpretation of the results should be confined to a point-data context. However, the preliminary result still gives insight to the model's performance with respect to different combinations of input data.

Input data involved are shortwave radiative flux R_s, maximum and minimum temperatures T_{max} and T_{min}, cloud cover C, air temperature T_a, vapor pressure e, wind velocity U, and soil temperature profiles. The model is operated on an event-based mode, i.e., the ET estimated depends entirely on the input data for that particular day only. Values for model parameters used are tabulated in Tables 1 and 2. In all cases, the surface roughness Z_o and the zeroplane displacement d are respectively taken as 0.13 times and 0.67 times the crop height h_c which is assumed as 0.1 m. Some of the input parameters are based on literature and some from site information. The parameters are not optimized because the results are only meant for preliminary interpretation. Given that information for the soil-temperature profile is available, the soil heat flux G is computed by Equation (29) but on a daily basis, G is found to be insignificant as compared to R_n and H.

The predicted ET values are compared with open evaporation pan measurements corrected by a pan coefficient of 0.7. Figure 4 shows the plots of predicted versus observed ET values for the 1988 April and December periods and Figure 5 shows the corresponding scattergrams. These two months are selected because in Bangkok April is a hot month while December a "cold" month.

A perusual of the figures show that on both months, some predicted values agree very well with the observed, some not so well, and several show great discrepancies, i.e., April 10, 15, 16, and December 11. Input data for these four particular days are examined to study the cause to these problems. On December 11, the recorded solar radiation R_s was of record low, 79 Wm^{-2}, as against its monthly mean radiation of 184.6 Wm^{-2} (see Figure 6 for R_n). On April 15 and 16, the recorded solar radiations were 103.4 and 255.3 Wm^{-2} respectively. It is found that solar radiation plays a major role in determining the ET because as expected, in a hot and humid environment such as Bangkok, a large part of the radiation goes to evaporating water instead of heating the air or the soil. On April 15, the low radiation is further aggravated by a high surface temperature of 38.10 °C which causes the net absorbed longwave radiation to be -118 W/m^2, giving a nonsensical net solar radiation R_n of -35.3 Wm^{-2} (see Figure 6). On contrary, the high radiation value on APril 16 gives rise to a high predicted ET value. Apparently, the absurd ET values computed are caused by measurement or recording errors in the radiation and temperature data. The observed ET on April 10 was 7.14 mm which is two standard deviations larger than its monthly mean value of 4.40 mm. Since the computed value is only 3.54 mm, it is possible that the observed value might be measured or again recorded wrongly.

Other than these four values, there are other values that differ from the observed up to 40 % or slightly more. However, inspection of the input data does not reveal any obvious errors as before. Table 3 shows that the computed values have higher standard deviations than the measured values which is of no surprise since ET is computed from eight different meteorological measurements, whose total variabilities and possible measurement errors (especially cloud cover and wind speed), reflected in the computed ET values, should be larger than that of pan evaporation alone. Moreover, the computations involve several empirical parameters whose values are not optimized, the stability of the aerodynamic resistance r_a is only approximately accounted for by Equation (28), and to adjust the daily absorbed longwave fluxes with a simple empirical relationship, Equation (21), using instantaneously measured cloud cover information is open to discussion. Some of the input data such as cloud cover, wind speed, and air temperature (equal to the mean of daily maximum and minimum temperature) may not represent the daily average correctly.

On a whole, this simple study shows that generally it is possible to predict reliable point-daily ET values adequately with the surface energy model if accurate meteorological data are available. It will be interesting to study the performace of this model with remotely sensed data.

CONCLUSION

With increasing focus in the applications of remotely sensed data for estimating evapotranspiration and soil moisture fluxes pertinent to hydrology, agriculture, forestry and other disciplines, discussions on models associated with such applications are presented in the first part of this paper. The number of models reviewed are limited but they are representative of major studies conducted in the past. The earlier soil-water and heat transfer models used Richard Equation or Philip De Vries's equation for modeling the water movement or water coupled with heat movement in the subsurface respectively. The major drawback of these models is that they are only applicable to local studies. Later versions of these models are more simplified yet are probably more applicable regionally. If the soil moisture information isn't essential, the energy budget model seems to be an attractive alternative because surface temperature is the only remotely sensed data required.

A preliminary analysis shows that mean daily ET predicted by the surface energy budget model presented agrees fairly well with the measured ET but individual daily totals may differ up to 40 % (ignoring the four cases with erroneous data) mainly because of many meteorological data involved and thus are subjected to higher variabilities and likely measurement or data recording errors. This model is quasi physical, implying that it is neither too complicated nor over simplified. However, the number of empirical parameters involved are still many. When satellite data becomes available, the model will be further tested to see its performance on a regional basis. However, even though remotely sensed data contain areal information, how valid it is to extrapolate point measurements such as wind speed, vapor pressure, air temperature, and surface roughness which is based on crop height to a regional scale, especially to complex land surface, so that the energy budget methods can provide adequate areal ET predictions on a regional basis? The question is yet to be fully addressed.

ACKNOWLEDGEMENTS

This work was partially supported by the Asian Institute of Technology under a research initiation grant. The author is indebted to Mr. Jaya Verrasingam for preparing the figures of this paper.

REFERENCES

Abbott, M.B., J.C. Bathurst, J.A. Cunge, P.E. O'Connell, and J. Rasmussen, An Introduction to the European Hydrological System - Systeme Hydrologique European, 'SHE', 2: Structure of a Physically-Based, Distributed Modeling System, J. of Hydrology, 87, pp. 61-77, 1986.

Bernard, R., M. Vauclin, and D. Vidal-Madjar, Possible Use of Active Microwave Remote Sensing Data for Prediction of Regional Evaporation by Numerical Simulation of Soil Water Movement in the Unsaturated Zone, Water Resour. Res., 17(6), pp. 1603-1610, 1981.

Bernard, R., J.V. Soares, and D. Vidal-Madjar, Differential Bare Field Drainage Properties from Airborne Microwave Observations, Water Resour. Res., 22(6), pp. 869-875, 1986.

Brutsaert, W., Evaporation into the Atmosphere, Theory, History and Application, Reidel, Dordrecht, The Netherlands, 299 pp., 1984.

Budyko, M.I., Climate and Life, Academic Press, N.Y., 508 pp., 1974.

Burnash, R.J.C., R.L. Ferral, and R.A. Mcguire, A Generalized Streamflow Simulation System, Conceptual Modeling for Digital Computers, U.S. National Weather Service, Sacramento, CA, 1973.

Camillo, P.J., R.J. Gurney, and T.J. Schmugge, A Soil and Atmosphere Boundary Layer Model for Evapotranspiration and Soil Moisture Studies, Water Resour. Res., 19(2), pp. 371-380, 1983.

Carlson, T.N., Regional Scale Estimates of Surface Moisture Availability and Thermal Inertia Using Remote Thermal Measurements, Remote Sensing Rev., 1, pp. 197-247, 1985.

Deardorff, J.W., A Parameterization of Ground Surface Moisture Content for Use in Atmospheric Prediction Models, J. Appl. Meteorol., 16, pp. 1182-1185, 1977.

Dunne, T. and L.B. Leopold, Water in Environmental Planning, W.H. Freeman and Company, San Francisco, 1978.

Engman, E.T., Hydrologic Research Before and After AgRISTARS, IEEE Trans, Geosci. & Remote Sensing, GE-24, 1, pp. 5-11, 1986.

Fuchs, M. and A. Hadas, The Heat Flux Density in a Non-Homogeneous Bare Loessial Soil, Boundary-Layer Meteorol., 3, pp.191-200, 1972.

Gan, T.Y., Applications of Scientific Modeling of Hydrologic Responses from Hypothetical Small Catchments to Assess a Complex Conceptual Rainfall-Runoff Model, Water Resources Series, Technicl Report No. 111, U. of Washington, Seattle, WA, 1988.

Girard, G., Modele global Orstom, Premiere application du modele journalier a discretisation spatiale sur le bassin versant de la crique Gregoire, en Guyanne, in Atelier Hydrologique sur les Modeles Mathematiques, ORSTOM, Paris, 1974.

Gurney, R.J., Prospects for Determining Global Land Surface Hydrological Parameters from Space Observations, Unpublished Manuscript,NASA/Goddard Space Flight Center, 1987.

Haan, C.T., A Water Yield Model for Small Watersheds, Water Resour. Res.

8(1), pp. 58-69, 1972.

Hatfield, J.L. , A. Perrier, and R.D. Jackson, Estimation of Evapotranspiration at One time-of-Day Using Remotely Sensed Surface Temperatures, Agricultural Water Management, 7, pp. 341-350, 1983.

Holton, H.N. , G.J. Stiltner, W.H. Hensen, and N.C. Lopez, USDAHL-74 Revised Model of Watershed Hydrology, USDA Tech. Bull., 1518 pp., 1975.

Huntley, P., On the Detection of Shallow Aquifers Using Thermal Infrared Imagery, Water Resour. Res.. 14, pp. 1075-1083, 1978.

Jackson, R.D., J.L. Hatfield, R.J. Reginato, S.B. Idsc, and P.J. Pinter, Jr., Estimation of Daily Evapotranspiration from One-Time-of-Day Measurements, Agricultural Water Management, 7, pp. 351-362, 1983.

Jackson, R.D., S.B. Idso, R.J. Reginato, and P.J. Pinter, Jr., Canopy Temperature as a Crop Water Stress Indicator, Water Resour. Res., 17(4), pp. 1133-1138, 1981.

Jackson, R.D., R.J. Reginato, and S.B. Idso, Wheat Canopy Temperature: A Practical Tool for Evaluating Water Requirements, Water Resour. Res., 13, pp. 651-656, 1977.

Kasahara, A. and W.M. Washington, General Circulation Experiments with a Six-Layer NCAR Model, Including Orography, cloudiness and Surface Temperature Circulation, J. Atmos. Sci., 28, pp.657-701, 1971.

Monteith, J.L., Principles of Environmental Physics, American Elsevier Publ. Co., N.Y., 241 pp., 1973.

Oliver, H.R., The Availability of Evaporation Data in Space and Time for Use in Water Balance Computations, from New Approaches in Water Balance Computations (Proceedings of the Hamburg Workshop, August 1983), IAHS Publ. No. 148, pp. 21-31, 1985.

Ottle, C., D. Vidal-Madjar, and G. Girard, Remote Sensing Applications to Hydrological Modeling, J. of Hydrol., 105, pp. 369-384, 1989.

Penman, H.L., Natural Evaporation from Open Water, Bare Soil and Grass, Proc. Roy. Soc. Lond. A193, pp. 120-145, 1948.

Philip, J.R. and D.A. de Vries, Moisture Movement in Porous Materials Under Temperature Gradients, EOS, Trans. AGU, 38, pp. 222-228, 1957.

Prevot, L., R. Bernard, O. Taconet, and D. Vidal-Madjar, Evaporation from a Bare Soil Evaluated Using a Soil Water Transfer Model and Remotely Sensed Surface Soil Moisture Data, Water Resour. Res., 20(2), pp. 311-316, 1984.

Price, J.C., The Potential of Remotely Sensed Thermal Infrared Data to Infer Surface Soil Moisture and Evaporation, Water Resour. Res., 16(4), pp. 787-795, 1980.

Priestly, C.H.B., and R.J. Taylor, On the Assessment of Surface Heat Flux and Evaporation Using Large Scale Parameters, Mon. Weath. Rev., 100, pp.81-92. 1972.

Satterlund, D.R., An Improved Equation for Estimating Long-Wave Radiation from the Atmosphere, Water Resour. Res., 15(6), pp. 1649-1650, 1979.

Saxton, K.E., H.P. Johnson, and R.H. Shaw, Watershed Evapotranspiration Estimated by the Combination Method, Trans. Am. Soc,. Agric. Engrs., 17(4), pp. 668-672, 1974a.

Saxton, K.E., H.P. Johnson, and R.H. Shaw, Modeling Evapotranspiration and

Soil Moisture, Trans. Am.Soc. Agric. Engrs., 17(4), pp. 673-677, 1974b.

Saxton, K.E., Soil Water Hydrology: Simulation for Water Balance Computations, from New Approaches in Water Balance Computations (Proceedings of the Hamburg Workshop, August 1983), IAHS Publ. No. 148, pp. 47-59, 1985.

Schmugge, T.J., T.J. Jackson, and H.L. McKim, Survey of In-Situ and Remote Sensing Methods for Soil Moisture Determination, in Satellite Hydrology, AWRA, pp. 333-352, 1979.

Schultz, G.A., Remote Sensing in Hydrology, J. of Hydrology, 100, pp. 239-265, 1988.

Seguin, B., and B. Itier, Using Midday Surface Temperature to Estimate Daily Evaporation from Satellite Thermal IR Data, Int. J. Remote Sensing, 4(2), pp. 371-383, 1983.

Soares, J.V., R. Bernard, O. Taconet, D. Vidal-Madjar, and A. Weill, Estimation of Bare Soil Evaporation from Airborne Measurements, J. of Hydrol., 99, pp. 281-296, 1988.

Soer, G.J.R., Estimation of Regional Evapotranspiration and Soil Moisture Conditions Using Remotely Sensed Crop Surface Temperatures, Remote Sensing of Environment, 9, pp. 27-45, 1980.

Taconet, O., R. Bernard, and D. Vidal-Madjar, Evaporation Over an Agricultural Region Using a Surface Flux/temperature Model Based on NOAA/AVHRR Data, J. Climatol. Appl. Meteorol., 25, pp. 284-307, 1986.

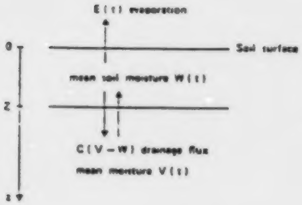
E(t) evaporation
0
Soil surface
mean soil moisture W(t)
Z
C(V − W) drainage flux
mean moisture V(t)
z

Figure 1 Representative of the Two-Layer Model Used to Follow the Water Budget of a Bare Soil Surface Layer (Source: Bernard et al.,1986)

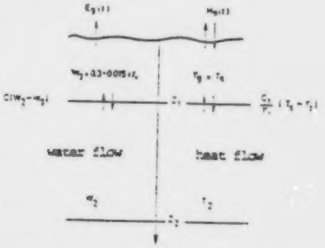
water flow
heat flow

Figure 2 Description of the Simplified Model to Monitor Vertical Transfer of Soil Water and Temperature (Source: Soarces et al., 1988)

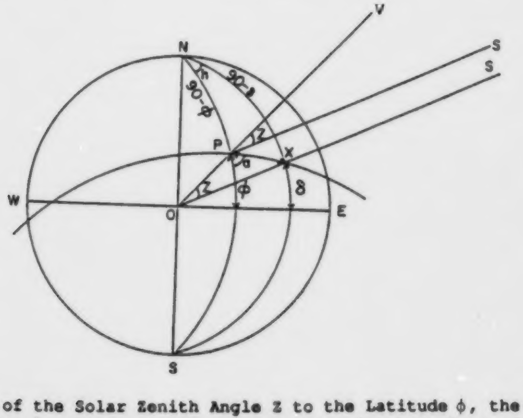
V
S
S
N
h
90-φ
90-δ
P
Z
a
X
W
O
Z
φ
δ
E
S

Figure 3 Relation of the Solar Zenith Angle Z to the Latitude ϕ, the Solar Declination δ, the Hour Angle h, and the Azimuth Angle a of the Sun from South (Source: Sellers, 1965)

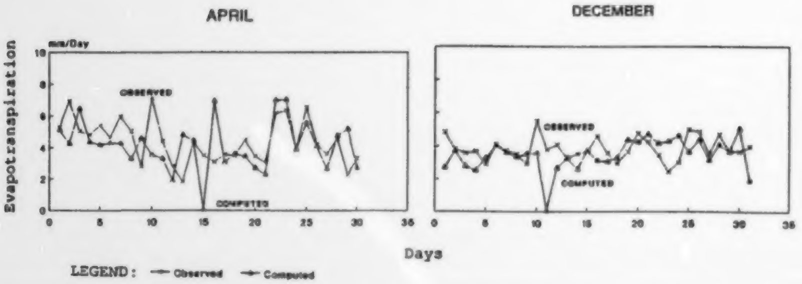

Figure 4 Daily Observed and Predicted Evapotranspiration Values for April and December

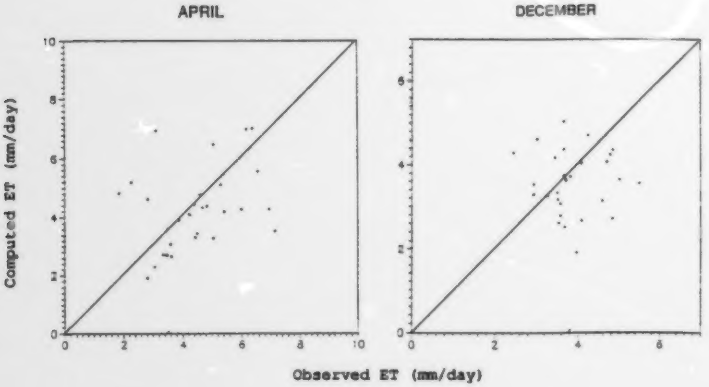

Figure 5 Scattergrams of Daily Evapotranspiration Values for April and December

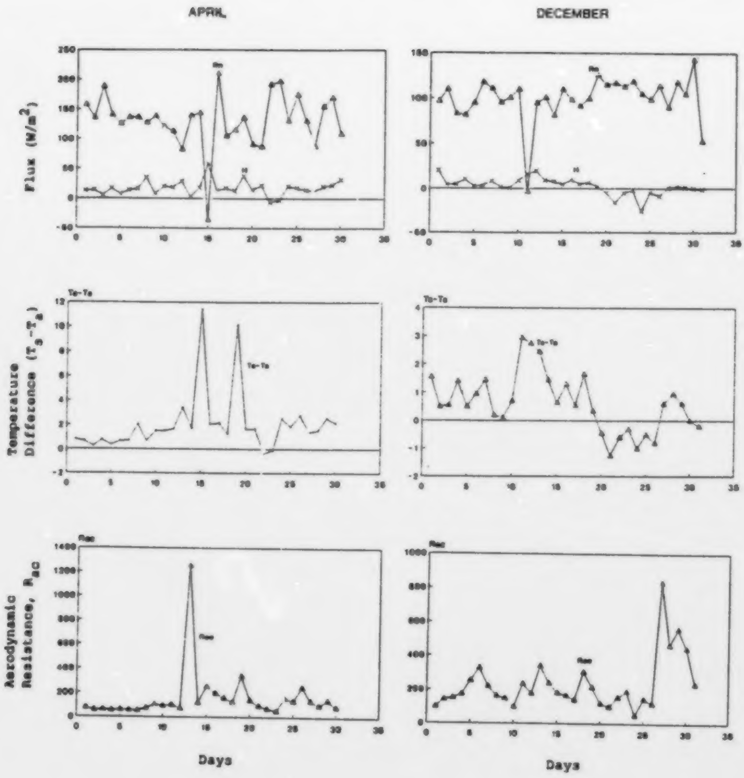

Figure 6 Plots of Daily Net Radiation R_n, Sensible Heat H, Temperature Difference (T_s-T_a), and Stability Corrected Aerodynamic Resistance R_{ac} for April and December

Table 1 List of Data the Energy Budget Model Required to Estimate Regional Evapotranspiration

Data Type	Description	Equation No.	Symbol
Satellite	Surface temperature	(21)	T_s
	Cloud cover	(20), (21)	C
	Surface albedo	(12)	α_s(0.20)
Meteorological	Air temperature	(21),(22),(24)	T_a
	Wind speed	(26)	u
	Air vapor pressure	(22),(23),(24)	ℓ_a
	Daily Solar Radiation	(12),(13)	R_s
	Actual number of hours of bright sunshine	(20)	n
Ground	Height at which T_a is measured	(26)	z_a(1.65m)
	Zeroplane displacement	(26),(28)	d (.067m)
	Vegetation height	(27)	h_c (0.1m)
	Latitude of point observed	(14),(18),(19)	ϕ*
	Solar declination	(14)	∂*
	Day of the year	(17)	D

Note: * Data not required if R_s is available

Table 2 List of Empirical Parameters for the Energy Budget Model

Model Parameters	Equation No.	Symbol	Literature Source
Constants of Prescott's(1940) model	(16)	a,b	Brusaert(1984)
Constant to relate cloud cover and fraction of daylight hour	(20)	f	Brusaert(1984)
Atmospheric emissivity	(21)	$\varepsilon_{\ell a}$	
Surface emissivity	(21)	$\varepsilon_{\ell e}$(0.97)	
Constant for cloud cover effects	(21)	η,q (0.2,2)	Brusaert(1984) Budyko(1974)
Aerodynamic resistance	(25),(26)	r_a	
Stability corrected aerodynamic resistance	(28)	r_{ac}	
Surface roughness parameter	(27)	Z_o	Table A.1
Soil thermal conductivity	(29),(30)	λ	Sellers(1985)
Soil heat capacity	(30)	C_s	Sellers(1985)
Constants of Brunt's(1932) model	(23)	υ,ψ	Brusaert(1984)
Soil flux constant related to sensible heat H	(31)	a_h(0.4)	
Soil flux constant related to net radiation R_n	(32)	a_r(0.4)	

Table 3

Summary of mean monthly input data and ET values for April and December

Variables		April	December
Total rainfall (mm)		80.73	0.0
Maximum temperature ^oC		34.71	31.35
Minimum temperature ^oC		22.80	18.64
Solar radiation Wm^{-2}		218.75	184.60
Air temperature ^oC		28.75	25.00
Observed ET (mm)	Mean	4.40	3.83
	Std dev	1.37	0.69
Predicted ET (mm)	Mean	4.13	3.45
	Std dev	1.53	0.94
Percent difference between predicted & observed ET		6.1	9.9

TABLE A.1

Examples of roughness parameters for various surfaces

Surface description	z_o (cm)	Reference
Mud flats, ice	0.001	Sutton(1953)
Smooth tarmac(airport runway)	0.002	Bradley(1968)
Large water surfaces('average' conditions)	0.01-0.06	Numerous references
Grass(lawn up to 1 cm high)	0.1	Sutton(1953)
Grass(airport)	0.45	Kondo(1962)
Grass(prairie in Nebraska)	0.65	Kondo(1962)
Grass(artificial, 7.5 cm high)	1.0	Chamberlain(1966)
Grass(thick up to 10 cm high)	2.3	Sutton(1953)
Grass(thin up to 50 cm)	5	Sutton(1953)
Wheat stubble plain(18 cm,Kansas)	2.44	Businger et al. (1971)
Grass(with a few scattered bushes and clumps of trees; regional value for Salisbury Plain, England)	4	Deacon(1973)
1-2m high vegetation(Cape Canaveral,Florida)	20	Fichtl and McVehil (1970)
Trees(10-15m high)(Cape Canaveral,Florida)	40-70	Fichtl and McVehil (1970)
Savannah scrub(25%trees 8m; 65% dry grass 1m; burnt grass and sand 10%)	40	Garratt(1978b)
Large city(Tokyo, Japan)	165	Yamamoto and Shimanuki(1964)

Source : Brusaert(1984)

Table A.2

Some published values of mean daily albedo for various surfaces. The range given for crops represents the variation of reflectivity from bare ground or low growth to full cover.

TYPE OF SURFACE	ALBEDO	LOCALITY	SOURCE
Water	0.05-0.10	Various	Various
Bare soil(wet)	0.11	W. Europe	Monteith(1959)
Bare soil(dry)	0.18	W. Europe	Monteith(1959)
Spruce forest	0.05-0.08	W. Europe	Baumgartner(1967), Tajchman(1971)
Pine forest	0.01-0.12	W. Europe	Szeicz et al.(1969)
Bamboo forest	0.12	Kenya	EAAFRO
Evergreen forest	0.14	Kenya	EAAFRO
Tropical hardwood forest	0.18	Kenya	EAAFRO
Pineapple	0.05-0.08	Hawaii	Chang(1968)
Sugar cane	0.05-0.18	Hawaii	Chang(1968)
Tea	0.16	Kenya	EAAFRO
Potatoes	0.15-0.27	W. Europe	Various
Rye and wheat	0.10-0.25	W. Europe	Monteith(1959)
Corn (maize)	0.12-0.24	N. America	Chang(1968)
Sugar beet	0.14-0.25	W. Europe	Monteith(1959)
Short grass	0.14-0.25	Various	Various
Cotton	0.17-0.25	Various	Various
Alfalfa(lucerne)	0.19-0.25	Various	Various
Kale	0.19-0.28	W. Europe	Chang(1968)
Green vegetables	0.25	N. America	Monteith(1959)
Green grass and other short vegetation(e.g., alfalfa, potatoes,beets)	0.15-0.25		Brusaert(1984)
Dry grass;stubble	0.15-0.20		" "
Dry prairie and savannah	0.20-0.30		" "
Coniferous forest	0.10-0.15		" "
Deciduous forest	0.15-0.25		" "
Forest with melting snow	0.20-0.30		" "
Old and dirty snow cover	0.35-0.65		" "
Clean,stable snow cover	0.60-0.75		" "
Fresh dry snow	0.80-0.90		" "

Source : Dunne and Leopold(1978), Brusaert(1984)

A QUALITATIVE EVALUATION OF DATA NETWORKS FOR STREAMFLOW SIMULATION IN MANITOBA

by

A. A. Warkentin, River Forecast Centre
Department of Natural Resources, Winnipeg, Manitoba

Presented at Workshop on Application of Remote Sensing in Hydrology-Saskatoon-February 13-14, 1990

1. Introduction

Data on precipitation, soil moisture, snow cover, streamflow and various meteorological elements have been collected in Manitoba for 40 years or more. This data has been employed to varying degrees in the development of river forecasting procedures. These traditional data networks are all based on point sampling whereas non-distributed hydrologic models require basin average inputs. Inaccuracies in the point sampling procedures and in the estimation of spacial averages from point samples create an unreliable data base which can have serious consequences in the formulation and calibration of hydrologic models.

During the period from 1981 to 1988 Manitoba, in conjunction with the Canada-Manitoba Flood Damage Reduction Program, undertook an investigation of various hydrological models to determine their suitability for river forecasting in the northern plains region. The study concluded with the finding that leading state-of-the-art models such as HSPF and SSARR do not perform significantly better than simple index models for single event simulation. An analysis of the reasons for the relatively poor performance of the more complex models suggested data unknowns as the most likely culprit, followed by inadequacies in the models. This paper consists of a discussion of the impacts of various data unknowns on hydrologic modelling, as perceived from Manitoba's study. This is followed by some speculations as to the potential advantages of remote sensing to estimate watershed state variables.

2. Networks for Estimation of Watershed State Variables

The major watershed state variables for spring water supply and flood forecasting are the snowpack and the initial soil moisture.

2.1 *Snowpack*

Cumulative winter precipitation is commonly used to estimate the water content of the snowpack. This data base works reasonably well for Manitoba because sublimation losses are generally minimal due to predominantly below freezing temperatures. Nevertheless significant errors can occur in the use of this data base to estimate snow cover. Such errors accrue from the inaccurate catch by snow gauges during strong winds (Goodison, 1978), from redistribution of the snowpack by winds causing non-representative ruler measurements of fresh snow (Hopkinson, 1978), from deviations from the 10:1 ratio of snow depth/water content assumed for most climatological observations, and from snowpack melt and sublimation losses during unusually mild winters.

A second data base used is that from the snow course network which has been operated by Manitoba Natural Resources since the early 1950's. The difficulties with this network relate to the low network density and the difficulty of obtaining samples which are representative of a substantial area. The low frequency of updating is a further drawback as manpower limitations preclude more than two or three surveys per season.

The River Forecast Centre of Manitoba Natural Resources relies mainly on the AES precipitation network to estimate snow cover. However, snow course data is used to modify estimates based on cumulative precipitation where the latter are suspect. For the Red River watershed upstream of Emerson, airborne gamma surveys conducted by the United States National Weather Service (NWS) are also used. Since 1989, satellite microwave snow surveys coordinated by the Canadian Climatic Centre and Ph.D. Associates have also been used to some degree, even though this product has been in the experimental stages.

River forecasters must make decisions when the various data bases available to estimate snow cover are conflicting. An example of such a conflict is that along the Red River boundary in mid-March, 1989. Cumulative winter precipitation in the area decreased from 204 mm at Emerson to 104 mm at Morden, a difference of 100 mm in about 40 miles. Snow course data suggested about 70 mm in the Emerson area and 50 mm in the Morden area, a difference of only 20 mm. There had been some snowstorms with strong winds during the winter so that both data sets were suspect. A microwave survey for March 30, 1989 showed about 50 mm of water in the Emerson area and about 45 mm at Morden. A United States NWS gamma survey just south of the area on March 31, 1989 suggested about 130 mm for the Emerson area and 95 mm for Morden. The decision on which data set was more representative would have a major effect on the predicted runoff.

2.2 *Soil Moisture*

As with snow cover, various data bases are available for use in estimating soil moisture. Manitoba Natural Resources have been conducting soil moisture surveys in early November, the average time of freeze-up, each year since 1955. Samples are taken at depths of 6, 12, 24 and 30 inches below ground level and moisture is determined using the gravimetric method. As with the snow course network, the soil moisture network is quite sparse and representative sites are difficult to find due to the high spacial variability of soil types, land use and rainfall.

Expression of the soil moisture as a percent of the long-term mean at each site is somewhat more useful, since samples are always taken in the same location and thus the soil type (and often the land use) are constant from year to year. Nevertheless the data base has been of little use for runoff forecasting.

A proxy value of soil moisture, the Antecedent Precipitation Index (API) is normally used in conjunction with index models for river forecasting. The API is the summation of weighted monthly precipitation expressed as a percent of the long-term average. Appropriate monthly weights used have been determined by optimization and are as follows: May 0.07, June 0.08, July 0.12, August 0.18, September 0.25, October 0.30. The assumption of constant evapotranspiration from year to year is implicit in the method. The API has been found to perform quite well for index models but is of little use for deterministic models.

Soil moisture may be estimated using procedures or models such as Thornthwaite, Versatile Soil Moisture Budget and others. The accuracy of such procedures depends heavily on the validity of the technique used to compute evapotranspiration. Use of Thornthwaite soil moisture estimates instead of API on the Shellmouth Reservoir watershed did not improve runoff forecasts. Nevertheless Manitoba Natural Resources is contributing to a project at the University of Manitoba which will compute historical soil moisture for three decades or so in southern Manitoba using a Baier and Robertson evapotranspiration routine. The results should be useful for river forecasting using both index and deterministic models.

3. Data Impacts on Calibration of Hydrologic Models

A study on the Boyne River Watershed in southern Manitoba was conducted to evaluate various hydrologic models for potential use in Manitoba. Two detailed reports on this study have recently been published (Manitoba River Forecast Development, 1985 and 1988). Three models were evaluated, namely the complex Hydrologic Simulation Program-Fortran (HSPF), the intermediate Streamflow Simulation and Reservoir Regulation (SSARR) and the Single Linear Unit Reservoir Parametric (SLURP). Results were compared with the simple index model MANAPI used in Manitoba. Models were first calibrated on summer data to determine values for most of the physical and process parameters. Calibration with spring data then followed. Each procedure involved many difficulties due to data unknowns, as briefly described in the following subsections.

3.1 *Calibration With Summer Data*

The main source of error due to data unknowns was in the estimation of watershed rainfall inputs. These errors were large due to the high spacial variability of summer precipitation and the relatively sparse rain gauge network. The magnitude of this source of error was manifested by instances where significant runoff occurred without any evident precipitation or where apparently heavy precipitation produced no runoff. Inaccuracies in basin precipitation estimates created serious difficulties in model calibration.

A further source of error was in the estimates of rainfall intensity. Rainfall intensity was found to be so important in calibrating the HSPF model that hourly data had to be used. Unknowns in rainfall intensity stemmed mainly from the very sparse network of recording rain gauges.

The water balance of the soil is a critical component of hydrologic modelling. Precipitation is the input to the water budget whereas evapotranspiration (ET) is the main loss. Models compute ET from an input time series on potential evapotranspiration (PET). Pan evaporation data was basically used to represent PET, with monthly modifying factors to account for the typical state of plant growth. The pan evaporation network is extremely sparse and the assumption of a direct relationship between pan evaporation and PET may be questioned.

Calibration of the model parametres controlling the water balance of the soil was severely hampered by the lack of soil moisture data for validation. The correct simulation of summer streamflow does not necessarily validate the soil moisture budget.

3.2 *Calibration With Spring Data*

Simulation of spring runoff involves the computation of snowmelt in addition to calibration of the lands phase components. Accurate simulation of snowmelt requires representative data on ambient temperature, dew point, wind speed and solar radiation. In addition, the albedo of the snow must be modelled before radiation melt can be computed. The greatest source of error in snowmelt computations appeared to be in the solar radiation estimates. There is only one station, Winnipeg, measuring solar radiation in southern Manitoba. It was necessary to modify observed solar radiation for differences in cloudiness between the watersheds and Winnipeg. This involved error, especially when sunshine recorders were located some distance from the watersheds. Temperature dew point and wind are generally not as variable spatially as radiation but inaccuracies in watershed estimates for these parameters did create calibration difficulties in some instances. The lack of data on snow albedo meant that this important parameter had to be modelled. The unavailability of snow pillow data to monitor the deterioration of the snowpack made it impossible to calibrate and validate the snowmelt routine independently. Uncertainties in the major state variable, the initial water content of the snowpack, compounded the problem.

With respect to the lands phase of the models, the lack of sufficient information on soil temperatures made it impossible to independently validate the infiltration routine. While AES monitors soil temperature at a few stations in Manitoba, the representativeness of the data for specific watersheds is questionable due to differences in soil type, land use and snow cover. Furthermore, there is virtually no information on overland flow, interflow or groundwater flow to validate model land phase subroutines. It was therefore necessary to calibrate the models almost entirely on one data time series, that of the measured streamflow at the downstream end of the watershed. An attempt was made at subdividing the watershed into areas of unique topography and soils and to calibrate these sub-areas separately. This procedure basically failed due to the lack of observed streamflows for the sub-areas and the substantial errors involved in computing these flows by reverse channel routing. Inaccuracies in the "recorded" hydrometric data due to river ice conditions and breakdowns in stage recording devices further complicated the calibration and validation of hydrologic models.

4. Complications Due to Inadequacies of Models

A full-blown state-of-the-art model such as HSPF is quite rigorous in its capacity to model the various aspects of the hydrologic cycle. Nevertheless the model has some shortcomings which seriously hampered its calibration on watersheds in Manitoba.

4.1 *Processes Poorly Modelled*

The most serious difficulty with all models tested was their inability to account for changes in the effective drainage area of a watershed due to widely different moisture inputs. In effect the drainage area is assumed to be constant. Most hydrologists are well aware of the fact that the portion of a watershed contributing to runoff can vary dramatically with the moisture input, particularly for a poorly drained pothole type of topography. Studies by PFRA show that gross drainage areas are frequently two to three times as large as the two-year return period drainage area (PFRA, 1989). The problem with effective drainage areas may be overcome by using a distributed watershed approach with very small response units. This approach has been impractical due to the lack of detailed physical data for watersheds.

A further difficulty with the models was their inability to effectively model infiltration under frozen or partially frozen soil conditions. Research done by the Division of Hydrology, University of Saskatchewan (Gray et al, 1985) on this topic was used to recalibrate the models so as to achieve more realistic infiltration under these conditions. This did improve simulations to a degree.

Problems were also found with the snowmelt routine employed by the HSPF model. Some research done by MacLaren Plansearch (1984) was employed to make changes in the algorithms computing the albedo, the negative heat storage of the pack, the long wave melt and the convection-condensation melt. These changes resulted in a slight improvement of the streamflow simulations.

A further inadequacy of the models was in the evapotranspiration routine. The underlying assumption made is that plants act as "wicks" and will routinely dispel available water. This assumption has been challenged by some researchers (Morton, 1982). According to Dr. Morton, there exists a complementary relationship between ET and PET such that ET actually decreases when PET increases and visa versa. The use of erroneous estimates of ET may have contributed significantly to calibration difficulties with summer data and hence to inaccuracies in the soil moisture estimates at freeze-up.

4.2 *Complex Versus Simple Models*

Complex models such as HSPF have the capacity to produce reasonably good simulations of streamflow if detailed and reliable data is available on the physical watershed characteristics, the state variables, meteorological data and transient watershed conditions such as albedo, overland flow, soil frost, evapotranspiration, etc. Such detailed and reliable data is seldom available and was not available for the watersheds on which the models were tested in southern Manitoba. The problem was compounded by some serious model inadequacies as listed in Section 4.1. As a result, the complex models did not live up to expectations and performed little better than simple index procedures for event spring streamflow simulation in Manitoba. This somewhat surprising result perhaps warrants another look at Manitoba's index model MANAPI. This index model takes the form of a product power type of equation relating runoff (R) to causal parameters such as API, winter precipitation (WP) and melt rate (MR) as follows:

$$R = c(WP)^k(API)^l(MR)^m \text{ ——————— Equation 1}$$

where the constant c and the exponents k, l and m are obtained statistically by regression optimization. Alternately MANAPI takes the form of a family of API curves drawn on a graph which has winter precipitation on one axis and spring runoff on the other axis. Conveyance of runoff is handled using unit hydrographs for various rates of moisture inputs.

One might ask whether changes in effective drainage area are implicitly embodied in these simple non-linear relationships. One might further speculate as to whether the API, defined in Section 2.2, represents antecedent watershed moisture conditions as well as modelled soil moisture. The latter would imply that evapotranspiration, as computed in the models, is no more accurate than the assumption of evapotranspiration being constant from year to year.

The Manitoba River Forecast Centre has concluded that the use of complex models such as HSPF is not waranted unless a more reliable database can be developed and significant model improvements can be made.

5. Potential for Improved River Forecasting with Remote Sensing Data

Airborne or spaceborne measurements of snow cover and soil moisture have the potential to greatly improve estimates of the state variables for watersheds. Airborne gamma measurements of snow cover and soil moisture are made on a routine basis for large areas in the United States by the U.S. National Weather Service. Manitoba Water Resources uses such data for the United States portions of the Red River and Souris River watersheds, at least on a qualitative basis. For the past five years or so, Manitoba Water Resources has been supporting the Atmospheric Environment Service, Downsview and Ph.D. Associates in the evaluation of satellite passive microwave techniques for snow cover measurements. Confidence in this product is increasing and it may soon be used qualitatively for river forecasting. Hopefully new distributed models being developed for use with remotely sensed state variables will prove to be superior to past models based on point data inputs.

For the past few years, Manitoba Water Resources has subscribed to AES Telidon Weather Radar for the purpose of storm tracking and improved rainfall mapping. Weather radar is also a very useful monitoring device upon which to base flash flood watches or warnings. It is hoped that improved types of radar employing CAPPI will prove to be even more useful and that these devices will soon be available to end users at a reasonable cost.

LITERATURE CITED

1. Goodison, B.E., 1978. Canadian Snow Gauge Measurements. Proceedings, Seventh Symposium on applied Prairie Hydrology, Saskatoon.

2. Hopkinson, R. F., 1984. The Doubtful Value of Snow Survey Data for Runoff Forecasting. 18th Annual Congress CMOS, Halifax.

3. Manitoba River Forecast Development-Phase I-Planning and Design September, 1985. Manitoba Natural Resources, Environment Canada.

4. Manitoba River Forecast Development-Phase II-Application and Evaluation, June, 1988. Manitoba Natural Resources, Environment Canada.

5. P.F.R.A., 1989. The Determination of Gross and Effective Drainage Areas in the Prairie Provinces; Regina, Saskatchewan.

6. Morton, F.I., 1982. Operational Estimates of Areal Evapotranspiration and Their Significance to the Science and Practice of Hydrology, NHRI, Ottawa.

7. Gray, D.M., Landine, P. G. and McKay G. A. (1985) Forecasting Streamflow Runoff from Snowmelt in a Prairie Environment, Saskatoon.

Questions and Answers

Brian Latham: Did you ever correct for winter precipitation or for other effects such as wind?

Alf Warkentin: We are aware of the problem, but as far as I know there is no quantitative reliable method to make that correction.

Barry Goodison: I think a point relative to that is we have a quantitative method for correction of our gauge data, but not all of those are gauge sites, some of those were rulered sites where you use a ten to one conversion. So you've got a multiple problem there; it is not just dealing with one type of measurement, it is several, so that can cause an artificial gradient.

Brian Lathan: Did you correct for and say something about trace precipitation as well?

Alf Warkentin: No. I know that is a problem in the arctic, but I don't think that it is important here. For these flood years we are talking about 200 millimeters and up of water content, so it is quite a bit. Trace amounts are relatively small for those years. At Emerson I did check into the exposure there, and the gage is placed in a fairly large treed area, a big clearing in a treed area. I think what might have happened there is that these trees acted under strong winds as a snow fence, and that snow was collecting with this clearing. So, it was a very good exposure for normal conditions, but for very strong winds it may have been just accumulating snow.

John Stewart: Just a comment. It is relevant to consider the results that we had at the Institute of Hydrology in comparing different types of models. In this discussion, now, we are going back to work done in the 1960's and early 70's. At that time we were looking at the Stanford model. It was certainly a very complex model; I can't remember now how many parameters you had to tweak or change somehow. I think there were a couple of dozen or maybe even more than that, and eventually we came to the feeling that really that tweaking was counterproductive. You've mentioned that you can not check that the sub-models at intermediate stages were actually right or if they have any physical reality. So we went back to much simpler models. I do not know whether they were actually the same sort of index you've used, but we certainly ended up with something like that. We really placed a lot more confidence in that, because at least we knew what we were dealing with. That is the basis of our runoff modelling.

Alf Warkentin: That is very much what happened to us too; lack of validation data kind of killed us. We started this whole thing at around 1980, and if we had known then what we know now of course we would not have gone to the trouble. But we didn't know then what we know now. Certainly you learn a lot more at workshops like this. It is pretty obvious we need a lot more data for validation and to develop better models.

John Stewart: Well we were, in fact, in a situation where we didn't have the problem with snow, because much of the lowlands of the U.K. does not have an appreciable amount of snow, so we were dealing with rainfall situations and we were doing it on an experimental basis where we had a great deal of data, but we decided it was actually better to use a simple index model, rather than to use a supposedly "physically based" model.

Alf Warkentin: I think that that question is still going to be here for a while too, even with remote sensing data that's not going to go away for a while. There will still be the temptation to use simple models even using remotely-sensed state variables, perhaps even index models still for a while. Until something comes along that is proven to be better; why do it the complicated way when you can do it the simple way? We have a couple of reports that describe in detail what we have done, in case anyone is interested.

WORKSHOP SESSION 1
REMOTE SENSING IN HYDROLOGIC MODELLING

Session Chairman: G.W. Kite, Canadian Climate Centre

Session 1 - Working Group Questions

1. Which types of remotely sensed data are presently useful in hydrologic modelling? Do they make a significant improvement to the performance of the models?

2. What other types of remotely sensed data are needed for modelling? What are the prospects of getting them in the near future?

3. How should existing models be changed to take advantage of RS data or does it require new types of model?

Workshop Chairmen & Rapporteurs

	Group 1	Group 2	Group 3
Chair	A Rango	G Leavesley	N Kouwen
Rapporteur	ED Soulis	JB Stewart	G Thomas

HYDROLOGIC MODELS

Summary

G.W. Kite - Session Chairman

1. There is a widespread awareness of the availability and utility of remotely sensed data for hydrologic modelling purposes. The relative importance of hydrologic variables, on a scale of 1 to 3 stars, and the relative success in deriving them from remote sensing may be summarised in the following table.

	Importance		Success
land use/land cover	***		***
snow covered area	***		**
snow water equivalent	***		*
ice	***		*
precipitation	***	radar	**
		satellite	*
radiation	***		***
albedo	**		*
cloud cover/type	**		*
soil surface moisture	***		*
surface temperature	**		*
frozen ground	**		*

Landsat MSS, TM or SPOT give good land use/ land cover data for hydrologic models and are available at less cost than from conventional maps. Snow cover data from NOAA AVHRR is useful to determine the distribution of snow within elevation bands of a basin and is used in several existing models.

Precipitation from radar is useful in areas of sparse raingauge networks (density < 1 gauge/400 km^2) and is especially important for short-term real-time flood forecasting. Precipitation data from satellite are useful in sparcely gauged tropical areas (e.g. Meteosat in Africa) but there are problems with stratiform clouds in temperate regions. There has been some success in combining satellite, radar and ground-based precipitation data on a monthly basis.

Snow water equivalent is currently estimated from cumulative precipitation but some success is being obtained with microwave imagery and with air-borne gamma surveys. Soil moisture is usually a model output at this stage although there is promise of results from microwave techniques.

2. Variables that may be estimated in the future include evaporation/evapotranspiration, precipitation (particularly in mountainous areas), runoff (stage, velocity), water quality, deep soil moisture and depth of water table.

3. To take advantage of the capabilities of remote sensing, hydrologic models must have the ability to update state variables such as snow depth. They must be able to accept data at different scales and be able to combine point and remotely sensed (spatial) data including data from digital terrain models and geographic information systems via extrapolation routines. The models should be flexible so that they can operate with differing degrees of complexity depending on the data available.

Algorithms to extract hydrological information from satellite data require considerable refinement as, at the moment, interpretation is usually undertaken in a qualitative framework. While satellite data is sometimes used to modify the variables in a model, problems of interpretation have prevented direct incorporation into a model; it is difficult to relate satellite derived variables with the hydrologic and climatologic variables used in current models. The current understanding of the physics of the interaction of electromagnetic energy with complex land surfaces limits such interpretation. Thus satellite data provides relative measures of soil wetness, for example, rather than volumetric soil moisture.

Three areas were identified in which it was felt that models using remotely sensed data could best contribute:

a) Watershed behaviour under high flood conditions. The needs here are for the spatial distribution of rainfall, rainfall excess and surface water. The models will need accurate simulation of the surface and subsurface routing processes.

b) Global change models. The need identified here is foe a scaling-up of basin-size fields for comparison with global-scale maps of, for example, precipitation, soil moisture, temperature and snow water equivalent.

c) Irrigation scheduling models could make use of remote sensing for estimation of the distribution of soil moisture.

It was also felt that researchers should lobby against the reduction of conventional sources of data and should develop statements of data requirements to influence future satellite planning.

SESSION 2A

RADAR REMOTE SENSING AND SOIL MICROWAVE RADIOMETRY

Session Chairman: A. Wankiewicz
National Hydrology Research Institute

UTILIZATION OF SAR DATA IN THE MONITORING OF SNOWPACKS AND WETLANDS

Robert Leconte
Canada Centre for Remote Sensing
1547 Merivale Road, Ottawa, Ontario K1A 0Y7

Terry J. Pultz
Intera Technologies Ltd.
1525 Carling Avenue, Suite 600, Ottawa, Ontario K1Z 8R9

ABSTRACT

Snow water equivalent (SWE) and the areal extent of snow cover are important parameters in the forecasts of spring flows and in monitoring environmental changes at the regional and global scales. The Synthetic Aperture Radar (SAR), with its ability to penetrate a dry snowpack and its high sensitivity to the occurrence of liquid water in snow and soils, represents a promising alternative to conventional methods to obtain snow parameters at a basin scale.

In this paper, the potential of the SAR for evaluating the total water equivalent of the snowpack is assessed. To that end, a set of airborne C-Band SAR data acquired in the Ottawa region during the winter of 1986-1987, in conjunction with point measurements of snow depths and water equivalent collected at nearby snow courses have been used to examine potential relationships between SWE and the radar backscatter from the snowpack. The SAR data were relatively calibrated using an airport runway and coniferous trees as reference calibration targets. Results obtained seem to indicate an inverse relationship between SWE and backscatter.

Also, a series of C-Band SAR images acquired in fall 1988 and winter 1988-1989 under wet and dry snowpack types were used to discriminate vegetated wetlands. The proposed methodology focusses on the changing response of wetlands when exposed to varying snow wetness conditions.

INTRODUCTION

Snow cover is an important factor that affects the global and regional weather and climate, as it significantly alters the surface heat and moisture exchange and the radiation balance, thereby interacting with the global atmospheric circulation. Knowledge of the extent and distribution of the snow masses is essential to improve weather forecasts, both medium and long-range, and for upgrading existing, and developing new general circulation models. The snow distribution and extent are good indicators of climate fluctuations. Monitoring the areal distribution and extent of snow masses would be useful in monitoring shifts in regional and global climates. At a regional level, snow is a valuable resource for irrigation, hydro-power generation, agriculture, and other human activities.

Wetlands are also sensitive indicators of climatic changes at the regional and the global scales. Furthermore, wetlands are a major source of methane (a greenhouse gas) production. Locating wetlands and monitoring their areal extent is critical to a better understanding of the links between atmospheric and terrestrial processes.

For operational uses in hydrology and in regional and global environmental monitoring, microwave techniques are very promising. Microwaves are able to penetrate clouds and therefore provide data on snow cover, freshwater ice regime and wetlands at regular time intervals. Because snow and ice extent change rapidly, timely observation of snow and ice parameters is highly desirable. Only with the use of microwaves can this requirement be fulfilled at a basin scale. Techniques employing gamma ray were shown to be very useful for monitoring snow water equivalent, but the areal coverage is lesser that than with microwave techniques. The time constraint is not as important in the case of wetlands, however, the ability to obtain multitemporal coverages is highly valuable in monitoring the wetlands hydrological regime, which is often not feasible with optical sensors.

In this paper, the potential of the Synthetic Aperture Radar (SAR) for monitoring the snowpack, and in particular the snow water equivalent (SWE), will be investigated. As well, a method that employs multitemporal SAR data sets for wetland identification and delineation will be presented. The multitemporal data sets were acquired during the winters of 1986-1987 and 1988-1989 by the Canada Centre for Remote Sensing in a test area in the vicinity of Ottawa, Ontario.

DATA SETS

Airborne SAR images were collected between August 6, 1986 and August 6, 1987 over a test area near Ottawa using the C-band airborne synthetic aperture radar installed in the Canada Centre for Remote Sensing (CCRS) Convair-580 aircraft. It is a digitally controlled, two channel radar, operating at C-band (5.30 GHz), transmitting either H or V polarization and receiving both polarizations simultaneously. It was demonstrated that this system could discriminate targets with low backscatter values (-20dB to -15dB) (Livingstone *et al*, 1987), making it attractive for snow monitoring. The system can process one received channel to a 7 look image using an onboard 7-look real-time SAR processor (RTSP) and subsequently display these data. Data can be acquired in three nominal modes: nadir, narrow, and wide swath. During the summer of 1987, the C-band antenna was changed and the system was upgraded into a dual frequency C/X band radar. The data set from September 1988 to February 1989 were collected with this system. The C/X band system offers the same options as the old C-band SAR system. In addition, it can acquire X-band (9.6 GHZ) data simultaneously, thus offering the option to analyze multi-frequency data sets. However, the present study focussed on the use of C-band data alone.

The location of the study site (45°23'N; 75°55'W; west of the city of Ottawa) was determined by the area of overlap of individual flight lines. Figure 1 shows the location of the imaged area. The total imaged area covers a surface of approximately 1000 sq. km. However, the present study focussed on a much smaller sub-area (approximately 50 sq. km.). Table 1 shows the SAR imaging parameters of each scene. The test site is composed of forest, water (open water bodies and bogs), pasture, urban and agricultural (grain, corn, hay, soybeans, sod) land cover types. Figure 2 illustrates the normal SWE (averaged over periods of 8-15 years) values in the vicinity of the study site. Data were obtained from the Mississippi Valley Conservation Authority, the Rideau Valley Conservation Authority, the Ontario Ministry of Natural Resources, and Ontario Hydro.

In order to assist in interpreting the SAR images, the meteorological history was compiled using the two nearest meteorological stations. These stations are located at the Ottawa International Airport, 22 km east of the site, and at a Canada Department of Agriculture facility, 21 km north east of the site. A study by Cihlar *et al* (1990) has shown the importance of accurate meteorological data for environmental change detection. Since the two meteorological stations exhibited some important variations, especially in relation to precipitation, and to a lesser extent the air temperature, it was decided to deploy a portable automated weather station at the site. The weather station began collecting hourly data (precipitation, solar radiation, air temperature, relative humidity, wind speed and direction) in early September 1988. All weather data are automatically stored in a "storage module" at the station. The module is removed periodically and the data downloaded to a personal computer. The weather station can be programmed to collect data for any time interval. During the SAR flights, the weather station collected data at every 5 minutes. Tables 2 to 4 summarize the meteorological conditions encountered before and during the SAR data acquisitions.

In addition, snow depths and water equivalent were collected at and in the vicinity of the study site. Figure 3 shows the SWE curves of selected stations within and in the vicinity of the study area for the 1986-1987 winter season.

Finally, soils maps, topographic maps, aerial photographs and a LANDSAT scene (path 16, row 29; acquired on October 11, 1986) were used as supplementary information for the interpretation of the SAR data.

In preparation for analysis, the TM image was registered to a Universal Transverse Mercator (UTM) map and resampled using a cubic convolution algorithm to 6.25 pixels. This image was used as a reference image to which all SAR data were registered using a nearest neighbour algorithm.

MONITORING OF THE SNOWPACK

Background information

For applications in hydrology and in climatology, the areal extent and the (SWE) are the most important parameters of the snowpack. The snow wetness, i.e. the amount of liquid water present in the snowpack, is also of interest, particularly in the forecasting of the onset of spring runoff.

The following snow properties affect the active and passive microwave signatures (Rott, *et al*, 1986):

- liquid water content (the snow wetness);
- snow depth;
- snow density;
- stratigraphy;
- grain size;
- grain shape;
- surface features.

In particular, active microwave signatures of snow are highly dependent on the liquid water content in the pack. Increasing the liquid water content in the snowpack significantly increases both the real and imaginary portions of the dielectric constant, therefore substantially altering the amount of incident microwave energy being scattered and absorbed in the snow medium. For instance, the penetration depth at X-band in a homogeneous dry snowpack is in the order of 10 meters. The penetration depth is reduced to the order of one wavelength (3-4 cm) with a 4-5% snow wetness (Matzler and Schanda, 1984). Under those circumstances, scattering is limited to the surface and a very thin layer at the top of snowpack, and absorption is the predominant process, wet snow behaving essentially as a black body.

The scattering processes of a dry snowpack are more difficult to describe because low absorption allows complete penetration of the microwave energy into the pack (Rott, 1986). Radar return from snow covered ground includes contributions from surface scattering at the air-snow boundary, from volume scattering in the snowpack, and if the losses in the snowpack are small, from scattering at the snow-ground boundary (Ulaby and Stiles, 1980). Schanda (1987) observed that at lower microwave frequencies (below 10GHz) the measured backscatter (σ°) values were strongly affected by reflections from the soil below the snow cover due to the large penetration depth at these wavelengths through dry snow. Scattering at the surface of a dry snowpack is very small and can usually be neglected (Ulaby *et al*, 1986).

Because of the large penetration depths of dry snowpacks, the task to estimate the SWE from radars becomes a difficult task.

However, a natural snowpack is rarely homogeneous. The presence of layers of ice and of snow with different characteristics (grain size, density) have been shown to have a non-negligible effect on scattering, especially at higher frequencies (Rott *et al*, 1988).

The task of discriminating areas covered with dry snow from snow-free areas is not straightforward. However, it may be possible to monitor changes in SWE through multidate observations. Ulaby *et al* (1986) suggest that the use of change detection techniques (implying the analysis of multitemporal data sets) may prove quite useful in estimating the SWE over large areas. Rott *et al* (1985) also state that improved capabilities for snow mapping are also expected by use of multitemporal data sets, relating temporal changes in radar return to snow coverage. This approach was used in the present study.

The potential of estimating SWE from active microwave sensors have been explored mainly by Matzler (1987), Matzler and Schanda (1984), and Ulaby and Stiles (1980). Data obtained from ground scatterometers were used for these studies. Ulaby and Stiles (1980) have reported a positive relationship, i.e. an increase of the scattering coefficient with increasing SWE, at X-band, 57° incidence angle, HH polarization, while Matzler and Schanda (1984) observed that backscatter decreased with increasing SWE. A possible explanation for this discrepancy may be related to the characteristics of the snowpack. An artificially packed snow was utilized in Stiles and Ulaby's work, while Matzler and Schanda worked with a natural snowpack. On the other hand, the utilization of SAR for estimating the SWE has only recently begun. Bernier and Fortin (1989) report a study of the utilization of the CCRS X/C SAR system to estimate the SWE in a small sub-basin of the Eaton River, Quebec. Preliminary results seem to indicate that stratified snow is not completely transparent at C- and X-band, and that in pastures, the radar backscatter increases with increasing SWE.

Methodology

The 1986-1987 multitemporal SAR data set were analyzed for trends between σ^0 and the SWE. The 1988-1989 data set were not used in the analysis, mainly because the data were acquired using a different antenna. Comparison between the two data sets would have lead to problems since the relative radiometric characteristics of the data sets are difficult to ascertain. One way to adjust the 1988-1989 data set against the 1986-1987 data set - called relative calibration - would have to employ point and/or distributed targets of known cross sections. Corner reflectors are mounted permanently in the area. Unfortunately, these targets did not appear on each SAR image, and furthermore there are no assurances that they were pointed correctly at each flight pass. Therefore, there was no attempt made to calibrate the 1988-1989 data set to the 1986-1987 set.

Data analysis was conducted in the following way. First, the SAR scenes were spatially averaged using a 5x5 median filter to reduce speckle, an inherent characteristic of any SAR system. The boundaries of the each land cover type were outlined on the interactive display of an image analysis system and identified as to field number and land cover type. The set of individually outlined fields thus constituted a ground truth map. In this manner, digital values for a given cover type could be easily extracted from any image of this area. Next, the SAR scenes were relatively calibrated. This is a crucial step to a multitemporal analysis, where change detection (in this case the detection of temporal variations of SWE) is concerned. In the selected calibration approach, distributed target areas were considered as reference targets. Unfortunately, it was impossible to select a target area for which the backscatter values would not change with time and which was in the mid- to upper region of the backscatter range of the scenes. Forested areas were considered, but the possible effects on the backscatter values caused by snow on the branches (which may alter the geometry of the trees, hence altering the σ° value) could not be assessed. As a compromise, an airport runway (the Carp airfield) was selected as a reference target despite the fact that the average runway pixel value was in the lower part of the scene dynamic range. As the runway was dry for all data acquisition dates, it is assumed that its backscatter was constant.

The calibration procedure consisted in subtracting the system noise power from the SAR image, followed by rescaling the dynamic range of each image based on the assumption that the runway backscatter value was constant. The system noise was obtained from a topographic shadow region on each image. Since the SAR processor generates output values in the voltage domain, the pixel values were squared (power domain) prior to subtracting the noise and rescaling the images. Possible impacts of this calibration procedure on the results obtained is presented in the next section.

Once the images were rescaled, statistics (mean and standard deviation) for each land cover type and each date were collected. It must be noted here that averaging the pixel values for each cover type eliminates the possibility of examining variations of SWE within the study area. Rather, it will allow investigation of temporal variations of the average SWE. This approach is quite different from that utilized by Bernier and Fortin (1989), where their analysis focused on individual fields. It also has the advantage of minimizing random fluctuations of the pixel values, since the averaging process is performed over a much larger sample population.

Results

Environmental conditions during SAR data acquisition

The maximum air temperature during, and the days preceding the SAR acquisition were below 0°C. Also, the snowpack was relatively shallow and the ground was frozen (see Table 3). Therefore it was assumed that the snowpack was dry (0% liquid water content) during all winter flights over the site. Minimum and maximum air temperatures at the Ottawa International airport and at the Agriculture Canada weather stations are shown in Tables 2 and 3. Because the ground was frozen, it is probable that soil moisture under the frozen layer had a little, if not negligible, influence on the backscatter values of the snowpack, especially since the images were acquired at shallow incidence angles (see Table 1). Finally, plants were either absent (harvested) or covered by snow (dry remnants of broken corn stalks following the harvest of the cobs in the fall), and with the possible exception of corn fields, the effects of vegetation on the radar backscatter are assumed negligible.

Backscatter values during winter

Average values of the backscatter coefficient for the three winter dates (December 11, January 12, February 25), the fall (October 21) and spring (May 8) dates for the agricultural areas (harvested corn, grain, hay, soy) are shown in Figure 4, along with the estimated average SWE for the study site. The SWE curve was obtained by performing a simple arithmetic average of the Huntley, Bells Corners, Kinburn, and Ottawa Airport snow courses. Note on Figure 4 that the backscatter values are expressed as digital counts. The units employed here are not what is commonly found in the literature (dBs are employed), where the backscatter values are dimensionless. Nevertheless, we are concerned here with possible correlations between radar returns and SWE, so that the choice of units is not critical to the analysis. The SAR images were calibrated with the airport runway at Carp arbitrarily set up to DN = 30.

From Figure 4, a consistent decrease in backscatter during winter is observed, along with an increase in the average SWE. It appears *a priori* that the snowpack is not transparent at C-band, as it was pointed out by Bernier and Fortin (1989). Matzler and Schanda (1984) and Rott *et al* (1988) mention that, although a dry snowpack is virtually transparent at frequencies smaller than 10 GHz, inhomogeneities in the snowpack, such as ice layers, impurities in the snow, and variations in snow crystal shapes and sizes and of density all contribute to an increased scattering from the pack. These inhomogeneities are the result of gravity and wet snow metamorphism, and are often associated with rainfall episodes. Meteorological records (see Tables 2 and 3) indicate that a rainfall event occurred on December 25. This event has substantially altered the metamorphism of the snow crystals, and has probably resulted in the formation of an ice layer in the pack.

The observed trend in Figure 4 seems to contradict the findings by Bernier and Fortin (1989) and the experimental results of Ulaby and Stiles (1980), who observed a positive correlation between SWE and σ°. This apparent contradiction may be partly explained by one or some of the following factors: 1- the attenuation of the radar signal from the underlying soil is larger than the increase in volumetric backscattering caused by an increase in SWE (characteristics of the snowpack and of the underlying soil may explain this trend); 2- the snowpack contained small amounts of liquid water at the time the SAR data were collected; 3- the calibration procedure employed here introduced an artifact on the derived backscatter values. Hypothesis 2 is unlikely considering the meteorological records the day of, and preceding, the SAR flights. Hypotheses 1 and 3 will be further explored in the following section.

Figure 4 also reveals that on October 21, substantial differences in backscatter values among the various crop types are observed, and that the differences are almost non-existent during the winter season. In winter, if the crops are harvested, the backscatter values of a dry snowpack become strongly affected by the scattering mechanisms of the underlying soil. Although the soil surface roughness may vary considerably, frozen soils have a low dielectric constant (similar to that of dry soil), hence surface roughness may not play an important role in the total backscatter from the soil. On May 8, the soils are probably high in liquid water content, and all the fields exhibit a high radar backscatter.

Discussion

SAR data calibration

As previously stated, the SAR calibration procedure utilized in this study suffered from the absence of reference target areas in the mid- to upper portions of the backscatter range of the scenes. Also, the possibility of using trees to calibrate the scenes was envisioned, but the lack of evidence that the backscatter coefficients of coniferous trees would remain constant throughout winter favoured the use of an airport runway as the only reference target. With this apparent shortcoming in the calibration procedure, the following questions arise: 1- what impact does the calibration procedure have on the output results?; 2- Is the observed trend between radar backscatter and SWE sensitive to the calibration procedure employed?

To try to answer the above questions, the average DN observed in Figure 4 were modified according to the hypothesis that the radar backscatter of coniferous trees would not vary in the course of the winter season. This implies the following underlying assumptions:

1- the radar backscatter results from scattering mechanisms in the tree canopies only, with a negligible contribution from the underlying soil and snowpack;

2- the occurrence of dry snow in the tree canopies have a negligible effect on radar backscatter. This implies that snow on branches did not substantially affect the geometry of trees;

Bernier and Fortin (1989) employed coniferous trees as calibration targets to remove the antenna pattern in SAR. The validity of the assumption 2 is difficult to assess since no ground observations were made during the winter flights.

Figure 5 shows the calibrated backscatter coefficients obtained by utilizing the trees and an airport runway as reference calibration targets. The calibration factor applied to the scenes was no longer a constant, but varied in a linear fashion with the DN. Linear relationships were obtained for each scene with reference DNs for coniferous trees and the airport runway arbitrarily set up at 100 and 30, respectively.

A look at Figure 5 reveals that the modified procedure did not affect substantially the relative DN of the agricultural targets. This was somewhat anticipated, since the agricultural fields all had low radar backscatter values (close to that of the airport runway) during the winter season. On the other hand, the backscatter values during the growing season would have experienced important changes since they would be closer to the values of the coniferous trees. As an example, the backscatter of corn on October 21 went from 136 (with the airport runway as the only reference target) to more than 160, when both coniferous trees and airport runway are used as calibration targets.

The trend between SWE and DN observed in Figure 4 is preserved in Figure 5. Note that the negative slope of the backscatter curves for corn grain, hay/pasture, and soy are nearly identical during the winter season. Consequently, it appears that grouping all the fields and developing one curve between SWE and DN is a possible approach to monitor the temporal evolution of a snowpack on agricultural areas.

Backscatter model

As it was pointed out in a previous section, the observed inverse relationship observed here between SWE and radar backscatter agrees with findings by Matzler and Schanda (1984), but is in apparent contradiction with the results observed by

Bernier and Fortin (1989) and Ulaby and Stiles (1980). In this particular case, the calibration procedure adopted did not seem to change the direction of the trend between SWE and DN. A possible explanation between those conflicting observations may be related to the nature of the snowpack and the underlying soil. For discussion of the scattering contributions in dependence of snow and soil parameters, a simplified one-dimensional approach developed by Ulaby *et al* (1982) is used here.

Ignoring diffuse scattering (which accounts for multiple scatter in the snowpack) and multiple reflections between the air-snow and the snow-soil interfaces within which the snow layer is bounded, σ° may be written in the following form:

$$\sigma^\circ(\theta) = \gamma^2(\theta) * \left[\frac{\sigma_v \cos\theta'}{2k_e} * \left(1 - \frac{1}{L^2(\theta')}\right) + \frac{\sigma_s^\circ(\theta')}{L^2(\theta')} \right] \qquad (1)$$

where

$\gamma(\theta)$ = power transmission coefficient of the snow-air boundary, dimensionless
θ = angle of incidence from nadir
σ_v = volume reflectivity of snow, 1/cm
k_e = volume extinction coefficient of snow, 1/cm
k_e = k_a+k_s, the absorption and scattering coefficients, respectively
$\sigma_s^\circ(\theta')$ = backscattering coefficient of the underlying ground medium
θ' = angle of refraction, related to θ by Snell's law
$L(\theta')$ = loss factor of the snow layer
$L(\theta')$ = $\exp(k_e\ d \sec\theta')$, where d is the snow depth in cm.

The above equation does not include the backscatter contribution of the snow-air interface, and therefore does not apply for σ° near nadir, nor can it account for changes in the snow surface roughness (Ulaby *et al*, 1982). Rearranging equation (1) leads to the following expression:

$$\sigma^\circ(\theta) = \frac{\gamma^2(\theta)\sigma_v \cos\theta'}{2k_e} - \gamma^2(\theta) * \left[\frac{\sigma_v \cos\theta'}{2k_e} - \sigma_s^\circ(\theta') \right] * \exp(-2k_e\ d \sec\theta') \qquad (2)$$

Note that the expression inside the brackets in equation (2) can be negative or positive depending on the relative contribution of the terms $\sigma_v \cos\theta'/2k_e$ and $\sigma_s^\circ(\theta')$. Note also that if the expression inside the brackets is positive, the model predicts an increase of σ° with increasing SWE, whereas if the expression is negative, the model predicts a decrease of σ° with increasing SWE.

According to this simplified model, the snowpack and the soils characteristics will determine the sign of the slope of the σ° vs SWE relationship.

If the backscatter contribution from the underlying ground medium is large, then it is possible that the expression inside the brackets of equation (2) becomes negative, and a decrease of σ° with increasing SWE is encountered. This particular situation would possibly occur in rough unfrozen soils. On the other hand, if the soil contribution is small (for example a smooth soil frozen to large depths), then the model would predict an increase in backscatter values with increasing SWE. Bernier and Fortin (1989) reported a positive relationship between σ and SWE over pasture fields, which are characterized by smooth surfaces.

The snowpack structure also plays a role in the scattering mechanisms. As the snow grain size increases the volume scattering coefficient of snow increases, as well as the volume reflectivity coefficient. For a weakly scattering medium with isotropic scattering, the volume reflectivity coefficient of snow may be approximated by $k_s/2$. Thus an increase in the snow grain size causes an increase in the expression inside the brackets of equation (2), which in turn modifies the slope of the σ° vs SWE curve. However, because the volume scattering coefficient is found in both the numerator and the denominator of the expression, the variation of σ^0 with grain size is likely to be small. This supports the findings of Stiles and Ulaby (1980), who noted that in the 9-16.6 GHz range, σ° appeared to be relatively insensitive to snow "type". Perhaps a more important factor in the backscatter values of snow is the presence of inhomogeneities such as ice layers. In the experiment by Stiles and Ulaby (1980), snow was piled up in horizontal layers that were 20-30 cm thick each, up to a depth of 170 cm. Dry, newly-fallen snow was used throughout, thereby maintaining approximately uniform snow density and crystal size distribution as a function of snow depth. A positive relationship between σ° and SWE was obtained. Bernier and Fortin (1989) also observed an increase of σ° with SWE in agricultural fields. However, the snowpack was relatively shallow (snow densities of 0.32-0.47 and depths of 15-43 cm), and was highly stratified (up to 9 layers (Bernier, pers. comm.)). Multiple layers generate diffuse scattering which may result in an increased volume backscatter as SWE increases. In this study, there were no ground data collected relative to the stratification of the snowpack. However, the meteorological records indicate that between December 86 and February 87, the air temperature was always below 0°C, with the exception of 4 consecutive days in December and two days in January. Therefore the snowpack may not be have been highly stratified. This may also explain why Bernier and Fortin observed a different trend than the one reported here.

MONITORING OF WETLANDS

Background information

Radar image investigations over wetlands have been rather limited to date. A majority of the studies were conducted on Seasat SAR images (L-band) (Harris and Digby, 1986; Benton *et al*, 1983; Waite *et al*, 1981; Wedler and Kessler, 1981), and also with the old airborne SAR-580 dual frequency system (X- and L-band) of CCRS (Harris and Digby, 1986; Wedler and Kessler, 1981). In a recent study, Cihlar *et al* (1990) examined the potential of C-band data for wetland monitoring.

Harris and Digby (1986) performed a detailed study of Seasat SAR and airborne SAR images for their potential in wetland mapping and concluded that it appears L-band spaceborne radar imagery can be useful for monitoring the spatial extent and locations of wetlands. They hypothesized that the very high backscatter characterizing wetlands, in the form of standing water and emergent vegetation results from a dihedral reflecting surface consisting of the water surface and the emergent vegetation. They also noticed that differences in radar response were tied to different surface cover types. The areas of very bright return corresponded to areas of dead trees in standing water, while areas of medium-bright return were predominantly from mature, live deciduous trees in areas of intermittent coverage (deciduous swamps). Frequency also appears to play an important role in identifying wetlands. For example, it was found that wetlands characterized by sedges and bulrushes in open water appear bright on the X-band imagery and dark on the L-band imagery.

Although L-band and X-band images appear suitable for wetland mapping, there are circumstances under which the detection can be problematic. For example, vegetated wetlands are difficult to distinguish, as the contrast between the vegetated wetland and the surrounding forested terrain is low. Harris and Digby (1986) observed that shrub bogs had a low return at L-band, which made them difficult to clearly separate from the surrounding terrain. One way to improve detection capability is to use multiple radar frequencies. Benton *et al* (1983) found that combining L- and X-bands should provide a significant breakthrough for wetlands reconnaissance and mapping. L-band, with its greater penetration through vegetation, is capable of sensing moisture under the canopy, while X-band, being more sensitive to small scale roughness, is potentially useful for discrimination of broad categories of plant species.

A method is proposed here to map vegetated wetland extent using a single frequency, (C-band). Rather than relying on multiple frequencies and/or polarizations, the proposed delineation method is based on the analysis of a multi-temporal data set. In particular, the method will take advantage of the inherent characteristic of wet snow to absorb microwave energy. As Radarsat will provide repetitive C-band coverage, the method would be valuable for monitoring the evolution of vegetated wetlands in Canada.

SAR data and qualitative analysis

The 1988-1989 multitemporal SAR data set (14 September 1988, 30 January 1989, 10 February 1989) were used in this analysis. The characteristics of the SAR data and the meteorological conditions prevailing during the SAR data acquisition are shown in Tables 1 and 4, respectively. It is important to note here that on January 30, 1989 the air temperature was above the freezing point and that the snowpack was wet. This situation contrasted with the February 10 flight, where the snowpack had 0 percent wetness.

Figures 6, 7 and 8 show the C-band SAR images acquired on August 1982, January 1989, and February 1989, respectively. The wooded area in the image is characterized by a large number of small open water bodies and marshes (vegetation, namely cattails, growing in water).

A look at the September scene (Figure 6) reveals that the open water bodies appear dark and are easy to detect, because of the high contrast with the surrounding land. Marshes are much more difficult to detect, because the radar return is, in many instances, similar to that of the surrounding trees.

The February scene also shows the open water bodies quite distinctly, as lake ice typically produces low returns (specular reflection at the ice/water interface, along with small volumetric scattering). Note however that marshes seem to be a little more apparent, as the emergent vegetation trapped in the ice cover and blanketed by the snow produces a somewhat weaker return than vegetation in standing water (corner reflector effect). Cihlar *et al* (1990) noticed that during the summer months marshes would generate returns somewhat larger than the deciduous and the coniferous trees, whereas during the winter months, the backscatter values were lower by 2-3 dB. This difference allows for some level of discrimination of the wetlands.

On the January scene, which corresponds to the wet snow conditions, a very different situation occurs. Because the penetration capability of microwaves in a wet snowpack is in the order of one wavelength, the open water bodies and the marshes appear very dark, since the dead vegetation in the marshes no longer contributes to the backscatter. Because marshes behave differently depending on snow wetness conditions, it appears that combining wet and dry snow scenes would allow discrimination of vegetated wetlands in an efficient manner. Below is a description of the steps suggested to achieve this goal.

Proposed methodology

In preparation for the analysis, the SAR scenes were spatially averaged using a 5x5 median filter. A median filter was chosen in order to minimize fading. Next the images were all registered to UTM coordinates. An accurate registration of the imagery is critical to the effectiveness of the proposed methodology.

The proposed methodology consists of the following steps:

1- Using the interactive display of an image analysis system, training areas around the open water bodies are created and statistics (mean DN and standard deviation S of the pixel intensities) are collected;

2- Pixels with a DN greater that DN + S are given a DN of 255, while the pixels with a DN less than DN + S are are given a DN of 0. On the resulting image, open water bodies imaged in the summer, and under dry snow conditions appear as black features on a white background. However, both open water bodies and marshes appear dark on the corresponding wet snow scene;

3- The resulting summer scene (and also the dry snow winter scene) is then subtracted from the corresponding wet snow winter scene. The difference image would show marshes as black features in a white background.

The proposed method is presently being tested for its accuracy in delineating wetlands. At the time of this paper, final results were not yet available.

CONCLUSIONS

Airborne SAR images collected in 1986-1987 and 1988-1989 near the Ottawa area were analyzed to determine the potential of radar data for monitoring snow water equivalent and wetland extent. Results of the analysis indicate an inverse relationship between SWE and backscatter. However, future work must carefully address the calibration issue in the analysis of multitemporal SAR data. The multitemporal approach also proved to be an effective way to identify wetlands due to the large, but systematic change in backscatter. More specifically, the analysis yielded the following findings:

* an inverse relationship between σ^o and SWE has been observed on the winter 1986-1987 C-band SAR data set. It appears that the snowpack is not completely transparent at C-band, as it was observed by Bernier and Fortin (1989);

- the observed inversed relationship between σ° and SWE is in apparent contradiction with findings by Bernier and Fortin (1989) an Ulaby and Stiles (1980), but is in accordance with the trend observed by Matzler and Schanda (1984);

- it was hypothesized that the SAR calibration procedure used in this study may have introduced an artifact in the SWE-σ° relationship. Using a different approach by which the SAR scenes are calibrated with reference targets in the lower and mid- to upper portion of the scene dynamic range, the DN values changed but the relationship between SWE and σ° was preserved. It was therefore assumed that the calibration procedure employed did not introduced a pseudo correlation between SWE and σ°;

- it was also hypothesized that the apparent contradictory behaviour of σ° vs SWE among various researchers was the result of different snowpack and soils conditions at the time the measurements were made. A simple scattering model developed by Ulaby *et al* (1982) was used to demonstrate that the backscattering contribution of the underlying soil could significantly affect the relationship. In particular, if the soil scattering contribution is large, the simplified model would predict an inverse relationship of σ° with SWE, whereas smooth soil surfaces would more likely produce a positive relationship. The grain size would probably have a less significant impact, however, layering in the snowpack is thought to significantly increase the backscatter values (multiple scattering in the snowpack);

- it is well known that wet snow is a highly absorbing medium. In this study, it was observed that wetlands (emerging vegetation in standing water) would appear as bright targets in summer and dry snow winter scenes. However, the same wetlands would produce a very dark return under wet snow conditions. This enabled the authors to develop a method by which vegetated wetlands could be easily discriminated.

ACKNOWLEDGEMENTS

The authors would like to express their appreciation to Tom Alföldi of the Canada Centre for Remote Sensing for constructive comments on a draft of this paper.

REFERENCES

Benton, A.R., A.J. Blanchard, R.W. Newton, 1983, "Determination of Mobility and Trafficability indicators with Multifrequency Imaging Radar". Proceedings of SPIE - The International Society for Optical Engineering, Vol. 414, pp 194-200.

Bernier, M., J.P. Fortin, 1989, "Suivi de la Couverture de Neige au Moyen d'un Radar a Ouverture Synthetique". IGARSS'89 12th Canadian Symposium on Remote Sensing, Vol. 3, pp 1251-1255.

Cihlar, J., T.J. Pultz, A.L. Gray, 1990, "Change Detection with Synthetic Aperture Radar". Paper submitted for publication at the International Journal of Remote Sensing.

Harris, J., S. Digby-Argus, 1986, "The Detection of Wetlands on Radar Imagery". Proceedings of the 10th Canadian Symposium on Remote Sensing, Vol. 1, pp 529-543.

Livingstone, C.E., A.L. Gray, R.K. Hawkins, J.C. Halbertsma, 1987, "CCRS C-band airborne Radar - System Description and Test Results". Proceedings of the 11th Canadian Symposium on Remote Sensing, pp 503-518.

Matzler, C., 1987, "Interaction of Microwaves with the Natural Snow Cover". Remote Sensing Reviews, Vol.2, pp 259-387.

Matzler, C., E. Schanda, 1984, "Snow Mapping with Active Microwave Sensors". International Journal of Remote Sensing, Vol. 5, No. 2, pp 409-422.

Rott, H., C. Matzler, D. Strobl, S. Bruzzi, K.G. Lenhart, 1988, " Study on SAR Land Applications for Snow and Glacier Monitoring". Final Report, ESA contract No. 6618/85/F/FL(SC), 185 pages.

Rott, H., C. Matzler, D. Strobl, 1986, "The Potential of SAR for Snow and Glacier Monitoring System". Proceedings of the SAR Applications Workshop held at Frascati, Italy, pp 25-35.

Rott, H., 1986, "Prospects of Microwave Remote Sensing for Snow Hydrology". IAHS Publication No. 160, pp 215-223.

Rott, H., G. Domik, C. Matzler, H. Miller, K.G. Lenhart, 1985, "Study on Use and Characteristics of SAR for Land Snow and Ice Applications". Final report, ESA contract No. 5441/83/D/IM(SC), 117 pages.

Schanda, E., 1987, "On the Contribution of Volume Scattering to the Microwave Backscattered Signal from Wet Snow and Wet Soil". International Journal of Remote Sensing, Vol. 8, No. 10, pp 1489-1500.

Stiles, W.H., and F.T. Ulaby, 1980, "microwave Remote Sensing of Snowpacks". NASA contractor report 3263, Contract NAS5-23777, 404 pages.

Ulaby, F.T., Stiles, W.H., 1980, "The Active and Passive Response to SNow Parameters. 2. Water Equivalent of Dry Snow". Journal of Geophysical Research, Vol. 85, No. C2, pp 1045-1049.

Ulaby, F.T., R.K. Moore, A.K. Fung, 1982, " Microwave Remote Sensing Active and Passive". Vol II, Chap 11, Addison-Wesley Publishing Company.

Ulaby, F.T., R.K. Moore, A.K. Fung, 1986, " Microwave Remote Sensing Active and Passive". Vol III, Chap 21, Addison-Wesley Publishing Company.

Waite, W.P., H.C. McDonald, V.H. Kaupp, J.S. Demarke, 1981, "Wetland Mapping with Imaging Radar", IGARSS'81, IEEE Digest Volume II, pp 794-799.

Wedler, E., R. Kessler, 1981, "Interpretation of Vegetative Cover in Wetlands using Four-Channel SAR Imagery". The American Society of Photogrammetry, 47th Annual Meeting, Washington, D.C., pp 111-124.

Table 1: SAR data sets

Date	Polarization	Incidence angle at north end of airport runway	Altitude in meters
21/10/86	HH	81	3000
11/12/86	HH	58	3600
12/01/87	HH	77	4900
25/02/87	HH	75	2800
08/05/87	HH	69	6100
14/09/88	HH	69	6100
30/01/89	HH	70	5800
10/02/89	HH	70	5800

Table 2: Hydrometeorological conditions at Ottawa International Airport

Date	Rain mm	Snow cm	Min T °C	Max T °C	Sunshine 2 hours	Snow on ground cm
20/10/86	0	0	3.4	15.3	7.6	0
21/10/86	5.8	0	6.6	12.9	0.2	0
09/12/86	0	13.6	-18.5	-7.8	0.0	13
10/12/86	TR	0.4	-10.6	-0.5	1.9	23
11/12/86	0	0.2	-8.4	-3.0	3.6	21
25/12/86	25.4	0.2	-2.3	1.2	0.0	14
11/01/87	0	1.2	-5.4	-2.9	0.0	25
12/01/87	0	0.4	-4.5	-1.0	0.0	26
24/02/87	0	0	-9.4	-2.6	9.1	40*
25/02/87	0	0	-12.4	-0.4	10.2	40*
07/05/87	0	0	6.0	15.3	13.7	0
08/05/87	0	0	1.8	18.5	12.1	0

TR: trace
* : estimated

Table 3: Hydrometeorological conditions at the Agriculture Canada Station

Date	Rain mm	Snow cm	Min T °C	Max T °C	Soil T at 10 cm °C	Snow on ground cm
20/10/86	3.0	0	2.0	14.7	9.9	0
21/10/86	0.0	0	5.1	13.4	10.0	0
09/12/86	0.6	8.4	-18.3	-7.1	-0.2	8
10/12/86	0	0.2	-12.1	-0.3	-0.2	13
11/12/86	0	TR	-8.8	-0.8	0.0	11
25/12/86	12.0	TR	-4.2	1.2	0.1	12
11/01/87	0	2.0	-4.6	-2.3	-0.2	17
12/01/87	0	TR	-4.8	-0.5	-0.1	18
24/02/87	0	0	-9.0	-2.2	-0.3	40*
25/02/87	0	0	-12.0	-0.4	-0.2	40*
07/05/87	0	0	5.0	14.8	9.9	0
08/05/87	0	0	1.6	18.1	8.7	0

TR: trace
* : estimated

Table 4: Hydrometeorological conditions at the Carp weather station

Date	Rain mm	Snow cm	Min T °C	Max T °C	Solar radiation cal/cm2	Snow on ground cm
13/09/88	0	0	6.1	14.7	400	0
14/09/88	8.2	0	3.3	14.8	245	0
29/01/89	0	0	-6.9	2.8	227	14
30/01/89	0	0	-1.2	2.2	---	12
01/02/89	0	0	-22.2	-9.4	267	12
10/02/89	0	0	-14.9	-4.9	256	12

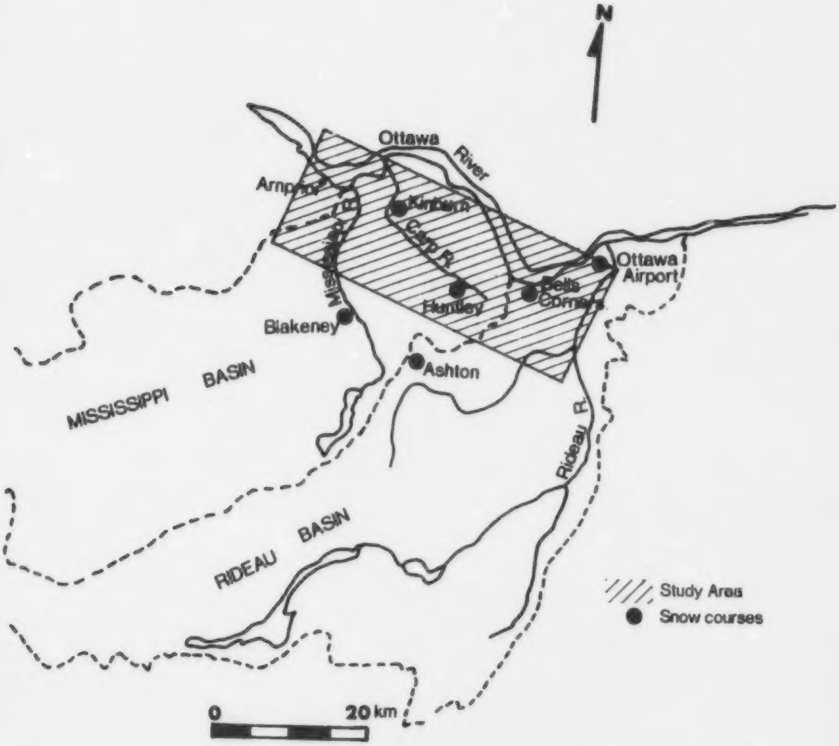
N
Ottawa River
Arnprior
Kinburn
Carp R.
Mississippi R.
Ottawa Airport
Bells Corners
Huntley
Blakeney
Ashton
MISSISSIPPI BASIN
RIDEAU BASIN
Rideau R.
Study Area
Snow courses
0
20 km

Figure 1: Study site

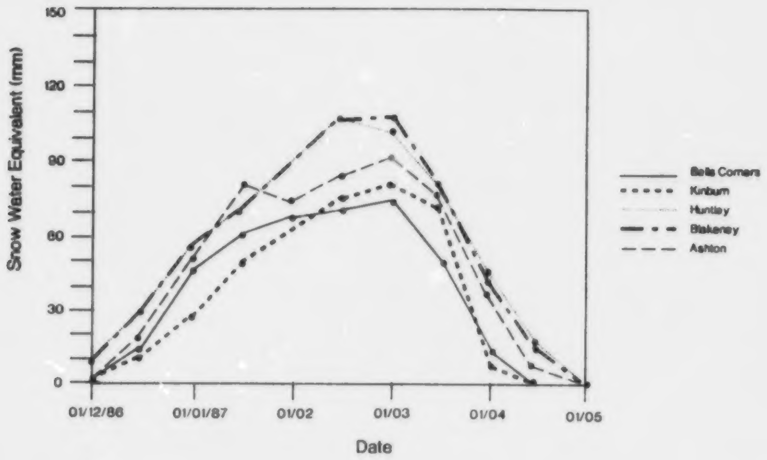

Figure 2: Mean snow water equivalent at or near study area

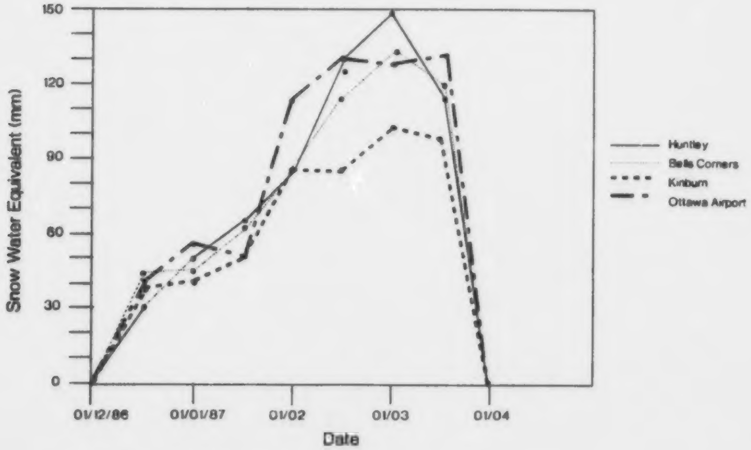

Figure 3: Snow water equivalent during winter 1986-1987

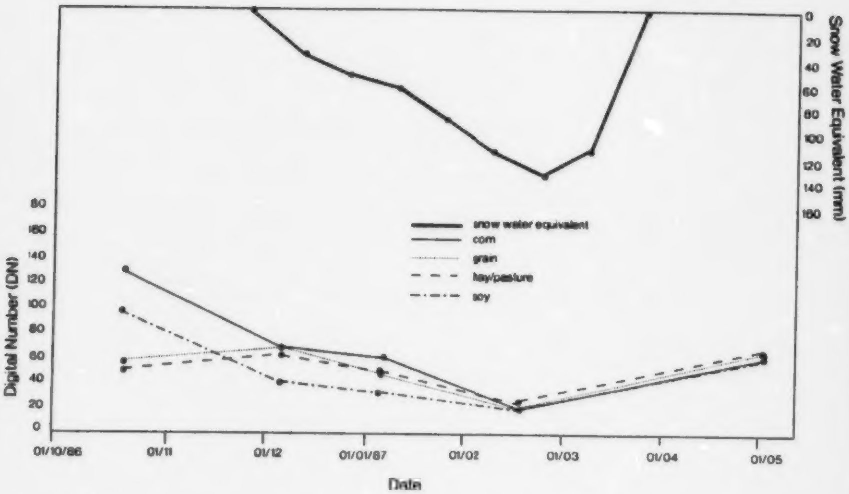

Figure 4: Relative calibrated C-SAR backscatter coefficients with airport runway as calibration target

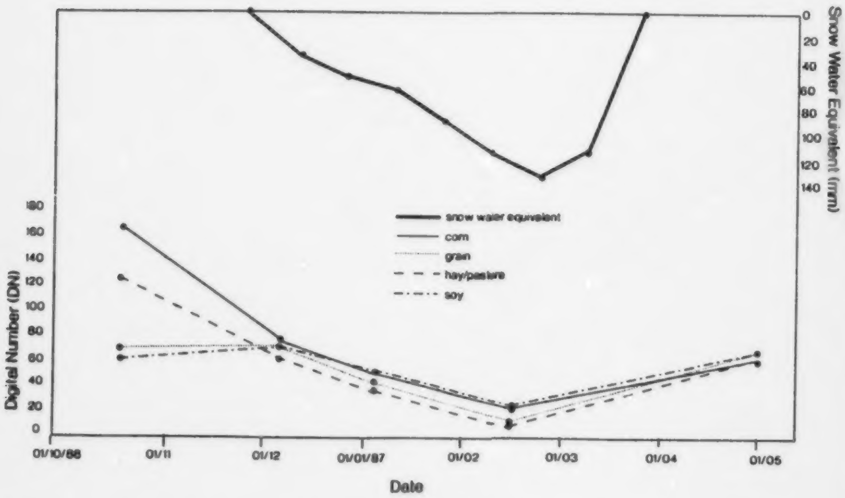

Figure 5: Relative calibrated C-SAR backscatter coefficients with airport runway and coniferous trees as calibration targets

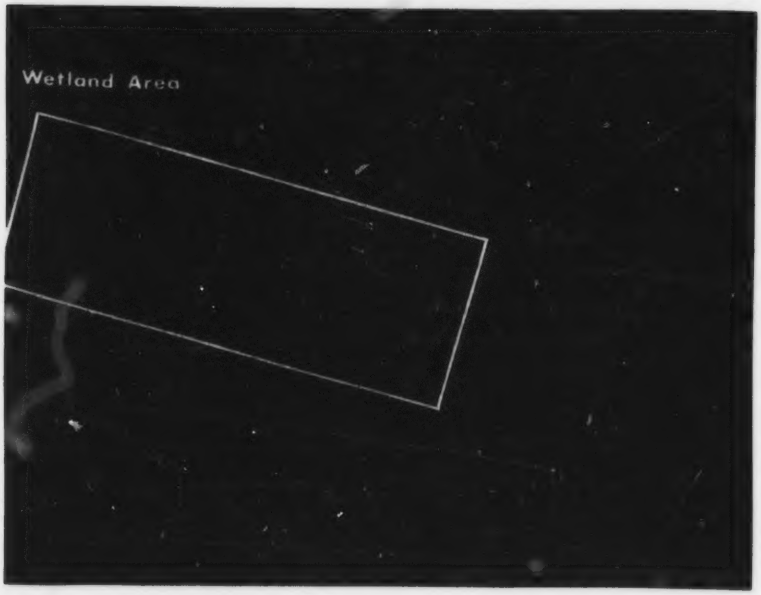
Wetland Area

Figure 6: C-HH SAR collected over Ottawa Test line August 5, 1987

Figure 7: C-HH SAR collected over Ottawa
Test line January 30, 1989 under wet snow conditions

Figure 8: C-HH SAR collected over Ottawa
Test line February 10, 1989 under dry snow conditions

Questions and Answers

Al Rango: Why wouldn't the X-band be more sensitive to the snow and why weren't you using it?

Robert Leconte: Probably, the X-band would be more sensitive to the snow. We had some X-band data, but not on all the scenes. Those data were collected [only] as part of testing of the S.A.R. system. They would fly a run and we would collect some C-band data, and sometimes we collect C- and X-band. So for that reason we did not analyse the X-band data.

John Stewart: In the images for during the winter, the very bright areas... what were they? Were those the trees that you were talking about that you used for secondary calibration?

Robert Leconte: That's correct.

John Stewart: If you did a comparison between, say, the value for the runway and for the trees in both winter and summer would you get a similar relationship?

Robert Leconte: Yes, the runway is more or less the same value over the course of the winter, but if the value changes over the course of the winter, then we adjust the images accordingly.

John Stewart: How well do the two methods agree?

Robert Leconte: Well, as I have shown on the graphs, using the trees and the runway, or the runway alone, didn't have great impact on the results we've obtained.

John Stewart: But the actual digital values changed, is that correct?

Robert Leconte: Yes, they changed. But the trend remained the same.

John Stewart: What about ... corner reflectors that were used on some overpasses?

Robert LeConte: On this batch, for example, the corner reflectors are north of this area, so we could not use them.

John Stewart: So are you reasonably happy that you have a stable calibration?

Robert Leconte: Yes. Of course, it is shaky ground. I cannot at this present time say this is the relationship, but at least we can see a trend.

INTERPRETATION OF PASSIVE AND ACTIVE MICROWAVE IMAGERY OVER SNOW-COVERED LAKES AND RIVERS NEAR FAIRBANKS ALASKA

Rae A. Melloh and Lawrence W. Gatto
U.S. Army Cold Regions Research and Engineering Laboratory
Hanover, New Hampshire 03755

ABSTRACT

Passive and active microwave imagery provide information about freshwater ice and snow environments needed for a better understanding of river and lake ice processes, winter stream habitats, winter water supply and ice management. The ability to image at night and through clouds is an advantage of microwave systems over shorter wavelength visible and infrared systems. Additionally microwave imagers have a different sensitivity to ice and snow conditions and thus provide added capability to observe features that could not be detected with visible and infrared instruments. To exploit the imagery data fully, a better understanding of microwave signatures created by freshwater ice conditions is needed.

An on-going CRREL investigation interprets snow and ice conditions on lakes and rivers near Fairbanks, Alaska, using both passive and active microwave imagery taken in March, 1988 during both wet and dry snow conditions. The imagery includes that obtained with the Jet Propulsion Laboratory's Synthetic Aperture Radar (SAR) in quad-polarized (HH,VV,HV and VH) C-, L- and P-bands, and that obtained with NORDA's Ka-band Radiometric Mapping System. Ground truth data taken during overflights includes aerial video, observations of snow depth and stratigraphy, ice core descriptions and thickness measurements and impulse radar traces. Our field data and available experimental studies of microwave interactions with snow and ice are used to interpret imagery patterns. Results to date confirm that the microwave imagery distinguishes snow and ice conditions including open leads, wet overflows, ice jams, and main channels on the Tanana River, and fracture patterns and changing snow conditions on nearby lakes. The specific geophysical characteristics and conditions of river and lake ice that produced the imagery patterns are being investigated.

INTRODUCTION

Passive and active microwave sensors provide a tool for monitoring and studying river and lake ice processes. The large area coverage afforded by airborne and spaceborne sensors provides a means of extrapolating known site conditions over long river reaches or lake surfaces. Microwave interaction with both surface, and in some cases subsurface, roughness and dielectric properties, allows observation of conditions that would not be detected with shorter wavelength, visible and infrared systems. Active radar systems, for example, have been used to distinguish areas of freshwater lakes that were frozen completely to the bed from those that were not based on the strength of radar backscatter (Weeks et al. 1978). Investigations using passive systems over freshwater lake ice have shown that shorter wavelength (.81 cm) radiometers are better suited for gathering information about the upper layers of ice and snow on the surface, while longer wavelengths (6 cm) probably sense the entire ice thickness (Hall et al. 1981).

A better understanding of active and passive microwave signatures created by freshwater ice conditions is needed in order to utilize current and future data sources fully. Current airborne passive microwave systems can provide adequate spatial resolution needed in river and small lake environments; however, this type of data is not widely available and its applications to freshwater ice studies have not been fully explored. Recently developed synthetic aperture radar (SAR) systems such as the one currently being tested by NASA and the Jet Propulsion Laboratory (JPL) (Held 1988) provide an opportunity to compare river and lake ice signatures on coincident images of three frequencies (C-, L- and P-band) and four polarizations (HH, HV, VH, and VV). This airborne system, called the NASA/JPL AIRSAR is representative of a new generation of radar imaging systems that will be deployed on space platforms during the next decade. Proposed launches of SAR systems including the European Space Agency's ERS-1, Canada's Radarsat, Japan's ERS-1 and the United States' Shuttle Imaging Radar, will make SAR imagery more widely available to user communities. The objective of our preliminary evaluation of SAR imagery in natural freshwater ice environments, is to provide an initial assessment of potential uses of the data in studies of river and lake ice, and to raise important questions to be addressed by later field and laboratory studies.

BACKGROUND AND APPROACH

During March 1988, an opportunity arose to acquire images from both passive and active systems over the Tanana River Valley in and near Fairbanks, Alaska. The two airborne systems flown were the NASA/JPL AIRSAR aboard a NASA DC-8 and the Naval Ocean Research and Development Activity (NORDA) Ka-band Radiometric Mapping System (KRMS) aboard a Navy RP-3. Image data were acquired over CRREL field sites on an opportunity basis while the aircraft were on their way to and from their primary mission sites over the Beaufort Sea, off the north coast of Alaska, and the Bonanza Creek Experimental Forest near Fairbanks.

Two CRREL field teams obtained aerial and ground truth data during a three week period coincident with the overflights for use in interpreting image patterns (Figure 1). A primary field team collected data at a number of sites along a 22 mile reach of the Tanana River, the lower 10 miles of the Chena River, small lakes adjacent to the Tanana near Fairbanks and Harding Lake (Figure 2). Aerial observations, photographs and videotapes were taken to document regional conditions. Field observations and measurements were made to determine site-specific conditions (Tables 1 and 2). In addition, impulse radar traces (e.g., Arcone et al. 1987) recorded from a helicopter were acquired to define horizontal changes in ice thickness and to detect channels of water under the ice. A second field team collected detailed information on frazil ice deposition and erosion on the Tanana River at the Chena River confluence in connection with another ongoing research project on sub-ice processes in braided subarctic rivers (e.g., Lawson et al. 1986).

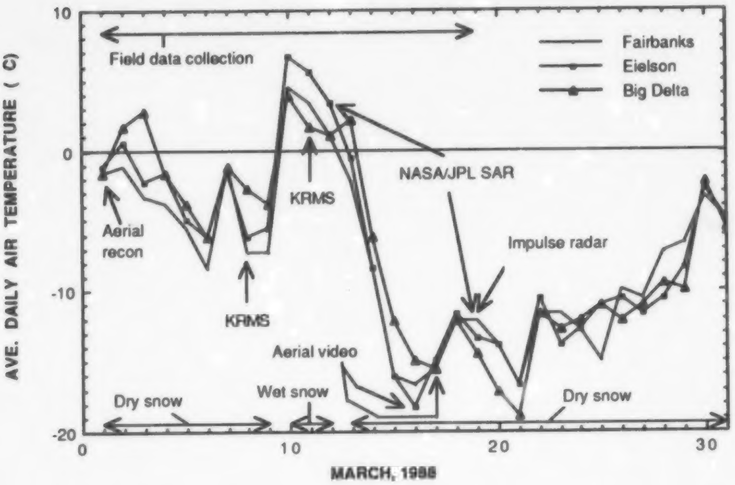

Figure 1. Air temperatures and observed snow wetness during aerial and ground data collection.

The purpose of this paper is to present results obtained to date which demonstrate the ability to distinguish certain freshwater ice conditions on passive and active microwave images. Topics of discussion include open leads, wet overflows, ice jams, main channels, fracture patterns and the effects of changing snow cover wetness on image patterns.

PHYSICAL SETTING

The study area lies within the discontinuous permafrost zone of the interior of Alaska, about 160 km south of the Arctic Circle. The climate is continental with long, cold winters and short, warm summers. The average annual temperature in Fairbanks is -3°C and precipitation averages 25.4 to 55.9 cm water equivalent including 76 to 152 cm of snow per year (Selkregg 1974).

The Tanana River changes from a braided river with unstable bars, multiple channels and a predominantly gravel bed upstream of Fairbanks to an anastomosing river with several main channels separated by stable vegetated islands and a sand bed downstream of Fairbanks (Neill et al. 1984). Width of the active floodplain ranges from 610 to 2130 meters. Eighty-five percent of the Tanana discharge comes from glacial tributaries out of the Alaska Range to the south, and 15% comes from non-glacial streams from the Yukon-Tanana Uplands to the north (Neill et al. 1984). Mean monthly discharge in March 1988, was 161 cms (5697 cfs), mean daily discharge was 164 cms (5600 cfs)

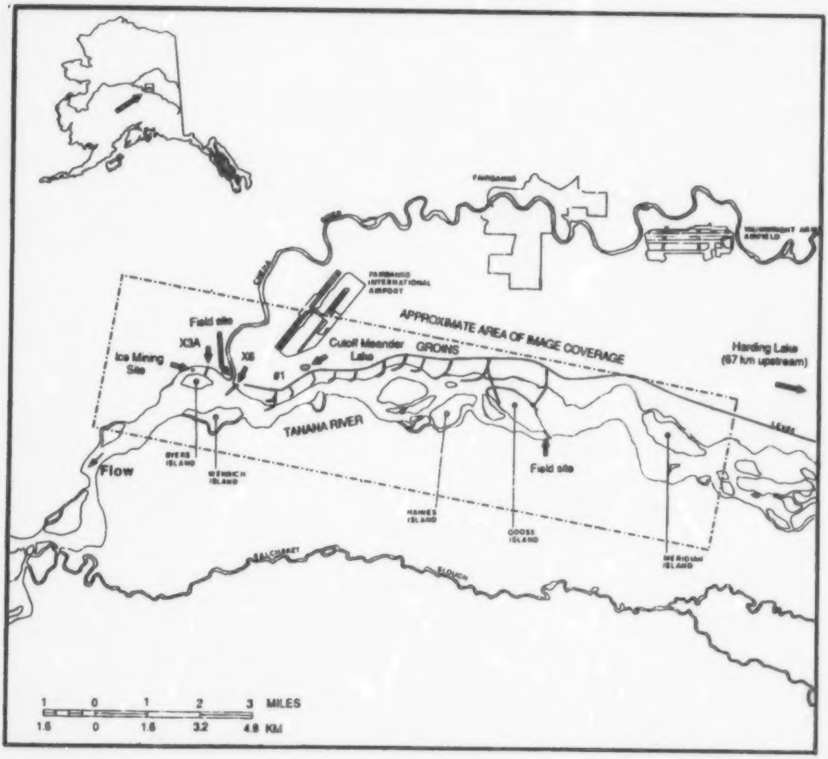
FAIRBANKS
CHENA
FAIRBANKS INTERNATIONAL AIRPORT
APPROXIMATE AREA OF IMAGE COVERAGE
Field site
X3A
X6
Ice Mining Site
Cutoff Meander Lake
GROINS
#1
Harding Lake (67 km upstream)
TANANA RIVER
LEVEE
BYERS ISLAND
WENRICH ISLAND
Flow
HAINES ISLAND
Field site
GOOSE ISLAND
MERIDIAN ISLAND
SALCHAKET
SLOUGH
1 0 1 2 3 MILES
1.6 0 1.6 3.2 4.8 KM

Figure 2. Location map (Moose Creek Dam, Eielson Air Force Base and Big Delta are upstream 27, 34 and 125 km, respectively).

from 1 to 15 March and 159 cms (5600 cfs) from 16 to 31 March (USGS data). These are the lowest discharges during the 1988 water year. A 20-mile-long (32 km), flood-control levee and a series of protective groins exists along the north bank of the Tanana River from the Moose Creek Dam floodway to the Chena River.

Harding Lake is roughly circular in shape and is underlain by the Tanana Gravel formation on the north and the Birch Creek Schist formation on the south. The surface of Harding Lake is about 10 km^3 in area and at an elevation of 220 km above sea level. The maximum depth of the lake is around 43 meters, and average depth is 16 meters (Nakao 1980).

Table 1. Field observations and measurements

	Tanana River						
	Cross Section X3A	Cross Section X6	Groin # 1	Goose Island	Cutoff Meander Lake	Chena River	Harding Lake
Snow Conditions							
Stratigraphy (1)	X	X	X	X		X	X
Depths (1,2)	X	X	X	X		X	X
Density (1)	X	X	X	X		X	X
Temperature (1)	X	X	X	X		X	X
Surface Topography (2)	X	X	X	X			X
Ice Conditions							
Surface Topography (2)	X	X	X	X			X
Thickness (2,3)	X		X	X	X	X	X
Stratigraphy (3)	X		X	X	X	X	X
Sub-ice Conditions							
Frazil Deposits (2,4)	X		X	X		X	
Water Depth (2,5)	X		X	X	X	X	X
Water Current (2,5)	X		X	X			
Bottom Sediment (2)	X		X	X			

Methods:
(1) Snow pits
(2) Graduated metal rod
(3) Ice Cores
(4) EM 31
(5) Weighted line

SENSOR CHARACTERISTICS

The ability to distinguish freshwater ice and snow conditions on microwave imagery depends on the characteristics of the sensor system and the physical properties of the materials. Passive systems measure naturally emitted radiation in terms of brightness temperature (T_B), which is the product of the physical temperature (T_0) of an object and its emissivity (E) at the wavelength being sensed, ($T_B = ET_0$). The ability to distinguish freshwater ice conditions in an environment where physical temperatures vary little, depends largely on differences in emissivity. For example, smooth, open water surfaces have a very low emissivity, resulting in the coldest brightness temperatures in a scene while wet snow is highly emissive, resulting in a much warmer signature. Active radar systems do not rely on naturally emitted radiation, but transmit energy of a given frequency and then record the magnitude of backscatter. Where surfaces are rough, relative to the wavelength, strong backscatter results. In contrast, low backscatter occurs where transmitted energy reflects specularly off of smooth air-water, air-ice and ice-water interfaces. The images constructed from brightness temperature or backscatter measurements display patterns and tonal variations that may be correlated with known site conditions.

The Ka-band Radiometric Mapping System (KRMS) is an airborne passive microwave imager that operates at a center frequency of 33.6 GHz. KRMS image

Table 2 Date and number of observations and measurements

					Graduated Metal Rod														Weighted Line					
	Snow Pits		Ice Cores		Snow Depths		Surface Topography		Ice Thickness		Frazil Deposits		Water Depth		Water Current		Bottom Sediment		Water Depth		Water Current		EM31	
	Day	No.	Day	No.	Day	Rdgs.	Day	Lines	Day	Rdgs.	Day	Obs.	Day	Rdgs.	Day	Obs.	Day	Obs.	Day	Rdgs.	Day	Obs.	Day	Lines
X3A	6	1	10	19	6	1	6	1			10	19											5 6 11 18 19	1 1 1 1 1
X6	6 11	1 1		0			6	6															5 6 11 18 19	1 1 1 1 1
Groin #1	8 11 12 17	1 1 2 1	8	16	8	9	8 12	1 1			8	16	8	15	8	16	8	2					9	3
Goose Island	2 3	2 1	2	11			3	3			2	9	2	9	2	8	2	9						
Cutoff Meander Lake		0	10	7							10	6					10	7	10	6	10	7		
Chena River	11	3	11	5	11	6					11	5	11	2	11	5			11	3			11	1
Harding Lake	3	1	3	7	3 10	42 1	3	1	3	1	3	6	3	3	3	2	3	2	3	3	3	4		
Totals		15		65		59		13		1		61		29		31		20		12		11		14

data has been extensively used in polar ice research to distinguish ocean surface types such as open water, first year ice and multi-year ice (Eppler et al. 1984, 1986). The imagery and analyses presented here represent the first use of the KRMS for analysis of freshwater ice conditions. KRMS technical characteristics are provided in Table 3. The sensor was flown at an altitude of 1524 m, resulting in an image width of 3.6 km. The angle of incidence along a scanline varies from 50° at the outer edges of the image to 0° at nadir, along the center-line of the image. A gradual increase in measured brightness temperature toward the edges of an image may occur due to the change in incidence angle along the scanline. Image tonal variations are thus best interpreted along vertical columns from the top to the bottom of an image. Overlap between successive scanlines (nominally 80% at nadir) and the sampling interval along a scanline are such that radiances are spatially averaged. The antennae beam width of 1° subtends a circular beamspot on the ground at nadir that is approximately 26.7 m in diameter for a 1524 m flight altitude. Both size and ellipticity of the beamspot increase with increasing off-nadir angle thus detail toward the edges of an image may appear blurred.

Table 3. KRMS technical characteristics

ANTENNAS	
number	3
diameter	24 inches
polarization	vertical
beam width	1.0°
isolation	40 dB (minimum)
SCANNER	
maximum scan rate	25 scans/second (40 ms/scan)
minimum scan rate	7.5 scans/second (133 ms/scan)
scan angle	60° from nadir
midscan incidence angle	0° (nadir)
scan width	3.46 x altitude
antenna position accuracy	2.5 minutes of arc
STABILIZATION	
method	cross-track roll gyro
accuracy	less than 0.25°
RF AMPLIFIER	
type	Superheterodyne (DSB)
noise	less than 5.0 dB
bandwidth	1.3 GHz
gain	greater than 60 dB
loss	1.2 dB (maximum)
RADIOMETER	
type	pulse stabilized, total power
pulse width	4.0 MS
local oscillator frequency	33.6 GHZ
IF bandwidth	greater than 500 MHz
video bandwidth	1.7 kHz (maximum)
video gain	72 dB (nominal)
minimum detectable signal	0.05 K/second
sensitivity	50 mV/K (nominal)
dynamic range	370 K

(from Eppler et al. 1984)

The NASA/JPL AIRSAR technical characteristics are described by Held et al. (1988). The AIRSAR replaces a previous single band (L-band) system built and operated by JPL, that was destroyed in a fire at takeoff in 1985. The March 1988 flights in Alaska were among the first science campaigns conducted with the new system. The system is capable of collecting three frequencies and four polarizations simultaneously, yielding 12 co-registered radar images. Flight dates and parameters for data used in this analysis are listed in Table 4. The images were processed by JPL to a standard compressed four-look format. The compression algorithm spatially averages four adjacent pixels to reduce speckle variance (Held et al. 1988, Dubois 1987). Data were collected over a swath width of roughly 8 km, and incidence angle across the swath varying between 22.5 to 52.5 degrees. Pixel resolutions are 12.1 meters in the azimuth direction and 6.662 meters in the slant range direction.

Table 4

NASA/JPL AIRSAR DATA SETS

Flight Dates	March 12	March 19	March 19
Heading	54°	234°	54°
Bands	P,L,C	L,C	L,C
Local Time	14:05	22:02	22:18
Altitude	8900 m	8540 m	8730 m

SAR PARAMETERS

Band	C	L	P
Center Frequency (MHz)	5299	1249	439
Bandwidth (MHz)	11	11	11
Wavelength (cm)	5.7	24	68.4

MARCH 1988 CONDITIONS

Average daily air temperatures were below 0° C for all but six days from 1 to 22 March when measurements and images were being acquired (Figure 1). The snow was wet during the afternoons on those six days and noticeably drier in the mornings and throughout the colder days. Temperatures in undisturbed snow ranged from 0.5°C to -14.5°C and in compacted snow from -1.0°C to -4.0°C. We measured snow depths on the river and lake ice surfaces ranging from 0 to 83.8 cm in windblown snow dunes and 20 to 30 cm in undisturbed snow.

The ice cover on the Tanana River consisted of ice jams separated by reaches of relatively smooth ice. The ice thickness we measured in jammed ice ranged from a maximum of 111.8 cm to a minimum of 63.5 cm. In unjammed river ice the maximum thickness we measured was 109.2 cm, the minimum 35.6 cm. Ice thickness measurements of up to 132.1 cm were measured on a "man-made" ice bridge at the Goose Island site, built-up by repeated floodings of the ice surface.

The maximum lake ice thickness measured was 83.3 cm on Harding Lake; the minimum was 13.5 cm at the cutoff meander lake.

PRELIMINARY RESULTS

Image interpretations are organized by those observed on rivers and those observed on lakes and by passive versus active systems. The passive microwave system, operating at 33.6 GHz (.89 cm) was sensitive to characteristics of the snow cover. KRMS image interpretations are thus primarily related to the presence or absence of snow, variation in snow properties, and occurrence of open water. The active radar systems at longer wavelengths 5.7 cm, 24 cm, and 68.4 cm were less affected by snow conditions and more affected by large-scale surface roughness. The AIRSAR interpretations thus are related to smooth versus rough surfaces.

Ka-band Radiometric Mapping System

River Patterns

Ice jams: Freeze-up ice jams on the Tanana River are not readily distinguished from level ice on the KRMS images (Figure 3). The jam areas appear white in tone which corresponds to cool brightness temperatures. The active radar system provided a much superior ability to distinguish ice jams, as discussed below.

Hard-packed snow: Radiometrically warmer (dark) lines, faint across the ice jams, and more pronounced along the river (Figure 3) are snowmobile, dogsled and our SUSV (Small Unit Support Vehicle) trails. Detection of the trails may be explained by compaction of the depth hoar into a hard-packed fine grained snow. Snow pit observations on a roughly 4 meter wide trail, showed 7 cm of very hard, dense snow (.46 g/cm^3) over 6 cm of a less dense snow (.33 g/cm^3).

Open leads: The low emissivity of the smooth water surface compared to the snow or ice surfaces makes open water readily detectable on KRMS imagery. Radiometrically cold (light tone) open water is seen on the Chena River in Fairbanks, and in open leads on the Tanana River. Observations from bridges at Cushman Street and Old Steese Highway showed the radiometrically warm (dark tone) reach on the Chena River (Figure 4) to be well traveled hardpacked snow over ice. The radiometrically cold (light tone) reach at Grant Street, Peger Road and University Avenue was open water bordered by snow-covered ice. The open lead on the Tanana River (Figure 5) is in the vicinity of Delta and Clear Creeks southeast of Harding Lake. The open water signature is so distinct on KRMS images that automated classification routines using simple level slicing algorithms could be used to map it.

Wet Overflows: The low emissivity of the water surface would also result in radiometrically cold signatures for relatively thin puddles of water on the ice. The second flight of the KRMS on March 11, followed two days of unseasonably warm weather with daily mean temperatures above freezing. Air temperature at the time of the March 11 flight was around 6.7° C. Two features that appear on the March 11 image, but are absent on the March 8 image (Figures 6 and 7) may be related to overflow of tributary streams or upflow through cracks due to a rise in river stage. Brightness temperatures of these features approach those of open water, suggesting either open water

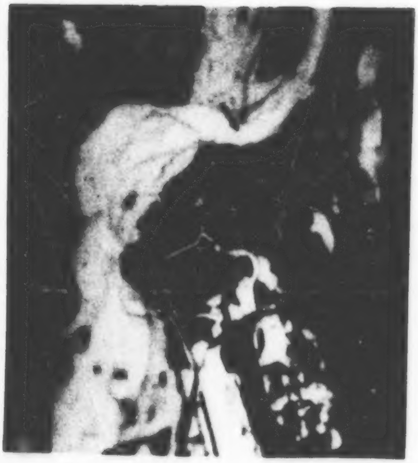

Figure 3. KRMS image of ice jam at the Tanana and Chena rivers confluence.

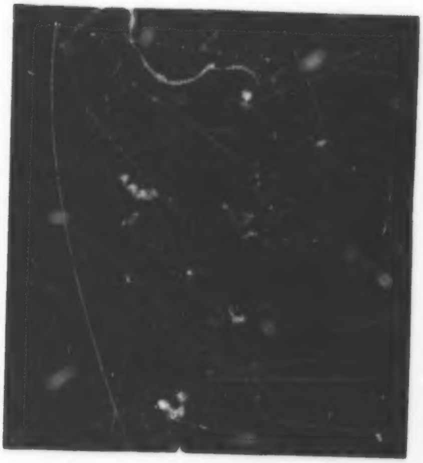

Figure 4. Open water (1) and hardpacked snow over ice (2) on the Chena R. in Fairbanks.

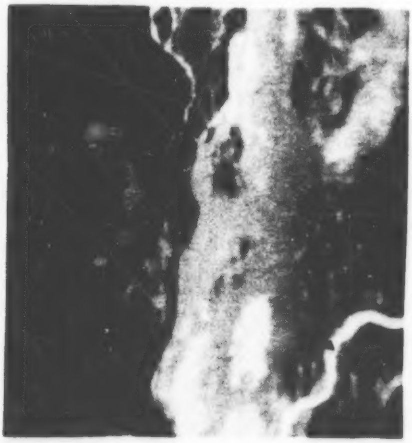

Figure 5. Open lead on the Tanana River southeast of Harding Lake near Delta Creek.

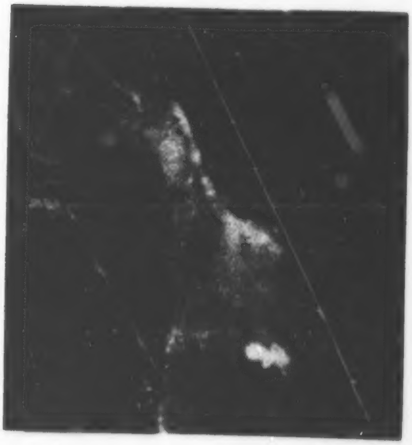

Figure 6. Potential overflow on the Tanana River southeast of Harding Lake, near Little Delta River.

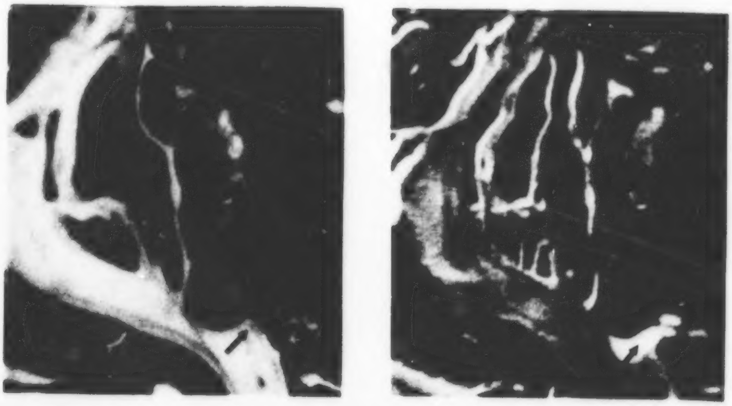

Figure 7. Site of potential overflow on the Tanana River west of Fairbanks on March 8 (left) and March 11 (right).

with floating ice or overflows with some contribution from wet snow and ice. Unfortunately, we have no ground verification or video coverage of these features.

Lake Patterns

Snow wetness : A comparison of images of Harding Lake acquired on March 8 and 11 show an overall increase of brightness temperature and decrease in image detail between the two dates (Figure 8). Snow wetness was low or absent on March 8 and very high on March 11 in response to air temperatures at the time of overflight of 0° C and 6.7° C, respectively. Increased emission due to moisture in the snow results in increased brightness temperature and thus a darker, more uniform image tone on the second flight date.

Wet snow has the effect of masking underlying features. As snow wetness increases, absorption becomes the dominant loss mechanism in snow and a rapid decrease in penetration depth occurs (Hallikainen, M.T. 1984). The wet snow layer itself is highly emissive, resulting in the observed increased brightness temperature.

Snow depth, distribution and grain size: The cold band along the north shore of the March 8 image of Harding Lake (Figure 8) corresponds to the most continuous and deepest snow cover on the lake surface. This cold band also overlies a shallow shelf where ice had frozen to the bed; however, the cold brightness temperature, in our opinion, is a result of the snow cover. Visual comparison of ice cores showed no apparent difference in ice stratigraphy over the shelf compared to the open lake.

The medium to light tones across the lake surface (excluding the dark linear features) are the result of the combined radiance from snow dunes and intervening pockets of bare ice. The snow dunes were composed primarily of coarse-grained depth hoar capped by fine-grained, wind-blown snow. Substantial scattering in the coarse-grained depth hoar on the surface of

Figure 8. Harding Lake KRMS images of March 8 (left) and March 11 (right); wet snow (1), deep continuous snow (2) and snow ice over fractures (3).

Harding Lake decreases brightness temperatures over snow-covered ice relative to snow-free ice. The result is colder brightness temperatures in areas with more continuous and deeper snow cover.

Volume scattering caused by dielectric discontinuities between air and ice crystals is the dominant loss mechanism in dry snow (Hallikainen, 1984). Scattering increases as the number of scatterers increases. Thus, keeping all else the same, a deep snowpack scatters more energy than a thin snowpack, resulting in colder brightness temperatures for the deep snowpack.

Scattering increases as grain size increases relative to the wavelength. The effect of grain size on brightness temperature of wind drifted and depth hoar-type snowpacks measured by Shiue et al. (1978) at 35 GHz over soil, show large temperature differences between the two types with the fine-grained snow being much warmer than the coarse-grained snow.

Fractures: The number and arrangement of the dark (radiometrically warm) linear features on the March 8 image of Harding Lake (Figure 8) suggest that they originated over fractures in the ice cover through which water seeped and wetted the overlying snow. Ground observations and aerial videos were used to identify these features as snow ice superimposed on lake ice. A linear snow ice feature observed in the field was roughly 60 meters wide, and lacked snow cover. The linear snow ice features are warmer in brightness temperature, presumably because the melted, refrozen snow scatters less energy than the depth hoar of the surrounding snow-covered ice.

NASA/JPL AIRSAR

River Patterns

Ice jams : The most obvious patterns on the Tanana River SAR images (Figure 9) are the light reaches interspersed with reaches of intermediate and dark tones. The light patterns generally correspond to river ice jams. The ice topography in jams is very irregular due to individual ice blocks of highly variable sizes and angles of tilt (Figure 10). We measured ice surface

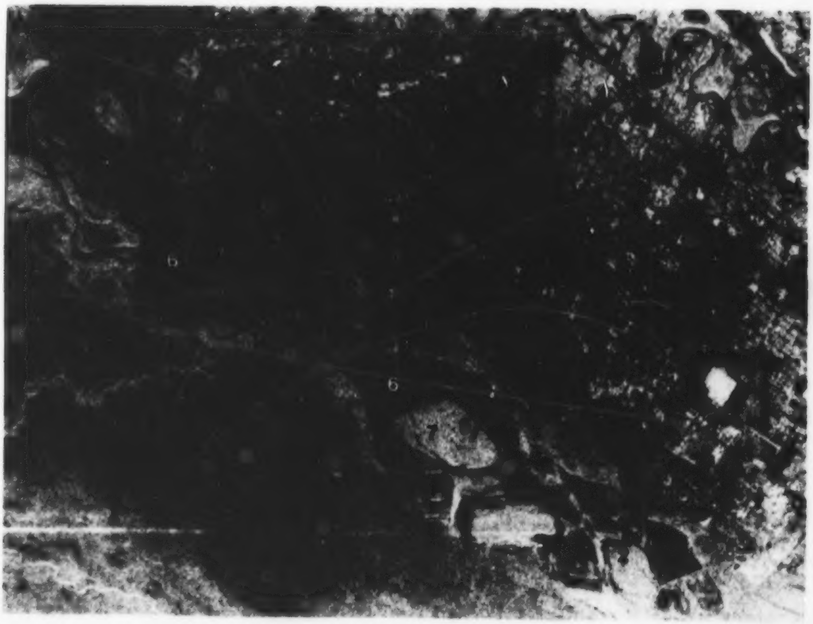

Figure 9a. NASA/JPL AIRSAR image, March 12, 1988; ice jams (1), less-rough ice (2), level ice (3), brash ice and ice chunks (4), open water (5), river bed and bars (6), vegetated islands (7) and lake ice (8).

relief between ice blocks up to 63 cm in some of the jams (Figure 10). The snow surface topography in the jams typically reflects the ice surface below.

Within the jams shown on the images, the lightest portion is the downstream end which corresponds to the area with the largest surface relief and thus highest radar backscatter. The jam tone darkens upstream because the surface roughness and relief within the jams typically decrease upstream resulting in less radar backscatter.

The longitudinal, linear, light pattern within the jams (Figure 9) probably delineates the main flow channel below the ice cover. The ice surface here may be rougher than along the channel margins because more ice would have moved down the middle of this channel than along its edges resulting in more ice being jammed and piled up within it than along its margins. Ground electrical conductivity measurements we made with the EM31 magnetic induction instrument (Arcone et al. 1987) across the river channel at the Groin #1 and X6 sites suggest that the main channel is in the location of the light patterns.

Ice cores taken from the rubble fields of the ice jams at the Groin #1 and the Goose Island sites were more variable than those from unjammed ice.

Figure 9b. NASA/JPL AIRSAR image, March 19, 1988; ice jams (1), less-rough ice (2), level ice (3), brash ice and ice chunks (4), open water (5), river bed and bars (6), vegetated islands (7) and lake ice (8).

Frazil ice predominated in the Groin #1 cores with less black ice and snow ice being the least. Black, bubbly and frazil ice occurred in approximately equal proportions, with some snow ice in the Goose Island cores. The interfaces between and within these ice types may act as volume scatterers and contribute to the increased radar backscatter from the ice jam sites, but the rough ice surface in the jams is the predominant scattering surface.

Less-rough ice: Snow-covered river channels with ice that appears level and unjammed on aerial photos and videotapes have image tones intermediate between the light ice jams and dark snow-covered river bars. The ice surface in these channels is not as rough as in jams but is sufficiently irregular to produce more radar backscatter than very level, smooth ice. These channels are often bordered by low scarps cut into river bars which help to define the channel limits on the SAR images. Open water bordered by slush ice zones and overflows also occur within these channels (Figure 11).

Level ice : Dark image patterns within the rivers (Figure 9) are formed by unjammed ice with a level surface such as at the X3 and Groin#1 sites on the Tanana and the Chena River site. The ice across the channel at X3 (35.6-109.2 cm thick) was predominantly black ice and bubbly ice on the south side.

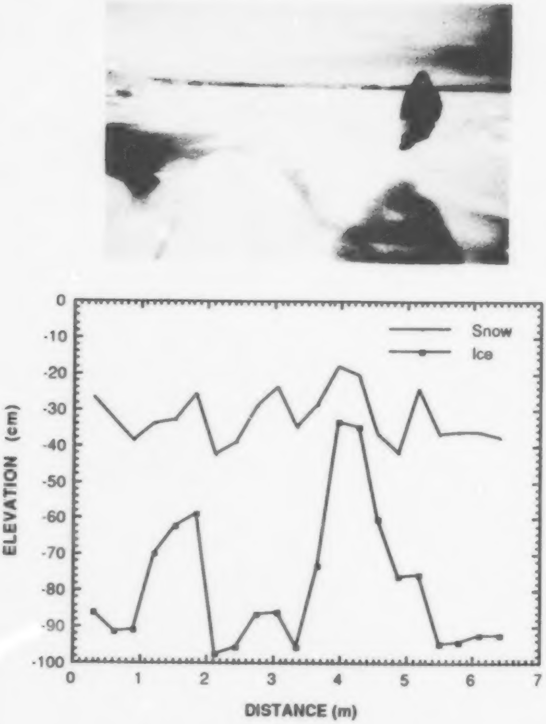

Figure 10. (Above) Ice jam at the Groin #1 site looking upstream, March 8, 1988; (Below) Typical snow and ice surface topography in the ice jam at Groin #1.

The level ice (50.8-76.2 cm thick) at the downstream end of the Groin #1 site was primarily black ice over frazil ice with surface snow ice present on a few cores. The ice at the Chena River site (46-94 cm thick) was predominantly clear, black ice below snow ice which contained bubbles and sediment layers. The generally flat, clear ice caused virtually no radar backscatter and thus appears black on the SAR images.

Open water : The darkest image patterns within the rivers (Figure 9) are formed by open water areas. The open areas were observed throughout the river during the aerial reconnaissance. The flat, smooth open water surface causes virtually no radar backscatter and thus appears black on the SAR images.

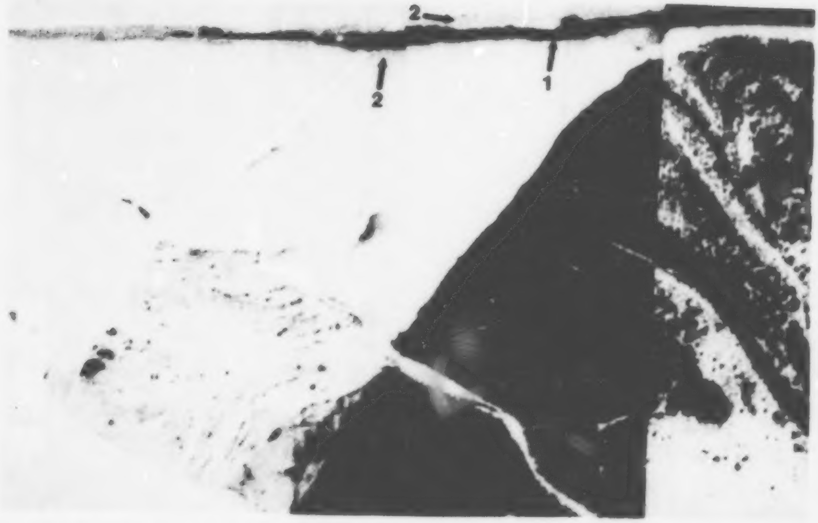

Figure 11. Open water (1) with bordering brash ice and ice chunks (2), March 17, 1988 (photographs made from an aerial videotape).

Snow : Although the snow was substantially wetter on 12 March than on 19 March, differences in the snow patterns on the images are subtle. Channel patterns and drainage ways in undeveloped, tree-covered areas of the Tanana River floodplain are more distinct in images acquired when the snow was wet. The contrast between the vegetated islands and the unvegetated bars of the Tanana River is greater when the snow was wet.

Some of the bright reaches of the river may be due to the presence of snow dunes that were observed at many locations along the Tanana River. The snow surface topography amongst the dunes was highly variable. A wind-blown crust of variable thickness also was present on the snow surface at some of the field sites. The irregularity of the snow surface could contribute to radar backscatter, especially where the snow had a hard crust.

Snow surface conditions on the river varied from loose granular snow to a hard crust with firm wind-blown and melt crusts at some sites. Snow densities varied from .15 to .44 g/cm^3 in undisturbed snow and from .33 to .46 g/cm^3 in compacted snow. Depth hoar was found below the surface snow at all sites and constituted 16 to 100 % of the snowpack where the snow was undisturbed. Depth hoar crystals were rectangular, hexagonal and prismatic shapes and ranged generally from 0.1 cm to 1.2 cm in size, with an occasional crystal as long as 2 cm. Some depth hoar layers had vertical channels between crystals.

On 13 March, we cleared an area (about 52 X 18 m) of flat ice downstream of the Groin #1 ice jam (Figure 12) to determine if the snow had a

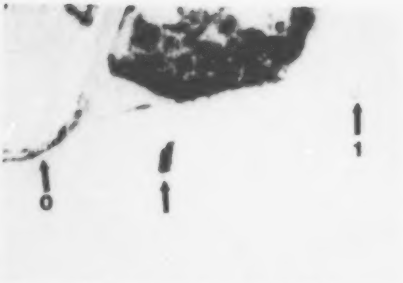

Figure 12. Cleared area of flat ice between Groins #0 and #1 (photograph made from an aerial videotape).

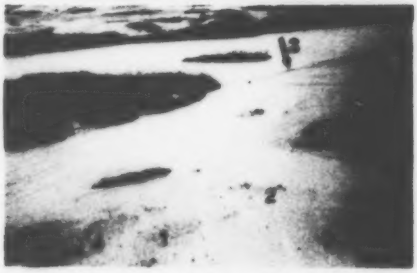

Figure 13. Typical configuration of river bars (1) and exposed river bed (2) near the Goose Island ice bridge (3).

detectable effect on the amount of backscatter from the river ice surface. Only 3.6 cm of new snow fell after the ice was cleared before the SAR image was taken on 19 March. The cleared area is not apparent on the image which suggests that the snow in this area is virtually transparent to the radar signals in the three bands.

River bed and bars : The river bars and exposed river bed (Figure 13) show up as mottled dark areas with variable light and dark tones caused by the irregular surface, scattered vegetation and ephemeral channels that flow water when river discharge is high. Some of the bars and exposed bed have light toned lines within them on the SAR images which are likely scarps less than 0.3 to 1 meter high which border these old channels (Figure 9).

Surface sediment on the river bars and exposed bed and nearshore sediment along the sampled lakes was likely frozen and ice-bonded at some sites. However, surface sand and silt at some sites was frozen but dry, such as at a sampled Goose Island snow pit where the upper 3.5 cm of sediment was frozen and desiccated. The depth of frost was not measured at any of the field sites.

Lake Patterns

Many of the lakes adjacent to the Tanana and Chena Rivers occur in old gravel borrow pits and have surface areas of less than 10 acres. Most of these lakes appear dark on the SAR images (Figure 9). We cored the ice on a small lake east of the Fairbanks airport that was formed when the flood control levee was built across a meander of the Tanana River. Ice in the seven cores ranged between 13.5 cm and 56.0 cm in thickness and consisted of less than 10 cm of snow ice and bubbly ice at the top with black ice below. The ice surface typically was smooth and the snow above on most of the lake was compacted by snowmobile passes. This lake is difficult to discern from the surrounding abandoned river bed.

Summary

A visual comparison of three overlay (color composite) images made from the HH-, VV- and HV-polarized data in each of P, L and C bands, was made to determine the relative ability of the bands to define the features discussed above. With PD meaning poorly defined, D is defined and WD is well defined, the results are as follows:

	P-band	L-band	C-band
Ice jams	PD	WD	D
Less-rough ice	D	WD	D
Level ice	D	D	D
Open water	WD	WD	WD
Snow	PD	PD	PD
River bed and bars	WD	D	D
Lake ice	D	D	D

This subjective evaluation suggests that L-band is better overall at distinguishing ice conditions.

The next step in our analysis, will include a more thorough comparison of detailed field data with the SAR images and will make use of additional images synthesized from digital data provided to us by JPL. The additional images will allow comparison of signatures of like (HH and VV) and cross (HV, VH) polarizations for each of the three bands. The digital data will also allow some quantitative analysis to support image interpretations.

CONCLUSIONS

1. Colder brightness temperatures at 33.6 GHz correlate with deeper and more continuous snow cover. This is pronounced because of the depth hoar.

2. Snow wetness greatly alters 33.6 GHz brightness temperatures, masking snow and ice features that were readily apparent during dry snow conditions.

3. Fracture patterns in lake ice can be detected where they result in a contrasting surface expression. On Harding Lake fractures are detected with the Ka-band passive microwave imager because of snow ice on the surface contrasting with surrounding snow-covered ice.

4. Open water is readily apparent on KRMS and AIRSAR imagery.

5. Ice jams are more apparent on SAR images. L-band images are the most sensitive to change in roughness along the jams.

6. Snow-covered river ice, smooth to rough, is clearly distinguishable from snow-covered river sediments on exposed river bed and unvegetated bars on SAR images.

7. Undisturbed to compacted and dry to wet snow does not appear to cause enough variation in backscatter to be visually differentiated on P-, L- and C-band imagery.

8. Smooth, level lake ice produces little backscatter on SAR images.

ACKNOWLEDGMENTS

We wish to acknowledge E. Chacho, B. Brockett, and D. Lawson of CRREL for field data collection, D. Eppler, D. Farmer of NORDA and B. Heydlauft of Naval Weapons Center, China Lake, CA for the KRMS data acquisition, T. George of the University of Alaska for obtaining aerial video, and B. Holt and numerous others at JPL and NASA for their assistance in obtaining the AIRSAR data. We would also like to thank D. Eppler and H. Boyne for their review of this paper.

REFERENCES

Arcone, S.A., A.J. Delaney (1986) Airborne river-ice thickness profiling with helicopter-borne UHF short-pulse radar. Journal of Glaciology, Vol. 33, No. 115, pp. 330-340.

Arcone, S.A., B.E. Brockett, D.E. Lawson and E.F. Chacho (1987) Evaluation of the magnetic induction conductivity method for detecting frazil ice deposits. CRREL Report 87-17, U.S. Army CRREL, Hanover, NH. 03755-1290.

Dubois, P.C., and L. Norikane (1987) Data Volume reduction for imaging radar polarimetry. Proceedings IGARSS '87, Michigan, USA, May 18-21, 1987. Vol. 1, pp. 691-696.

Eppler, D.T., L.D. Farmer, A.W. Lohanick (1984) Digital processing of passive Ka-band microwave images for sea-ice classification. Naval Ocean Research and Development Activity, NSTL, Mississippi, Report 51.

Eppler, D.T., L.D. Farmer, A.W. Lohanick and M. Hoover (1986) Classification of sea ice types with single-band (33.6 GHz) airborne passive microwave imagery. Journal of Geophysical Research, Vol. 91, No. C9, pp 10,661-10,695.

Hall, D.K., J.L. Foster, A.T.C. Chang, and A. Rango (1981) Freshwater ice thickness observations using passive microwave sensors. IEEE Transactions on Geoscience and Remote Sensing, Vol. GE-19, No.4, pp. 189-193.

Hallikainen, M., F.T. Ulaby, and M. Abdelrazik (1984) The dielectric behavior of snow in the 3- to 37-GHz range. Proceedings IGARASS '84, Strasbourg, France, August 27-30, 1984. Vol. 2, pp. 169-174.

Held, D.N., W.E. Brown, A. Freeman, J.D. Klein, H. Zebker, T. Sato, T. Miller, Q. Nguyen, and Y. Lou (1988) The NASA/JPL multifrequency, multipolarisation Airborne SAR system. Proceedings IGARSS '88, Edinburgh, Scotland, Sept. 13-16, 1988. Vol. 1, pp. 345-347.

Lawson, D.E., E.F. Chacho, B.E. Brockett (1986) Sub-ice sheet channels and longitudinal frazil bars, ice-covered Tanana River, Alaska. Proceedings IAHR Symposium on Ice, 8th, Iowa City, Aug. 18-22, 1986. Vol. 1, pp. 465-474.

Nakao, K. (ed) (1980) Climatic Changes in the Interior Alaska, Report of the

Alaskan Paleolimnology Research Project - 1977/78/79, Laboratory of Hydrology. Department of Geophysics, Hokkaido University.

Neill, C.R., J.S. Buska, E.F. Chacho, C.M. Collins and L.W. Gatto (1984) Overview of Tanana River monitoring and research studies near Fairbanks, Alaska. Special Report 84-37, U.S. Army CRREL, Hanover, NH. 03755-1290.

Selkregg, L.L. (1974) Alaska regional profiles. Vol. 6, Yukon Region, AEIDC, University of Alaska, Anchorage, Alaska.

Shiue, J.C..A.T.C. Chang, H. Boyne and D. Ellerbruch (1978) Remote sensing of snowpack with microwave radiometers for hydrologic applications. Proceedings of the 12th International Symposium on Remote Sensing of the Environment, Ann Arbor, Michigan, pp. 887-896.

Weeks, W.F..A.G. Fountain, M.L. Bryan, and C. Elachi (1978) Differences in radar returns from ice-covered lakes. Journal of Geophysical Research, Vol. 83(C8), pp. 4069-4073.

USE OF MICROWAVE REMOTELY SENSED SOIL MOISTURE IN HYDROLOGIC MODELING

E. T. Engman
USDA Hydrology Laboratory, Beltsville, Maryland 20705, U.S.A.

INTRODUCTION

Many of the models that hydrologists have used during the past couple of decades have a soil moisture component. In most cases the soil moisture component is actually an intermediate step in the water balance computations and not an input or output variable that can be compared with measured data. In these models, soil moisture is a system state that must be initiated and then, timewise, recomputed by increasing it when precipitation is added or decreased by drainage and evapotranspiration. In general, existing models' representation of soil moisture is simply a step to make the model work and not a physical representation of soil moisture. This also illustrates a contention of Morton (1982) that our models tend to make reality conform to our model concepts rather than vice versa. In many respects this approach can be justified because soil moisture data are not generally available and hydrologists have not been able to account for the spatial distribution of soil moisture and soil hydraulic properties.

Recent research in microwave remote sensing of soil moisture has demonstrated the potential for obtaining spatial and temporal maps of soil moisture within a natural drainage area. These are entirely new data and data forms that hydrologists have not had previously to work with and, consequently, the models currently available do not represent soil moisture in a way compatible with these new data. This paper presents an example of how a time series or remotely sensed soil moisture maps might be used in hydrologic modeling. The paper then addresses the needs in hydrologic research and in microwave remote sensing to fully exploit the potential of future microwave data.

FIFE EXAMPLE

During the First International Satellite Land Surface Climatology Project Field Experiment (FIFE) (Sellers et al., 1988) that was conducted at and around the Konza Prairie Long Term Ecological Research site near Manhattan, Kansas in the summer of 1987, we had the opportunity to collect time series of spatial soil moisture data. One phase of FIFE was an investigation of soil moisture and its role in the biology and climatology of the region. Although there are no operational satellite sensors suitable for measuring soil moisture, an aircraft-borne microwave radiometer was used to make remotely sensed measurements of soil moisture. The following describes the relationship between measured streamflow and soil moisture during an eight day period in late May and early June 1987.

STUDY SITE AND DATA COLLECTION

In order to conduct a water balance a small drainage basin was instrumented with a streamgaging station. Other hydrologic variables, with the exception of groundwater, were measured as part of the basic FIFE instrumentation network. The drainage basin selected for study is a 37.7 ha area totally in natural grasses. The area is drained by a stream system that flows only during the winter and late spring when ET rates are low and precipitation frequent. Streamflow was measured with a 120° sharp crested weir and a clock driven analog recorder. Low flow calibration was accomplished with timed volumetric measurements. Figure 1 is a detailed map of watershed 1D that shows the stream network, approximate elevation contours and instrument locations. Evapotranspiration (ET) and rainfall were measured as part of the overall FIFE instrument network. ET was measured by several techniques including the Bowen ratio and eddy correlation methods. General weather conditions were measured by several automatic meteorological stations.

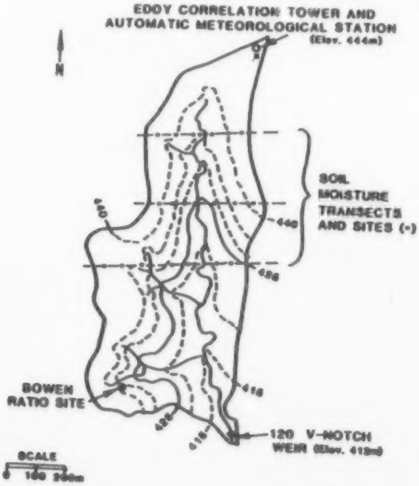
EDDY CORRELATION TOWER AND
AUTOMATIC METEOROLOGICAL STATION
(Elev. 444m)
N
SOIL
MOISTURE
TRANSECTS
AND SITES (•)
440
440
426
416
BOWEN
RATIO SITE
426
416
120 V-NOTCH
WEIR (Elev. 412m)
SCALE
0 100 200m

Fig. 1. Detailed map of watershed 1D showing approximate elevation contours, instrument locations and soil moisture sampling transects.

The period of study commenced with a soaking rain on May 27 and was followed by an essentially rain-free period of drydown for the next eight days. This provided the opportunity to trace the changes in soil moisture in response to a high ET demand and gravity drainage to the stream. Table 1 summarizes the daily climatic conditions (soil sampling and flight opportunities) during this period.

Table 1 Summary of climatology for the period May 27 to June 4, 1987. Dates of microwave flights and soil moisture are also shown

Date	Rain (mm)	ET (mm)	Streamflow (mm)	Flight	Soil moisture samples
May 27	61.72	0.00	0.54		
May 28	0.08	3.63*	0.16	yes	yes
May 29	0.68	2.37*	0.10	yes	yes
May 30	1.69	5.69	0.08	yes	yes
May 31	0.00	6.22	0.09		yes
Jun 1	0.00	5.70	0.08		yes
Jun 2	0.25	1.17*	0.10		
Jun 3	0.00	5.91	0.07		yes
Jun 4	0.00	6.40	0.06	yes	yes

*Full day's data not available; total daily value estimated using data from other Bowen ratio sites.

Near surface soil moisture was measured with a push broom microwave radiometer (PBMR) mounted in a NASA C-130 aircraft. The radiometer operates at the 21-cm wavelength which has been shown to be most effective for measuring soil moisture (Schmugge et al., 1986). It operates with four beams which sweep a path with a width of about 1.2 times the aircraft's altitude above the ground. The resolution of each beam is about 0.3 times the altitude. A schematic of the PBMR is shown in Fig. 2. The PBMR measures the electromagnetic emission from the soil surface as a brightness temperature. The PBMR provides a quasi two-dimensional data set. Each of the four beams traces out a swath about 90 m wide so that the total swath is about 350 m wide for an aircraft altitude of 300 m.

Ground measurements were taken to support the remotely sensed data. Three transects were established under the aircraft flight lines for taking gravimetric soil moisture samples. The transects and sample sites are also shown in Fig. 1. The bulk density of the soil at each site was measured by a water displacement method. Full or partial transect data were taken on all except one day (June 2) of the study period. Aircraft PBMR data were taken on four of the days.

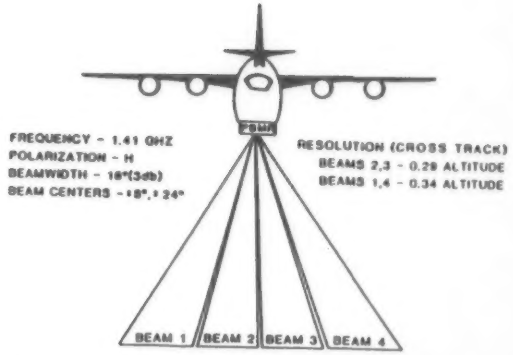

Fig. 2. Schematic of push broom microwave radiometer and aircraft.

Figure 3 shows the results of remotely sensed soil moisture in a two-dimensional map format for the days of May 28 and 30, and June 4. The north and south ends of the basin are missing soil moisture data for two days because the aircraft flight lines were displaced slightly. Examination of soil moisture maps for the three dates points up both the temporal changes and certain locations where the changes in soil moisture are occurring at different rates. The June 4th map shows rather uniformly low soil moisture over most of the basin except along the southern boundary. This relatively high area of soil moisture is probably the result of down gradient redistribution of the soil moisture. This area also would represent the more dynamic region of the basin, in partial area or source area terms.

MODEL SELECTION

The availability of spatial and temporal soil moisture data provided a unique opportunity to model the hydrology of the basin where the soil moisture aspects could be emphasized. Our search for a model that has a reasonably sound theoretical base and focuses on the between storm base flow led us to several models that are all based on Hewlett & Hibbert (1963) experiments. This class of models, which will be referred to as sloping slab models, was developed to simulate subsurface stormflow from relatively steep and primarily forested watersheds. Our search led us to a simple storage-discharge model developed by Sloan & Moore (1984). Figure 4 is a schematic of the Sloan & Moore (1984) model. This model is based on a water balance of a hillside segment that acts as the control volume for the continuity of mass equation. The water balance aspect of the model is particularly important to this study because the change in storage may be a measurable quantity with remote sensing.

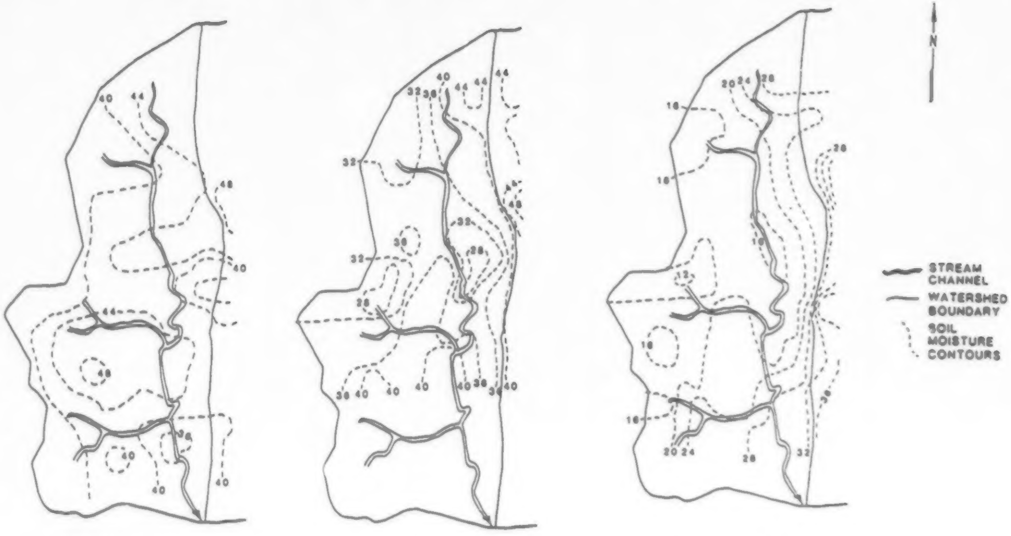

N
STREAM CHANNEL
WATERSHED BOUNDARY
SOIL MOISTURE CONTOURS
40
44
48
36
32
28
24
20
16
12

WATERSHED 1D
MAY 28, 1987

WATERSHED 1D
MAY 30, 1987

WATERSHED 1D
JUNE 4, 1987

Fig. 3. Volumetric soil moisture map developed from PBMR data for three dates: May 28, May 30 and June 4 (Wang et al., 1989).

The Sloan & Moore (1984) model assumes an idealized slope segment of length L, slope angle α, and an impermeable boundary at depth D as shown in Fig. 4. The mass balance is written as

$$\frac{S_2 - S_1}{t_2 - t_1} = (r+i-ET)L - \frac{q_1 + q_2}{2} \tag{1}$$

where q is the discharge out of the slab, t is time, r is the rainfall input, ET is the evapotranspiration, i is the vertical flux from the unsaturated zone to the saturated zone, S is the drainable volume of water in the saturated zone.

$$q = H_o K_s \sin\alpha \tag{2}$$

where K_s is the saturated conductivity. H_o, the saturated thickness normal to the hill slope, is computed by

$$H_{o_2} = \frac{[H_{o_1} (L\theta_d - K_s \sin\alpha\Delta t) + 2L(r+i-ET)\Delta t]}{(L\theta_d + K_s \sin\alpha\Delta t)} \tag{3}$$

where θ_d is the drainable porosity of the soil. The saturated region is recharged from the overlying unsaturated zone by

$$i = K(\theta) \tag{4}$$

where $K(\theta)$ is estimated by the Brooks-Corey (1964) approximation, using a value of soil moisture, θ, calculated by a mass balance of the unsaturated zone from

$$\theta_2 = \theta_1 U_u + L\Delta t\ (r-ET-i)/U_u \tag{5}$$

where U_u is the total volume of the unsaturated zone.

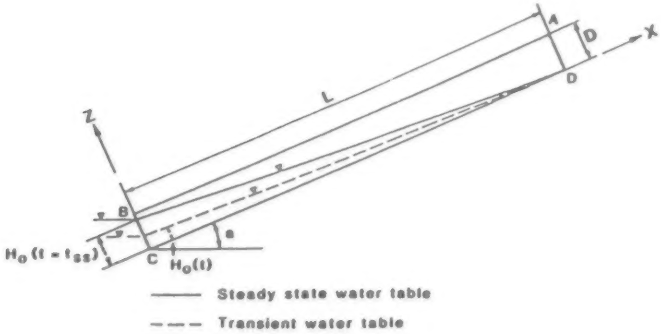

Fig. 4. Schematic of sloping slab model.

MODEL DATA

Simulation of the discharge requires site specific data from the study basin. Some of these data could be measured and some had to be estimated from published descriptions and relationships. The soil depth D was estimated to be 400 mm which corresponds to the A horizon depth (16 in) in the Riley County Soil Survey (SCS, 1975). The soils in the basin are mapped as Tully silty clay and Tully silty clay loam in the aluvial areas and as Benfield/Florence silty clay and silty clay loam in the remainder of the basin. The saturated hydraulic conductivity $K_s = 0.5$ mm/hr was estimated to be between the SCS permeability (10 mm/h) and that which would be estimated from the work of Rawls & Brakensiek (1983) (0.1 mm/h). The Brooks-Corey $\lambda = 0.15$ value was estimated from Rawls et al., (1981). The drainable porosity of the soil was taken to be 45% which compares favorably to the total porosity for these soils. The land slope $\alpha = 0.1$ was estimated from the southern portion of the topographic map, west side of the channel and $\alpha = 0.2$ for the east side of the channel. The slope length L of 200 m and an L of 30 m for the east side of the channel were "judicially chosen" to give good results but they also fit the topography of the basin reasonably well. A channel length of 600 m was chosen to match the total volume of streamflow.

MODEL SIMULATIONS

The Sloan & Moore (1984) sloping slab model was used to simulate the eight day recession flow from watershed 1D. As initial conditions, the hydraulic head, H, was assumed equal to the soil depth, D. The initial unsaturated volumetric soil moisture content was taken to be 43% which was estimated to be a reasonable average for May 28 from the microwave measurements. The saturated volume was assumed to be 50% of the total slab volume. The time step Δt was taken as one hour and the data for ET were taken from Bowen ratio measurements.

The model simulation results are given for a unit width of slab, in this case, 1 mm. In order to evaluate the results, a total length of channel must be determined so that the simulated discharge can be compared to the discharge measured at the weir. The results shown in Fig. 5 are for a channel length of 600 m. This result also assumes that most of the drainage comes from the west side of the channel which is based on the asymmetrical location of the channel in the basin.

A second means for evaluating the simulation results is to compare the simulated and measured soil moisture results. Figure 6 traces the temporal change of the simulated soil moisture; measured data are shown at the time they were taken for two points in the southernmost transect.

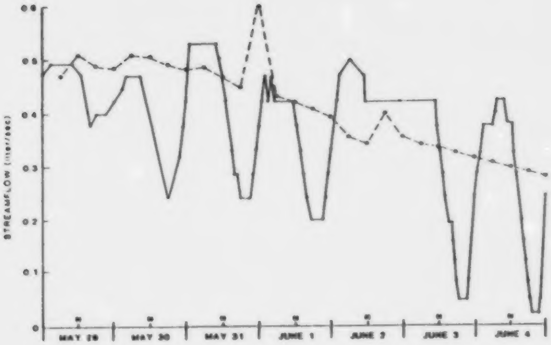

Fig. 5. Comparison of measured and simulated streamflow from watershed 1D. Measured data is represented by solid line and simulated data by dashed line.

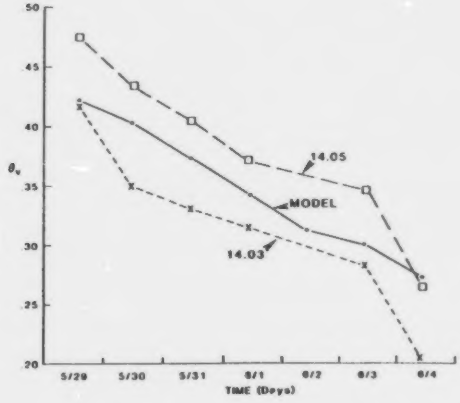

Fig. 6. Comparison of model simulated soil moisture and measured soil moisture at two locations on transect 14 (southern most transect).

DISCUSSION

The results shown in Figs. 5 & 6 demonstrate that the model has simulated the discharge and change in storage (soil moisture) reasonably well, at least for the study period. The large diurnal change during the latter part of the study period distorts the match between simulated and measured discharge. Most of the diurnal decrease in measured streamflow can be accounted for by free water evaporation from the stream surface and weir pond.

The slab dimensions were chosen to "fit" the runoff data; that is, the channel length and slab widths were varied until the simulated runoff volume matched the measured runoff volume. However, use of the microwave data can give some indication as to whether or not the values are reasonable. Re-examination of Fig. 3 may yield some information on the dimensions of the slab. Note that in the southern end of the basin there is a region of relatively high soil moisture on June 4. Unfortunately these equal moisture contours do not quite extend to the basin boundary. Figure 7 is a reproduction of Fig. 3 with the dimensions of the slab used in the simulations shown. One can see that the high moisture area detected with the microwave overflights is approximately the same as the sloping slab dimensions chosen for the simulations.

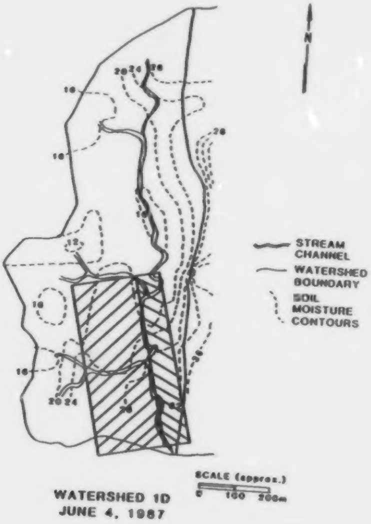

Fig. 7. Dimensions of sloping slab necessary to simulate streamflow superimposed on June 4 soil moisture map.

After examining the remotely sensed soil moisture maps and the good model simulations of soil moisture for the study period, one is tempted to speculate on how soil moisture could be used as direct input to the model to predict the base flow. To do this we first must examine the model, and in particular Eqs. 1 and 5.

Equation 1 shows that the change in streamflow is related to the change in storage represented by the net flux to the saturated zone, which in turn is made up of the rainfall and recharge from the unsaturated zone and the ET loss. The rate of recharge, i, depends on the water balance on the unsaturated zone (Eq. 5). It is in Eq. 5 that one would like to use soil moisture as data. Rewriting this equation to solve for i gives

$$iL\Delta t = (r - ET)L\Delta t + (\theta_1 - \theta_2)U_u \qquad (6)$$

In this form it can be seen that i depends upon the change in soil moisture and the net balance between rainfall and ET. Thus, i cannot be estimated from soil moisture data alone but must also have an estimate of the ET for a rain-free period.

It was pointed out above that the model and the microwave measurements of the soil moisture both reflected the June 2 ET which was considerably lower than the other days' ET (Table 1). This being the case, one may be able to use estimates of ET based on simplified potential ET considerations rather than local short term measurements requiring significant micrometeorological instrumentation. The consequences of this would be that for any one day (such as June 2), the ET may be overestimated and the model calculation of soil moisture would be lower than the actual. But subsequent measurements of soil moisture would show this discrepancy and allow correction so that the model predicted soil moisture would agree with the measured value. Thus, by using the remotely sensed soil moisture as feedback to the model, one may be able to run water balance models calibrated for a basin without the need of detailed on-site ET measurements.

The implications of this approach are that this type of model structure could be used to verify an intermediate step in the simulation process; that is, the unsaturated soil moisture balance during drainage and ET. Thus, a time series of soil moisture would provide an important check on the model performance and possibly provide feedback data so that the model could be corrected and updated if the simulations were under or over estimating the streamflow.

FUTURE MICROWAVE REMOTE SENSING

Future microwave remote sensing of soil moisture is veiled in hope and potential future sensors and platforms. For the next few years hydrologists will be limited by the lack of suitable data. Only intensive and hydrologically driven aircraft experiments will be available for collecting soil moisture data in a form that hydrologists will find useful. Unfortunately, the money and manpower costs of performing aircraft experiments limit these oportunities. However, there are a few experiments planned in the next few years and these should be invaluable for providing sample data for developing and testing hydrologic models.

Looking ahead to when there may be microwave sensors on orbiting platforms, one confronts the basic differences between passive and active instruments and the intended use of the data. Comparing the instruments simplistically, the active sensors have the capability to provide high spatial resolution data (on the order of 10's of meters) but their sensitivity to soil moisture may be confused more by roughness, topographic features, and vegetation than the passive systems. On the other hand, the passive systems, although less sensitive to target features, can provide spatial resolutions only on the order of kilometers to 10's of kilometers from a space platform.

One then must consider how the data will be used. Meteorological and climate models currently use computational cells on the order of 10 to 100 km which may be well within the capability of future passive systems. However, if one is interested in more detailed hydrologic process studies and partial area hydrology, the passive data would appear to be of little use. It is in this context that the active systems, specifically Synthetic Aperture Radar (SAR) appears promising. For example, the Shuttle Imaging Radar (SIR-C/X) to be flown in 1992 is capable of at least 20 m resolution over a swath width of 15 to 30 km. SAR also has the capability of a scanning mode (SCANSAR) to cover a much wider swath (300 to 500 km) at a reduced resolution (250 m). At this stage, SCANSAR is a theoretical option; it has not been demonstrated nor has its sensitivity to useful soil moisture values been demonstrated.

Future space launch manifests include several SARs but no passive systems that have frequencies low enough to be useful for soil moisture. Table 2 lists the principal characteristics of the scheduled SARs. It should be noted that the shuttle missions will be rather short, a week to ten days at this date. Past space ventures, SEASAT, SIR-A, and SIR-B, all provided useful data; these data are available but, unfortunately, very little hydrologically useful ground data were collected during these missions.

As hydrologists, there is at least a glimmer of hope in obtaining soil moisture data from these new systems and from a few aircraft experiments. However, along with this are a number of research questions that must be addressed before these data are valuable on a routine basis. The research questions can be split up into two categories for the purpose of discussion, one focusing on the microwave response and the other on hydrologic modeling.

Table 2. Comparison of international SAR missions.

Parameters	E ERS-1	SIR-C/X-SAR	JERS-1	RADARSAT	Eos SAR (NEW)
Launch date	1990	1992,93,94	1992	1994	1998
Altitude (km)	800	225	568	792	620
Spectral coverage	C	L,C,X	L	C	L,C,X
Polarization	W	Quad(L&C) VV(X)	HH	HH	Quad(L) Dual(C,X)
Incidence angle	23°	15°-60°	35°	20°-50°	15°-43°
Antenna size	1.0m x 10m	4.1m x 12m	2.2m x 12m	1.6m x 15m	2.6m x 10.9m
Antenna feed network	passive	active, distri.(L&C) passive (X)	passive	passive	active, distri. arrays
Antenna beamsteering	no	electronics(L&C) mechanical(L,C.X)	no	electronics	electronics
Flight system mass (kg)	---	+500	1400	1424	1800
Noise equiv. sigma zero (dB)	-18	-50/-40/-26	-20	-21	-36/-28/-22
Swath coverage (km)	100	15-150	75	50-500	15-360
Main objective	ice/ocean	scientific algorithm development	geology	polar ice, northern latitude coverage	global biomass, soil moisture, polar ice, snow
Equator cross time	10:30 a.m.	variable	10:30 a.m.	6 a.m./6 p.m.	1:30 p.m. (?)

Microwave responses: There are a number of unanswered questions regarding the microwave-target interactions that need to be answered before soil moisture can be routinely determined with microwave instrumentation. Most of the following comments will apply directly to the SAR because it appears these data will be the first that we have to work with. However, to a certain degree (in many cases a lesser degree) these needs also apply to the passive systems.

1. There is a need to develop algorithms to abstract volumetric soil moisture directly from the microwave measurement (backscatter coefficient or brightness temperature). To do this the other target characteristics of vegetation and surface roughness will have to be parameterized.

2. There is a need to better understand the effects of surface roughness on the measured microwave response with respect to incidence angle, azimuth angle, wavelength, and polarization.

3. There is a need to understand the effect of the vegetation canopy on the microwave response. Vegetation variables include the geometry for the individual plant as well as the canopy as a whole, the water content (and perhaps the biochemical make-up) of the plant, and its stage of growth. Microwave variables would include the incidence angle, the azimuth angle, wavelength, and polarization.

4. There is a need to investigate the use of change detection algorithms for determing the relative soil moisture of an area and whether or not this information can be useful for hydrologists. Change detection may minimize the influence of target variables such as roughness and vegetation, at least over short time intervals.

5. There is a need to develop software procedures for correcting the effects of terrain on the microwave response. Active microwave (SAR) is especially sensitive to this. This includes fore-shortening, layover and local incidence angle effects. Also, a potential issue is the relative accuracy of the DEM data with respect to the spatial resolution of the microwave data.

6. There is a need to investigate the potential for polarimetric SAR and its potential for abstracting target information such as the surface roughness and vegetation characteristics.

7. There is a need to explore the potential of other SAR analysis techniques such as multiple bounce response from vegetated canopies and polarization ratios for abstracting information of hydrologic interest.

Hydrologic modeling: Because soil moisture has not been used as measured data in hydrologic modeling, there are a number of issues that hydrologists must address and solve in anticipation of actually working with spatial and temporal soil moisture.

1. There is a need to modify existing models or develop new models that reflect soil moisture in a way that is more physically realistic and so that soil moisture data can be used as input or to verify output.

2. There is a need to develop procedures for modeling or estimating profile soil moisture from time series near surface measurements and/or using multifrequency data.

3. There is a need to understand the relationship between point ground data, the pixel size, and larger representation of remotely sensed soil moisture.

4. There is a need to investigate the potential for direct determination of hydrologic variables and basin characteristics with the microwave response in a way that is as yet unknown. The general idea is that a time series of microwave patterns within a basin may integrate the soil moisture, vegetation, topography, and relative position with respect to the natural drainage system. These patterns would be in effect a hydrologic signature of the basin.

5. There is a need to be able to estimate spatial evapotranspiration losses with soil moisture based algorithms, either as direct input or as feedback to a water balance model.

6. There is a need to develop software, perhaps within a work station concept, that can truly integrate GIS, remote sensing data from several sensors, and the hydrologic models so that all the calibration, scale, format, etc., problems become transparent to the hydrologist and he can concentrate on the hydrologic analysis.

REFERENCES

Brooks, R. H. & Corey, A. T. (1964) Hydraulic properties of porous media, Hydrol. Paper 3, Colorado State University, Ft. Collins, CO, 27 pp.

Hewlett, J. D. & Hibbert, A. R. (1963) Moisture and energy considerations within a sloping soil mass during drainage. J. Geophys. Res., 68(4), 1081-1087.

Morton, F. I. (1982) Integrated basin response - A problem of synthesis or a problem of analysis, Proceedings Canadian Hydrology Symposium, Assoc. Committee on Hydrology National Research Council, Canada, 361 pp.

Rawls, W. J., & Brakensiek, D. L. (1983) Green-Ampt infiltration model parameters for hydrological classification of soils, Proc. of Specialty Conference on Advances in Irrigation and Drainage, Irrigation and Drainage Div., ASCE, Jackson, Wyoming, 8 pp.

Rawls, W. J., Brakensiek, D. L. & Saxton, K. E. (1981) Soil water characteristics, Am. Soc. Agr. Engr. Paper 81-2510, ASAE Winter Meeting, Chicago, IL.

Schmugge, T. J., O'Neill, P. E. & Wang, J. R. (1986) Passive microwave soil moisture research, IEEE Trans. Geosci. and Remote Sens., GE-24(1), 12-22.

Sellers, P. J., Hall, F. G., Asrar, G., Strebel, D. E., & Murphy, R. E. (1988) The first ISLSCP field experiment (FIFE), Bull. Am. Met. Soc., 69(1), 22-27.

Sloan, P. G., & Moore, I. D. (1984) Modeling subsurface stormflow on steeply sloping forested watersheds. Water Resour. Res., 20(12), 1815-1822.

Soil Conservation Service (1975) Soil survey of Riley County and part of Gery County, Kansas, USDA, Washington, D.C. 20250.

Wang, J. R., Shuie, J. C., Schmugge, T. J., & Engman, E. T. (1989) Mapping surface soil moisture with L-band radiometric measurements. Remote Sens. Environ., 27, 305-312.

RETRIEVAL OF LAND SURFACE TEMPERATURE AND SURFACE MOISTURE WITH SSM/I BRIGHTNESS TEMPERATURE

M.J. McFarland & R.L. Miller
Texas A&M University, College Station

C.M.U. Neale
Utah State University, Logan

ABSTRACT

Passive microwave brightness temperatures from the DMSP Special Sensor Microwave/Imager were used to determine surface temperature over land areas in the Central Plains of the United States. The data presented are for calendar days 231, 232, 235, and 240, 1987. The temperature range was from 1.1 to 26.7 C. Pixels containing large amounts of water, snow and falling rain, as classificed with SSM/I brightness temperatures, were excluded from the analysis. No attempt was made to stratify the data set based on degree of cloudiness. Three categories of land surface were used: crops/range, moist soils, and dry soils. A regression analysis between all of the SSM/I channels and minimum air temperatures at screen height (representing the surface temperature) showed good correlations, with coefficients of dertermination as high as 0.85. The root mean square errors were in the range of 2 to 3 C. The channels with the highest correlations were the 85 GHz vertical and horizontal polarization. The use of independent ground truth data such as soil moisture or land surface type was not required to obtain the correlations between brightness temperatures and surface temperatures.

Questions and Answers

Unidentified: How did you achieve that [particular frequency]?

Robert Miller: We are using the minimum temperatures at a given station.

SESSION 2B
SNOW MICROWAVE RADIOMETRY

Session Chairman: R. Perla, National Hydrology Research Institute

DETERMINATION OF SNOW WATER EQUIVALENT ON THE CANADIAN PRAIRIES USING NEAR REAL-TIME PASSIVE MICROWAVE DATA

B.E. Goodison
Canadian Climate Centre
Atmospheric Environment Service
4905 Dufferin Street
Downsview, Ontario
M3H 5T4

A.E. Walker
PhD Associates Inc.
Research Offices
Kinsmen Building
4700 Keele Street
North York, Ontario
M3J 1P3

F.W. Thirkettle
PhD Associates Inc.
1115-605,5th Street SW
Calgary, Alberta
T2P 3H5

BACKGROUND

The distribution and amount of snow cover over the Canadian Prairies is extremely important as snow is one of the main local sources of water for crop growth and water supply. In Canada snow courses have formed the basis of the conventional Canadian snow survey network for over 50 years for determining the amount and distribution of snow water equivalent on the ground. Recent advances in remote sensing technology, however, offer the potential for significant change in snow survey procedures. A combination of ground-based, airborne and satellite information, or eventually remote sensing methods alone, may provide the most effective and efficient means of snow survey data collection to meet a variety of user needs. Snow course data will continue to provide the standard against which any new techniques will be evaluated.

A major advance in the remote sensing of snow cover is the development of algorithms which determine snow depth, water equivalent, areal extent and snow state (wet/dry) using sensors having all-weather capabilities, most notably, microwave radiometers data sensors. Investigations (Goodison, 1989; Goodison et al., 1986a; Hallikainen and Jolma, 1986a, 1986b; Kunzi et al., 1982; Chang et al., 1982; Foster et al., 1980) using data from ESMR on NIMBUS 5 and 6 and from the Scanning Multichannel Microwave Radiometer (SMMR) on NIM-

BUS-7, have shown that passive microwave sensors can be used to monitor snow cover.

Goodison (1989) provides a general discussion on the development and testing of algorithms for the monitoring of areal snow water equivalent over the Canadian prairies using passive microwave satellite data. This paper focuses on the production, delivery and assessment in near real-time of an accurate satellite derived snow water equivalent map to complement existing snow data collection methods in the prairie regions.

ALGORITHM DEVELOPMENT AND VALIDATION

A multi-agency snow survey experiment was initiated in southern Saskatchewan in February, 1982 (Goodison et al., 1984; 1986) to assess the utility of passive microwave data for mapping prairie snow cover. Research has since focussed on the derivation and validation of algorithms to estimate snow water equivalent (SWE) using microwave radiometer data. Airborne microwave measurements (18GHz and 37GHz horizontally and vertically polarized) and airborne gamma measurements of SWE were collected along an 1100km flight line network established specifically for this research. The airborne gamma measurements provided one type of "ground true" data against which the microwave data were calibrated. Carroll et al. (1983) provide a complete discussion of the airborne gamma surveys and the associated errors. The gamma and airborne microwave data were averaged over 20-25km segments, this resolution being similar to the 30km x 30km resolution of the 37GHz satellite data collected on the same days. Intensive, specially designed snow surveys were also conducted along the flight lines and served as the more conventional snow survey data against which the airborne gamma and microwave radiometer data were validated. Goodison et al. (1987) provide a summary of Canadian snow survey procedures, errors, accuracies and problems which can influence algorithm development or validation.

Using the different data sources as "ground true", a series of empirical airborne based algorithms were derived for determining snow water equivalent from passive microwave measurements. Goodison (1989) summarizes the relationships developed from this field experiment. Figure 1 shows the relationship between the NWS airborne gamma derived SWE (NWS SWE) and airborne radiometer brightness temperature gradient (GTV) for dry snow conditions using vertically polarized brightness temperatures (R^2=.89). In the airborne analyses, comparison of SWE and 37H or 18H brightness temperatures showed considerably more scatter than those for vertically polarized data. For 37H versus NWS SWE, the R^2 was only 0.29. Many different combinations of horizontally and vertically polarized 37 and 18GHz airborne microwave data were tested against the "ground true" estimates of SWE. It was concluded that the "best" algorithms to test in a case study of real-time snow cover monitoring were the NWS SWE vs 37V GHz and the NWS SWE vs the brightness temperature gradient between 37V and 18V GHz (37V and 19V for SSM/I). An important point to remember when mapping snow water equivalent is that melting snow can be distinguished from dry snow, but snow water equivalent cannot be determined for wet snow conditions (see Goodison, 1989, 1986a). Therefore, snow cover must be monitored regularly, and preferably at 1-2 day intervals, if SWE is to be determined or the onset of melt identified.

MAPPING AREAL SNOW WATER EQUIVALENT: DATA ACQUISITION PROCESSING AND DELIVERY OF SWE PRODUCTS

During initial algorithm testing, selected maps of snow water equivalent during the 1979-1986 period were produced from archived NIMBUS-7 SMMR data for southern Saskatchewan and Manitoba. The distribution and amount of SWE determined from SMMR data were generally comparable to the maps produced from conventional snow surveys (Goodison et al., 1986b), but it was evident that analysis of individual days could be complicated by melt events, occurrence of significant snowfalls and lack of knowledge of developing snowpack structure. A more complete test of the algorithms was to monitor snow cover on a daily basis, with periodic comparison with available snow survey and airborne gamma measurements, or SWE estimates from water budget computations (Goodison, 1989). Data from the DMSP (Defense Meteorological Satellite Program) Special Sensor Microwave/Imager (SSM/I) are most suited to such a real-time test. The SSM/I sensor has four frequencies (19.3, 22.2, 37.0 and 85.5 GHz) scanning a swath of 1400km. Robles (1988) provides a summary of the SSM/I configuration, initial data problems and archiving activities for these data. The important difference from NIMBUS-7 SMMR data is the use of a 19.3 GHz channel, instead of an 18 GHz one. This will have a slight effect on the brightness temperature gradient calculation, but for the initial test, the coefficients for the GTV equation were not changed. During the 1988/89 and 1989/90 winter season, a trial demonstration of delivering snow water equivalent maps in near real-time to twelve provincial and federal agencies in Manitoba, Saskatchewan and Alberta was undertaken. Assessment of the results continue.

SSM/I is currently on one of two U.S. DMSP satellites. These are "operational" spacecraft; therefore, the data from the instruments are processed in a near real-time mode on an orbit-by-orbit basis. The global coverage of an orbit is recorded by an onboard tape system and played back to the ground receiving station in Maine, Washington or Hawaii. The data are then relayed to the Fleet Numeric Operations Center (FNOC) in Monterey, California where they are converted into Temperature Brightness units, time stamped and latitute/longitude tagged. As part of the FNOC processing, two tailored SSM/I data files are transmitted to the computer system of the National Oceanic Data Distribution System (NODDS) also situated in Monterey. One file contains the 19 and 37 GHz channels and the other, much larger file, holds all the instrument channels (including 85 GHz with its data volume being four times that of any of the other channels). Ph.D. Associates can direct dial into the NODDS system and retrieve a file using matching high speed modems in Monterey and on the company's IBM PC/AT.

Once the data for a particular region of the earth have been transferred to Ph.D. Associates, all further processing can be performed "in-house" except possible mainframe support that may be required for certain products requested by the user. The local processing consists of unpacking the compressed NODDS format, identifying each instrument footprint as to being over land or water, selecting land locations, running the snow water equivalent algorithm, passing the results through the requested map projection, contouring the snow water equivalent values as required, displaying the final product in the desired format and transmitting that image to the user's site. This entire task can be completed, if necessary, within four to six hours of the original satellite viewing. The format requested by the co-operating agencies was a facsimile map at 1:2,000,000 scale or a colour printer map from Ph.D. Associates' IBM PC-based Geographic Analysis and Display System (GADS). Both of these products were enhanced with individual user requirements such as town locations, basin outlines, airborne flight lines or the tree line. Furthermore, a data product could consist solely of a file created to the user's specifications and delivered on diskette, 9-track computer tape or modem-to-modem interface. Users with their own analysis system or GADS could produce hardcopy maps themselves and undertake further processing of the data.

The SSM/I data are available on a 24-hour, seven days-a-week basis. The data files on the NODDS computer remain online for about three days. After that time, the data may be obtained on 9-track tape, but these will be at least one month old. For this intercomparison, PhD Associates acquired daytime or nighttime passes once per day over the target area. Facsimile maps of SWE were produced once per week and distributed to co-operators. There are four more SSM/I systems ready for launch with the intent of having at least one instrument operational at all times throughout the next ten years. Since there are always two DMSP satellites functioning at any time, there will be periods when two SSM/I instruments are in operation. The next planned launch of a DMSP satellite is October 1990 and it will be carrying another SSM/I sensor. Should that occur, the current twice daily coverage of the Canadian Prairies will increase to four times daily.

VALIDATION OF REAL-TIME SWE MAPS.

For this real-time exercise the NWS SWE vs GTV (37V and 19V GHz) algorithm (Figure 1) was used to map snow cover over the prairie regions. No changes were made to the algorithm during the winter accumulation/ablation season to account for possible effects of changing snowpack structure and density, including those related to diurnal freeze/thaw. The need for adjustments to the algorithm to account for structure/density/grain size changes is being assessed as part of the validation process. The experimental results of Hallikainen and Jaaskelainen (1988) clearly show the potential hysteresis in the 37GHz brightness temperature versus snow water equivalent due to changes in surface snowpack structure. Over a large region, such as the Canadian prairies, it will be necessary to regionalize these effects, before making any modification to microwave algorithms. As well, it is necessary to assess the accuracy of the algorithm in forested regions in the northern parts of the provinces. This is difficult because of the limited amount of conventional data available for validation of the satellite maps.

An extensive snow survey was conducted in southern Saskatchewan during the week of February 13, 1989. Regular ground surveys were done by the Saskatchewan Water Corporation. Figure 2 shows the contoured distribution of snow water equivalent over southern Saskatchewan (degraded fax map product) as determined from SSM/I data for February 14, 1989 (0127 GMT; orbit 8543). The numbers are the ground snow survey measurements of snow water equivalent. The regional pattern of snow distribution from both data sources agree very well; the average SWE values are generally within 10mm of each other, although in south-west Saskatchewan, the ground data exhibit more local variability which is directly related to the land use, terrain and exposure of the individual snow course. Fallow fields were often blown clear, while stubble fields retained or accumulated wind blown snow. These effects are integrated in the microwave signal, since each "pixel" is approximately 25km x 25km. The resolution of current microwave sensors precludes the data being used to map small scale variability in snow cover over small regions or basins, yet Figure 2 clearly shows their utility in defining the snow cover distribution over larger areas.

Figure 3 illustrates the ability of this satellite technique to detect localized early season snowfalls. Snow was observed on the ground during an aircraft overflight from Saskatoon to Winnipeg on October 29, 1989 for an area near Wynyard and the Quill Lakes. A SWE map produced for October 31, 1989 showed local snowcover in the Quill Lakes region. This early snowfall resulted in this area showing a subsequent persistent local high SWE for much of the early winter season.

Algorithm validation has focussed on the open prairie regions, south of the treeline. It is for this area that most of the conventional snow survey data exist. However, there is a need to assess the use of passive microwave data for mapping snow cover in the forested areas of these provinces. The retrieval of snow water equivalent from passive microwave brightness temperatures is influenced by the type of land cover present. In forested areas, the microwave response to SWE is decreased as a result of attenuation by the tree canopy. Previous studies in Finland using Nimbus-7 SMMR data (Hallikainen and Jolma, 1986a and 1986b) have shown that the microwave response to SWE in forested regions may be reduced by as much as 50% as compared to open agricultural areas (eg. farmland).

Decreased SWE retrievals have been observed on the SSM/I snow cover maps over areas characterized by forest cover. Figure 4 depicts SSM/I SWE contours over Saskatchewan and the bordering areas of Alberta and Manitoba for November 12, 1989. The few AES snow course SWE measurements (mm) for November 15, 1989 are plotted; the boundary (treeline) between open prairie (south) and forest (north) is also shown. The effect of the forest on the SSM/I SWE retrievals can be readily observed; north of the treeline the SSM/I SWE values indicate no snow, while the AES snow courses report SWE measurements exceeding 30 mm.

The forest cover appears to mask completely the microwave response to the underlying snowpack.

The SSM/I SWE retrievals depicted in Figure 4 were derived using the current operational algorithm, which utilizes the 37V-19V brightness temperature gradient. Although this algorithm performs well over the open prairie, results over forested regions are not reliable, as indicated in Figure 4. Cooperators using the SSM/I SWE map products have expressed interest in receiving information over the forested regions in order to better predict spring runoff. A dual-algorithm approach is currently being tested, where the existing SSM/I SWE operational algorithm is applied only to the prairie region and a second algorithm is used over the forest. Preliminary results indicate that a single frequency algorithm using 37GHz vertically polarized data only yields more realistic SWE retrievals over the forested areas. Figure 5 presents results of applying the dual-algorithm approach to the November 12, 1989 SSM/I data. The SSM/I SWE retrievals north of the treeline are significantly higher and more representative of the AES snow course measurements than those of the single algorithm approach (Figure 4). These preliminary results are encouraging, but further testing is required before the dual-algorithm method can be used operationally to produce the SSM/I SWE map products.

One problem identified in the 1988/89 analyses was an error in the geolocation of the data (Goodison, 1989). This was noted during the 1987/88 analysis of snow cover and has also been reported by other investigators (Robles, 1988). Goodison (1989) found shifts in the snow cover pattern between some successive orbits of up to 1° latitude. This geo-location error was acknowledged by the satellite operators and since then measures have been taken to bring the geo-location of pixels within the planned pre-launch accuracy of ± 15km. Shifts in the location of snow cover are not as evident in the 1989/90 analyses, although some smaller shifts have been noted.

SUMMARY

The real-time application of passive microwave satellite data for mapping snow cover in prairie regions has been shown to be feasible. A map is produced and delivered to users within hours of the satellite overpass. Initial comparison of the SWE maps with available "ground true" data shows generally good agreement. There are areas where differences exist; the reasons are yet to be determined, but snowpack structure including the development of ice layers is one logical factor. It is clear that different algorithms will be required for determining snow cover in forested areas. Initial tests suggest a single channel algorithm may be suitable, but full assessment of the appropriate coefficients remains to be done.

At this time, it is reasonable that snow cover maps derived from passive microwave data provide a complementary data set for analysis of regional snow cover. They provide another piece of information for the practitioner who must provide day-to-day operations.

ACKNOWLEDGEMENTS

This snow cover validation experiment would not be possible without the co-operation and financial support of may Canadian federal and provincial agencies. Development of this work has been made possible with the support of:

Manitoba Water Resources Branch
Saskatchewan Research Council
Saskatchewan Water Corporation
Alberta Water Resources Branch
Prairie Farm Rehabilitation Administration
Saskatchewan Crop Insurance Corporation
Atmospheric Environment Service
Inland Waters Directorate
National Hydrology Research Centre
U.S. National Aeronautics and Space Administration
U.S. National Weather Service
U.S. Navy

REFERENCES

Carroll, T.R., J.E. Glynn and B.E. Goodison, 1983. "A comparison of U.S. and Canadian gamma radiation snow water equivalent measurements". Proc. Western Snow Conf., 51st Annual Meeting, Vancouver, Washington, April 19-21. pp. 27-37.

Chang, A.T.C., J.L. Foster, D.K. Hall, A. Rango and B.K. Hartline, 1982. "Snow water equivalent estimation by microwave radiometry". Cold Regions Science and Technology, Vol. 5. pp. 259-267.

Foster, J.L., A. Rango, D.K. Hall, A.T.C. Chang, L.J. Allison and B.C. Diesen III. 1980. "Snowpack monitoring in North America and Eurasia using passive microwave satellite data". Remote Sensing of Environment, Vol. 10. pp. 285-298.

Goodison, B.E., A. Banga and R.A. Halliday. 1984. "Canada-United States prairie snow cover runoff study". Can.Water Res. J., 9,1. pp. 99-107.

Goodison, B.E., I. Rubinstein, F.W. Thirkettle and E.J. Langham, 1986a. "Determination of snow water equivalent on the Canadian Prairies using microwave radiometry". In, Modelling Snowmelt Irduced Processes. (Proceedings of the Budapest Symposium, July, 1986). IAHS Publ. No. 155. pp. 163-173.

Goodison, B.E., I Rubinstein, F.W. Thirkettle, 1986b: Snow cover determination the Canadian Prairies using microwave radiometry. Paper presented at 20th Annual CMOS Congress, Regina, Saskatchewan, 3-6 June 1986, Abstract Volume, pp. 59-60.

Goodison, B.E., J.E. Glynn, K.D. Harvey, J.E. Slater, 1987. "Snow surveying in Canada: A perspective". Can.Water Res J., 12, 1. pp. 28-42.

Hallikainen, M.T. and V.I. Jaaskelainen, 1988: Microwave emission behaviour of snow.Proc. IGARSS'88 Symposium, Edinburgh, Scotland, 13-16 Sept. 1988. ESA SP-284 (IEEE 88CH2497-6), pp. 437-438.

Hallikainen, M. and P. Jolma, 1986a: "Applications of satellite microwave radiometry in Finland", Geocarto International, 4, pp. 17-25.

Hallikainen, M. and P. Jolma, 1986b: "Development of algorithms to retrieve the water equivalent of snow cover from satellite microwave radiometer data", Proceedings of IGARSS '86, Zuerich, September 8-11, 1986, pp. 611-616.

Kunzi, K.F., S. Patil and H. Rott. 1982. "Snow cover parameters retrieved from NIMBUS-7 Scanning Multi-Channel Microwave Radiometer (SMMR) data". IEEE Trans. Geosc. Rem. Sens., GE-20(4). pp. 453-467.

Robles Jr., J. 1988. "Ocean and ice communities begin archiving microwave data". Information Systems Newsletter. December, 1988, pp. 32-34.

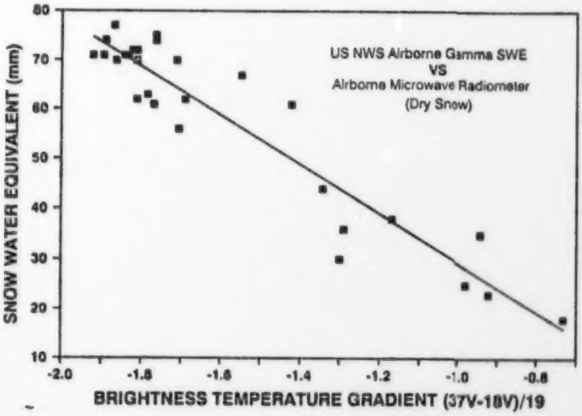

Figure 1: Relationship between NWS airborne gamma SWE and MFMR airborne microwave radiometer brightness temperature gradient for dry snow.

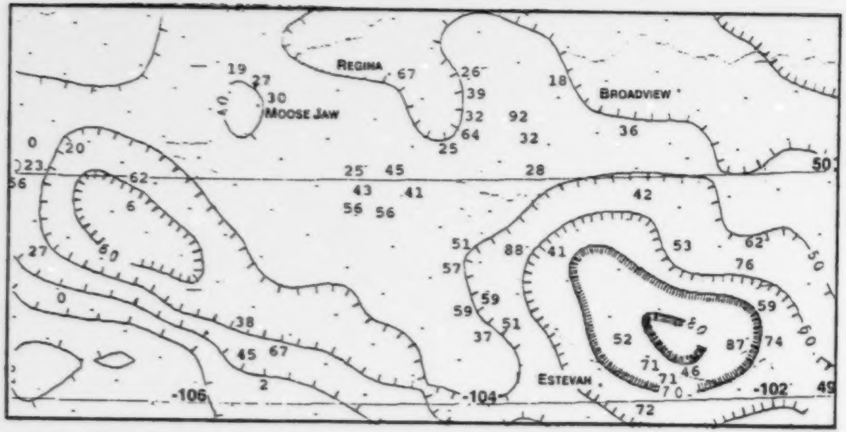

REGINA
MOOSE JAW
BROADVIEW
ESTEVAN
50
49
-106
-104
-102
19
27
30
67
26
39
32
64
25
92
32
18
36
28
0
20
23
56
25
45
43
41
56
56
62
6
60
27
0
38
45
67
2
51
57
59
59
37
51
88
41
42
53
62
76
59
87
74
52
71
71
46
70
72
50
60

Figure 2: Distribution of SWE (mm) on February 14, 1989, derived from SSM/I data using NWS/GTV algorithm. Numerical values are coincident ground snow survey measurements (mm).

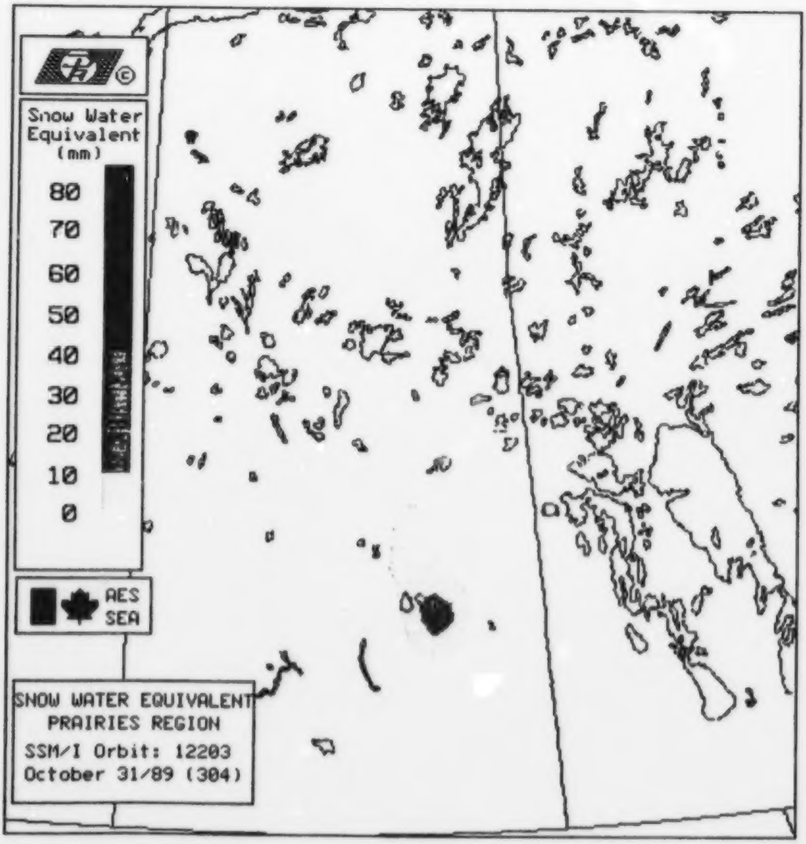
Snow Water
Equivalent
(mm)
80
70
60
50
40
30
20
10
0
AES
SEA
SNOW WATER EQUIVALENT
PRAIRIES REGION
SSM/I Orbit: 12203
October 31/89 (304)

Figure 3: Distribution of SWE (mm) over southern Prairies on October 31, 1989, as derived from SSM/I data using NWS/GTV algorithm.

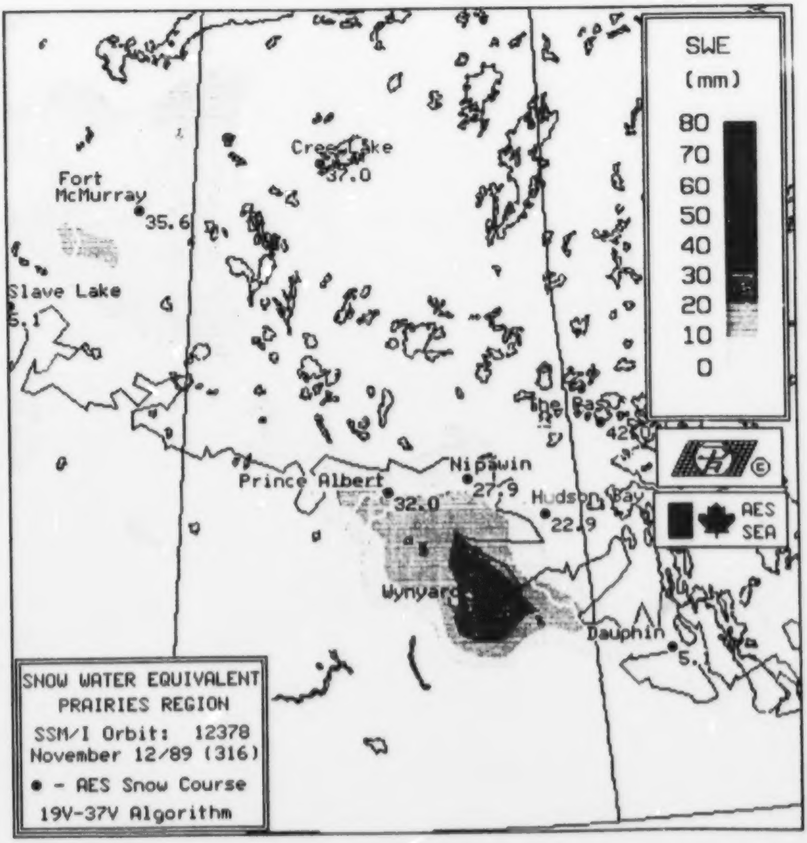
SWE
(mm)
80
70
60
50
40
30
20
10
0
Cree Lake
37.0
Fort McMurray
35.6
Slave Lake
5.1
The Pas
42
Nipawin
27.9
Prince Albert
32.0
Hudson Bay
22.9
Wynyard
Dauphin
5.
AES
SEA
SNOW WATER EQUIVALENT
PRAIRIES REGION
SSM/I Orbit: 12378
November 12/89 (316)
● - AES Snow Course
19V-37V Algorithm

Figure 4: Distribution of SWE (mm) over Prairie Provinces on November 12, 1989, as derived from SSM/I data using NWS/GTV algorithm.

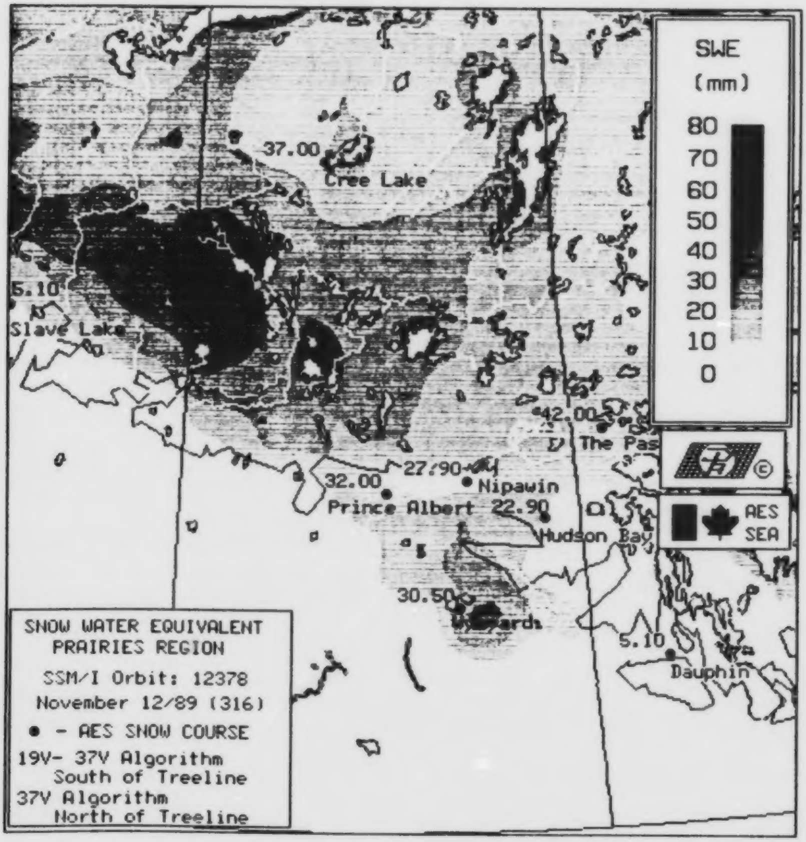
SWE
(mm)
80
70
60
50
40
30
20
10
0
AES
SEA
37.00
Cree Lake
5.10
Slave Lake
42.00
The Pas
32.00
27.90
Nipawin
Prince Albert
22.90
Hudson Bay
30.50
5.10
Dauphin
SNOW WATER EQUIVALENT
PRAIRIES REGION
SSM/I Orbit: 12378
November 12/89 (316)
● - AES SNOW COURSE
19V- 37V Algorithm
South of Treeline
37V Algorithm
North of Treeline

Figure 5: Distribution of SWE (mm) over Prairie Provinces on November 12, 1989, as derived from SSM/I data using NWS/GTV algorithm south of the treeline and NWS/37V algorithm north of the treeline.

Questions and Answers

Robert Miller: Did you notice big differences between different types of snow, when there is melting, when there's wet snow?

Barry Goodison: Yes. Certainly for wet snow, once there's any bit of moisture on the surface, passive micro-wave can not be used to detect snow-water equivalent at depth. That is the nature of the dielectric properties. Robert refered to it in the morning in the case of active; it's similar for passive. You can not detect quantitatively the amount of snow, but what you can tell is the onset of melt or melt-refreeze events.

Rick Soulis: How deep do you think you can get?

Barry Goodison: The deepest we have mapped is 109 millimeters. This was obtained in Manitoba in the Riding Mountain Park, a few years ago. We have not been getting those high ends since this experiment started. The highest we've seen is 110 mm.

Jean-Pierre Fortin: Considering the accuracy for passive micro-wave, what would be the smallest basin for which you could obtain data?

Barry Goodison: I think we could derive a number for a small basin, but I wouldn't put a lot of faith in it. I would think you would have to be on the order of 2500 square kilometers. I would want a number of pixels in the area, to have some faith in the estimate. If on EOS we get a micro-wave radiometer up in orbit with a pixel size of about 10 by 10 kilometers, that will change things and you will be able to get the smaller basins.

Unidentified: The wind causes a fair bit of snow distribution, have you been able to pick that up?

Barry Goodison: No. We have done individual case studies of particular weather events, trying to detect through snow storms and we did not find an effect. In this cold environment, even though it is snowing, it's still very low moisture in the atmosphere. We still penetrated and got similar numbers. Snow in the atmosphere did not seem to cause a big effect. I have not seen anything on a map that I could honestly say "that is because of redistribution". That does not mean to say it does not occur, just that I have not been able to pick it up. This is probably because often redistribution is associated with a snow event and therefore you have a mixed situation that you are looking at.

Robert Miller: Back to the basin question. Assuming you did have a huge basin, wouldn't your algorithm kind of "go to pot" because you did not have the fifty degree angle with the earth, assuming you were in a mountainous area.

Barry Goodison: For example, [although] we have not tried to go to a mountainous basin; there are some maps out there showing 0 or 10 millimeters, which you don't believe. In the mountains that we have been working in we have not had sucessful results with this particular algorithm. Probably the point I should stress here is I am a strong believer that we will need regional algorithms. It is not just for this sensor or this element. It applies to all the sensors, I think, and elements that we are trying to derive. So, what may be suitable for central North America, may not apply to a boreal forest zone or an arctic zone. They may work or they may not. The global algorithm is good for a start, but I think it is tenuous if you are really trying to pull geophysical numbers out.

Average Areal Snow Water Equivalent Determination in a Mountain Basin Using Passive Microwave Satellite Data

Albert Rango
USDA Hydrology Laboratory
Beltsville, Maryland 20705 U.S.A.

ABSTRACT

Satellite microwave data have been used to evaluate the average areal water equivalent of snow cover in the mountainous Rio Grande basin (3419 km^2) of Colorado. Because of poor satellite passive microwave resolution (approximately 25 km x 25 km), it took only eight satellite footprints to cover the entire Rio Grande basin. The average microwave values from these footprints on April 1 was correlated with areal water equivalent data for the basin obtained by two methods, namely, from contoured values of point measurements and from elevation-zone water volume values generated by a reliable snowmelt-runoff model. Although there was a high correlation between the model and contoured values, the areal water equivalent values derived from the model consistently exceeded the contoured values. The model values were higher most likely because the conventional point measurement sites, from which the contoured values were derived, were concentrated in the lower elevations of the basin.

A significant relationship between the difference in microwave brightness temperature at two different frequencies (37 and 18 GHz) and the basin-wide average snow water equivalent value was obtained. Either the contoured or model values could have been used, but the model values were chosen for the relationship because of the inclusion of information from the higher elevation zones. This relationship was developed for the period 1979-1985 using

Nimbus-7 SMMR satellite data and snowmelt runoff model simulations for the same years. The relationship and the satellite microwave data for two reserved test years, 1986 and 1987, were used to estimate the average areal water equivalent of the snow cover to within 15% of the observed value. Subsequent tests indicated that the results would not always be as good in other years, especially extreme years.

The approach is not ready for true operational use because of several problems. The resolution is still too poor from space to give anything but an average value for an entire basin. Even the approach used to obtain this value needs to be refined by acquiring additional years for the relationship and testing in other basins. As resolutions improve with future sensors, the improved microwave data could be used on smaller basins and for determining the snow water equivalent of individual elevation zones. Such data could be used for selecting elevation zone snow cover depletion curves for particular years, for use in snowmelt-runoff forecasts, or for directly inputting areal water equivalent data to snowmelt-runoff models.

REFERENCE

Rango, A., Martinec, J., Chang, A.T.C., Foster, J. L., and van Katwijk, V., 1989: Average areal water equivalent of snow in a mountain basin using microwave and visible satellite data, IEEE Transactions on Geoscience and Remote Sensing, GE-27(6).

ANALYSIS OF MOS-1 MICROWAVE SCANNING RADIOMETER DATA FOR CANADIAN PRAIRIE SNOW COVER

A.E. Walker and S.A. Gray
Ph.D. Associates Inc.
4700 Keele Street
North York, Ontario
M3J 1P3

B.E. Goodison
Atmospheric Environment Service
4905 Dufferin Street
Downsview, Ontario
M3H 5T4

R.A. O'Neil
Canada Centre for Remote Sensing
2464 Sheffield Road
Ottawa, Ontario
K1A 0Y7

INTRODUCTION

In the remote sensing of snow cover, passive microwave sensors have the advantages of all-weather and day-or-night sensing capabilities. Recent investigations (Goodison, 1989; Goodison et al., 1986, Kunzi et al., 1982; Foster et al., 1980) have demonstrated the potential of satellite-based passive microwave sensors, such as the NIMBUS-5 and 6 ESMR, the NIMBUS-7 SMMR and the DMSP SSM/I, to monitor the areal extent, depth and water equivalent of snow.

The Marine Observational Satellite-1 (MOS-1) was launched by Japan in February 1987, with a Microwave Scanning Radiometer (MSR) as one of three sensors on board. Under a special agreement with the National Space Development Agency of Japan (NASDA), the Canada Centre for Remote Sensing (CCRS) began receiving MOS-1 data at its Gatineau satellite receiving station in May 1988. As part of the Canadian MOS-1 Project (Butlin et al., 1989) a collaborative project involving Ph.D. Associates Inc., CCRS and the Atmospheric Environment Service (AES) was established to investigate the hydrologic applications of MSR data for the Canadian Prairies. The application of the MSR to snow cover sensing is an important aspect of this investigation.

This paper focuses on a preliminary evaluation of the MSR data with respect to the potential for deriving useful snow cover information for the Canadian Prairies. This evaluation is based on comparisons of the MSR brightness temperatures to coincident data obtained from the Special Sensor Microwave/ Imager (SSM/I) on board the U.S. Defense Meteorological Satellite Program (DMSP) F-8 satellite and SSM/I-derived values of snow water equivalent (SWE). Values of SWE from snow suveys (AES and Provincial Agencies) are incorporated into the comparisons to represent ground-truth information. Coincident data from the MOS-1 Visible and Thermal Infrared Radiometer (VTIR) will eventually be incorporated into the project in order to determine if the combination of infrared and microwave data provides improved snow cover information.

MSR AND SSM/I DATA SETS

The MOS-1 MSR is a dual-frequency radiometer which measures earth-emitted microwave radiation at 23 and 31 GHz. Other sensor characteristics include a swath width of 317 km and data resolutions of 23 km (31 GHz) and 32 km (23 GHz). The MOS-1 satellite has a sun-synchronous, near-polar orbit with a local descending time between 10:00 and 11:00 am and repeat coverage every 17 days. A detailed description of the MOS-1 satellite and the MSR is available in NASDA (1987).

For the purposes of this investigation, MOS-1 data were collected by CCRS at the Gatineau receiving station for selected tracks (Paths 179-187) over the Canadian Prairies during February and March 1989. Processed data in the form of brightness temperatures in degrees Kelvin were provided on CCT. Latitude/longitude locations for each of the scan data points were also included, in order that the data could be displayed on the Geographic Analysis and Display System (GADS) (Ph.D. Asscociates, 1989).

The DMSP SSM/I orbits selected for comparison to the MSR data were acquired in near real-time from the Civilian Navy/ NOAA Oceanographic Data Distribution System (CNODDS) by Ph.D. Associates Inc. The SSM/I sensor operates at four frequencies (19.3, 22.2, 37.0 and 85.5 GHz) with a swath width of 1400 km and ground resolution cells of 25 km x 25 km at 37 GHz and 12.5 km x 12.5 km at 85 GHz. With an average of two orbits a day over the Canadian Prairies, repeat coverage is available for some areas on a daily basis. For this investigation, orbits were chosen which best coincided with the MSR orbits in terms of time and ground coverage.

ANALYSIS OF MSR DATA FOR PRAIRIES SNOW COVER

To date, a total of six MSR orbits have been examined for Canadian Prairies snow cover applications. Table 1 lists the dates of these orbits and indicates the Provincial area of coverage of each one. Also noted are the corresponding SSM/I orbits.

Table 1

MSR and SSM/I Data Sets Analysed for Prairies Snow Cover

Date	MSR Path	Provincial Coverage	SSM/I Orbit
Day 038/89	180	Manitoba	8451
Day 039/89	181	Manitoba	8465
Day 041/89	183	S.W. Manitoba and S.E. Saskatchewan	8493
Day 042/89	184	S.E. Saskatchewan	8507
Day 071/89	179	S.E. Manitoba	8924
Day 073/89	180	Manitoba	8945

The display and analysis of the MSR and SSM/I data sets were facilitated using an IBM PC-based Geographic Analysis and Display System (GADS). For each of the days listed in Table 1 the MSR V31 and H23 GHz brightness temperatures were contoured separately on a Prairies base map. Figure 1 depicts V31 GHz brightness temperature contours for Day 041/89 (February 10) from MOS-1 Path 183. The patterns present over the swath may be generally related to the amount of snow present on the ground. When the H23 GHz values were contoured, there was less variation in brightness temperature observed over the swath. Since the microwave response to snow cover is frequency dependant, the H23 GHz channel would be less sensitive to the snow than the higher frequency V31 GHz channel.

In order to compare the MSR microwave data to the coincident SSM/I data, the SSM/I brightness temperatures were contoured on the same geographic base map as the MSR data. Based on qualitative comparisons, the MSR V31 GHz and SSM/I V37 GHz patterns appeared similar, although the V37 GHz brightness temperatures were approximately 10 degrees higher than the V31 GHz values. Areas of highs and lows were observed to coincide on the geographic display of the two data sets.

In relating the MSR data to the snow cover on the ground, values of snow water equivalent (SWE) were derived from the SSM/I data using an algorithm which is currently being used to provide operational Prairie snow maps (Goodison, 1989; Goodison et al., 1990). Figure 2 presents an overlay of SSM/I snow water equivalent contours on MSR V31 GHz brightness temperature data for S.E. Saskatchewan and S.W. Manitoba on Day 41/89, which provides a visual comparison of the two data sets. In several places on the image the shapes formed by the SWE contours match very closely the MSR brightness temperature contours, with highest and lowest SWE values corresponding to the lowest and highest brightness temperatures, respectively. This would indicate that the variability in snow cover is reflected in the MSR V31 GHz microwave data. It is important to note that in this case the SSM/I data are shifted slightly to the northeast due to a geolocation problem associated with data from the sensor. This problem was subsequently corrected by the U.S. Navy in the summer of 1989.

Figure 3 presents a second example of the MSR and SSM/I SWE comparison for Day 073/89 (March 14) over S.W. Manitoba. The contour patterns associated with the two data sets are generally comparable. The spot values indicate SWE values measured during the March 13-17, 1989 ground snow surveys. In the regions where the SSM/I SWE contours indicate 90-100+ mm the ground measured SWE values are much lower. Above zero temperatures were recorded during the days previous to March 14, which may have caused some thawing and refreezing to take place. If ice layers form in the snow pack as a result of this refreezing, increased attenuation of the microwave radiation will occur and over-estimations of SWE may result. In Figure 3, the areas where the SSM/I SWE values are the highest also coincide with the lowest MSR brightness temperatures. The two microwave sensors therefore appear to have the same behavior under these conditions.

The relationship between the MSR brightness temperatures and the SSM/I SWE values was further investigated by regridding the SSM/I values onto the MSR data locations. A data subset was extracted from each of the 6 MSR swaths consisting of values located over the non-forested southern portions of Manitoba and Saskatchewan. A regression analysis was applied to each of the data subsets and correlation coefficients were determined for the MSR V31 GHz and H23 GHz brightness temperatures versus the SSM/I SWE values. Overall, the V31 GHz versus SSM/I SWE comparisons exhibited higher correlation coefficients than H23 GHz versus SSM/I SWE; reaffirming the greater sensitivity of the V31 GHz microwave response to snow cover. Figures 4a and 4b present two examples of these comparisons for Day 039/89 (February 8) and Day 073/89 (March 14), respectively. Both graphs depict decreasing trends in MSR V31 and H23 GHz brightness temperatures with increasing SSM/I SWE. The V31 GHz trends depict the strongest decreases, which indicate that this MSR frequency has the higher potential for deriving useful snow cover information, such as snow water equivalent.

CONCLUSIONS

The evaluation of MOS-1 MSR passive microwave data for Canadian Prairies snow cover applications is an ongoing project. The preliminary results presented in this paper are very encouraging and indicate that the V31 GHz channel has the greater sensitivity to snow cover. An evaluation of the MSR's potential for snow water equivalent algorithm development will be made at the conclusion of this project. Further analysis is planned using additional MSR orbits from February 1989 and March 1990.

Another aspect of the MSR evaluation involves a comparison of the microwave data with coincident thermal infrared data obtained from the MOS-1 Visible and Thermal Infrared Radiometer (VTIR). The overall objective is to determine if the interpretation of the passive microwave data can be improved with the incorporation of thermal infrared data.

The investigation described in this paper involves the comparison of coincident data from two microwave radiometers which are on board separate satellites. This represents a unique research opportunity, which may contribute to a better understanding and interpretation of passive microwave satellite data.

ACKNOWLEDGEMENTS

This research work described in this paper was done under DSS contract No. 18SR.23413-8-7192.

REFERENCES

Butlin, T., J. Lam, M. Manore and R.A. O'Neil, (1989) "The Canadian MOS-1 Project", Proceedings IGARSS '89, Vancouver, Canada, July 10-14, 1989, Vol. 2, pp. 982-986.

Foster, J.L., A. Rango, D.K. Hall, A.T.C. Chang, L.J. Allison and B.C. Diesen III, (1980) "Snowpack Monitoring in North America and Eurasia Using Passive Microwave Satellite Data", Remote Sensing of Environment, Vol. 10, pp. 285-298.

Goodison, B.E., (1989) "Determination of Areal Snow Water Equivalent on the Canadian Prairies Using Passive Microwave Satellite Data", Proceedings IGARSS '89, Vancouver, Canada, July 10-14, 1989, Vol. 3, pp. 1243-1244.

Goodison , B.E., I. Rubinstein, F.W. Thirkettle and E.J. Langham, (1986) "Determination of Snow Water Equivalent on the Canadian Prairies Using Microwave Radiometry", in Modelling Snowmelt Induced Processes, Proceedings of the Budapest Symposium, July, IAHS Publication No. 155, pp. 163-173.

Goodison, B.E., A.E. Walker and F.W. Thirkettle, (1990) "Determination of Snow Water Equivalent on the Canadian Prairies Using Near Real-Time Passive Microwave Data", Submitted to Proceedings of Workshop on Application of Remote Sensing in Hydrology, Saskatoon, Saskatchewan, February 13-14, 1990.

Kunzi, K.F., S. Patil and H. Rott, (1982) "Snow Cover Parameters Retrieved from NIMBUS-7 Scanning Multi-Channel Microwave Radiometer (SMMR) Data", IEEE Trans. Geosc. Rem. Sens., GE-20(4), pp. 453-467.

NASDA, (1987) "MOS-1 Data User's Handbook", National Space Development Agency of Japan, Earth Observation Center.

Ph.D. Associates, (1989) "Technote: GADS", Ph.D. Associates Technote Series, No. 1989-5.

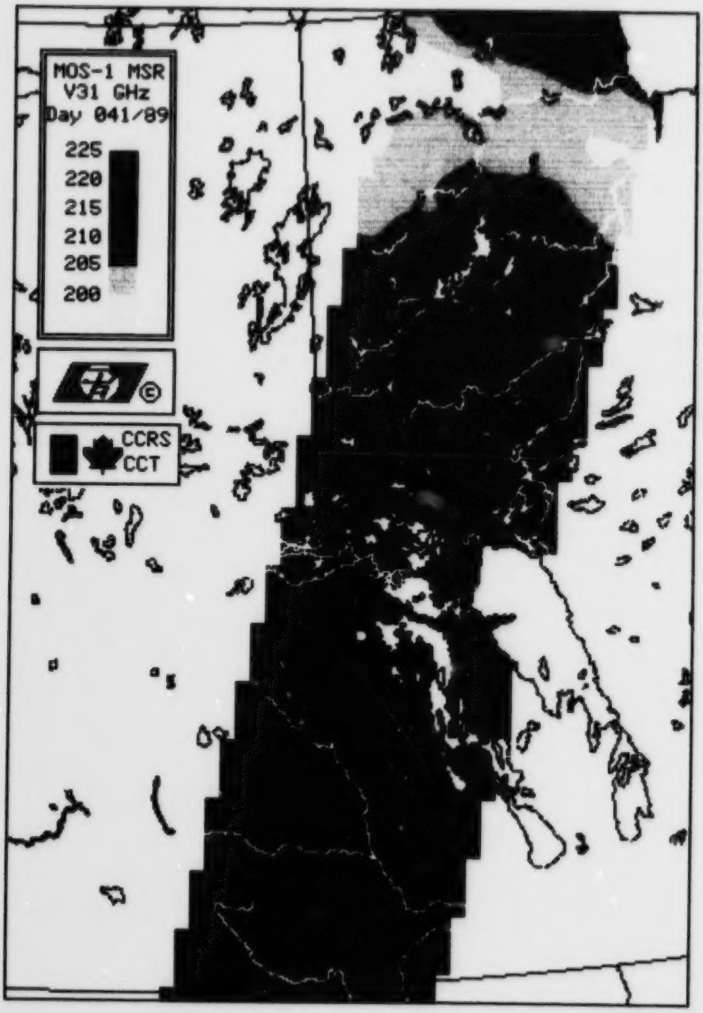
MOS-1 MSR
V31 GHz
Day 041/89
225
220
215
210
205
200
CCRS
CCT

Figure 1. MOS-1 MSR V31 GHz brightness temperature contours over Manitoba and S.W. Saskatchewan (MOS-1 Path 183), February 10, 1989.

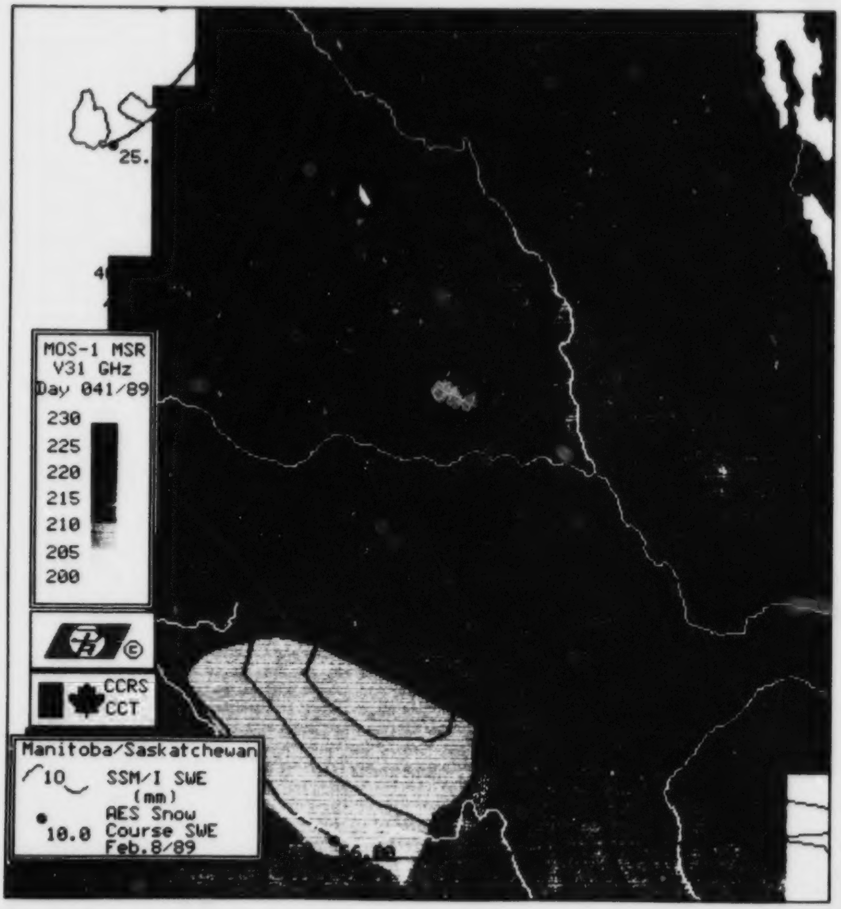
MOS-1 MSR
V31 GHz
Day 041/89
230
225
220
215
210
205
200
CCRS
CCT
Manitoba/Saskatchewan
10 SSM/I SWE (mm)
AES Snow Course SWE Feb.8/89
10.0
25.

Figure 2. Overlay of SSM/I SWE contours (black lines) on MSR V31 GHz brightness temperature contours, S.E. Saskatchewan and S.W. Manitoba (MOS-1 Path 183), February 10, 1989.

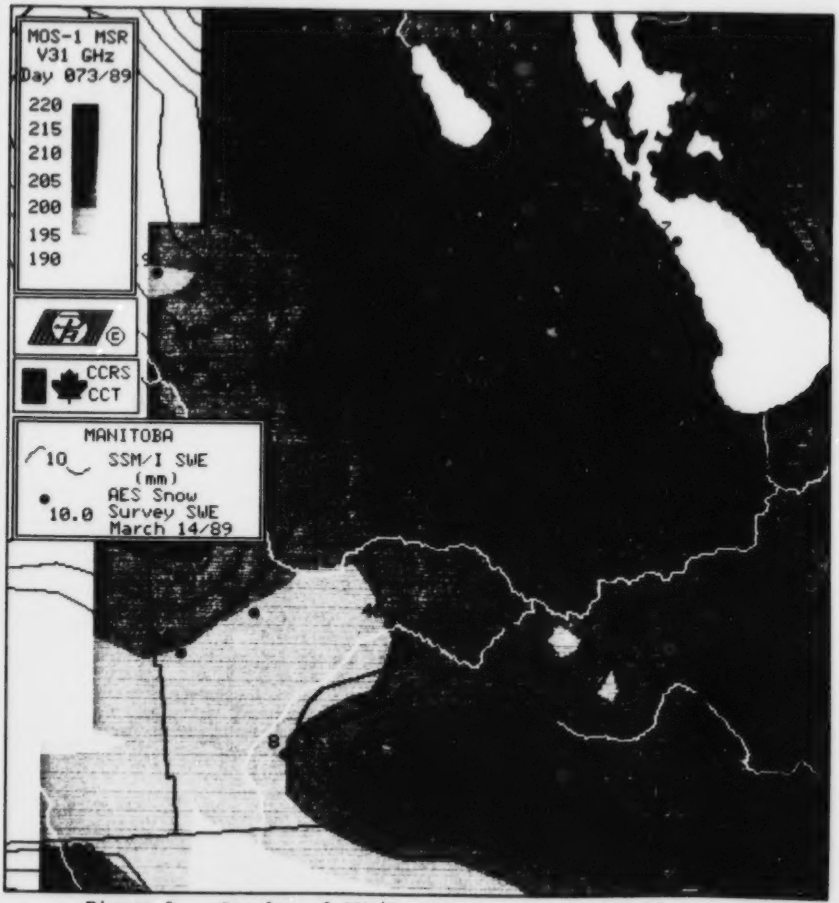
MOS-1 MSR
V31 GHz
Day 073/89
220
215
210
205
200
195
190
CCRS
CCT
MANITOBA
10
SSM/I SWE
(mm)
AES Snow
10.0
Survey SWE
March 14/89
8

Figure 3. Overlay of SSM/I SWE contours (black lines) on MSR V31 GHz brightness temperature contours, S.W. Manitoba (MOS-1 Path 180), March 14, 1989. The spot values indicate SWE values measured at ground survey stations during the week of March 13-17, 1989.

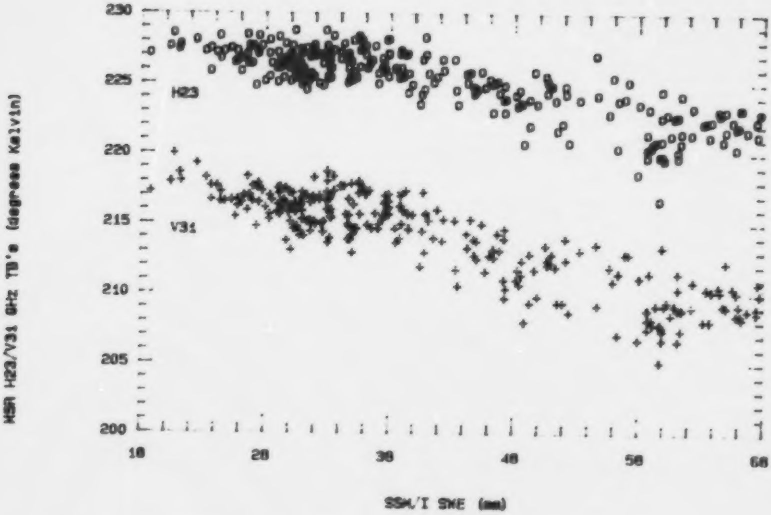

Figure 4a. Relationship between MSR H23 and V31 GHz brightness temperatures and SSM/I-derived SWE values over Southern Manitoba, February 8, 1989.

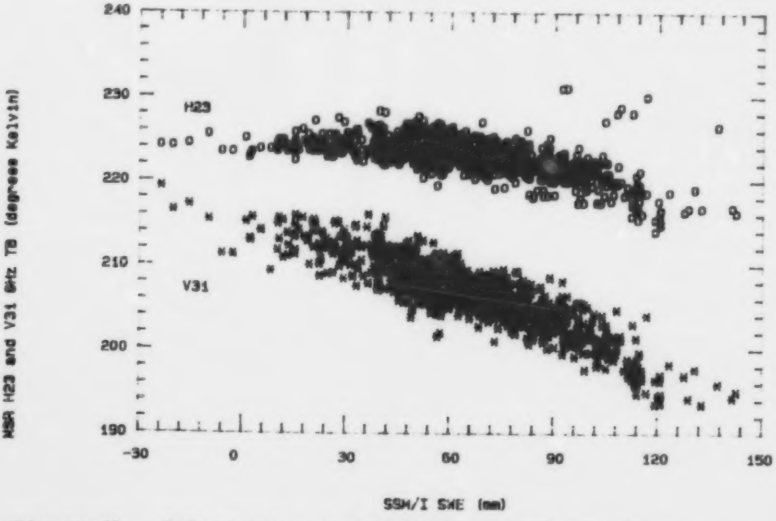

Figure 4b. Relationship between MSR H23 and V31 GHz brightness temperatures and SSM/I-derived SWE values over Southern Manitoba, March 14, 1989.

Questions and Answers

Unidentified: What is the repeat coverage?

Anne Walker: There is 17 day repeat coverage. In fact, when we asked for data this week, for example, we could only get data for tomorrow and Friday, that was all that they could collect for us and that is only over Manitoba. What we try to do when we ask for this data is to coincide with the snow surveys that are being done, so that we can make a proper comparison of data types.

Tony Wankiewicz: Was there a change in snowfall or was it fairly constant?

Anne Walker: The February data that we looked at was all from consecutive days, so it was all pretty much the same type of snow cover.

Tony Wankiewicz: Is the snow pretty much constant in that region?

Anne Walker: Yes.

MICROWAVE SATELLITE SPRING RUNOFF CORRELATIONS

Anthony Wankiewicz

National Hydrology Research Institute
11 Innovation Blvd, Saskatoon, Canada S7N3H5

ABSTRACT

Winter microwave satellite observations are used to forecast spring runoff volumes from river basins in the Rocky Mountains and Plains. A significant multiple correlation was found with three Plains basins for forecasting runoff from winter microwave brightness and previous October streamflow. Significant correlations were also found with four large Rocky Mountain watersheds (median basin area 10000 km^2) for forecasting runoff from winter brightness only. The microwave fluctuations appeared to be localized to the 500 km scale of physiographic regions. Similar correlations were found for thirty-six small mountain watersheds (median area 250 km^2). Snowpack in High-Alpine basins, computed from runoff and precipitation measurements, was found to have a highly significant correlation of -0.92 with microwave brightness temperature. The significance of the microwave-runoff correlations for the Mountain and Plains watersheds is demonstrated by six different statistical tests.

1. INTRODUCTION

Since the first microwave satellite in the Nimbus series was launched in late 1972, the potential of microwave radiometry for monitoring winter snowpacks has become evident. The algorithms for determining snow water equivalent from microwave brightness have been investigated from airborne/satellite correlations with ground measurements, modeling of electromagnetic interaction with snow grains, and ground studies with truck mounted radiometers. Good results were shown early on for targets in the Plains region, in spite of difficulties in obtaining representative ground truth measurements.

An alternative test procedure is to correlate satellite microwave observations of watersheds with the runoff measured at the basin outlet. Since watershed spring runoff is a function of upstream snowpack conditions, runoff volume is a variable that could be representative of the basin area. Furthermore, significant correlations could have direct application to streamflow forecasting.

Historically, seasonal runoff has been forecast using correlations with many years of snow survey data. A typical case is May-August Bow River runoff at Banff, Alberta which has a correlation coefficient of $r = -0.68$ with April 1 snow course water equivalent for the period 1940-1959. Alternative methods of snowpack measurement, such as satellite observations, could similarly correlate with spring runoff. Whatever the method used, individual runoff years will be scattered about the regression line of runoff from snowpack, whenever r differs from + or - 1.0 in value. Reasons for this scatter usually include such factors as: (1) Late winter or early spring precipitation subsequent to the snow course measurements; (2) Losses to storage resulting from moisture deficits in soil and depressions during the previous fall; and (3) Evapotranspiration during the runoff period.

New methods of measurement are currently limited to shorter periods of record. A corollary to the existence of scatter about a regression from a long series of observations, is that the r-values of sample correlations (using shorter series taken from the population) will be distributed about the population r-value [Yevjevich, 1982]. For random sampling with N observations, the Fisher z-values, given by $z = 0.5 \ln (1+r)/(1-r)$, are normally distributed with a standard deviation of $1/(N-3)^{1/2}$. For short series, there will be a small scatter in r only for r-values quite different from zero. The significance level for a particular case can be computed from the z distribution.

The objective of this paper is to demonstrate spring runoff correlations with the four-years of winter observations by Nimbus 5 ESMR between 1973 and 1976. With N=4, the theoretical standard deviation for r-values is unity. The correlations will be shown to be significant for both Plains and Mountain watersheds.

2. RUNOFF AND MICROWAVE OBSERVATIONS

The two primary variables are spring runoff and microwave brightness temperature. To account for differences in timing of spring runoff from basins in different regions, runoff volumes are computed for periods characteristic of the freshet for that region. Spring runoff is defined to be the total May to August runoff for mountain basins; and total April and May runoff for Foothills and Plateaus basins. Direct computation of snowmelt was performed for the short and sudden melt periods on the Plains, using a hydrograph separation technique.

The late-winter microwave brightness for a basin, is taken to be the average January and February brightness of all microwave grid cells with centres located within the watershed. Microwave brightness temperatures were obtained from Nimbus 5 ESMR magnetic tapes decribed in Parkinson et al [1987a]. The data provided are monthly averages of 19 GHz nadir brightness temperatures, from observations taken at noon and midnight local time. The microwave observations are displayed on a polar stereographic grid with 30 km X 30 km cells. (March was not used because satellite observations are missing for 1973). This paper uses the Northern Oceans calibration for the microwave observations, described in Appendix A of Parkinson et al [1987b], unless otherwise noted.

3. LARGE WATERSHEDS IN FIVE DIFFERENT REGIONS

An examination of the full range in microwave-streamflow correlations requires an investigation of a large number of watersheds with a wide variety of relief and vegetation cover. The location of seventeen large gauged watersheds in Western Canada are shown in Figure 1. The basins have a median area of 8000 km^2 and are located in five different physiographic regions: Coast Mountains, Rocky Mountains, Foothills, Plateaus, and Plains [Table 1, Wankiewicz, 1989]. Unregulated basins between 2500 and 25000 km^2 were selected for analysis, if they contained less than 7% lake area on a 1:2000000 map.

Intra-regional comparisons between Rocky Mountain watersheds shows that the average cross-correlation of the runoff series was 0.96, for the years 1973-76. The stream runoff in this region is highly correlated from one basin to another ("average r" is the r-value that corresponds to mean z-value in a set of correlations). Large cross-correlations were also obtained for basins in the Coast Mountains; basins in the Foothills, and basins in the Plateaus. Consequently the equivalent sample size from each region is only N=4, i.e. four years. An exception in these intra-regional comparisons is the low cross-correlation r between the three Plains basins, 0.42, due to the large separation among them. The equivalent sample size, for the Plains region only, is assumed to be N=12, i.e.four years by three basins. Inter-regional comparisons between basins in different regions had an average cross-correlation r of 0.1. The different regions have independent spring runoffs.

A significant feature of the 1973-76 observation period is the complete lack of any positive serial correlation between successive annual runoffs. In fact the median basin lag-one autocorrelations in each region are either close to zero or anti-correlated. Consequently the four annual spring runoffs were independent in time. Furthermore, both extreme floods and dry spells were recorded in all regions over the four-year period, so that the information content in the four-year series is greater than would be expected for such a short series.

Microwave correlations, in contrast to those from snow courses, would be expected to display a negative slope with runoff. An increasing thickness of snow results in decreasing microwave emission from the underlying ground; because of greater backscatter of upwelling thermal energy by microwave-length sized snow grains. The microwave and runoff observations for 1973-76 result in the correlations summerized in Table 1. The Rocky Mountains and Foothills basins have mean correlation coefficients r of -0.76 and -0.80, respectively. These r values have significance levels SL of 15%, i.e. the null hypothesis results in r-values equal of higher than those found, only 15 times out of 100. Because the runoff is correlated between basins in each region, the sample size is effectively 1 basin and 4 independent years. The Plains watersheds have mean r-values of -0.44. Even this lower r has a SL of 20%, because there are three uncorrelated Plains basins for each of 4 independent years. The over-all average r for all seventeen basins is -0.35, with a SL=20% for five independent regions.

The higher absolute r-values for the Rocky Mountains and Foothills results from the higher runoff to precipitation ratios for those basins, compared to the Plains. The median annual runoff ratios are 76% in the Rocky Mountains; 44% in the Foothills; 21% in the Plateaus; and only 2% in the Plains. Although the Coast Mountains have runoff ratios approaching 100%, no significant correlation was found, perhaps due to their proximity to sources of interfering liquid water clouds.

4. DISCUSSION OF ERRORS

The median range in winter microwave brightness on the Plains was 5 K because the median tree cover is only 4%. The range in brightness for the Rocky Mountains was reduced to 3.5 K because of interfering vegetation below the tree line in those watersheds. Differences between microwave observations at different points in time and space are believed to be accurate to better than 1 K [Kunzi et al, 1976].

To check the accuracy of microwave brightness temperatures, cross-correlations of winter microwave brightness were computed between pairs of basins. Any significant inter-annual change in sensor calibration would appear as a long-range spatial persistence in microwave-microwave correlation between widely separated pairs of basins. Figure 2 shows this cross-correlation as a function of basin separation for observations calibrated against the Northern Ocean targets. The left axis is the Fisher z transformation of r-values. The All-basins trend (solid line) is a third-order polynomial regression using 145 basin pairs. A trend was also computed for the Rockies and Foothills (dash-dot line), separately, because of the smaller inter-annual variation in that region. Additional trends are also shown for correlations that use the 1973-76 observations calibrated against an alternative target: the Greenland Icecap.

All the trends are consistent with a localization in the microwave-microwave cross-correlations, with a correlation distance of 500 km. The significance of this localization is SL=5%, assuming five independent regions. The lack of long range persistence means that no calibration bias can be detected. The two calibrations produce results too similar for this method to discriminate between them. (The slight negative correlation at longer distances is not significant because of few basin pairs at large distances).

The localization scale for microwave variations would be related to localization scales in the underlying physical variable. Cross correlations between basins were also computed for annual snowpack variations, which presumably result in microwave brightness variations. The November-February snowfall from 15 Nipher snow gauges across Western Canada showed a localization scale of about

1500 km. March 1 snow-course water-equivalent from 10 snow course networks and 11 individual snow courses, also shows a localization scale of 1500 km.

The fact that microwave correlation is localized on a smaller scale than snowpack probably reflects the effect of regionalization on snowpack signatures. 500 km is about the scale of physiographic regions in the area. 500 km is also the scale for localization of cross-correlations of spring runoff between basin pairs. As seen in Section 3, basin spring runoff is uncorrelated between different regions.

5. PLAINS WATERSHEDS

The three Plains watersheds investigated have median basin areas of 3500 km^2. Iron Creek basin, 3500 km^2, is only 4% forest covered, has 5% frozen pond area at maximum stage, and an annual runoff/precipitation ratio of only 2%. Antler River basin, 3200 km^2, is 0% forest covered, and the same frozen pond area and runoff ratio as Iron Creek. Swan River basin, 4200 km^2, is 56% forest covered, with similar pond area as the others, and a runoff ratio of 9%. The low runoff ratios mean that antecedent moisture conditions in the fall are just as important to spring runoff as winter snowpack. For example, a wet fall that saturates basin storage, greatly increases the potential for large spring runoff volumes from snowmelt.

The relationship between winter microwave brightness and spring snowmelt runoff is shown in Figure 3 for the Plains watersheds. A third variable, previous October streamflow in mm (an antecedent moisture index, AMI), is also shown beside each symbol and in isopleths drawn across the Figure. There is a good multiple correlation between fall AMI, winter brightness, and spring runoff. The multiple correlation coefficient R is 0.75. The SL of R is 5%, assuming the three basins are independent. The independence assumption is supported by inter-basin correlation coefficients for the 4-year data series that average only 0.00, +0.07 and +0.42 for the three respective variables, and have no apparent pattern.

The significance of the multiple correlation for the three basins suggest that microwave satellite observations can be applied to spring runoff forecasing, if estimates are available for the AMI. Wankiewicz (1990) has shown that a moisture index, indicated by monthly streamflow, can be estimated using Nimbus 5 ESMR for the snow-free period, from microwave emissivity of Iron Creek and Antler River watersheds. The potential exists for spring runoff forecasting for ungauged watersheds on the Plains using only microwave observations. A comparison study using snow course data was not done because of there were no courses near Iron Creek.

6. LARGE MOUNTAIN WATERSHEDS

The four large Rocky Mountain watersheds investigated have median basin areas of 10000 km^2. Fraser River basin, 18000 km^2, is 30% unforested Alpine, and has an annual runoff/precipitation ratio of 91%. Athabaska River basin, 9800 km^2, is 44% Alpine, and has a runoff ratio of 82%. Columbia River basin, 9700 km^2, is 26% Alpine, and has a runoff ratio of 59%. Kootenay River basin, 5400 km^2, is 25% Alpine, and has a runoff ratio of 71%. The high runoff ratios mean that snowpack measurements should be highly correlated with spring runoff. The median Alpine area is 28% for these large basins, so at least this fraction of the snow is observable by satellite, without interference from forest cover.

Rocky Mountain spring runoff correlations are compared in Figure 4, using both March 1 snow course measurements and Jan-Feb microwave brightness observations. (Each correlation line is a bisector of a regression of runoff from snowpack and regression of snowpack from runoff). The conventional snow-course runoff correlations (left diagram) for 1973-76 have a mean r of +0.90 with a significance level SL= 5%. Precipitation subsequent to the snow measurement date would produce scatter in the correlation with runoff. An analysis of variance was performed on long-term monthly precipitation, using accumulated values up to a March 1 measurement date and subsequent precipitation to the end of the runoff period. This analysis suggest that the large r-value for snow courses is a sampling fluctuation for the short 4-year period; a value of less then +0.81 would be more consistent with long-term seasonal precipitation records.

By comparison, the microwave runoff correlations have an r of -0.75 with and SL=15%. This value is close to that suggested by an analysis of variance (less than -0.74), for the Jan-Feb satellite observation period. Comparison of r-values between the snow course and microwave methods shows that a single-channel microwave radiometer is almost as good as ground measurements of snowpack for forecasting spring runoff from large watersheds.

7. SMALL MOUNTAIN WATERSHEDS

Thirty-six small watersheds in the Rocky Mountains and Columbia Mountains were investigated to clarify the correlation properties of Mountain basins. The median area of the Mountain basins is 250 km^2, which is much smaller than the microwave grid area (900 km^2). The location of the small watersheds in shown in Figure 5. The shaded basins have Alpine areas in excess of 50% of the basin. The microwave brightness for each basin was computed from a weighted average of neighboring grids, with a weighting inversely proportional to the distance between grid centre and basin centroid. An example of a basin and ESMR grid set-up is shown in Figure 6 for the Whirlpool watershed near Jasper. The computed brightness is effectively a spatial average of the local microwave pattern evaluated at the watershed centroid.

Regression lines for the thirty basins are shown in Figure 7. Each line is a regression of May-August runoff for one basin from Jan-Feb brightness, for the period 1973-76. The correlation coefficients are: (1) Columbia Mountain basins, r=-0.72, SL=20%; Rocky Mountain basins, r=-0.71, SL=20%; and Foothills basins r=-0.69, SL=20%. These results show that the correlations established for the large Mountain basins also apply to small basins as well, even though they are smaller than the microwave grid squares. The regional similarities in slope of the regression lines for the gauged basins shown in Figure 7, suggest that this Figure may help define regressions for ungauged basins as well.

Winter microwave brightness should be a better indicator of observation period snowpack than spring runoff, since the latter includes precipitation subsequent to the observation. Subsequent precipitation could then be added afterwards, from weather network data. To show this, spring runoff was corrected for the effect of subsequent precipitation after the Jan-Feb microwave observations. The estimate of snowpack, ES, is that portion of total precipitation prior to the mid-winter observation. ES was calculated from ES = R X 0.33(AP1+AP2+AP3)/(TP). R is the May-August runoff observed at the basin outlet. The AP's are accumulated precipitation previous to a microwave observation: AP1, Oct-Dec; AP2, Oct-Jan; and AP3, Oct-Feb. TP is total precipitation from October to August. Approximate precipitation values were obtained for each basin, from maps of monthly precipitation found in the Canada Atmospheric Environment Service's Monthly Record series.

The estimated snowpack correlations with microwave brightness are summarized in Table 2. The first line of the Table (All Basins) shows that both the total runoff and winter snowpack microwave correlations are significant, but a significant difference between the two cannot be established from the short record.

When the seven High Alpine basins are considered separately, however, the second line of the Table shows a definite improvement in snowpack over total runoff forecasting (High Alpine means Alpine area greater than 50% of the basin). The difference in r-values, from -0.69 to -0.92, has an SL=20%. The microwave snowpack r, -0.92, is highly significant for the High Alpine basins, SL= 5%. Improvement in the correlations is visually apparent in the comparison of microwave-runoff correlations vs microwave-snowpack correlations shown in Figure 8., for the High Alpine basins.

As a final test for significance, the above correlation of ES with brightness was recomputed for the High Alpine basins, this time using microwave observations calibrated against the Greenland Icefield target. This target should introduce different biases in the microwave data than any introduced by the Northern Oceans calibration. Nevertheless, the correlation retained its significance, with an r-value of -0.73 and an SL=20%. This shows the Mountain correlations are robust with respect to selection of calibration target.

8. CONCLUSIONS

The following conclusions may be drawn about the significance of microwave runoff correlations for Mountain and Plains watersheds. A stated significance level (SL) is the probability that the indicated correlation coefficient r (between two variables), or R (for multiple correlations) is a random fluctuation about a zero value (the Null Hypothesis).

1. Plains microwave correlations with spring runoff are significant by two different statistical tests.

1a. Null Hypothesis Rejection #1, SL=20%. r=-0.42 for microwave brightness vs spring runoff; using Plains basins correlations.

1b. Null Hypothesis Rejection #2, SL=2%. R=0.75 for multiple correlation with AMI; using Plains basins correlations.

2. Mountain microwave correlations with spring runoff are significant by four different statistical tests.

2a. Null Hypothesis rejection #1, SL=15%. r=-0.76 for microwave bightness vs spring runoff; using Rocky Mountain big-basin correlations.

2b. Null Hypothesis rejection #2, SL=5%. 500 km scale localization in microwave variation; using Western Canada inter-basin spatial correlation.

2c. Null Hypothesis rejection #3, SL=5%. r=-0.92 for runoff corrected for subsequent precipitation (mid-winter snowpack); using High Alpine small-basin correlations.

2d. Null Hypothesis rejection #4, SL=20%. r=-0.73 for Greenland Icefield calibration; using High Alpine small-basin correlations.

REFERENCES

Kunzi, K., S. Patil and H. Rott, 1982. "Snow cover parameters retrieved from Nimbus-7 SMMR data", IEEE TRANS. GEOSCI. REMOTE SENSING, vol. 20, no. 4, pp. 452-467.

Parkinson, C., J. Comiso and H. Zwally, 1987a. SATELLITE-DERIVED ICE DATA SETS NO.2: ARCTIC MONTHLY AVERAGE MICROWAVE BRIGHTNESS TEMPERATURES AND SEA ICE CONCENTRATIONS, 1973-1976, NASA Technical Memorandum 87825, Washington D.C., 38pp.

Parkinson, C., J. Comiso, H. Zwally, D. Cavalieri, P. Gloerson and W. Campbell, 1987b. ARCTIC SEA ICE, 1973-1976: SATELLITE PASSIVE-MICROWAVE OBSERVATIONS, NASA-SP-489, Washington D.C., 296pp.

Wankiewicz, A., 1989. "Microwave satellite forecasting of snowmelt runoff", IGARSS'89, Volume 3, 1235-1238.

Wankiewicz, A., 1989. "Watershed Moisture Monitoring by Microwave Satellite", IGARSS'90, In Press.

TABLE 1 MICROWAVE SPRING-RUNOFF CORRELATIONS
Average for Regional Watersheds

REGION	CORR COEF r	NUMBER n	SIGNIF LEVEL % N=1	N=n
ROCKY MOUNTAINS	-0.76	4	15%	n/a
COAST MOUNTAINS	0.29	3	none	n/a
FOOTHILLS	-0.80	2	15%	n\a
PLAINS	-0.44	3	none	20%
PLATEAUS	0.18	4	none	n/a
West Road R.	-0.24	1	none	n/a
BASINS IN ALL 5 REGIONS	-0.35	5	n/a	20%

TABLE 2 MICROWAVE CORRELATIONS FOR FORECASTING TOTAL RUNOFF AND FOR ESTIMATING WINTER SNOWPACKS
Rocky and Columbia Mountain Watersheds

	MAY-AUG RUNOFF		JAN-FEB SNOWPACK	
	r	SL	r	SL
ALL BASINS	-0.72	20%	-0.77	20%
ALPINE > 50%	-0.69	20%	-0.92	5%

This difference for the Alpine
has an SL of 20%

ESTIMATED SNOWPACK = RUNOFF X ACCUMULATED PRECIP / TOTAL PRECIP

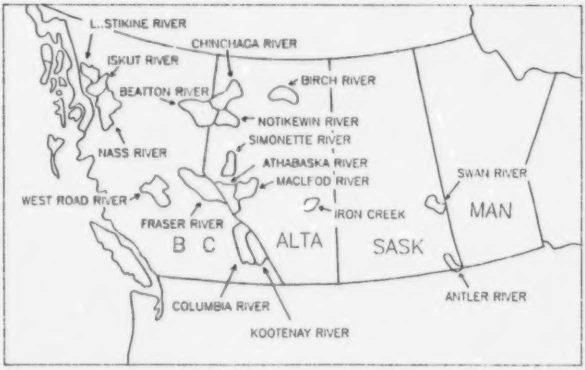
L..STIKINE RIVER
CHINCHAGA RIVER
ISKUT RIVER
BIRCH RIVER
BEATTON RIVER
NOTIKEWIN RIVER
SIMONETTE RIVER
NASS RIVER
ATHABASKA RIVER
MACLEOD RIVER
SWAN RIVER
WEST ROAD RIVER
IRON CREEK
MAN
FRASER RIVER
B C
ALTA
SASK
ANTLER RIVER
COLUMBIA RIVER
KOOTENAY RIVER

FIGURE 1. LOCATION OF REGIONAL WATERSHEDS

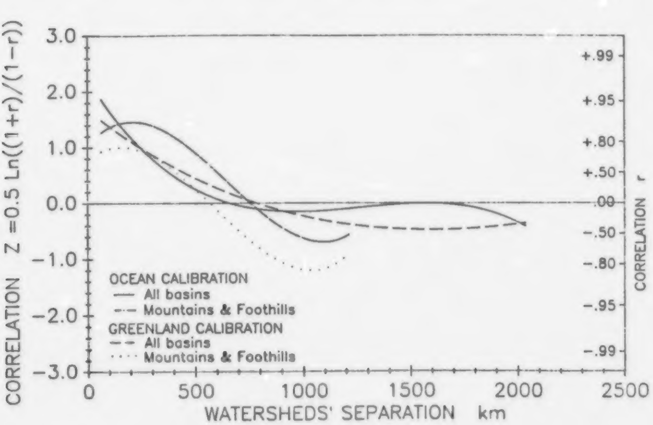

FIGURE 2. MICROWAVE BRIGHTNESS CROSS-CORRELATION BETWEEN PAIRS OF WATERSHEDS VS SEPARATION

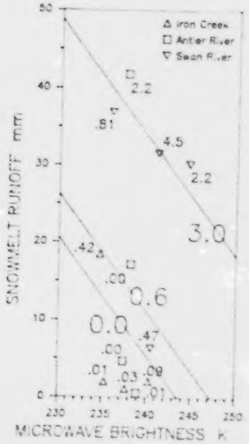

FIGURE 3. PLAINS SNOWMELT RUNOFF CORRELATIONS WITH JAN-MAR MICROWAVE OBSERVATIONS. ISOPLETHS ARE OCT. FLOWS (mm)

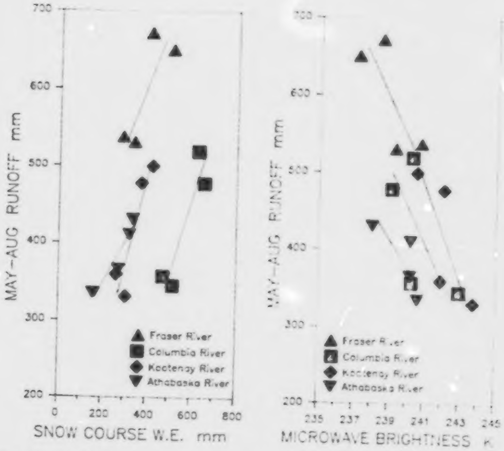

FIGURE 4. ROCKY MOUNTAIN SNOWMELT RUNOFF CORRELATIONS WITH MAR 1 SNOW COURSE MEASUREMENTS (LEFT) AND WITH JAN-FEB MICROWAVE OBSERVATIONS (RIGHT) FOR 1973-76

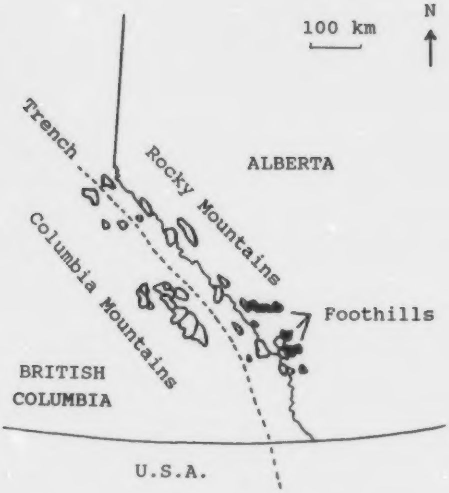
N
100 km
Trench
Rocky Mountains
ALBERTA
Columbia Mountains
Foothills
BRITISH COLUMBIA
U.S.A.

FIGURE 5. LOCATION OF SMALL BASINS IN ROCKY AND COLUMBIA MOUNTAINS

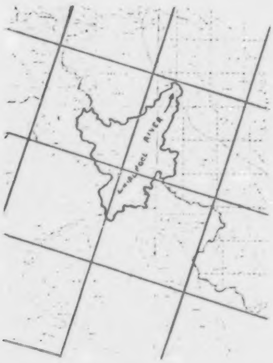

FIGURE 6. EXAMPLE OF SMALL BASIN AND ESMR GRID FOR BRIGHTNESS COMPUTATION. 30 KM X 30 KM GRID

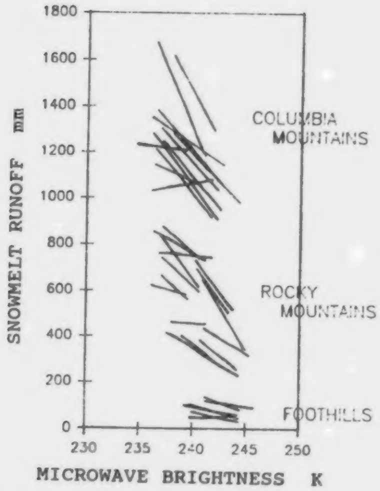

FIGURE 7. RUNOFF REGRESSIONS FOR 36 SMALL BASINS FROM JAN-FEB MICROWAVE OBSERVATIONS

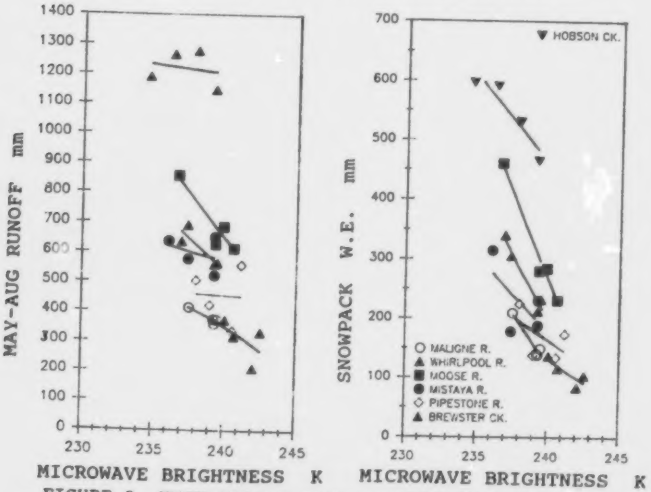

FIGURE 8. HIGH-ALPINE BASIN REGRESSIONS FROM MICROWAVE BRIGHTNESS FOR FORECASTING TOTAL RUNOFF (LEFT) AND ESTIMATING WINTER SNOWPACK (RIGHT)

CLASSIFICATION OF SNOW AND FROZEN GROUND SURFACES WITH SSM/I SIGNATURES

CHRISTOPHER M. U. NEALE

Department of Agricultural and Irrigation Engineering, Utah State University
Logan, Utah 84322-4105

MARSHALL J. McFARLAND and MATT M. BATCHELOR

Department of Agricultural Engineering, Texas A&M University
College Station, Texas 77843

INTRODUCTION

Microwave brightness temperatures from the Special Sensor Microwave/Imager are used to obtain information on certain meteorologic and surface phenomena over the oceans and land. Parameters such as ice edge, wind speed over the ocean, precipitation over the ocean and over land, land surface temperature, snow depth and water equivalent etc. can be retrieved with algorithms as described by Hollinger et. al (1987). These parameter retrieval algorithms consist of linear combinations of brightness temperatures from the seven possible channels of the SSM/I. Due to the empirical nature of these algorithms, it is necessary to properly characterize ground surface types according to their microwave emission properties and group the SSM/I data into appropriate regression data sets for each parameter of interest.

The classification of snow presents an additional problem as the microwave signature from a snowpack with constant depth can vary with snow morphology, snow ripeness and cycles of melting and re-freezing under spring weather conditions. Therefore, the interpretation of microwave signatures from a snow covered surface at any point in time would benefit from the knowledge of previous weather and snowpack conditions.

The objective of this paper is to describe some preliminary snow classification rules for the SSM/I as well as present the methodology used in their development.

BACKGROUND

The SSM/I is a seven channel, four frequency, linearly polarized, passive microwave radiometer onboard a U.S. Air Force DMSP satellite (Hollinger et al., 1987). Table 1 contains information regarding the characteristics of this sensor.

The characterization of snow signatures and their relationships with parameters such as snow wetness, snow depth and water equivalent has been studied by many authors such as Stiles and Ulaby (1980), Ulaby and Stiles (1980), and Chang and Shiue (1980). Other research concerning snow microwave properties has been described by Ulaby et al. (1986).

Most of the previous research on surface type characterization based on microwave brightness temperatures from satellite platforms, has been conducted within the development context of specific retrieval algorithms, using data from the Electrically Scanning Microwave Radiometer (ESMR) and the Scanning Multichannel Microwave Radiometer (SSMR). Among this research is the work done by Wilke and McFarland (1986) in soil moisture identification. Ferraro et al. (1986) presented a classification technique to identify several surface types using SSMR data. The surfaces included dry land, rain, wet flooded land, dry snow, sea ice and open water.

Specific research on snow classification has been done by Kunzi et al. (1982) in the development of snow extent, snow depth and water equivalent algorithms. Schanda et al. (1983) proposed a snow classification scheme based on several years of observations which included classes such as winter snow, wet spring snow and dry, refrozen spring snow. McFarland et al, (1987) investigated snowpack properties using SMMR brightness temperatures and were able to detect dry snow accumulation, and snow melting and refreezing processes.

METHODOLOGY

Database Development

SSM/I data from overpasses of interest were obtained from the Navy Research Laboratory (NRL). The data arrived on DEF tapes and segments of orbits were down-loaded to hard disk using a VAX 8650 computer. The data were then preprocessed and stripped of inter-record blank spaces, header records and saved in compact files for type A and B scans of the SSM/I (see Table 1 for explanation of scans). The SSM/I sensor data records (SDR) were then loaded into database files for several regions of interest. These regions consisted of large boxed areas identified and bounded by meridians and parallels. A typical database file would contain SDR data pertaining to several orbits over the boxed regions during a period of a week to ten days.

The "ground truth" data consisted of maximum and minimum temperatures, snow depth and snowfall amounts from the NOAA cooperative weather network, obtained from Asheville, NC. This is a relatively dense network of weather stations in the central plains states of the United States. The climatic data for each day of interest were gridded into 0.5 degree latitude/longitude boxes and merged with the corresponding SSM/I brightness temperature data.

CLIPS Expert System Land Surface Type Classifier

The C language production system (CLIPS) expert system shell developed by NASA (Cosmic, 1987), was used for the development of snow covered surface classification rules. This environment allowed for the addition, removal or modification of classification rules without the necessity of changing and re-compiling software code. To preserve the maximum of flexibility, the CLIPS module and rule base were imbedded within a C language program which handled input/output routines, passed the brightness temperatures to the CLIPS module, and executed the appropriate parameter retreival algorithms(snow depth and water equivalent) according to the results of the surface type classification. A dynamic database accessed by the C program was developed to store surface type classification codes for each 0.5 degree box over a region. Classification data from a time series of ascending (6 am) and descending (6 pm) overpasses of the SSM/I instrument over a region for the preceding 3 days was stored providing a surface type "memory" which was used within the CLIPS framework to classify snow covered surfaces. Thus, snow classification rules concerning dry snow/wet snow signatures as well as refrozen snow could be considered by observing the previous history over a region.

SSM/I data were classified on a footprint by footprint basis, using the concentric footprints of the SSM/I A scans. At the 85.5 GHz frequency, the brightness temperatures assigned to the concentric 85.5 GHz footprint was an average of nine footprints, eight of which surrounded the concentric footprint. Thus, the resolution of the 85.5 GHz channel (approximately 14 Km) was decreased to the same order as that of the 37.0 GHz channels (approximately 33 Km).

DISCUSSION AND RESULTS

Classification of Relevant Surface Types

Polarization dependence at the SSM/I frequencies will vary from almost no dependence in the presence of a dense canopy (with large optical thickness) to a large dependence in the presence of bare soil. This is shown in Figure 1, using the average difference between vertically polarized and horizontally polarized brightness temperatures at the 19.35 GHz and 37.0 GHz frequencies as an indicator. Smooth lines have been plotted through the center of each 0.5 K histogram class constructed from data obtained over appropriate control (training) areas. For data over dense vegetation the mean T_B polarization difference was 0.67 K with a standard deviation of 0.53 K. In the case of total absence of vegetation such as in the Sahara desert, the mean T_B polarization difference was 32.24 K with a standard deviation of 3.46.

The amount of vegetation cover over the central plains of the United States will vary considerably according to the seasons. The peak green vegetation cover for an agricultural region in the central plains of the U.S. can occur during the months of May through August depending on the climate zone, type of crop and if the crop is irrigated or rainfed. Vegetation densities in grasslands and savannas will vary according to the precipitation distribution throughout the year. Figure 1 shows the distribution of average polarization difference over the central plains states of the U.S. in the summer, for regions with natural rangeland vegetation as well as agricultural crops. Seasonal variations of vegetation cover within the arable soil classification group can be observed in Table 2 for the central plains of the United States, by comparing the distribution of average brightness temperature polarization differences in the 19.35 GHz and 37.0 GHz channels (combination [b]) during the summer and winter seasons respectively. Footprints classified as rain, snow, water, or dense vegetation were removed from the dataset. The larger influence of natural vegetation and crop cover during the summer, resulted in a lower mean T_B polarization difference. In the winter months, the T_B polarization differences were higher as the soil is mostly bare or partially covered with dry senesced vegetation.

Classification of Snow

a) Dry Snow

When dry, mostly bare soil is covered with a dry snowpack of a certain depth, a depression of brightness temperatures in the 37.0 GHz channels with respect to the 19.35 GHz channels occurs due to scattering. At 37.0 GHz, scattering is the dominant component of the total extinction loss of the medium (Ulaby et al, 1986). Channel combination data for footprints containing snow over the northern plains of the U.S are shown in Table 3. Brightness temperatures at 19.35 GHz were also lower, partly due to scattering and partly due to the physical temperature of the snow and underlying soil. However the latter will depend on the depth of the snowpack. The classification rule for dry snow consists in examining the conditions [b], [c], [d], [e] and [f] in

Table 3, which together differentiate snow from cold bare soil as well as large precipitating thunderstorm clouds.

Figure 2 shows the GT factor proposed by Kunzi et al. (1982) calculated from the 19.35 H and 37.0 H GHz channels for mostly dry snow cover. The GT factor was sensitive to snow depth up to between 300 and 400 mm of snow. However not enough data was available for higher snow depths to conclusively determine the slope of the trend as well as the threshold of sensitivity to snow depth. The considerable scatter in the data could be a result of the SSM/I geo-location error as well as the inclusion of some wet snow data points. In general however, Figure 2 shows the general trends presented by Kunzi et al. (1982) for SMMR data.

b) Wet snow or spring snow

The classification of wet snow or melted snow containing water in liquid form requires the use of the dynamic database scheme, as the signature could be confused with other surfaces. A small amount of liquid water (volumetric water content of 0.01) will increase the volume absorption coefficient of the medium to a value greater than the scattering coefficient, thus reducing the scattering albedo to a very small value (Ulaby et al., 1986). For higher volumetric water contents, scattering is practically non-existent and the snowpack begins to behave like a blackbody radiator.

Such conditions are normally encountered in the spring, when the snowpack undergoes successive cycles of thawing and refreezing. During the day, when temperatures are above the freezing point, the top layers of the snowpack will partially melt, increasing the volumetric water content of the snow. As a result, the microwave brightness temperatures at 37.0H GHz will increase with respect to the T_B at 19.35H GHz. This is shown in Figure 3 for a 7 day sequence of SSM/I data over north-central Nebraska during February, 1988. The last snowfall over that region occurred on day 51 with 50 to 75 mm of new snow being reported by the weather stations in the area. Snow depth changed throughout the period from 190 mm on day 53, 178 mm on day 56, 140 mm on day 57 to 90 mm on day 59. Minimum and maximum air temperatures are also shown in Figure 3, corresponding to ascending and descending overpasses respectively. The first available SSM/I data after the snowfall is for the ascending overpass on day 53. The T_B difference of approximately 20 K between the 19.35H and 37.0H GHz channels as well as the low brightness temperatures in both channels is an indication of dry snow. The minimum air temperature, which probably occurred a few hours prior to the overpass, was below the freezing point. The descending overpass on the same day, shows a marked increase in the 37.0H GHz brightness temperature to within 1 K of the 19.35H GHz channel as a result of a wet snow surface layer. Thawing at the snow surface occurred during the day due to warm air temperatures (maximum temperature of 7° C). Later overpasses beginning with day 56 descending, indicate a cycle of thawing during the day with freezing overnight. During this period, the variability in the 19.35H - 37.0H GHz T_B difference for the descending overpasses was probably due to different volumetric water content in the snowpack. It is important to note as well that the snowpack depth on day 59 was half its depth on day 53.

The rule for classification of wet snow within the CLIPS framework would check for dry snow, wet snow or refrozen snow on previous overpasses as well as brightness temperatures in the 19.35H and 37.0H Ghz channels.

c) Refrozen snow

Successive cycles of freezing and thawing will result in larger, more spherical ice crystals in the snowpack which will increase the scattering albedo. and decrease the polarization dependence. Figure 4 shows brightness temperatures in the horizontal and vertical polarizations for the 19.35, and 37.0 GHz channels for the same period. Brightness temperatures for the ascending overpass on day 57 were lower than those of day 53 for both frequencies and polarizations while the polarization dependence was smaller, indicating a partial refrozen snow surface layer. The rule for refrozen snow surface would check the previous descending overpasses for the presence of wet snow.

d) Snow edge

No particular classification rule was developed to detect snow edge due to lack of precise ground truth data. However under the present scheme, footprints would be classified as dry or wet snow, moist soil or dry soil. Thus, the position of the snow edge would be determined geographically by the classification of congruent footprints as one of these classifications.

CONCLUSIONS AND RECOMMENDATIONS

Land surface types can be independently classified using SSM/I channel combinations. The identification of proper surface types, is required for parameter retrieval algorithm development and subsequent algorithm application.

The brightness temperature threshold values used in the classification rules were based on statistical analysis and observations of SSM/I SDR data and are therefore subject to the present calibration of the instrument.

The classification of dry snow was based on the 37.0 - 19.35 GHZ and 85.5 - 37.0 GHz channel combinations (both polarizations) as well as average polarization difference in the 19.35 and 37.0 GHz channels. Wet snow and refrozen snow classification rules, were derived by examining conditions over past days using surface type classification information from previous SSM/I overpasses stored in a dynamic database.

The results presented herein are preliminary. Future research should include additional times series of SSM/I data over different climatic regions and snow conditions to better derive brightness temperature threshold values for the appropriate channel combinations. Frozen ground surfaces should also be included in future analysis.

REFERENCES

Chang, A.T.C. and J.C. Shiue. A comparitive study of microwave radiometer observations over snowfields with radiative transfer model calculations. Remote Sensing of Env. 10:215-229, 1980.

Cosmic. CLIPS reference manual, Version 4.0. Cosmic Software Information Services, University of Georgia, Computer Services Annex, Athens, Georgia 30602. 1987.

Ferraro, R.R., N.C. Grody and J.A. Kogut. Classification of geophysical parameters using passive microwave satellite measurements. IEEE Trans. Geosci. Remote Sensing. GE-24, No. 6. pp 1008-1013. 1986.

Hollinger, J., R. Lo, G. Poe, R. Savage and J. Pierce. Special Sensor Microwave/Imager User's Guide. Naval Research Laboratory, Washington, D.C. 1987.

Kunzi, K.F., S. Patil, and H. Rott. Snow-cover parameters retrieved from Nimbus-7 Scanning Multichannel Microwave Radiometer (SMMR) data. IEEE Trans. Geosci. Remote Sensing. GE-20, pp 452-467. 1982.

Schanda, E., C. Matzler, K. Kunzi. Microwave Remote Sensing of Snow Cover, Int. J. Remote Sensing, 4, pp149-158. 1983.

Stiles, W. H. and F.T. Ulaby. The active and passive microwave response to snow parameters 1. Wetness. Journal of Geophysical Research, Vol 85, No. C2 pp 1037-1044, 1980.

SCS Agricultural Handbook 296. Land Resource Regions and Major Land Resource Areas of the United States. USDA-SCS, Washington D.C. 1981.

Ulaby, F.T. and W.H. Stiles. The active and passive microwave response to snow parameters 2. Water equivalent of dry snow. Journal of Geophysical Research, Vol. 85, No. C2, pp1045-1049, 1980.

Ulaby, F. T., R. K. Moore, A. K. Fung. Microwave Remote Sensing, Active and Passive. Volume II: Radar remote sensing and surface scattering and emission theory. Artech House Inc. 1982.

Ulaby, F. T., R. K. Moore, A. K. Fung. Microwave Remote Sensing, Active and Passive. Volume III: From theory to applications. Artech House Inc. 1986.

Wilke, G. D. and M. J. McFarland. Correlations between Nimbus 7 scanning multichannel microwave radiometer (SMMR) data and an antecedent precipitation index. JCAM, vol 25, pp 227-238, 1986.

Table 1. Summary of Special Sensor Microwave/Imager characteristics.

Channel	Frequency (GHz)	Polarization	Noise Equiv. Temperature Differential (K)	Approximate Footprint Size (Km)
19V	19.35	Vertical	0.45	56
19H	19.35	Horizontal	0.42	56
22V	22.235	Vertical	0.74	45
37V	37.0	Vertical	0.37	33
37H	37.0	Horizontal	0.38	33
85V	85.5	Vertical	0.69	14
85H	85.5	Horizontal	0.73	14

Swath Width: 1400 Km
Scan A: 64: 19.35, 22.235 and 37.0 GHz concentric footprints and
128: 85.5 GHz footprints, concentric with the above, every other footprint
Scan B: 128: 85.5 GHz footprints

Table 2. Brightness temperature combination values for the Central Plains states of the U.S. corresponding to the arable soil classification.
Box size: NW corner: 50°N 105°W SE corner: 32°N 95°W

SUMMER SEASON

Combination	Mean (K)	St. Dev. (K)	Lower Limit (K)	Upper Limit (K)	Calendar Date and Node
19V - 22V [a]	-1.90	1.31	-4.52	0.72	
$\frac{(19V+37V)}{2} - \frac{(19H+37H)}{2}$ [b]	5.72	1.25	3.22	8.22	Asc. (1987) 211 222 235 244 253
37V - 19V [c]	-3.59	0.94	-5.47	-1.71	
85V - 37V [d]	-1.17	1.15	-3.47	1.13	
85H - 37H [e]	1.30	1.61	-1.92	4.52	

WINTER SEASON

22V - 19V [a]	-1.47	0.94	-3.35	0.41	
$\frac{(19V+37V)}{2} - \frac{(19H+37H)}{2}$ [b]	7.34	1.27	4.80	9.88	Asc. (1988) 55 59
37V - 19V [c]	-4.06	0.99	-6.04	-2.08	
85V - 37V [d]	-2.17	1.25	-4.67	0.33	
85H - 37H [e]	-0.87	1.79	-4.45	2.71	

Table 3. Mean and standard deviations for selected brightness temperature combinations over dry snow in the central plains of U.S.
Approximate box size:
NW corner: 49°N 105°W SE corner: 45°N 100°W

Combination	SNOW		NO SNOW		Julian Date of Overpass
	Mean (K)	St. Dev. (K)	Mean (K)	St. Dev. (K)	
22V - 19V [a]	-2.62	1.04	-0.95	1.06	
$\frac{(19V+37V)}{2} - \frac{(19H+37H)}{2}$ [b]	12.02	2.33	10.09	1.41	Asc. 51 55 Desc. 55 (1988)
37V - 19V [c]	-11.55	4.10	-2.24	1.21	
85V - 37V [d]	-8.36	5.92	-0.86	1.34	
85H - 37H [e]	-4.48	5.72	1.42	1.37	

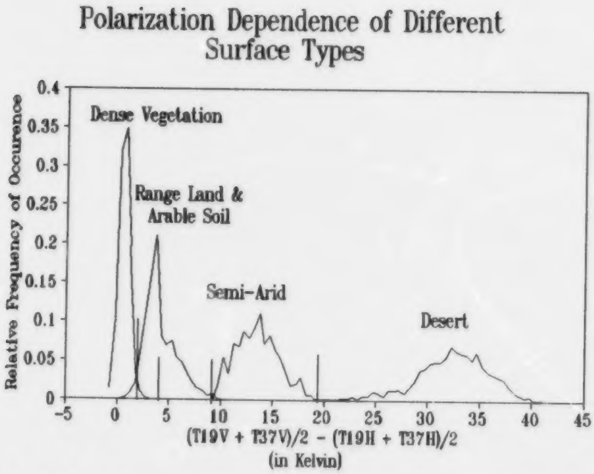

Figure 1 Polarization dependence of different surface types

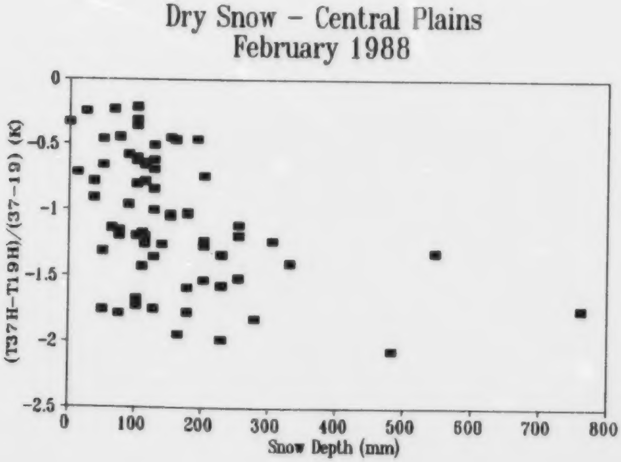

Figure 2. Snow depth versus the GT factor for mostly dry snow

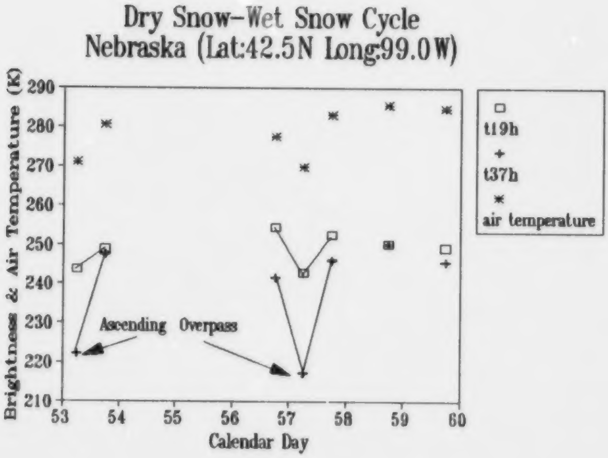

Figure 3. A sequence of SSM/I data over north-central Nebraska showing the influence of wet snow on brightness temperatures in the 19.35H and 37.0H channels

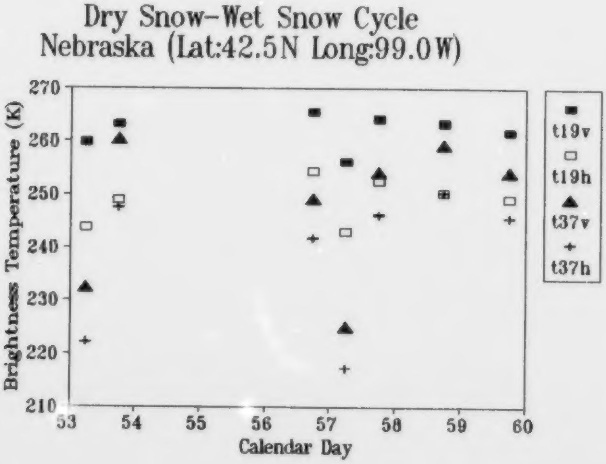

Figure 4. Influence of thawing and refreezing on SSM/I signatures.

WORKSHOP SESSION 2
RADAR AND MICROWAVE RADIOMETRY

Session Chairman: A. Wankiewicz
National Hydrology Research Institute

Session 2 - Working Group Questions

Group 1

Discussion Question:
Given the differences between microwave and visible/IR bands, how would microwave satellite observations complement conventional satellite methods; in terms of resolution, frequency of coverage, atmospheric interference, and sensitivity to surface hydrological properties.

CMU Neale, Chairman & Rapporteur
D Ambleur
H Assaf
D Euteneier
GA Fuller
BE Goodison
A Hougham
A Khan
G Latham
RM Leith
RA Melloh
T Prowse
A Rango
M Shome
F Thirkettle
N Yasmin
J Whiting
V Whittrock

Group 2

Discussion Question:
Given the differences between satellite and surface observations, what types of data networks or surveys provide suitable ground-truthing information for microwave radiometry and RADAR observations; in terms of resolution, scheduling or frequency of measurement, electromagnetic vs hydrological properties; and archived vs real time surveys.

ET Engman, Chairman
D Harvey, Rapporteur
J Andrews
M Black
R De Jong
C Faucher
TY Gan
JN Jasper
N Kouwen
G Leavesley
A Mainali
P Marsh
R Miller
G Schaefer
ED Soulis
JB Stewart
G Thomas
LA Warner
L Wiens

Group 3

Discussion Question:
Given the sensitivity of microwave emission or reflectance to important hydrological variables like basin snowpack and moisture, how can the monitoring and forecast needs of water resource agencies be met; in terms of providing registered and calibrated imagery within a useful time frame and supplying up-to-date algorithms for interpreting the images?

R Leconte, Chairman
JP Fortin, Rapporteur
N Bussieres
M Drews
J Donald
C Gignac
F Hicks
R Hopkinson
B Kochtubajda
E Mekis
W Nicholaichuk
MC Quick
C Rooney
LP Shan
B Stolte
A Walker
A Warkentin
WB Wilkinson

RADAR AND MICROWAVE RADIOMETRY

Summary

A. Wankiewicz - Session Chairman

GROUP 1

Group 1 discussed the integration of microwave remote sensing with information from visible and infra-red bands. The general conclusion was that the microwave band complements other bands because of its high frequency of coverage, as a result of it's cloud-penetrating properties. In contrast, other bands can provide higher spatial resolution, e.g. NOAA satellites can define snow cover at 1 km resolution. But the frequency of coverage of the high resolution radiometers is poor because they are blocked by cloud conditions.

In addition, it was recognized that microwaves are particularly sensitive to surface water, due to water's high dielectric constant; and to dry snow, due to scattering from microwave-scale snow grains. The papers presented earlier demonstrated that RADAR had promise for snow sensing and for ice roughness detection. Microwaves also have potential for vegetation mass and geometry measurements that are complementary to other bands, because microwaves penetrate further into the biomass. Finally, there appears to be promising results for rainfall measurement over land, using the new high frequency microwave channels.

GROUP 2

Group 2 discussed methods for ground truthing the microwave satellite sensors. They concluded that hydrological models are needed to help interpret the surface point measurements. The most useful ground truth provides data for both microwave and hydrologic needs at the same time. Because microwave radiometry is characterized by large resolution elements, ground truth measurements require large-scale planning with many volunteer observers. The data collection effort must be coordinated so that all monitoring devices are calibrated to a common basis, and measurement techniques standardized. All components of a scene should be sampled, to assess all the parameters of interest. Otherwise, ground truth would have to be estimated from data sources unrelated to remote sensing and not optimized for the experiment in question.

The group considered an alternative ground truth procedure using a network for continuous data collection. This would ensure that short-term events are monitored for comparison with satellite observations. Continuous data collection would be especially useful for airborne and Shuttle-based RADAR studies, because scheduling problems often make these observations difficult to synchronize with ground truth. Also, natural integrators, such a measured basin streamflow, show promise for verifying the large footprint observations of microwave radiometers.

GROUP 3

Group 3 discussed means of facilitating user application of microwave remote sensing. They concluded that, for the present, users prefer to have the raw data processed by one, specialized agency and receive only the end product, such as water equivalent or snow cover. Eventually, it might be useful for users to get user-friendly software to process the raw data to suit their own needs. As more confidence develops in application algorithms, the software could be tailored for particular needs or for specific watersheds. An expert system might also be incorporated within the program. There was concern expressed about the continuity of microwave observations. Algorithms developed for a particular satellite sensor(s) would have to be extended to apply to new bands, polarizations, or angles, if different sensors are flown on future satellites.

It was decided that users require satellite observations of variables such as: snow cover area, snow water equivalent, soil moisture, and ground frost. Snow cover areal extent is especially important during melt-time. Receipt of data must be timely to be incorporated in user forecasts. Passive microwave snowcover is received every week for the Prairies. Timing and coverage of this variable is good, but it is still at the experimental stage. For example, effects of liquid water or of snow grain size remains to be included in the water-equivalent algorithm.

INVITED PAPER

OPPORTUNITIES FOR REMOTE SENSING INITIATIVES WITHIN A CANADIAN GEWEX PROGRAM

R.G. Lawford
Associate Director, NHRI
Saskatoon, Saskatchewan

ABSTRACT: The World Meteorological Organization and the International Council of Scientific Unions are developing joint plans for a Global Energy and Water Cycle Experiment. This presentation outlines the nature and status of these plans and discusses the steps which Canada is taking to develop a national GEWEX initiative. Possible issues and opportunities for remote sensing initiatives within this context are identified.

INTRODUCTION:

The following presentation outlines the objectives and the current status of the international GEWEX program and summarizes the discussions which have taken place in developing a Canadian GEWEX program.

THE INTERNATIONAL GEWEX PROGRAM

The Global Energy and Water Cycle Experiment (GEWEX) is a program currently being developed under the auspices of the World Climate Research Program. An international program plan has been developed by the Joint Scientific Committee (JSC). This committee brings together experts from the International Council of Scientific Unions (ICSU) and the World Meteorological Organization (WMO) to develop and manage major international science programs. The International Association of Hydrological Sciences (IAHS) is also planning some GEWEX initiatives. Currently there are two IAHS committees concerned with the GEWEX Program. One committee is studying precipitation measurement techniques and the other is reviewing research needs in the area of hydrological models.

The international program objectives have been documented in the JSC's report on the concept of a GEWEX experiment (WMO, 1988). These objectives are as follows:

i) To determine the hydrological cycle and energy fluxes by means of global measurements of observable atmospheric and surface properties;

ii) To model the global hydrological cycle and its impacts in the atmosphere and the ocean;

iii) To develop the ability to predict the variations of global and regional hydrological processes and water resources, and their response to environmental change;

iv) To foster the development of observing techniques, data management and assimilation systems suitable for operational application to long-range weather forecasts, hydrology and climate predictions.

The task of meeting these objectives will involve the analysis of remotely sensed data. It appears that remote sensing will make its largest contributions in initiatives related to objectives 1 and 4. Remote sensing data will be required over the oceans and many land areas to obtain sufficiently dense measurements of atmospheric and surface properties. Clearly, Objective 4, which is considered as the major technical objective for the GEWEX program, will involve the development of new remote sensing capabilities and the improvement of techniques and facilities for analyzing and interpreting the data. If Objective 4 can be realized, it will improve significantly our ability to predict variations in global and regional hydrological processes.

There is sometimes confusion regarding the relationship between GEWEX and projects being developed under ICSU's International Geosphere-Biosphere Program (IGBP). In general, the IGBP will study all aspects of global change. One aspect of the program deals with the cycles of chemicals in the environment. GEWEX focuses on the cycling of water on a global scale. It is also designed to exploit the new satellite technologies which will become operational after 1995. Since many preparatory studies will be needed prior to data becoming available from these satellites, GEWEX projects should be in place and carried out during a build-up phase prior to the satellite launches.

The common overall objectives of the IGBP and GEWEX programs are implicit in the structure of the U.S. Global Change project. The U.S. Government has accorded the highest priority for IGBP programs to climate and hydrology, a theme which clearly encompasses many initiatives related to GEWEX. Within the U.S. federal government, NASA (National Aeronautical and Space Administration) has made a major commitment to support the IGBP and assist in putting in place many of the sensors needed for GEWEX. NASA initiatives are included in plans for the Earth Observing System (EOS) sometimes referred to as "Mission to Planet Earth". NASA is presently cooperating with other international agencies in the International Cloud Climatology Project (ISCCP) and the Global Precipitation Climatology Project. It should be noted that the Canadian Climate Centre of the Atmospheric Environment Service is the data archiving and processing centre for the ISCCP. The U.S.A. is currently developing a GEWEX plan, although progress to date has been slow. Consequently, it is too early to assess how the linkages between U.S. Global Change program and GEWEX will develop.

CANADA AND GEWEX

Given the nature and broad scope of the GEWEX program and the scientific problems it proposes to address, program managers may ask whether there is a rationale for Canadian involvement in GEWEX. In my view, there are a number of reasons why Canada should commit itself to this program. Each year the observational networks for meteorological and hydrological parameters change. Over the past decade, there has tended to be a reduction in the number of observing stations as operating costs increased and budgets were reduced. Presently, Canada averages approximately one climatological station every 3500 km^2 and one first order meteorological station every 35,000 km^2. If we are going to improve our capability to make long range weather and streamflow forecasts, we need new sources of data to assist us in specifying the initial atmospheric, hydrological and oceanographic conditions. Projects being proposed under GEWEX would provide us with many of the techniques required to derive this information from satellite data.

There are other reasons why Canada should be involved in GEWEX. Recent experiences on the Canadian prairies have shown that we need a better capability to monitor and predict using both climatological and biological data. Canada has a special requirement to understand the physical environment in northern Canada where our data networks are very sparse. There is a growing concern that the increasing concentration of greenhouse gases in the atmosphere will lead to climatic change and to the geographical redistribution of water resources. Water supply and demand patterns will be affected by changes in the distribution of precipitation and by the response of water mangers through the construction of drought-proofing reservoirs. In summary, the knowledge and techniques gained through GEWEX projects could provide us with the capability to more effectively monitor changes in the atmosphere, in surface and ground water regimes and in land cover conditions.

By the late 1990's we will be able to observe the world in much greater detail than we ever have before. Remote sensing data from a wide range of spectral bands, sampled simultaneously and regularly, will be available. If Canada does not have the capability of processing this data, we will not be able to provide natural resource managers with the information required to husband Canada's resources in a sustainable fashion and to take maximum advantage of opportunities to market our products in global markets. This will put Canada at a distinct disadvantage in its area of major economic strength, natural resources. On the other hand, active participation in GEWEX could put Canada on the leading edge in terms of developing new applications for these new data sets.

While it is clear Canada needs GEWEX, it is equally apparent that GEWEX needs Canada. Canada is a unique portion of the earth's land mass. It has the longest coastline in the world (when the Arctic Islands are included), large readily accessible areas of homogeneous vegetation cover (for studies of land-atmosphere interactions), large freshwater flows into the Arctic Ocean which influence circulation patterns. It is also home to at least three of the major ecozone boundaries in the north-south transition of biomes.

GEWEX needs Canada because of the contributions which we can make to the international program. Canadians such as Gord McBean of the University of British Columbia have been very influential in the conceptual design of the international experiment. Canadian universities have internationally recognized expertise in virtually all aspects of the hydrological sciences including precipitation processes, hydrological models, ground water and oceanography. Federal laboratories offer expertise in remote sensing (CCRS), atmospheric modelling (AES), hydrological processes (NHRC) and oceanography (IOS and BIO), to name only a few. In addition, provincial research agencies and our "high-tech" industrial sector have a great deal to contribute.

Canada also has an excellent track record in facilitating and contributing to international science programs. Based on past experience, it is clear that Canadian scientists have the international credibility and the reputations to make GEWEX a success.

TOWARDS A CANADIAN GEWEX PROGRAM

Given the complexity of the international GEWEX program, it is not clear what form a Canadian program would take. Figure 1 shows one possible structure for a Canadian GEWEX program. The program would have linkages to the Canadian Climate Program, the Canadian Global Change Program and the international GEWEX program. In addition, it would have connections with appropriate Canadian learned societies such as CMOS (Canadian Meteorological and Oceanographic Society) and professional associations such as ACH (Associate Committee of Hydrology).

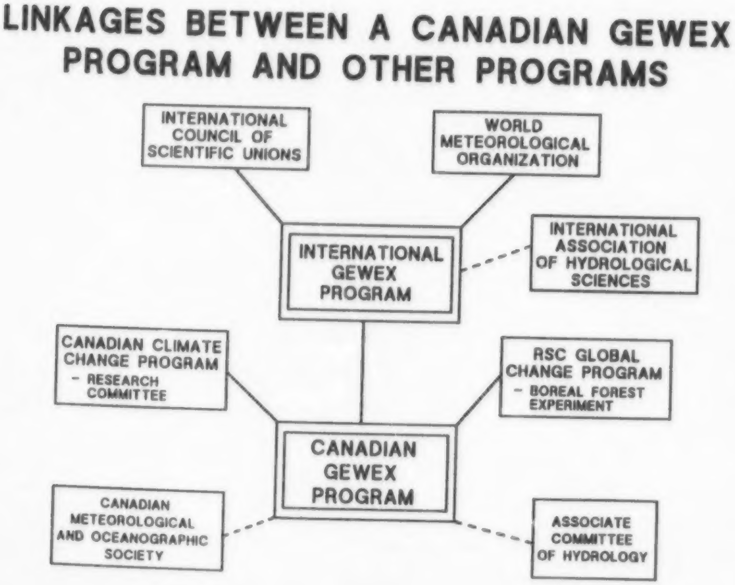
LINKAGES BETWEEN A CANADIAN GEWEX PROGRAM AND OTHER PROGRAMS
INTERNATIONAL COUNCIL OF SCIENTIFIC UNIONS
WORLD METEOROLOGICAL ORGANIZATION
INTERNATIONAL GEWEX PROGRAM
INTERNATIONAL ASSOCIATION OF HYDROLOGICAL SCIENCES
CANADIAN CLIMATE CHANGE PROGRAM - RESEARCH COMMITTEE
RSC GLOBAL CHANGE PROGRAM - BOREAL FOREST EXPERIMENT
CANADIAN GEWEX PROGRAM
CANADIAN METEOROLOGICAL AND OCEANOGRAPHIC SOCIETY
ASSOCIATE COMMITTEE OF HYDROLOGY

Figure 1. Schematic showing the possible program linkages for a Canadian GEWEX program.

Canada, under the leadership of the Canadian Climate Program, is undertaking an initiative to develop a plan for a Canadian GEWEX program. The first step in the process occurred at the National Hydrology Research Centre in October 1989. Approximately 50 scientists with expertise in oceanography, hydrology, remote sensing and meteorology met to discuss some of the major scientific and technical problems to be addressed as part of a Canadian GEWEX program. Table 1 provides a list of a number of the priority scientific problems which were identified at the workshop.

TABLE 1

LIST OF SOME OF THE PRIORITY SCIENCE ISSUES IDENTIFIED AT THE OCTOBER 1989 GEWEX WORKSHOP

- Integration of data from different space and time scales and to develop an understanding of the scale interactions of atmospheric and hydrologic processes.
- Development of reliable methods for measuring hydrologic variables in northern environments.
- Dynamics of the water balance in northern environments.
- Role of clouds in the arctic environment.
- Role of fresh water inflows to the Arctic Ocean and outflow from the Arctic Ocean in driving the thermohaline circulation.
- Determination of the biological parameters to be monitored in understanding and assessing changes in the global carbon cycle.

The need to develop an understanding of the relationships between the state variables and the hydrological processes was recognized. Hydrometeorological and hydrological processes operate on many scales. While the information from remote sensing provides us with some insight into these processes, we must have reliable models or algorithms to infer rates of evaporation, precipitation and other processes from the satellite data. Currently, satellite data are collected at different spatial resolutions (ranging from 10 m for some data at visual wavelengths to 25 km for Nimbus SMMR microwave data). Furthermore, the data from some satellites are received every 30 minutes (GOES) while data from Landsat are received every 16 days. Satellite sensors and even the satellites themselves are subject to failure from time to time. Before such highly variable data can be effectively integrated into operational hydrological models it will be necessary to develop robust models which can accept and utilize all these different data sources. Future remote sensing programs, which will make data available from many spectral bands simultaneously, will allow these models to perform more effectively. One proposal tabled at the GEWEX workshop involved the instrumentation of one or two research watersheds to provide data sets for calibrating and ground truthing remote sensing data.

Issues affecting remote sensing applications were also discussed at the workshop. Table 2 lists some of the issues and problems related to the use of remote sensing in hydrology which were articulated by the working groups.

TABLE 2

LIST OF SOME REMOTE SENSING ISSUES IDENTIFIED AT THE OCTOBER 1989 GEWEX WORKSHOP

- Development of time-independent algorithms based on inherent properties of the biosphere.
- Better design of remote sensing experiments.
- More emphasis on understanding the information contained in the atmospheric absorption parts of the spectrum.
- Need for ground based remote sensing methods to complement point and airborne measurements.

A process for developing a Canadian GEWEX plan is now in place. Hopefully, the relevant ideas and recommendations tabled at this Remote Sensing Applications Workshop will find their way into the Canadian GEWEX program. A writing team is currently preparing a "straw man" proposal. This team will be meeting at the end of March 1990 at the University of British Columbia to consolidate their ideas in initial draft. Members of the writing team are listed in Table 3. A second workshop will be held in late 1990 to discuss and refine this initial proposal.

TABLE 3

Participants in a Writing Team for a Canadian GEWEX Proposal

M. Beland	Global observations and weather prediction
M. Brugman	Glacial hydrology
B. Goodison	Precipitation detection
E. Carmack	Runoff and the thermohaline circulation - Pacific Ocean circulation
O. Hertzman	Atlantic Ocean/atmosphere interactions
R. Lawford	Precipitation processes and why Canada needs GEWEX
P. Marsh	Hydrology in the North
G. McBean	International context of the GEWEX program
L. Mysak	Arctic sea ice
W. Nicholaichuk	Prairie hydrology
M. Quick	Mountain hydrology
B. Swanson	Forestry hydrology
G. Kite	Remote sensing and hydrology models
R. Leconte	Remote sensing and land classification: remote sensing for GEWEX
R. Daley	Land surface processes in GCM's

From my perspective, there are a number of research opportunities and challenges which face the remote sensing community. They involve projects aimed at addressing and answering the following questions:

How can we design and implement a data management system which will give researchers economical and reliable access to remote sensing and conventional data bases?

How should satellite sensors be optimized in order to provide the most comprehensive and meaningful data possible for GEWEX studies?

What new algorithms will be needed to interpret data from the new sensors?

What types of models are needed in order to allow us to derive hydrological and meteorological processes from observations of state variables?

How can remote sensing data be effectively integrated into regional and global scale hydrological models and global climate models?

No doubt each one attending this workshop has ideas for projects and initiatives which could strengthen the remote sensing component of the plan for a Canadian GEWEX program. I would encourage you to document your ideas and forward them to me in the next 6-8 weeks.

REFERENCES:

World Meteorological Organization, 1988: Concept of the Global Energy and Water Cycle Experiment. Report of the JSC Study Group on GEWEX (Montreal, Canada, 8-12 June 1987 and Pasadena, USA, 5-9 January 1988), World Climate Research Program, WCRP-5, 67 pp. plus Appendices.

ACKNOWLEDGMENTS:

The author would like to express his appreciation to Mr. Kurt Loescher for assisting in preparing the graphics for this talk. He also thanks Mrs. Cindy Heseltine for her assistance in typing this manuscript.

POSTER PAPER

SNOWMELT STAGES ON LANDSAT IMAGES

by

G. A. Fuller, Faculty of Engineering
University of Regina, Regina, Saskatchewan

and

R. D. Hofer, Water Planning and Management Branch
I.W.D., Environment Canada, Regina, Saskatchewan

Abstract

Landsat imagery was used to study snowmelt in northern Canada. Band 5 and band 7 imagery were used. Band 5 imagery was chosen because it was of better quality than the band 4 imagery. Band 7 imagery was selected because it had the greatest potential of the four bands for analyzing melting snow. Four stages of snowmelt were observed on the imagery. The stages were: the disappearance of snow cover along ridges; water covering the ice on lakes; the appearance of dark open river reaches and finally the disappearance of the general snow cover.

Introduction

Much of the runoff in northern Canada occurs from snowmelt. Consequently information on snowmelt volumes, peaks and time of occurrence are useful. This paper reports on a study that attempted to evaluate the last day of snow cover using early Landsat imagery and Environment Canada climatic data. Due to financial restrictions, data from only two bands, bands 5 (0.6 to 0.7 µm) and band 7 (0.8 to 1.1 µm) were used. Band 5 images were selected because there were more useable images available and because they were of better quality than the band 4 images. Band 7 imagery was chosen because of its potential for identifying melting snow.

Results

It was impossible to accurately determine the last day of snow cover at specific locations due to the Landsat coverage cycle and the extensive cloud cover that occurred during the snowmelt period. Attempts were made to use images from adjacent flight paths to estimate conditions at the climate station but this did not prove to be satisfactory. Although it was not possible in this study to determine the last date of snow cover at specific locations, a pattern of snowmelt stages was observed on the Landsat images as the snowmelt process progressed.

The first snowmelt stage observed, the start of melt due to radiation, occurred when snow began to melt along ridges and southward facing valley slopes. This occurred before any melt was apparent on the general snow cover. Ridges and valley walls are more susceptible to melt because of a thinner snow cover and a more perpendicular aspect to the incoming energy.

Some time after the melt process began, the small lakes on the images appeared dark, especially on band 7 images, as a result of water on ice and snow covering the lakes. This stage was not evident on band 5 images for up to three weeks after the first stage but was evident sooner on band 7 images.

The third snowmelt stage, that of open river reaches, occurred soon after the second stage. The third stage was generally evident earlier on band 7 images. Small open streams were longer on band 7 images than on band 5 images, again demonstrating the near infrared band's greater sensitivity to the presence of water in the snow.

As melt increased, the general snow cover became increasingly gray on band 7 images until the snow generally disappeared except for snow remaining in the valleys. This was the fourth stage. Shortly after the snow cover had melted, vegetation began to grow. The land area on band 7 imagery appeared very similar to freshly fallen snow when the vegetation developed. This land area in band 5 imagery was much darker than in band 7, thereby indicating the presence of vegetation rather than fresh snow.

Conclusions

It was found that the progression of snowmelt on Landsat images could be divided into four general stages. The first stage was the start of snowmelt when the snow cover disappeared along ridges and southward facing valley walls. Then surface water appeared on ice covered lakes, followed shortly afterwards by the appearance of open river reaches. Finally the general snow cover became increasingly gray until the snow disappeared. All four stages of snowmelt were not observed at each location due to the Landsat coverage cycle and the extensive cloud cover that existed during the snowmelt period.

WORKSHOP PARTICIPANTS

Don C. Ambler
Regional Hydrologist
Environment Canada, IWD
Water Resources Branch
4th Floor, Queen Square
45 Alderney Drive
Dartmouth, Nova Scotia
B2Y 2N6

Jay Anderson
Environment Canada, AES
Prairie Weather Service
900-266 Graham Ave.
Winnipeg, Manitoba
R3C 3V4

Hamed Assaf
Dept. of Civil Engineering
University of British Columbia
Vancouver, B.C.
V6J 1Z9

Malcolm Black
Agriculture Canada, PFRA
1901 Victoria Ave.
Regina, Saskatchewan
S4P 0R5

Russell G. Boals
Regional Chief
Environment Canada
Water Resources Branch
G.M.C. Building, Room 210
1102 - 8th Avenue
Regina, Saskatchewan
S4R 1C9

Melinda (Mindy) Brugman
Glacial Hydrologist
Environment Canada
National Hydrology Research Centre
11 Innovation Blvd.
Saskatoon, Saskatchewan
S7N 3H5

Normand Bussières
Hydrometeorology & Marine Division
Canadian Climate Centre
Atmospheric Environment Service
4905 Dufferin Street
Downsview, Ontario
M3H 5T4

Reinder De Jong
Central Experimental Farm
Land Resource Research Centre
Neatby Bldg.
Ottawa, Ontario
K1A 0C6

Henry Desjarlais
Saskatchewan Parks and
Renewable Resources
Forest Fire Management Branch
P.O. Box 3003
Prince Albert, Saskatchewan
S6V 6G1

T. Milne Dick
Director
National Hydrology Research Centre
11 Innovation Blvd.
Saskatoon, Saskatchewan
S7N 3H5

John Donald
Dept. of Civil Engineering
University of Waterloo
Waterloo, Ontario
N2L 3G1

Manfred D. Drews
Environment Canada, AES
Twin Atria Building
4999-98th Ave.
Edmonton, Alberta
T6B 2X3

E.T. (Ted) Engman
Hydrology Laboratory, NRI
Bldg. 256, Rm. 205, BARC-East
Beltsville Agricultural Research
Centre
Beltsville, Maryland 20705
U.S.A.

Dalvin Euteneier
Hydrology Section
Saskatchewan Water Corporation
111 Fairford St.
Moose Jaw, Saskatchewan
S6H 7X9

Claude Faucher
Environment Canada, IWD
Water Planning & Management Br.
Ottawa, Ontario
K1A OH3

Jean-Pierre Fortin
Université de Québec, INRS-Eau
2800 rue Einstein
C.P. 7500,
Sainte Foy, Québec
G1X 4N8

Gerald A. Fuller
Faculty of Engineering
University of Regina
Regina, Saskatchewan
S4S OA2

Thian Yew Gan
Division of Water Res. Engineer
Asian Institute of Technology
G.P.O. Box 2754, Bangkok 10501
Thailand

Claude Gignac
Alcan Smelters & Chemicals Ltd
1954 Davis St.
Jonquière, Québec
G7S 4R5

Barry E. Goodison
Hydrometeorology & Marine Divis
Canadian Climate Centre
Atmospheric Environment Service
4905 Dufferin Street
Downsview, Ontario
M3H 5T4

K. David Harvey
Senior Hydrologist
Environment Canada, IWD
Water Resources Branch
8th Floor, Place Vincent Massey
351 St. Joseph Blvd.
Hull, Québec
K1A 0C3

Faye Hicks
University of Alberta
Room 220, Civil/Elec Bldg.
Edmonton, Alberta
T6G 2G7

Ronald F. Hopkinson
Scientific Services
Environment Canada, AES
P.O. Box 4800
Regina, Saskatchewan
S4P 3Y4

Arnold Hougham
PCI Inc.
50 West Wilmot St.
Unit # 1
Richmond Hill, Ontario
L4B 1M5

Jesse N. Jasper
Environment Canada, IWD
NWT Programs Branch
Yellowknife, N.W.T.
X1A 2R3

Abdul Khan
Dept. of Civil Engineering
University of Alberta
Edmonton, Alberta
T6G 2G7

Geoff Kite
Hydromet. Research Division
Environment Canada, AES
National Hydrology Research Centre
11 Innovation Blvd.
Saskatoon, Saskatchewan
S7N 3H5

Bob Kochtubajda
Resource Technologies Dept.
Alberta Research Council
P.O. Box 8330, Postal Station 'F'
Edmonton, Alberta
T6H 5X2

Nick Kouwen
Dept. of Civil Engineering
University of Waterloo
Waterloo, Ontario
N2L 3G1

Brian G. Latham
Regional Hydrologist
Indian & Northern Affairs Canada
P.O. Box 1500
Yellowknife, N.W.T.
X1A 2R3

R. G. (Rick) Lawford
Associate Director
Environment Canada, IWD
National Hydrology Research Centre
11 Innovation Blvd.
Saskatoon, Saskatchewan
S7N 3H5

George Leavesley
Project Chief, Water Resources
Division USGS
Denver Federal Center
Box 25046, MS412
Denver, Colorado 80225
U.S.A.

Robert Leconte
Canada Centre for Remote Sensing
1547 Merivale Road
Ottawa, Ontario
K1A 0Y7

Rory M. Leith
Environment Canada, IWD
502, 1001 West Pender St.
Vancouver, B.C.
V6E 2M9

L. Li Pi Shan
Saskatchewan Institute of Applied
Science and Technology
Palliser Campus
P.O. Box 1420
Moose Jaw, Saskatchewan
S6H 4R4

Arbind Mainali
Dept. of Civil Engineering
University of Alberta
Edmonton, Alberta
T6G 2G7

Philip Marsh
Research Scientist
Physical Hydrology Division
Environment Canada
National Hydrology Research Centre
11 Innovation Blvd.
Saskatoon, Saskatchewan
S7N 3H5

Robert Miller
Department of Agricultural
Engineering
Texas A & M University
College Station, Texas 77843-2117
U.S.A.

Eva Mekis
Hydrometeorology & Marine Division
Canadian Climate Centre
Atmospheric Environment Service
4905 Dufferin Street
Downsview, Ontario
M3H 5T4

Rae Ann Melloh
U.S. Army Cold Regions Research
and Engineering Lab (CRREL)
Hanover, New Hampshire 03755
U.S.A.

C. M. U. (Christopher) Neale
Dept. of Agricultural Engineering
Texas A & M University
College Station, Texas
77843-2117
U.S.A.

Walter N. (Wally) Nicholaichuk
Chief, Physical Hydrology Division
Environment Canada
National Hydrology Research Centre
11 Innovation Blvd.
Saskatoon, Saskatchewan
S7N 3H5

Ron Perla
Snow Properties Specialist
Physical Hydrology Division
Environment Canada
National Hydrology Research Centre
11 Innovation Blvd.
Saskatoon, Saskatchewan
S7N 3H5

Terry D. Prowse
Head, Northern Hydrology
Environment Canada
National Hydrology Research Centre
11 Innovation Blvd.
Saskatoon, Saskatchewan
S7N 3H5

Michael C. Quick
Dept. of Civil Engineering
University of British Columbia
Vancouver, B.C.
V6J 1Z9

Albert Rango
Chief, USDA Hydrology Laboratory
Agricultural Research Service
Beltsville Agr. Res. Centre-West
Building 007, Room 139
Beltsville, Md 20705
U.S.A.

Colleen Rooney
Sask. Crop Insurance Corp.
484 Prince William Drive
Box 3000
Melville, Saskatchewan
SOA 2PO

D. Garry Schaefer
A/Chief, Hydrometeorological
Research Division
Environment Canada, AES
National Hydrology Research Centre
11 Innovation Blvd.
Saskatoon, Saskatchewan
S7N 3H5

Manas Shome
Dept. of Civil Engineering
University of Alberta
Edmonton, Alberta
T6G 2G7

E.D.(Ric) Soulis
Dept. of Civil Engineering
University of Waterloo
Waterloo, Ontario
N2L 3G1

A. S. (Alan) Stanley
A/C Water Quality and
Aquatic Science Division
Environment Canada
National Hydrology Research Centre
11 Innovation Blvd.
Saskatoon, Saskatchewan
S7N 3H5

John B. Stewart
Institute of Hydrology
Wallingford, Oxon. OX10 8BB
U.K.

Bill Stolte
Civil Engineering Department
University of Saskatchewan
Saskatoon, Saskatchewan
S7N OWO

Frank Thirkettle
Ph.D Associates
1115, 505 5th Ave. S.W.
Calgary, Alberta
T2P 3H5

Graham Thomas
Department of Geography
University of British Columbia
#217-1984 West Mall
Vancouver, B.C.
V6T 1W5

Anne Walker
Ph.D. Associates
107 Fordwich Cr.
Rexdale, Ontario
M9W 2T6

Anthony Wankiewicz
Physical Hydrology Division
Environment Canada
National Hydrology Research Centre
11 Innovation Boulevard
Saskatoon, Saskatchewan
S7N 3H5

L. A. (Lyman) Warner
Water Survey of Canada
Environment Canada, IWD
Room 854, 220 - 4th Ave. SE
Calgary, Alberta
T2P 2M7

Alf Warkentin
Water Resources Branch
Government of Manitoba
1577 Dublin Ave.
Winnipeg, Manitoba
R2Y 0K4

Jeff Whiting
Saskatchewan Research Council
15 Innovation Blvd
Saskatoon, Saskatchewan
S7N 2X8

Larry Wiens
Water Planning & Management Branch
Motherwell Building
1901 Victoria Ave.
Regina, Saskatchewan
S4P 3R4

Virginia Wittrock
Saskatchewan Research Council
15 Innovation Blvd.
Saskatoon, Saskatchewan
S7N 2X8

Nighat Yasmin
Dept. of Civil Engineering
University of Alberta
Edmonton, Alberta
T6G 2G7